Nano Tungsten Oxides

Physical & Chemical Properties, Production Process, & Applications

CTIA GROUP LTD

CTIA GROUP LTD
Global Leader in Intelligent Manufacturing for Tungsten, Molybdenum, and Rare Earth Industries

INTRODUCTION TO CTIA GROUP

CTIA GROUP LTD， a wholly-owned subsidiary with independent legal personality established by CHINATUNGSTEN ONLINE , is dedicated to promoting the intelligent, integrated, and flexible design and manufacturing of tungsten and molybdenum materials in the Industrial Internet era. CHINATUNGSTEN ONLINE, founded in 1997 with www.chinatungsten.com as its starting point—China's first top-tier tungsten products website—is the country's pioneering e-commerce company focusing on the tungsten, molybdenum, and rare earth industries. Leveraging nearly three decades of deep experience in the tungsten and molybdenum fields, CTIA GROUP inherits its parent company's exceptional design and manufacturing capabilities, superior services, and global business reputation, becoming a comprehensive application solution provider in the fields of tungsten chemicals, tungsten metals, cemented carbides, high-density alloys, molybdenum, and molybdenum alloys.

Over the past 30 years, CHINATUNGSTEN ONLINE has established more than 200 multilingual tungsten and molybdenum professional websites covering more than 20 languages, with over one million pages of news, prices, and market analysis related to tungsten, molybdenum, and rare earths. Since 2013, its WeChat official account "CHINATUNGSTEN ONLINE" has published over 40,000 pieces of information, serving nearly 100,000 followers and providing free information daily to hundreds of thousands of industry professionals worldwide. With cumulative visits to its website cluster and official account reaching billions of times, it has become a recognized global and authoritative information hub for the tungsten, molybdenum, and rare earth industries, providing 24/7 multilingual news, product performance, market prices, and market trend services.

Building on the technology and experience of CHINATUNGSTEN ONLINE, CTIA GROUP focuses on meeting the personalized needs of customers. Utilizing AI technology, it collaboratively designs and produces tungsten and molybdenum products with specific chemical compositions and physical properties (such as particle size, density, hardness, strength, dimensions, and tolerances) with customers. It offers full-process integrated services ranging from mold opening, trial production, to finishing, packaging, and logistics. Over the past 30 years, CHINATUNGSTEN ONLINE has provided R&D, design, and production services for over 500,000 types of tungsten and molybdenum products to more than 130,000 customers worldwide, laying the foundation for customized, flexible, and intelligent manufacturing. Relying on this foundation, CTIA GROUP further deepens the intelligent manufacturing and integrated innovation of tungsten and molybdenum materials in the Industrial Internet era.

Dr. Hanns and his team at CTIA GROUP, based on their more than 30 years of industry experience, have also written and publicly released knowledge, technology, tungsten price and market trend analysis related to tungsten, molybdenum, and rare earths, freely sharing it with the tungsten industry. Dr. Han, with over 30 years of experience since the 1990s in the e-commerce and international trade of tungsten and molybdenum products, as well as the design and manufacturing of cemented carbides and high-density alloys, is a renowned expert in tungsten and molybdenum products both domestically and internationally. Adhering to the principle of providing professional and high-quality information to the industry, CTIA GROUP's team continuously writes technical research papers, articles, and industry reports based on production practice and market customer needs, winning widespread praise in the industry. These achievements provide solid support for CTIA GROUP's technological innovation, product promotion, and industry exchanges, propelling it to become a leader in global tungsten and molybdenum product manufacturing and information services.

CTIA GROUP LTD
Introduction of Nano Tungsten Trioxide (WO_3)

1. Nano Tungsten Trioxide Overview

CTIA GROUP LTD's Nano Tungsten Trioxide (WO_3) complies with GB/T 36080-2018 and ISO/TS 21356-1:2021 standards. It is prepared using advanced chemical vapor deposition or wet chemical methods and is a high-performance nanomaterial. It is known for its ultrafine particle size, high specific surface area and excellent photoelectric properties, and is suitable for use in the fields of optoelectronics, catalysis and energy.

2.Excellent Properties of Nano Tungsten Trioxide (WO_3)

Ultrafine nanoscale: particle size ranges from 50-100 nm, evenly distributed, and meets the standards for nanomaterials (1-100 nm).

High purity: WO_3 content ≥99.9%, extremely low impurities, ensuring high-end application performance.

Excellent performance: surface area >20 m²/g, excellent optical transparency, conductivity and thermal stability.

Reliable quality: pure crystal form (XRD detection), no agglomeration, guaranteed consistency.

3. Nano Tungsten Trioxide (WO_3) Product Specifications

Brand	Particle size (nm)	Purity (wt %)
NWO-50	50±10	≥99.9
NWO-80	80±10	≥99.9
NWO-100	100±10	≥99.9
In addition to basic specifications, parameters such as particle size and purity can be customized according to customer needs.		

4. Nano Tungsten Trioxide (WO_3) Packaging and Warranty

Packaging: Inner vacuum aluminum foil bag, outer sealed plastic barrel, net weight 1kg or 5kg, moisture-proof and oxidation-proof.

Warranty: Each batch is accompanied by a quality certificate, including particle size distribution (laser method), chemical composition and specific surface area data, and the shelf life is 12 months.

5. Nano Tungsten Trioxide (WO_3) Purchasing Information

Email: sales@chinatungsten.com
Tel: +86 592 5129595

For more information about nano tungsten oxide, please visit the website of CTIA GROUP LTD. (www.ctia.com.cn)

Table of Contents

Chapter 5: Applications of Nano-Tungsten Oxide

References

Appendix

Appendix A: Physical and Chemical Data Sheet of Nano-Tungsten Oxide

Including Detailed Parameters Such as Density, Melting Point, Band Gap, etc.

Appendix B: Experimental Procedures for Commonly Used Analytical Methods

XRD, FTIR, SEM, TEM, UV-Vis, BET, etc. Operation Guide

Appendix C: List of Patents Related to Nano-Tungsten Oxide

Detailed Listing of Patent Number, Title, and Abstract

Appendix D: List of Nano-Tungsten Oxide Standards

Comparison with Chinese, Japanese, German, Russian, Korean, and International Standards

Appendix E: Nano-Tungsten Oxide Multi-Language Terminology Table

Chinese, English, Japanese, and Korean Terminology Comparison Table

Preface

Trioxide (Nano-WO_3) , as a transition metal oxide with excellent physical and chemical properties, occupies an important position in the fields of materials science, chemical engineering and nanotechnology. Its unique semiconductor properties, optical properties and high specific surface area make it show a wide range of application potential in many fields such as photocatalysis, electrochromism, gas sensors and energy storage. The purpose of this book is to systematically sort out the scientific basis, preparation process, characterization method and application scenarios of nano tungsten trioxide, and at the same time combine patented technology, international standards and safety assessment to provide a comprehensive and practical reference guide for academic researchers, engineers and industry practitioners. By integrating the latest research progress and industrial practice, we hope to reveal the complete path of nano tungsten trioxide from laboratory exploration to industrial application, and promote its technological innovation in the fields of new energy, environmental protection and intelligent manufacturing.

Research significance and development history of nano-tungsten oxide

The research significance of nano tungsten oxide first comes from its excellent performance as an n-type semiconductor material. Its band gap energy range (2.4-2.8 eV) gives it strong visible light absorption ability, which gives it significant advantages in the field of photocatalysis, such as water splitting to produce hydrogen and degradation of organic pollutants. Compared with traditional photocatalysts (such as TiO_2) , nano-WO_3 is more responsive in the visible light region and can effectively utilize solar energy, which makes it a key material for solving energy crises and environmental pollution problems. In addition, WO_3 's electrochromic properties—the ability to control color and transmittance through electric fields—make it a core component for smart windows, displays, and dynamic thermal management devices. Nanoscale WO_3 also performs well in gas sensors (such as detecting NO_2 and H_2)

and energy storage materials (such as lithium-ion battery anodes and supercapacitor electrodes) due to its high specific surface area (20-50 m^2 / g , compared to 5-10 m^2/ g of micron - scale WO_3) and abundant surface active sites. Nanoscale quantum effects and surface effects further enhance their catalytic activity, ion diffusion rate, and photoelectric conversion efficiency, making them irreplaceable in interdisciplinary applications.

The unique properties of nano-tungsten oxide have not only promoted basic scientific research, but also opened up broad prospects for industrial applications. For example, its application in photocatalytic air purification and self-cleaning coatings has entered the commercialization stage, while its exploration in the fields of flexible electronics and biomedicine indicates the future development direction. However, the widespread application of nano-WO_3 is also accompanied by challenges, including how to achieve low-cost large-scale production, improve performance stability in complex environments, and evaluate its biological and environmental safety at the nanoscale. These issues are not only the focus of academic research, but also the focus of industry and policymakers.
The research and development of nano tungsten oxide can be traced back to the initial exploration of tungsten compounds in the late 19th century. As a rare metal, tungsten oxides first attracted attention due to the needs of the metallurgical industry. Yellow tungsten oxide (WO_3), as the main oxidation state of tungsten , has been widely studied due to its chemical stability, high temperature resistance (melting point of about 1473°C) and bright yellow appearance. At the end of the 19th century, chemists prepared WO_3 through the acidification reaction of tungstates (such as sodium tungstate Na_2WO_4) , and initially revealed its amphoteric oxide properties - it can react with acids to form tungstates, and react with alkalis to form tungstates. The research at this stage mainly focused on the chemical properties and industrial preparation of WO_3 , laying the foundation for subsequent applications.

In the mid-20th century, with the rise of semiconductor physics, the study of WO_3 entered a new stage. In the 1960s, researchers first discovered that WO_3 could change color after applying an electric field. This electrochromic property was driven by the formation of tungsten bronze structures (such as H_xWO_3). This discovery quickly triggered research on its optical applications, such as anti-glare glasses and early display devices. Subsequently, the proposal of the Honda-Fujishima effect (TiO_2 photocatalytic decomposition of water) in the 1970s set off a wave of photocatalytic research. WO_3 was regarded as a strong competitor to TiO_2 due to its lower band gap and better photochemical stability . For example, a study in 1976 showed that WO_3 could decompose water to produce oxygen under ultraviolet light, and this achievement promoted its in-depth exploration in the field of photocatalysis.

The rise of nanotechnology marks another leap forward in WO_3 research . Entering the 21st century, especially after 2000, with the breakthrough of nano-preparation technology (such as hydrothermal method and vapor deposition method), the synthesis of nano-scale WO_3 has become a reality. In 2004, researchers used a hydrothermal method to prepare WO_3 nanoparticles with a diameter of about 20 nm for the first time . Their photocatalytic activity was nearly three times higher than that of micron -sized materials . Subsequently, the development of morphologies such as nanowires, nanosheets, and porous structures further optimized their performance. For example, a 2010 study showed that WO_3 The

nanowires have a high surface area of 40 m^2 / g, which increases their sensitivity in NO_2 detection by 5 times . At the same time, doping modification (such as N and S doping) and composite material design (such as WO_3 /gC_3N_4 , WO_3 / TiO_2) significantly improved its photocatalytic efficiency and electrical properties. In recent years, the application of nano-WO_3 in the field of energy storage has expanded rapidly. For example, a study in 2018 demonstrated the high capacity (>600 mAh /g) and cycle stability of WO_3 /graphene composites in lithium-ion batteries . In addition, its potential in emerging fields such as antibacterial coatings (using photocatalysis to produce active oxygen), thermochromic materials (doping V to adjust the color change temperature) and bioimaging (quantum dots WO_3) is gradually emerging.

Although the research on nano-WO_3 has made remarkable progress, its development still faces many challenges. The complexity of the preparation process limits large-scale production, the agglomeration effect of nanoparticles may reduce performance, and their long-term safety in the body still needs in-depth evaluation. These issues have driven technological innovations around the world, such as China's breakthrough in high-purity WO_3 production (YS/T 572-2007 standard) and Europe and the United States' efforts on nanomaterial safety specifications (ASTM B922-20). This book was written in this context. It aims to build a bridge from basic research to industrial application by systematically analyzing the structure, preparation, application and safety of nano-WO_3 , and to provide scientific support for solving major challenges in the fields of energy, environment and intelligent technology.
This book is divided into nine chapters, starting with the structure and properties of nano-tungsten oxide, and gradually exploring its preparation process, characterization technology, application fields, patents and standards, safety assessment and future prospects. The appendix provides data sheets, experimental guides, patent lists, standard comparisons and multilingual glossaries, striving to create a comprehensive and practical knowledge platform for readers around the world. We hope that this book will not only inspire new ideas for academic research, but also inject momentum into the industrialization process of nano-WO_3 .

CTIA GROUP LTD
Introduction of Nano Tungsten Trioxide (WO_3)

1. Nano Tungsten Trioxide Overview

CTIA GROUP LTD's Nano Tungsten Trioxide (WO_3) complies with GB/T 36080-2018 and ISO/TS 21356-1:2021 standards. It is prepared using advanced chemical vapor deposition or wet chemical methods and is a high-performance nanomaterial. It is known for its ultrafine particle size, high specific surface area and excellent photoelectric properties, and is suitable for use in the fields of optoelectronics, catalysis and energy.

2.Excellent Properties of Nano Tungsten Trioxide (WO_3)

Ultrafine nanoscale: particle size ranges from 50-100 nm, evenly distributed, and meets the standards for nanomaterials (1-100 nm).

High purity: WO_3 content ≥99.9%, extremely low impurities, ensuring high-end application performance.

Excellent performance: surface area >20 m²/g, excellent optical transparency, conductivity and thermal stability.

Reliable quality: pure crystal form (XRD detection), no agglomeration, guaranteed consistency.

3. Nano Tungsten Trioxide (WO_3) Product Specifications

Brand	Particle size (nm)	Purity (wt %)
NWO-50	50±10	≥99.9
NWO-80	80±10	≥99.9
NWO-100	100±10	≥99.9
In addition to basic specifications, parameters such as particle size and purity can be customized according to customer needs.		

4. Nano Tungsten Trioxide (WO_3) Packaging and Warranty

Packaging: Inner vacuum aluminum foil bag, outer sealed plastic barrel, net weight 1kg or 5kg, moisture-proof and oxidation-proof.

Warranty: Each batch is accompanied by a quality certificate, including particle size distribution (laser method), chemical composition and specific surface area data, and the shelf life is 12 months.

5. Nano Tungsten Trioxide (WO_3) Purchasing Information

Email: sales@chinatungsten.com

Tel: +86 592 5129595

For more information about nano tungsten oxide, please visit the website of CTIA GROUP LTD. (www.ctia.com.cn)

Chapter 1: Introduction to Nano-Tungsten Oxide

Nano Tungsten Trioxide (Nano-WO_3) is an important transition metal oxide. It plays a pivotal role in the fields of materials science, chemical engineering and nanotechnology due to its diverse physical and chemical properties and broad application prospects. This chapter aims to provide readers with a comprehensive introductory knowledge of nano tungsten trioxide, starting with its basic definition, chemical formula and color variants, deeply exploring its unique characteristics at the nanoscale, reviewing the historical context of its research and development, and analyzing its status and research hotspots in materials science. Through the detailed introduction of this chapter, readers will have a comprehensive understanding of the scientific basis and application potential of nano tungsten trioxide, laying the foundation for a deep understanding of its preparation, properties and applications.

1.1 Basic Concepts of Tungsten Oxide

1.1.1 Definition and chemical formula (WO_3)

Tungsten trioxide is a compound composed of tungsten (W) and oxygen (O), with the chemical formula WO_3 , which means that each tungsten atom is combined with three oxygen atoms through a mixture of covalent bonds and ionic bonds to form a stable oxide structure. As the main oxidation state of tungsten element , tungsten in WO_3 is in the +6 oxidation state, belonging to the family of transition metal oxides, and its molecular weight is 231.84 g/mol. The crystal structure of WO_3 is highly dependent on the preparation conditions and temperature, usually presenting a monoclinic phase (Monoclinic, stable state, common at room temperature), an orthorhombic phase (Orthorhombic, 300-720°C) or a tetragonal phase (Tetragonal, >720°C), and the transition of these phases is closely related to its thermodynamic properties.

WO_3 is an amphoteric oxide with chemical versatility. It can react with strong acids (such as HCl) to form soluble tungsten salts (such as WCl_6), and can also react with strong bases (such as NaOH) to form tungstates (such as Na_2WO_4), which makes it valuable in industrial purification and chemical synthesis. In addition, WO_3 has a melting point of up to 1473°C and a boiling point of decomposition above 1700°C, showing excellent thermal stability, making it suitable for applications in high temperature environments, such as ceramic additives and refractory materials. At the nanoscale, these properties of WO_3 are further amplified by the enhancement of surface effects and quantum effects, giving it greater potential in the field of functional materials.

1.1.2 Color variations of tungsten oxide (yellow, blue, black)

Tungsten oxide is known for its various color variants, including yellow, blue and black, which not only reflect the differences in its chemical composition, crystal structure and defect state, but also directly determine its application potential in photocatalysis, electrochromism, gas sensors and energy storage. The following is a comprehensive description of these three color variants, covering their origin, preparation process, characteristics and nanoscale performance, and explores their specific applications in scientific research and industry.

Yellow Tungsten Oxide (YTO, WO_3)

Origin and Structure

of Yellow Tungsten Oxide (YTO, WO_3) Yellow tungsten oxide is a typical form of tungsten oxide (WO_3), usually existing in monoclinic or orthorhombic phase. Its yellow color originates from the electronic transition with a band gap energy between 2.6-2.8 eV, corresponding to strong absorption in the visible light region (about 450-500 nm). The crystal structure of monoclinic WO_3 is composed of WO_6 octahedral units, which are connected by corner-sharing or edge-sharing to form a three-dimensional network with lattice parameters of a=7.306 Å , b=7.540 Å , c=7.692 Å , β=90.91°. This ordered structure gives it high chemical and thermal stability. The yellow color is also related to trace defects in the lattice (such as oxygen vacancies). Although these defects are rare in pure WO_3 , they may increase slightly at the nanoscale, affecting the color depth. X-ray diffraction (XRD) and Raman spectroscopy analysis show that the characteristic peaks of the monoclinic phase (such as 717 cm^{-1} and 807 cm^{-1}) reflect the strong vibration of the WOW bond, further confirming its structural integrity .

Yellow Tungsten Oxide (YTO, WO_3) Preparation Method There are various methods for preparing yellow WO_3 , which are mainly divided into wet chemical method and thermochemical method:

Yellow Tungsten Oxide (YTO, WO_3) Acid Precipitation Preparation Method

the sodium tungstate (Na_2WO_4) solution to adjust the pH to 1-2 to generate tungstic acid (H_2WO_4) precipitation , which is then calcined at 500-600°C for 2-4 hours to decompose into WO_3 . The calcination temperature is critical. If the temperature is lower than 450°C, hydrates (such as $WO_3 \cdot H_2O$) may remain , and if the temperature is higher than 650°C, the color may become lighter or the grain size may be too large (>10 μm).

Thermal decomposition method: Ammonium metatungstate ($(NH_4)_5H_5[H_2(WO_4)_6]\cdot H_2O$, referred to as AMT) is commonly used in industry as a precursor . It is calcined at 550 ° C in air , and the decomposition reaction is: $(NH_4)_5H_5[H_2(WO_4)_6] \rightarrow WO_3 + NH_3\uparrow + H_2O\uparrow$. This method can control the grain size, usually obtaining micron-sized WO_3 of 1-5 μm , but a hydrothermal method is required at the nanoscale. The roasting atmosphere (such as oxygen content) has a significant effect on color purity, and insufficient oxygen may produce blue WO_3 .

Yellow Tungsten Oxide (YTO , WO_3) Hydrothermal Preparation

The reaction of sodium tungstate and HCl in an autoclave at 180°C for 12-24 hours can directly generate yellow WO_3 nanoparticles of 20-100 nm . The addition of surfactants (such as hexadecyltrimethylammonium bromide, CTAB) can adjust the morphology to spherical (20-50 nm in diameter), rod-shaped (100-200 nm long) or flake-shaped (10-20 nm thick). For example, a study in 2017 prepared 30 nm yellow WO_3 nanoparticles with a purity of 99.9% by optimizing hydrothermal conditions (pH=1.5, 180°C, 24 h) .

These methods each have their own advantages. The wet chemical method is suitable for nanoscale preparation, while the thermochemical method is more suitable for industrial mass production, with a

yield of more than 90%.

Physical and Chemical Properties of Nano Yellow Tungsten Oxide (YTO, WO_3)

Optical properties of nano yellow tungsten oxide (YTO, WO_3)

The band gap is 2.6-2.8 eV, reflecting yellow light (wavelength 570-590 nm), with high transmittance in the infrared region (>700 nm). The UV-Vis spectrum shows an absorption edge around 450 nm, high color purity, and an optical density (OD) between 0.5-1.0. The band gap value is determined by The Tauc plot method is used for calculation, and the formula is $(\alpha h\nu)^2 = A(h\nu - Eg)$, where α is the absorption coefficient and hν is the photon energy.

Density of Nano Yellow Tungsten Oxide (YTO, WO_3)

monoclinic WO_3 is 7.16 g/ cm^3 , and the density of orthorhombic phase is slightly lower (about 7.1 g/cm^3) due to looser lattice arrangement. The apparent density of nanoscale WO_3 may be slightly reduced to 6.8-7.0 g/cm^3 due to porosity as determined by Archimedes method .

Thermal stability: Stable up to 1100°C in air, it starts to volatilize above this temperature to generate $WO_{2.9}$ or other low oxidation state substances , and the decomposition reaction is: $2WO_3 \rightarrow 2WO_{2.9} + 0.5O_2\uparrow$. Thermogravimetric analysis (TGA) shows that the mass loss does not exceed 1% before 1200°C.

Chemical Properties of Nano Yellow Tungsten Oxide (YTO, WO_3)

It is slightly soluble in water (solubility <0.02 g/100 mL, 25°C), soluble in strong base (such as 1 M NaOH) to form Na_2WO_4 , with a dissolution rate of about 0.1 g/min; it is partially soluble in concentrated acid (such as 98% H_2SO_4) to form tungstate derivatives, and the reaction equilibrium takes several hours.

Electrical Properties of Nano Yellow Tungsten Oxide (YTO, WO_3)

As an n-type semiconductor, the electron concentration is about 10^{16} -10^{18} cm^{-3} , the conductivity is low (10^{-6} -10^{-5} S/cm), and is significantly affected by temperature and defects. For example, the conductivity can increase to 10^{-4} S/cm at 300°C due to the increase in thermally excited carriers.

Nanoscale properties

of yellow tungsten oxide (YTO, WO_3) Nanoscale yellow WO_3 (particle size 20-100 nm) exhibits significant advantages due to quantum effects and surface effects:

Specific surface area of nano yellow tungsten oxide (YTO, WO_3)

It can reach 20-30 m^2 / g (micron level is only 5-10 m^2 / g), which is verified by BET (Brunauer -Emmett-Teller) nitrogen adsorption test. The high specific surface area increases the surface active sites. For example, in the photocatalytic reaction, the ability to adsorb dye molecules is increased by 3-5 times , and the adsorption isotherm conforms to the Langmuir model.

Bandgap variation of nano yellow tungsten oxide (YTO, WO_3)

The reduction in particle size leads to a slight increase in the band gap. For example, the band gap of 20 nm WO_3 can reach 2.85 eV, the light absorption edge blue-shifts to 435 nm, and the color may be slightly lighter, which is attributed to the quantum confinement effect . Theoretical calculations show that the band gap increment is inversely proportional to the particle size (d), $\Delta Eg \propto 1/d^2$.

Photocatalytic activity of nano yellow tungsten oxide (YTO, WO_3)

When degrading methylene blue (MB), the reaction rate constant (k) of nano-WO_3 can reach 0.05 min^{-1} , far exceeding the 0.01 min^{-1} of the micron-level , attributed to the higher electron-hole separation efficiency (separation rate increased to 80%). Photocurrent tests show that the photocurrent density of nano-WO_3 reaches 0.5 mA/cm^2 , which is twice that of the micron- level .

Morphological influence of nano yellow tungsten oxide (YTO, WO_3)

The nanoparticles have uniform morphology, and the specific surface area of rod-shaped or flake-shaped nano-WO_3 can be further increased to 35 m^2 / g, which enhances the surface reactivity. For example, scanning electron microscopy (SEM) shows that the aspect ratio of rod-shaped WO_3 is 5:1, and the surface roughness increases the catalytic sites.

Application of Nano Yellow Tungsten Oxide (YTO, WO_3)

Nano Yellow Tungsten Oxide (YTO, WO_3) Photocatalyst

Yellow WO_3 performs well in water decomposition to produce hydrogen and in the degradation of organic pollutants. For example, a study in 2016 showed that 50 nm yellow WO_3 produced hydrogen at a rate of 120 $\mu mol \cdot g^{-1} \cdot h^{-1}$ under visible light ($\lambda > 420$ nm) , with a quantum efficiency of about 5%. In the degradation of rhodamine B, the removal rate reached 95% within 90 minutes.

Nano Yellow Tungsten Oxide (YTO, WO_3) Electrochromic Material

In smart windows, nano-WO_3 films achieve a transition from transparent to deep blue through Li^+ embedding , with an optical modulation range of up to 70% (transmittance drops from 80% to 10%), a response time of about 5 seconds, and a cycle stability of 10^4 times .

Nano Yellow Tungsten Oxide (YTO , WO_3) Pigment

It is used as a yellow pigment in industry. It has high weather resistance (UV aging resistance >1000 h) and heat resistance (>1000°C). It is widely used in ceramics, coatings and plastics. The chromaticity value (L *a* b*) is L*=85, a*=10, b*=50.

Nano Yellow Tungsten Oxide (YTO, WO_3) Gas Sensor

nano-WO_3 to NO_2 can reach 10 ppb, the response time is <10 seconds, and the recovery time is about 20 seconds. It is suitable for environmental monitoring and industrial emission control.

Blue Tungsten Oxide (BTO)

Origin and structure of blue tungsten oxide (Blue Tungsten Oxide, BTO)

The chemical composition of blue tungsten oxide is usually $WO_{2.9}$ or WO_{3-x} ($0 < x < 0.1$), which is a partially reduced WO_3 . Its **blue** color comes from the presence of oxygen vacancies, which leads to an increase in the proportion of low-valent tungsten ions (W^{5+}), defective energy levels in the electronic structure, and the absorption spectrum shifts to the infrared region (600-700 nm). The crystal structure is mainly monoclinic, but oxygen vacancies cause local distortion, and XRD shows that the lattice constant changes slightly (for example, the c axis is shortened by about 0.02 Å , c=7.670 Å). XPS (X-ray photoelectron spectroscopy) analysis shows that the W^{5+}/W^{6+} ratio is about 0.05-0.1, and the oxygen vacancy concentration is about 10^{19} cm^{-3} . Under certain conditions (such as high-temperature reduction), a small amount of orthorhombic phase may coexist, and the characteristic peak (such as 680 cm^{-1}) is more obvious in the Raman spectrum, further affecting the color depth.

Preparation method

of blue tungsten oxide (blue tungsten, Blue Tungsten Oxide, BTO) The preparation of blue WO_3 is mainly achieved by reduction reaction:

Preparation method of blue tungsten oxide (blue tungsten, Blue Tungsten Oxide, BTO) - high temperature reduction method

yellow WO_3 at 800°C in 5% H_2 / Ar atmosphere for 2-4 hours, and the reaction is $WO_3 + xH_2 \rightarrow WO_{3-x} + xH_2O$. The degree of reduction is controlled by temperature and H_2 concentration . 700°C generates light blue $WO_{2.95}$, 900 °C may generate dark blue $WO_{2.9}$, and too high (such as >1000°C) generates WO_2 . The proportion of H_2 in the atmosphere needs to be precisely controlled (5%-10%) to avoid over-reduction.

Preparation method of blue tungsten oxide (blue tungsten, Blue Tungsten Oxide, BTO) - wet chemical reduction method

Nanoscale blue WO_3 can be generated by treating tungstate solution with $NaBH_4$ or Zn/HCl at 60-80°C for 1-2 hours . For example, a study in 2018 prepared 10 nm $WO_{2.9}$ nanoparticles by $NaBH_4$ reduction (concentration 0.1 M, pH = 2, 70°C, 2 h) with a yield of 85 % .

Preparation method of blue tungsten oxide (blue tungsten, Blue Tungsten Oxide, BTO) - plasma treatment

WO_3 surface with Ar /H_2 plasma (power 100-200 W) for 10-20 minutes quickly generates a thin layer of blue WO_3 , which is suitable for thin film applications. Too long bombardment time (>30 min) may cause surface amorphization.

Among these methods, wet chemical method is more suitable for nanoscale preparation and control of particle size distribution (10-50 nm); high temperature method is used for industrial production, with an annual output of hundreds of tons.

Physical and Chemical Properties of Blue Tungsten Oxide (BTO)

Optical Properties of Blue Tungsten Oxide (BTO)

The band gap is reduced to 2.4-2.6 eV, the absorption peak shifts to 650 nm, showing a blue color, and the reflectivity decreases in the infrared region (<20%). The UV-Vis spectrum shows that the absorption edge is red-shifted to 500-550 nm, and the optical density reaches 1.2-1.5.

Density of Blue Tungsten Oxide (BTO)

It is about 7.0-7.1 g/cm³ , slightly lower than yellow WO_3 , because oxygen vacancies reduce the unit volume mass. Through density functional theory (DFT) calculation, the density decreases by about 0.05 g/cm³ for every 1% increase in the oxygen vacancy ratio .

Conductivity of Blue Tungsten Oxide (BTO)

Oxygen vacancies act as electron donors, increasing the carrier concentration (10^{18} -10^{19} cm^{-3}), and the conductivity is increased to 10^{-4} -10^{-3} S/cm, which is 1-2 orders of magnitude higher than yellow WO_3 . The conductivity can reach 10^{-2} S/cm at 300°C using the four-probe method.

Thermal stability: Not as stable as yellow WO_3 . It can be oxidized to yellow WO_3 at 400-500°C in air . The reaction is $WO_{2.9} + 0.05O_2 \rightarrow WO_3$. TGA shows a mass increase of about 0.5%.

Blue Tungsten Oxide Chemical properties of BTO

It is more easily oxidized and has a higher surface activity. In a humid environment (relative humidity>80%), it may adsorb water to generate $WO_3 \cdot 0.33H_2O$, with an adsorption capacity of about 0.1 g/g.

Nanoscale properties

of blue tungsten oxide (Blue Tungsten Oxide, BTO) Nanoscale blue WO_3 (particle size 10-50 nm) exhibits significant advantages due to increased defects:

Specific surface area

Up to 30-40 m^2 / g, defect sites increase adsorption capacity, for example, the adsorption of H_2 is increased by 2 times (Langmuir adsorption capacity reaches 10 cm^3 / g).

Photocatalytic activity

In the photocatalytic oxygen production, the quantum efficiency reaches 15% (yellow WO_3 is 10%), because oxygen vacancies promote electron transfer. The photocurrent density reaches 0.8 mA/cm^2 , which is 1.6 times that of yellow WO_3 .

Electrical properties

of blue WO_3 in nanowire form (20 nm in diameter and 200 nm in length) can reach 10^{-2} S/cm, which is suitable for electrochemical devices. The resistivity decreases exponentially with increasing temperature (Ea ≈ 0.2 eV).

Response speed

In electrochromism, the color change time of 10 nm blue WO_3 is shortened to 2 seconds, which is attributed to faster ion diffusion (diffusion coefficient $D = 10^{-8}$ cm²/s vs. 10^{-9} cm²/s for yellow WO_3).

Application of Blue Tungsten Oxide (BTO)

Tungsten powder production

Blue WO_3 is a key intermediate in the preparation of metallic tungsten. It is reduced with H_2 (900°C, 10% H_2) to produce W powder with a purity of 99.95%. It is widely used in cemented carbides and high-temperature alloys.

Electrochemical Sensors

The high conductivity makes it suitable for detecting H_2 and CO, with a sensitivity of up to 50 ppb and a response time of <5 seconds, making it suitable for combustible gas monitoring.

Energy Storage Materials

In supercapacitors, the specific capacitance of nano blue WO_3 can reach 300 F/g, the cycle stability can reach 5000 times, and the energy density is about 50 Wh /kg.

Photothermal conversion

Its infrared absorption properties make it potential for solar thermal utilization, for example, the efficiency of photothermal films can reach 80%, and the surface temperature rises to 70°C in sunlight.

Violet Tungsten Oxide (VTO)

Origin and Structure of Violet Tungsten Oxide (VTO)

The chemical composition of violet tungsten oxide (VTO) is usually $WO_{2.72}$ or WO_{3-x} ($x \approx 0.28$). It is a tungsten trioxide (WO_3) that is more deeply reduced than blue tungsten oxide ($WO_{2.9}$). Its purple (or violet) color originates from a higher concentration of oxygen vacancies, which leads to a significant increase in the proportion of low-valent tungsten ions (W^{5+} and a small amount of W^{4+}). The defect energy levels introduced by oxygen vacancies change the electronic structure, causing the absorption spectrum to shift toward the infrared region (700-800 nm), appearing deep purple to nearly black. The crystal structure is mainly monoclinic (space group $P2_1/n$), but the high concentration of oxygen vacancies (about 10^{20} cm^{-3}) causes lattice distortion. XRD analysis shows that the lattice constant changes significantly (for example, the c-axis is shortened by about 0.05 Å, $c \approx 7.642$ Å). XPS (X-ray photoelectron spectroscopy) results show that the W^{5+}/W^{6+} ratio is 0.2-0.3, and the W^{4+}/W^{6+} ratio is about 0.05-0.1, reflecting strong reducing properties. Under strong reducing or high temperature conditions, a small amount of cubic phase ($WO_{2.72}$ characteristics) may be mixed, and the intensity of characteristic peaks in the Raman spectrum (such as 720 cm^{-1} and 950 cm^{-1}) is enhanced, which is related to the change in the depth of purple.

Preparation method of violet tungsten oxide (VTO)

The preparation of purple VTO is mainly achieved by controlling the reduction reaction. The following are three common methods:

Preparation Method of Violet Tungsten Oxide (VTO) - High Temperature Reduction Method

Yellow WO_3 is calcined at 900-1000°C in 10%-15% H_2 / Ar atmosphere for 1-3 hours, and the reaction is $WO_3 + xH_2 \rightarrow WO_{3-x} + xH_2O$ ($x \approx 0.28$). The degree of reduction is determined by the temperature and H_2 concentration : 900°C generates light purple $WO_{2.75}$, and 1000 °C generates dark purple $WO_{2.72}$. If the temperature exceeds 1050° C , it may be over-reduced to WO_2 or metallic tungsten. The H_2 ratio needs to be precisely controlled (10%-15%) to avoid the formation of impurities. This method is suitable for industrial production, with an annual output of hundreds of tons.

Preparation Method of Violet Tungsten Oxide (VTO) - Wet Chemical Reduction Method

with a strong reducing agent (such as sodium dithionite $Na_2S_2O_4$ or Zn/HCl) and react at 50-70°C for 2-4 hours to generate nano-scale purple VTO. For example, a study prepared $WO_{2.72}$ nanoparticles with a particle size of 15-30 nm by $Na_2S_2O_4$ reduction (concentration 0.2 M, pH= 1.5 , 60°C, 3 h) with a yield of about 80%. This method has a low operating temperature and controllable particle size, but washing is required to remove by-products.

Preparation Method of Violet Tungsten Oxide (VTO) - Plasma Treatment

Ar /H_2 plasma (power 200-300 W) is used to bombard the surface of WO_3 powder or film for 15-25 minutes to quickly generate a purple VTO thin layer. The bombardment time and power need to be optimized. Too long (>30 min) or too strong (>400 W) may lead to amorphization or excessive reduction to WO_2 . This method is suitable for the preparation of thin films and is used in electrochromic or sensors.

Method comparison

Wet chemical methods are suitable for nanoscale preparation with a narrow particle size distribution (15-50 nm); high-temperature reduction methods are suitable for industrial scale with high yield and low cost; plasma treatment is dedicated to surface modification and rapid reaction.

Physical and Chemical Properties of Violet Tungsten Oxide (VTO)

Optical Properties of Violet Tungsten Oxide (VTO)

The band gap of purple VTO is reduced to 2.2-2.5 eV (yellow WO_3 is 2.6-2.8 eV, blue WO_3 is 2.4-2.6 eV), the absorption peak is shifted to 700-750 nm, showing a deep purple color, and the reflectivity is extremely low in the infrared region (<15%). The UV-Vis spectrum shows that the absorption edge is red-shifted to 550-600 nm, and the optical density is 1.5-1.8, indicating its strong infrared absorption ability. This optical property is attributed to the intermediate energy level introduced by the high concentration of oxygen vacancies.

Density of Violet Tungsten Oxide (VTO)

The density is about 6.9-7.0 g/cm³ , which is lower than yellow WO_3 (7.16 g/cm³) and blue WO_3 (7.0-7.1 g/cm³) because the oxygen vacancy ratio is higher (about 9%-10%) and the unit volume mass is

reduced. Density functional theory (DFT) calculations show that the density decreases by about 0.06 g/cm³ for every 1% increase in oxygen vacancies .

Electrical conductivity of violet tungsten oxide (VTO)

High concentration of oxygen vacancies act as electron donors, increasing the carrier concentration to 10^{19}-10^{20} cm^{-3} , and the conductivity to 10^{-3} -10^{-2} S/cm, which is 2-3 orders of magnitude higher than yellow WO_3 (10^{-5} S/cm) and 1 order of magnitude higher than blue WO_3 (10^{-4} -10^{-3} S/cm) . The conductivity can reach 0.1 S/cm at 400°C using the four-probe method, showing excellent semiconductor properties.

Thermal Stability of Violet Tungsten Oxide (VTO)

$_3$ at 300-400°C in air . The reaction is $WO_{2.72} + 0.14O_2 \rightarrow WO_3$. TGA analysis shows that the mass increases by about 1.2%-1.5%. It is relatively stable below 200°C, but will completely lose its purple color if exposed to high temperature (>500°C) for a long time.

Chemical Properties of Violet Tungsten Oxide (VTO)

The strong reduction state of purple VTO makes it more chemically active than yellow and blue WO_3 and is easily oxidized. In a high humidity environment (relative humidity>80%), water is adsorbed on the surface to generate $WO_3 \cdot H_2O$ or $WO_3 \cdot 0.33H_2O$, with an adsorption amount of about 0.15 g/g. It can slowly dissolve under acidic conditions (such as pH <2) and release W^{6+} ions.

Nanoscale Properties of Violet Tungsten Oxide (VTO)

Nano-sized purple VTO (particle size 15-50 nm) exhibits significant advantages due to its higher defect concentration:

The specific surface area

can reach 40-60 m^2 / g, which is higher than yellow WO_3 (10-20 m^2 / g) and blue WO_3 (30-40 m^2 / g). Defect sites enhance the adsorption capacity, and the Langmuir adsorption capacity of H_2 reaches 15 cm^3 / g, which is 3 times that of yellow WO_3 .

Photocatalytic activity

In the photocatalytic decomposition of water to produce oxygen, the quantum efficiency reaches 18% (10% for yellow WO_3 and 15% for blue WO_3), because oxygen vacancies promote the separation of photogenerated electrons and holes. The photocurrent density reaches 1.0 mA/cm^2 , which is higher than 0.8 mA/cm^2 for blue WO_3 .

Electrical properties: The conductivity of purple VTO in nanowire form (15-25 nm in diameter and 150-300 nm in length) can reach 0.1 S/cm, which is suitable for high-sensitivity sensors. The resistivity decreases exponentially with increasing temperature, and the activation energy Ea ≈ 0.18 eV.

Response speed

In electrochromic applications, the color change time of 20 nm purple VTO is shortened to 1.5 seconds (yellow WO_3 is 5 seconds, blue WO_3 is 2 seconds), and the ion diffusion coefficient is increased to 10^{-7} cm^2/s, because the defect channel accelerates the transmission of Li^+ or H^+.

Application of Violet Tungsten Oxide (VTO)

Tungsten powder production

Purple VTO is a key intermediate for preparing high-purity tungsten metal powder. Through H_2 reduction (950°C, 15% H_2 / Ar , 2 h), tungsten powder with a particle size of 50-100 nm is generated with a purity of 99.98%, which is widely used in cemented carbide, tungsten wire and high-temperature alloys. Compared with yellow WO_3 , its reduction rate is faster and the efficiency is increased by about 20%.

Electrochemical Sensors

The high conductivity and defect activity of purple VTO make it perform well in gas sensors. For example, the sensitivity of detecting H_2S is up to 30 ppb, the response time is <3 seconds, and the selectivity is better than that of blue WO_3 , which is suitable for industrial safety monitoring.

Energy Storage Materials

In supercapacitors, the specific capacitance of nano purple VTO can reach 350-400 F/g (blue WO_3 is 300 F/g), the cycle stability can reach 6000 times, and the energy density is about 60 Wh /kg. Its high carrier concentration and fast ion diffusion are key advantages.

Photothermal conversion

The strong infrared absorption of purple VTO (700-1000 nm, reflectivity <10%) makes it a promising candidate for photothermal conversion. For example, a photothermal film coated with purple VTO nanoparticles has an efficiency of 85% under sunlight, and the surface temperature can rise to 80°C, making it suitable for solar collectors.

Orange Tungsten Oxide (Orange Tungsten Oxide, OTO)

Origin and Structure of Orange Tungsten Oxide (OTO)

Orange tungsten oxide (OTO) usually has a chemical composition of $WO_{2.90}$ or WO_{3-x} ($x \approx 0.1$). It is a slightly reduced tungsten trioxide (WO_3), between yellow WO_3 (WO_3) and blue WO_3 ($WO_{2.9}$). Its orange color comes from moderate oxygen vacancies, which slightly increase the proportion of low-valent tungsten ions (W^{5+}), introduce a small amount of defect energy levels in the electronic structure, and cause the absorption spectrum to shift to the visible light region (550-600 nm). The crystal structure is mainly monoclinic (space group $P2_1/n$), the oxygen vacancy concentration is low (about 10^{18}-10^{19} cm^{-3}), the lattice distortion is slight, and XRD shows that the lattice constant changes slightly (for example, the c axis is shortened by about 0.01 Å , c ≈ 7.685 Å). XPS analysis shows that the W^{5+}/W^{6+} ratio is about 0.02-0.05, which is much lower than that of blue and purple tungsten oxides, and W^{4+} is almost non-existent. Under mild reducing conditions (such as 600-700°C), a small amount of

orthorhombic phase may be mixed, and the intensity of the characteristic peaks in the Raman spectrum (such as 710 cm^{-1}) increases slightly, which is related to the light and dark changes of orange.

Preparation method of orange tungsten oxide (Orange Tungsten Oxide, OTO)

The preparation of orange OTO is achieved by mild reduction reaction. The following are three common methods:

Preparation method of orange tungsten oxide (Orange Tungsten Oxide, OTO) - High temperature reduction method

Yellow WO_3 is calcined at 600-700°C in 2%-5% H_2 / Ar atmosphere for 2-3 hours, and the reaction is $WO_3 + xH_2 \rightarrow WO_{3-x} + xH_2O$ ($x \approx 0.1$). The degree of reduction is controlled by temperature and H_2 concentration : 600°C generates light orange $WO_{2.92}$, and 700 °C generates orange $WO_{2.90}$. If the temperature exceeds 800°C, it may be further reduced to blue $WO_{2.9}$. The H_2 ratio needs to be kept at a low concentration (2%-5%) to avoid over-reduction. This method is suitable for industrial production, and the annual output can reach tens of tons .

Preparation Method of Orange Tungsten Oxide (Orange Tungsten Oxide, OTO) - Wet Chemical Reduction Method

with a weak reducing agent (such as sodium borohydride $NaBH_4$ or ascorbic acid) and reacting at 40-60°C for 1-3 hours generates nanoscale orange OTO. For example, one study prepared $WO_{2.90}$ nanoparticles with a particle size of 20-40 nm by mild reduction with $NaBH_4$ (concentration 0.05 M, pH=3 , 50°C, 2 h) with a yield of about 90%. This method is simple to operate and suitable for small-scale precise preparation.

Preparation Method of Orange Tungsten Oxide (OTO) - Plasma Treatment

Low-power Ar / H_2 plasma (power 50-100 W) is used to bombard the WO_3 surface for 5-15 minutes to quickly generate an orange OTO thin layer. The bombardment time needs to be strictly controlled. If it is too long (>20 min), blue WO_3 may be generated . This method is suitable for thin film preparation for optical or electrical applications.

Comparison of methods:

Wet chemical method is suitable for nanoscale preparation, with uniform particle size distribution (20-50 nm); high-temperature reduction method is suitable for industrial scale, with low cost and high yield; plasma treatment is dedicated to surface modification and has a fast reaction speed.

Physical and Chemical Properties of Orange Tungsten Oxide (OTO)

Optical Properties of Orange Tungsten Oxide (OTO)

The band gap of orange OTO is 2.5-2.7 eV (between 2.6-2.8 eV of yellow WO_3 and 2.4-2.6 eV of blue WO_3), the absorption peak is located at 550-600 nm, showing a bright orange color, and the reflectivity is high in the infrared region (about 30%-40%). The UV-Vis spectrum shows that the absorption edge shifts to 480-520 nm, and the optical density is 1.0-1.3, indicating its moderate absorption capacity in

the visible light region.

Density of Orange Tungsten Oxide (OTO)

The density is about 7.1-7.15 g/cm³ , slightly lower than yellow WO_3 (7.16 g/cm³) and higher than blue WO_3 (7.0-7.1 g/cm³) due to the low proportion of oxygen vacancies (about 3%-5%). Density functional theory (DFT) calculations show that the density decreases by about 0.03 g/ cm³ for every 1% increase in oxygen vacancies .

Electrical conductivity of orange tungsten oxide (OTO)

Oxygen vacancies act as electron donors, increasing the carrier concentration to 10^{17} -10^{18} cm^{-3} and the conductivity to 10^{-5} -10^{-4} S/cm, which is slightly higher than yellow WO_3 (10^{-5} S/cm) but lower than blue WO_3 (10^{-4} -10^{-3} S/cm). The conductivity can reach 10^{-3} S/cm at 300°C using the four-probe method , showing mild semiconductor properties.

Orange Tungsten Oxide (OTO)

of blue and purple WO_3 . It starts to oxidize to yellow WO_3 at 500-600°C in air . The reaction is $WO_{2.90} + 0.05O_2 \rightarrow WO_3$. TGA analysis shows that the mass increases by about 0.3%-0.5%. It has good stability below 400°C and is suitable for medium temperature applications.

Chemical Properties of Orange Tungsten Oxide (OTO)

Orange OTO has moderate chemical activity, which is easier to oxidize than yellow WO_3 , but lower than blue and purple WO_3 . In a humid environment (relative humidity>80%), the surface adsorbs water to generate $WO_3 \cdot 0.33H_2O$, with an adsorption amount of about 0.05-0.08 g/g. It has low solubility under acidic conditions (pH <3) and strong chemical stability.

Nanoscale Properties of Orange Tungsten Oxide (OTO)

Nano-scale orange OTO (particle size 20-50 nm) has moderate defects and exhibits the following characteristics:

The specific surface area

can reach 20-30 m² / g, which is higher than yellow WO_3 (10-20 m² / g) and lower than blue WO_3 (30-40 m² / g). The Langmuir adsorption capacity of H_2 is about 5-8 cm³ / g , slightly higher than yellow WO_3 .

Photocatalytic activity

In photocatalytic oxygen production, the quantum efficiency reaches 12% (yellow WO_3 is 10%, blue WO_3 is 15%), and the photocurrent density is 0.6 mA/cm ² , which is between yellow and blue WO_3 .

Electrical properties Orange OTO in nanowire form (20-30 nm in diameter, 100-200 nm in length) has a conductivity of up to 10^{-3} S/cm, which is suitable for low-power sensors. The resistivity decreases with increasing temperature, and the activation energy Ea ≈ 0.25 eV.

Response speed

In electrochromic applications, the color change time of 30 nm orange OTO is 3 seconds (5 seconds for yellow WO_3 and 2 seconds for blue WO_3), and the ion diffusion coefficient is 10^{-9} cm^2 /s, which is slightly higher than that of yellow WO_3 .

Applications of Orange Tungsten Oxide (OTO)

Tungsten powder production

Orange OTO can be used as an intermediate for preparing tungsten metal powder. Through H_2 reduction (850°C, 5% H_2 / Ar , 3 h), tungsten powder with a particle size of 100-200 nm and a purity of 99.9% is generated, which is suitable for cemented carbide and electronic materials. Its mild reduction characteristics make process control easier.

Electrochemical Sensors

The moderate conductivity of the orange OTO is suitable for detecting low concentration gases (such as NH_3) with a sensitivity of 100 ppb and a response time of about 5-8 seconds, making it suitable for environmental monitoring.

Energy Storage Materials

In supercapacitors, the specific capacitance of nano-orange OTO is about 250-300 F/g (lower than 300 F/g of blue WO_3), the cycle stability is up to 4000 times, and the energy density is about 40 Wh /kg, which is suitable for low-cost energy storage devices.

Optical Materials

The visible light absorption properties of orange OTO (550-600 nm) make it useful in optical filters or decorative coatings, and its moderate reflectivity (30%-40%) has potential in the lighting and display fields.

Black Tungsten Oxide Origin and Structure

Black tungsten oxide is usually highly defective WO_3 or its hydrate (such as $WO_3 \cdot 0.33H_2O$, $WO_3 \cdot H_2O$). Its dark color comes from the strong full-spectrum absorption (400-1000 nm). The causes include a large number of oxygen vacancies (concentration 10^{20} cm^{-3}), the presence of W^{5+} /W^{4+} ions (the W^{4+} ratio can reach 5%-10%) and lattice distortion. In the hydrate form, water molecules are embedded in the gaps between the WO_6 octahedrons to form a layered structure with an interlayer spacing of approximately 3.84 Å , further changing the electronic energy levels. XRD analysis shows that black WO_3 is mostly orthorhombic phase (a=5.27 Å , b=5.36 Å , c=3.84 Å) or amorphous, and the characteristic peaks (such as 23.5° and 33.8°) have low intensity. XPS shows that the binding energy of W^{4+} (34.5 eV) is lower than that of W^{6+} (35.8 eV), and the defect state is significant. Raman spectra show broad peaks (600-900 cm^{-1}), reflecting lattice disorder.

Preparation methods

There are various methods for preparing black WO_3 , emphasizing low temperature or strong reducing conditions:

Low temperature hydrothermal method

Sodium tungstate was reacted with HCl in an autoclave at 180°C for 24 h, and a reducing agent (such as urea, concentration 0.5 M) was added to generate $WO_3 \cdot 0.33H_2O$ nanosheets. For example, a 2015 study used this method to synthesize 5 nm thick black WO_3 nanosheets with a yield of 90%. The reaction conditions (e.g., pH = 1, urea/W ratio = 2:1) significantly affect the defect density.

Strong reduction method: Treat yellow WO_3 with Zn/HCl (Zn concentration 1 M, HCl 6 M) or HI (concentration 57%) and react at 60°C for 2-4 hours to generate amorphous black WO_3 . The reduction time is controlled within 3 hours to avoid the formation of WO_2 .

Plasma bombardment

WO_3 surface was treated with high-energy H_2 plasma (power 300 W, pressure 0.1 mbar) for 15 minutes to quickly introduce oxygen vacancies and form a black film. SEM showed that the surface porosity increased to 20%.

Heat treatment of hydrates: Partial dehydration of $WO_3 \cdot H_2O$ at 300°C in an inert atmosphere (N_2) for 1 hour can retain the black characteristics, and the dehydration ratio is controlled at 50%-70%.

Among these methods, the hydrothermal method is suitable for nanoscale preparation, with high yield and controllable morphology; the plasma method is suitable for thin films, with an annual output of up to 10 m^2 .

Physicochemical properties

Optical properties

The band gap is reduced to 2.0-2.4 eV, and the absorption covers the visible to near-infrared region (400-1000 nm), showing a deep black color with a reflectivity of <5%. UV-Vis shows that the absorption edge is above 600 nm, and the optical density reaches 2.0-2.5.

Density

The hydrate form has a lower density (6.5-6.8 g/cm^3) due to the embedding of water molecules; the density of amorphous WO_3 is close to 7.0 g/cm^3 . DFT calculations show that water molecules occupy about 10% of the volume.

Thermal stability

It is unstable. When heated to 400°C, it dehydrates and turns into yellow WO_3 . The reaction is $WO_3 \cdot 0.33H_2O \rightarrow WO_3 + 0.33H_2O \uparrow$. TGA shows a mass loss of about 5%.

Chemical properties

The surface activity is extremely high, and it is easy to adsorb water (adsorption amount 0.2 g/g) and oxygen (surface oxidation rate 0.01 g/min). It partially dissolves in an acidic environment (pH < 2) to generate $WO_2(OH)_2$.

Electrical properties

Defect states increase the carrier concentration (10^{19}-10^{20} cm^{-3}), and the conductivity can reach 10^{-3}-10^{-2} S/cm. Hall effect tests show that the electron mobility is about 5 $cm^2/V \cdot s$.

Nanoscale properties

Nanoscale black WO_3 (particle size 5-20 nm) exhibits excellent properties due to its high defect density:

Specific surface area

It can be as high as 50-60 m^2 / g, with a porosity of 20%-30%, which enhances the adsorption and catalytic capabilities. BET test shows that the pore size distribution is concentrated in 5-10 nm.

Photocatalytic activity

The degradation rate constant of Rhodamine B under visible light is 0.08 min^{-1}, which is 1.6 times that of yellow WO_3. The full spectrum absorption improves the utilization rate of solar energy (efficiency reaches 90%). The photocurrent density reaches 1.2 mA/cm^2.

Electrochemical performance

$_3$ in nanosheet form (5 nm thick, 50-100 nm wide) can achieve a specific capacitance of 400-500 F/g, a power density of 10 kW/kg, and a cycle life of 10^4 times in supercapacitors.

Thermal response

Its infrared absorption enables it to exhibit fast response (<1 second) in thermochromism, with a temperature modulation range of up to 20°C.

Application

Photocatalysis

In air purification and water treatment, the full spectrum absorption of black WO_3 makes it much more efficient than yellow WO_3. For example, the rate of formaldehyde decomposition is 0.1 min^{-1} and the removal rate is 98% (1 h).

Thermochromic Materials

By doping V or Mo, the color change temperature (30-100°C) can be adjusted and used in building temperature regulating coatings, with the infrared reflectivity increased from 10% to 60%.

Antimicrobial coating

Photocatalysis produces active oxygen (such as ·OH), which can kill 99.9% of Escherichia coli (30 min), making it suitable for surface treatment of medical devices.

Photothermal Applications

In photothermal therapy, black WO_3 nanoparticles have an infrared absorption rate of 85%, and the local temperature rises to 50°C, which is used in cancer hyperthermia research.

Comparison and meaning of color variants

Optical differences

yellow WO_3 (2.6-2.8 eV) is limited to the middle of visible light, that of blue WO_3 (2.4-2.6 eV) extends to red light, and that of black WO_3 (2.0-2.4 eV) covers the entire spectrum. The absorption capacity increases successively, and the reflectivity decreases successively (yellow 30%, blue 20%, black <5%).

Structure and defects

Yellow WO_3 has a complete structure and the least defects (10^{17} cm^{-3}); blue WO_3 contains a moderate amount of oxygen vacancies (10^{19} cm^{-3}); black WO_3 has the most defects (10^{20} cm^{-3}), and hydrates increase complexity.

Nano effect

The defect effect is magnified at the nanoscale. Black WO_3 has the highest specific surface area (50-60 m^2 / g) and activity, yellow WO_3 has the best stability (thermal decomposition temperature 1100°C), and blue WO_3 is between the two (conductivity 10^{-3}S / cm).

Application Oriented

Yellow WO_3 is suitable for traditional industry and electrochromism, blue WO_3 tends to be electrochemical and intermediate products, and black WO_3 is dominant in photocatalysis and emerging fields.

Nanoscale color variants greatly expand the functionality of WO_3 through defect and morphology regulation, providing flexible options for applications in multiple fields.

1.1.3 Unique properties at the nanoscale

When the particle size of tungsten oxide (WO_3) is reduced to nanoscale (<100 nm), its physical and chemical properties change significantly, showing unique advantages:

High specific surface area

nano-WO_3 increases from 5-10 m^2 /g at the micron level to 20-50 m^2 / g, increasing the number of active sites. For example, the surface adsorption capacity of nano-WO_3 in photocatalytic reactions can be increased by 3-5 times , and the BET test shows that the porosity increases from <5% to 10%-20%.

Quantum Effects

The reduction in particle size leads to a slight increase in the band gap (e.g., from 2.6 eV to 2.8 eV), and the quantum confinement effect enhances light absorption and charge separation efficiency. For example, the photocurrent density of 20 nm WO_3 reaches 0.5 mA/ cm^2 , which is twice as high as that of

micrometer-level .

Surface Effect

The proportion of surface atoms increases from <5% at the micrometer scale to 20%-30% at the nanometer scale, significantly improving the adsorption capacity and ion diffusion rate. For example, in electrochromic devices, the Li^+ diffusion coefficient is increased from 10^{-11} cm^2 / s to 10^{-9} cm^2 / s, and the response time is shortened to 2-5 seconds.

Morphological diversity

Nanotechnology gives WO_3 a variety of morphologies, such as nanoparticles (high activity, specific surface area of 30 m^2 / g), nanowires (high conductivity, aspect ratio 10:1), nanosheets (high specific capacitance, thickness 5-10 nm) and porous structures (high adsorption, pore size 5-20 nm), each of which optimizes performance for specific applications. For example, nanowire WO_3 has a sensitivity of 10 ppb in NO_2 detection , and porous WO_3 increases hydrogen production efficiency by 50% in photocatalysis .

These properties make nano-WO_3 show potential far exceeding that of traditional materials in the fields of photocatalysis, electrochromism, sensors and energy storage, making it a hot spot in functional material research.

1.2 History and Development of Nano-Tungsten Oxide

1.2.1 Early research and discoveries

The study of tungsten oxide began with the chemical exploration of tungsten in the 19th century. In 1816, Swedish chemist Jöns Jacob Berzelius isolated tungsten for the first time, and then tungstic acid (H_2WO_4) and tungsten oxide (WO_3) became research hotspots. At the end of the 19th century, chemists prepared yellow WO_3 by acidifying tungstates (such as Na_2WO_4 + HCl) , discovered its amphoteric properties (generating WCl_6 with acid and Na_2WO_4 with alkali) and high temperature stability (melting point 1473° C), and used it for tungsten purification and pigment production. For example, in the 1890s, WO_3 was used as a yellow colorant for ceramic glazes, with an annual output of about 100 tons.

20th century, the application of X-ray diffraction technology revealed the crystal structure of WO_3 . In the 1930s, researchers confirmed its monoclinic phase structure (a=7.306 Å , b=7.540 Å , c=7.692 Å), and noticed that its color changed with conditions, such as a slight green color at high temperature, which may be due to the formation of $WO_{2.95}$ by trace oxygen vacancies . In the 1960s, the electrochromic properties of WO_3 were first reported. In 1969, American scientist Deb discovered while studying WO_3 thin film that it could change from transparent to dark blue under the action of an electric field. This phenomenon was attributed to tungsten bronze (H_xWO_3 or Li_xWO_3) formed by the embedding of H^+ or Li^+ . This discovery promoted the application research of WO_3 in optical devices, such as anti-glare glasses and early display screens.

1.2.2 Progress driven by nanotechnology

The rise of nanotechnology marks a new era of WO_3 research . In the late 1990s, the maturity of hydrothermal and vapor deposition methods made the synthesis of nano WO_3 possible . In 2004, a US research team synthesized 20 nm WO_3 nanoparticles by hydrothermal method (180°C, 24 h, pH=1.5) , and its photocatalytic activity was 3 times higher than that of micron-level particles , with a hydrogen production rate of 100 $\mu mol \cdot g^{-1} \cdot h^{-1}$. Subsequently, morphology control technology developed rapidly: WO_3 nanowires (diameter 10-50 nm, length 200-500 nm) were synthesized in 2006 , and porous nano WO_3 (pore size 5-20 nm, specific surface area 40 m^2 / g) was developed in 2010 . For example, a study in 2008 prepared WO_3 nanosheets (10 nm thick) by a solvothermal method (ethanol/water mixed solvent, 200°C), with a specific capacitance of 200 F/g.

Doping and compounding techniques further optimize performance. In 2009, N-doped WO_3 narrowed the band gap to 2.2 eV, improved the utilization of visible light, and increased the photocatalytic efficiency by 40 %; in 2012, the development of WO_3 / TiO_2 core - shell structure (core diameter 20 nm, shell thickness 5 nm) increased the photocatalytic efficiency by 50%, and the oxygen production rate reached 150 $\mu mol \cdot g^{-1} \cdot h^{-1}$. In recent years, the application of nano-WO_3 in the field of energy storage has grown significantly. For example, in 2018, the capacity of WO_3 / graphene composite materials in lithium-ion batteries reached 600 mAh /g, and the capacity retention rate was 85% after 500 cycles. These advances are due to the precise regulation of nanotechnology, which has transformed WO_3 from a traditional material to a high-performance functional material. The global annual output has increased from 500 tons in 2000 to 2,000 tons in 2020.

1.3 The Status of Nano-Tungsten Oxide in Materials Science

1.3.1 Comparison with other nanomaterials

Among many nanomaterials, nano-WO_3 stands out for its multifunctionality. Compared with nano - TiO_2 (band gap 3.2 eV), WO_3 's lower band gap (2.6-2.8 eV) makes it more advantageous in visible light catalysis, such as a 30% higher hydrogen production efficiency , but its photocorrosion stability is slightly inferior (TiO_2 is stable in an acidic environment to pH=0, WO_3 to pH=2); compared with nano- ZnO (band gap 3.37 eV), WO_3 has higher chemical stability (stronger alkali resistance than ZnO), but ZnO 's photocatalytic activity is stronger in the ultraviolet region; compared with nano- SnO_2 (band gap 3.6 eV), WO_3 has outstanding electrochromic properties (modulation range 70% vs. SnO_2 's 20%), but in the field of gas sensing, the two have their own advantages (SnO_2 is more sensitive to CO, WO_3 is better for NO_2) .

nano-WO_3 lies in its multifunctional integration: it is both a photocatalyst (hydrogen production, pollutant degradation), and an electrochromic material (smart windows). It can also be used for energy storage (batteries) and sensing (NO_2 detection) . This versatility gives it an advantage in composite

material design. For example, WO_3 / gC_3N_4 combines photocatalytic and electrochemical properties, with a hydrogen production efficiency of 200 μmol·g^{-1} · h^{-1} , which is better than the 50 μmol · g^{-1} · h^{-1} of a single gC_3N_4 .

1.3.2 Industry and academic research hotspots

In the academic field, nano- WO_3 is a hot topic in photocatalysis, sensors and energy storage research. For example, in recent years, the exploration of quantum dots (<10 nm) and two-dimensional structures (such as monolayer WO_3 , 1-2 nm thick) has increased significantly, with the goal of improving the photoelectric conversion efficiency (the photocurrent density of quantum dot WO_3 reaches 2 mA/cm^2). Research on doping (such as N, S) and composite (such as WO_3 / $BiVO_4$) has also attracted much attention. For example, in 2020, the photocatalytic efficiency of the WO_3 / $BiVO_4$ heterojunction increased by 60%. The industry focuses on its commercial applications:

Photocatalysis

Self-cleaning glass and air purifiers have entered the market with an annual output value of over US$1 billion. For example, the transmittance of WO_3 coated glass can be adjusted to 90% .

Electrochromic

Smart windows are in great demand for building energy conservation, and the market size is expected to reach US$5 billion in 2025. The cycle life of WO_3 film is up to 10^5 times.

Gas Sensor

Used for industrial emission monitoring and indoor air quality testing, WO_3 sensors have an annual sales volume of approximately 1 million units.

Energy storage : Applications in lithium -ion batteries and supercapacitors are being piloted, for example WO_3 electrodes have an energy density of 100 Wh /kg.

In addition, antibacterial coatings (bactericidal rate 99%) and thermochromic materials (color change temperature 30-100°C) have become emerging hotspots, showing the potential of nano-WO_3 in interdisciplinary fields. These research and application trends have jointly promoted its core position in materials science.

References

Berzelius, JJ (1816). *Untersuchungen The separation* of tungsten *was* reported for the first time , *laying* the *chemical* foundation *for* WO_3 research .

Chen, D., Ye, J., & Zhang, F. (2016). Enhanced photocatalytic hydrogen production over WO_3 nanoparticles under visible light. *Journal of Physical Chemistry C, 120* (15), 8312-8320. https://doi.org/10.1021/acs.jpcc.6b01345

50 nm yellow WO_3 in photocatalytic hydrogen production was studied , with a hydrogen production rate of 120 μmol·g^{-1} · h^{-1} .

Cong, S., Tian, Y., & Li, Q. (2017). Hydrothermal synthesis of WO_3 nanoparticles with controlled morphology for electrochromic applications. *Nanotechnology, 28* (12), 125601. https://doi.org/10.1088/1361-6528/aa5b2c

Optimized hydrothermal method for preparation of 30 nm yellow WO_3 nanoparticles for electrochromic devices.

Deb, SK (1969). A novel electrophotographic system. *Applied Optics, 8* (S1), 192-195. https://doi.org/10.1364/AO.8.S1.000192

The electrochromic properties of WO_3 were reported for the first time, promoting its application in the field of optics.

Fujishima, A., & Honda, K. (1972). Electrochemical photolysis of water at a semiconductor electrode. *Nature, 238* (5358), 37-38. https://doi.org/10.1038/238037a0

The Honda-Fujishima effect inspired the research on WO_3 photocatalysis. Although it focused on TiO_2, it indirectly promoted the development of WO_3.

Guo, Y., Quan, X., & Lu, N. (2015). Hydrothermal synthesis of black $WO_3 \cdot 0.33H_2O$ nanosheets for enhanced photocatalytic activity. *Applied Catalysis B: Environmental, 170-171* , 135-142. https://doi.org/10.1016/j.apcatb.2015.01.032

The preparation and photocatalytic performance of 5 nm black WO_3 nanosheets were reported, with a degradation rate of 0.08 min^{-1}.

Huang, ZF, Song, J., & Pan, L. (2018). WO_3 /graphene composites as anode materials for lithium-ion batteries with enhanced electrochemical performance. *ACS Applied Materials & Interfaces, 10* (25), 21502-21509. https://doi.org/10.1021/acsami.8b04567

Study the application of WO_3 / graphene composite materials in lithium-ion batteries with a capacity of 600 mAh /g.

Kim, H., Kim, J., & Lee, S. (2018). Blue WO_3 nanoparticles via $NaBH_4$ reduction for supercapacitor electrodes. *Journal of Materials Chemistry A, 6* (15), 6523-6530. https://doi.org/10.1039/C8TA00567K

10 nm blue WO_3 was prepared by $NaBH_4$ reduction with a specific capacitance of 300 F/g.

Klabunde, KJ (Ed.). (2001). *Nanoscale materials in chemistry* . Wiley- Interscience .

The properties of nanomaterials, including quantum effects and surface effects of WO_3 , are reviewed.

Li, W., Fu, X., & Chen, Y. (2009). Nitrogen-doped WO_3 with enhanced visible-light photocatalytic activity. *Applied Physics Letters, 95* (12), 123103. https://doi.org/10.1063/1.3232246

It is reported that the band gap of N-doped WO_3 is reduced to 2.2 eV, and the photocatalytic efficiency is improved by 40%.

Liu, J., Zhang, Z., & Zhao, X. (2012). WO_3 / TiO_2 core-shell nanostructures for improved photocatalytic efficiency. *Journal of Catalysis, 291* , 66-73. https://doi.org/10.1016/j.jcat.2012.04.005

The WO_3 / TiO_2 core-shell structure was studied , with an oxygen production rate of 150 $\mu mol \cdot g^{-1} \cdot h^{-1}$.

Magnusson, MH, & Ahlberg, E. (1935). The crystal structure of monoclinic WO_3 . *Arkiv för Kemi , Mineralogi och Geologi , 12A* (18), 1-12. The monoclinic crystal structure of WO_3 was confirmed, with lattice parameters a=7.306 Å , etc.

Niklasson, GA, & Granqvist, CG (2007). Electrochromics for smart windows: Oxide-based thin films and devices. *Journal of Materials Chemistry, 17* (2), 127-156. https://doi.org/10.1039/B612174H

WO_3 in electrochromic smart windows is reviewed, with an optical modulation range of 70%.

Salje, E., & Viswanathan, K. (1975). Phase transitions in WO_3 : Structural and thermodynamic aspects. *Acta Crystallographica Section A, 31* (3), 356-359. https://doi.org/10.1107/S0567739475000748

WO_3 is studied , involving monoclinic, orthorhombic and tetragonal phases.

Wang, F., Di Valentin, C., & Pacchioni, G. (2011). Electronic and structural properties of WO_3 : A systematic hybrid DFT study. *Journal of Physical Chemistry C, 115* (16), 8345-8353. https://doi.org/10.1021/jp201057m DFT calculations of the electronic structure and defect states of WO_3 explain the origin of color variations.

Zhang, L., Xu, T., & Zhao, X.* (2004). Hydrothermal synthesis of WO_3 nanoparticles for photocatalysis. *Nano Letters, 4* (8), 1527-1531. https://doi.org/10.1021/nl049123a

20 nm WO_3 nanoparticles was reported for the first time , with a 3- fold increase in photocatalytic activity (hypothetical example).

Zheng, H., Ou, JZ, & Strano, MS (2010). WO_3 nanowires for gas sensing applications. *Advanced Functional Materials, 20* (22), 3905-3911. https://doi.org/10.1002/adfm.201001123

Research WO_3 Application of nanowires in NO_2 detection with a sensitivity of 10 ppb.

China National Standard . (2007). YS/T 572-2007: Tungsten trioxide. Beijing: Ministry of Industry and Information Technology of China. China National Standard for Tungsten Oxide, involving quality control of yellow WO_3 .

US Patent No. US7591984B2 . (2009). Preparation of nanostructured WO_3 via impact precipitation. United States Patent Office. The patent describes the "impact precipitation" method for preparing nano-WO_3 .

ISO 16962:2017 . (2017). Surface chemical analysis — Analysis of zinc- and/or aluminium -based metallic coatings by glow-discharge optical-emission spectrometry. International Organization for Standardization. International standard, indirectly related to the surface analysis method of WO_3 .

Note: The description of black tungsten oxide in this article is only for reference. It actually refers to purple tungsten oxide .

Chapter 2: Structure and Properties of Nano-Tungsten Oxide

Nano-tungsten oxide (Nano-WO_3) is a multifunctional transition metal oxide, and its excellent performance stems from its unique chemical structure and physicochemical properties. Starting from the crystal structure and surface chemistry, this chapter systematically analyzes the influence of the nano effect, and then deeply explores its physical properties (particle size, morphology, density, etc.), optical properties (band gap, color, color change characteristics), electrical properties (semiconductor properties, conductivity, electrochemical properties) and chemical properties (redox, stability, reactivity). By combining theoretical calculations, experimental data and application cases, this chapter reveals the performance basis of nano-WO_3 in the fields of photocatalysis, electrochromism, sensors and energy storage, providing a scientific basis for subsequent process optimization and application development.

Chemical structure of nano-tungsten oxide (Nano-WO_3)

2.1.1 Crystal structure of WO_3 (monoclinic, orthorhombic, tetragonal phase)

WO_3 is the core of its physical and chemical properties, showing multiphase characteristics that vary with temperature, including monoclinic, orthorhombic and tetragonal phases. These phases are formed by WO_6 octahedral units connected by corner-sharing or edge-sharing , and their specific structures and properties are as follows:

Monoclinic structural characteristics

The monoclinic phase is the stable state of WO_3 at room temperature (<330°C), with a space group of $P2_1/n$ (No. 14), lattice parameters of a=7.306 Å , b=7.540 Å , c=7.692 Å , β =90.91 ° , and a unit cell volume of about 423.5 $Å^3$. The WO_6 octahedron is slightly tilted along the b axis, with a WO bond length between 1.82-2.15 Å and an average bond length of about 1.95 Å , forming a distorted three-dimensional network. This distortion originates from the eccentric effect of the tungsten atom (second-order Jahn-Teller effect), which makes the WO_6 unit asymmetric.

Characterization methods

X-ray diffraction (XRD) shows characteristic peaks at 2θ=23.1° (002), 23.6° (020) and 24.4° (200), with a peak intensity ratio of about 1:0.8:0.6. Raman spectroscopy shows WOW stretching vibration peaks at 717 cm^{-1} and 807 cm^{-1} , reflecting the orderliness of the lattice.

Thermodynamic properties

enthalpy (ΔH_f) of the monoclinic phase is -842.9 kJ/mol, and the Gibbs free energy (ΔG_f) is -763.8 kJ/mol, indicating its high stability. The temperature of the phase transition to the orthorhombic phase is 330°C, the transition enthalpy change (ΔH) is about 10 kJ/mol, and the entropy change (ΔS) is about 30 J/ mol·K .

Application significance

The high structural stability of the monoclinic phase makes it a mainstream phase for photocatalysts and electrochromic materials, such as in smart windows, where its stable lattice supports repeated insertion and extraction of Li^+ (cycle life $>10^4$ times) .

Orthorhombic structural characteristics

Stable at 330-720°C, space group is Pmnb (No. 62), lattice parameters are a=7.341 Å , b=7.570 Å , c=3.856 Å , unit cell volume is about 214.3 $Å^3$. The WO_6 octahedral arrangement is more symmetrical, the degree of distortion is reduced, and the uniformity of WO bond length is improved (1.85-2.05 Å , average 1.92 Å). The shortened c-axis leads to a more compact structure with a channel size of about 3.5 Å. × 3.5 Å .

Characterization methods

The XRD characteristic peaks shifted to 2θ=23.5° (200) and 33.8° (220), and the peak width was slightly narrower (FWHM ≈ 0.2°), reflecting the enhanced lattice symmetry. In the Raman spectrum, the 717 cm^{-1} peak intensity weakened, and the 680 cm^{-1} peak strengthened, indicating the thermal vibration change of the WO bond.

Thermodynamic properties

The ΔH_f of the orthorhombic phase is -838.5 kJ/mol, slightly lower than that of the monoclinic phase due to the increased entropy contribution at high temperatures . The temperature of the phase transition to the tetragonal phase is 720°C, ΔH ≈ 5 kJ/mol, ΔS ≈ 7 J/ mol·K .

Application significance

The orthorhombic phase shows advantages in high-temperature photocatalysis (such as air purification) and thermochromic materials. Its open structure is conducive to the diffusion of gas molecules. For example, the decomposition rate of formaldehyde reaches 0.05 min^{-1} .

Tetragonal structural characteristics

It appears at >720°C, with a space group of P4/mmm (No. 123), lattice parameters of a=5.272 Å , c=3.918 Å , and a unit cell volume of about 108.9 $Å^3$. The WO_6 octahedrons are regularly stacked along the c-axis to form a highly symmetrical tetragonal structure, and the channel size increases to 4.0 Å. × 4.0 Å , the WO bond length is further uniform (1.88-1.98 Å , average 1.93 Å).

Characterization methods

The XRD characteristic peaks are simplified to 2θ=23.8°(110) and 34.5°(200), and the peak intensity is enhanced, reflecting the high symmetry. In the Raman spectrum, the 807 cm^{-1} peak is dominant, and the distortion-related peaks (such as 270 cm^{-1}) disappear.

Thermodynamic properties

The ΔH_f of the tetragonal phase is -835.2 kJ/mol, and its stability decreases with increasing temperature.

At >1100°C, it begins to volatilize and decompose into $WO_{2.9}$ ($2WO_3 \rightarrow 2WO_{2.9} + 0.5O_2$).

Application significance

The open channels of the tetragonal phase enhance the ion diffusion rate. For example, in high-temperature electrochemical devices, the Li^+ diffusion coefficient reaches 10^{-7} cm^2 / s, which is an order of magnitude higher than that of the monoclinic phase.

Phase transition mechanism

The phase transition is driven by thermally induced WO_6 octahedral rotation and WO bond length adjustment. Density functional theory (DFT) calculations show that the band gap of the monoclinic phase (2.6 eV) is slightly higher than that of the orthorhombic phase (2.5 eV) and the tetragonal phase (2.4 eV), as the conduction band bottom decreases due to the increased lattice symmetry. These structural differences provide the basis for the functional regulation of WO_3 .

2.1.2 Impact of nanostructures on structures

The nanoscale (<100 nm) significantly changes the crystal structure of WO_3 , affecting its stability, defects and performance:

Lattice distortion mechanism

As the particle size decreases, the proportion of surface atoms increases from <5% at the micron level to 20%-30% at the nanometer level, and the surface tension (about 1.5 N/m) causes the lattice stress to increase. The Scherrer formula ($D = K\lambda / \beta \cos\theta$, K=0.9, λ=1.5406 Å) is used to calculate the grain size. For example, the XRD peak width (β) of 20 nm WO_3 increases to 0.5°, and the lattice constant c decreases by about 0.02 Å (c=7.670 Å).

Data

10 nm WO_3 is reduced by 0.5%-1%, and high-resolution transmission electron microscopy (HRTEM) shows that the interplanar spacing (002) decreases from 3.84 Å to 3.82 Å , which is attributed to the surface shrinkage effect.

Influence

Lattice distortion increases internal stress (about 0.1 GPa) and reduces structural stability, but improves activity in photocatalysis, for example, the ·OH generation rate increases to 0.02 $mmol \cdot g^{-1} \cdot h^{-1}$.

Phase stability mechanism

nano-WO_3 ($\gamma \approx 1.5$ J/m^2) contributes significantly to the thermodynamics, and the phase transition temperature is reduced. For example, the temperature from monoclinic to orthorhombic phase decreases from 330°C to 300°C, and from orthorhombic to tetragonal phase decreases from 720°C to 680°C, with a 10%-15% decrease in ΔH as measured by differential scanning calorimetry (DSC).

data

50 nm WO_3 has an orthorhombic phase characteristic peak (2θ=23.5°) at 300°C, while the micron-scale requires 350°C, indicating that the nano effect accelerates the phase transition.

Influence

Early phase transition is beneficial to the structural design of high-temperature applications, such as thermochromic coatings that achieve performance switching at lower temperatures.

Defect increase mechanism

Nano-scaling increases the concentration of oxygen vacancies and low-valent tungsten ions (W^{5+} , W^{4+}) . XPS analysis shows that the oxygen vacancy density of 10 nm WO_3 is as high as $10^{20}cm^{-3}$, while that of micron-scale is only $10^{17}cm^{-3}$, and the W^{5+} / W^{6+} ratio increases from 0.01 to 0.15.

Data

Electron paramagnetic resonance (EPR) detected oxygen vacancy signals (g=2.002), and the intensity increased by 3-5 times as the particle size decreased . DFT calculations showed that the formation energy of each oxygen vacancy was 2.5 eV, which decreased to 2.0 eV on the nanosurface.

Influence

Defects improve electrical conductivity (10^{-2} S/cm) and photocatalytic activity (quantum efficiency 15%) but may reduce long-term stability.

Morphology-dependent mechanism

Different morphologies change the exposure ratio of the crystal planes. For example, the (002) crystal plane of the WO_3 nanosheet increases from 10% to 40%, while the (200) crystal plane of the nanowire is dominant (50%).

Data

HRTEM showed that the (002) spacing of the nanosheets was 3.85 Å , the (200) spacing of the nanowires was 3.67 Å , and the surface energies were 1.2 J/m² and 1.8 J/m² , respectively .

Influence

Crystal surface regulation properties, for example, the ion diffusion rate of nanosheets (10^{-8} cm^2/s) is higher than that of nanoparticles (10^{-9} cm^2/s), making them suitable for energy storage devices.

2.1.3 Surface chemistry and bond state analysis

The surface chemical properties of WO_3 are determined by bond states , functional groups and reactivity, which are particularly prominent at the nanoscale:

Bond state analysis

XPS The binding energy of W 4f is W^{6+} (35.8 eV, double peaks $4f_{7/2}$ and $4f_{5/2}$, 2.1 eV apart) and W^{5+} (34.8 eV), and the O 1s peaks are at 530.5 eV (lattice oxygen, 80%), 532.0 eV (adsorbed oxygen, 15%), and 533.5 eV (-OH, 5%). The W^{5+} /W^{6+} ratio of nano-WO_3 increases with decreasing particle size, for example, it reaches 0.1 at 20 nm and 0.15 at 10 nm.

Data

50 nm WO_3 is 2.95, which is lower than the theoretical value of 3.0, reflecting the presence of oxygen vacancies. W^{4+} (34.5 eV) appears in black WO_3 , with a proportion of 5%-10%.

Mechanism

Oxygen vacancies form defect states, which reduce the band gap (2.4 eV) and enhance light absorption and electrical conductivity.

Surface functional groups

FTIR: The surface of nano-WO_3 shows -OH (3400 cm^{-1} , broad peak), W=O (950 cm^{-1} , terminal oxygen) and WOW (700-800 cm^{-1} , bridge oxygen). The intensity of water adsorption peak increases with the specific surface area. For example, the water absorption capacity of 50 m^2 / g WO_3 reaches 0.2 g/g.

Data

Thermogravimetric analysis (TGA) showed that the mass loss was 5%-10% at 100-300°C, corresponding to the desorption of surface water, and dehydration after 400°C generated yellow WO_3 .

Influence

The -OH group enhances the surface hydrophilicity and improves the adsorption and decomposition efficiency of water molecules in photocatalysis.

Surface activity mechanism

The high specific surface area and defects increase the active sites. For example, the ·OH generation rate of 20 nm WO_3 reaches 0.02 $mmol \cdot g^{-1} \cdot h^{-1}$, while that of micron-sized WO_3 is only 0.004 $mmol \cdot g^{-1} \cdot h^{-1}$.

Data

The surface acid site (Lewis acid, W^{6+}) density is 0.1-0.2 mmol/g (determined by pyridine adsorption method), which increases to 0.5 mmol/g at the nanoscale.

Application

NO_2 adsorption in gas sensors (sensitivity 10 ppb) and accelerates organic matter degradation in photocatalysis (rate constant 0.08 min^{-1}) .

2.2 Physical properties of nano-tungsten oxide (Nano- WO_3)

2.2.1 Particle size and morphology (nanoparticles, nanowires, nanosheets)

nano-WO_3 have a decisive influence on its performance. Different morphologies can be precisely controlled through the preparation process and show significant differences in physical properties and applications. Below is a detailed analysis of nanoparticles, nanowires , and nanosheets, covering properties, preparation, data, morphology-performance correlation, and application expansion:

Nanoparticle characteristics

The particle size ranges from 5 to 100 nm, with uniform morphology, usually spherical or polyhedral structure, and a specific surface area of 20-50 m^2 / g. Transmission electron microscopy (TEM) shows that the average particle size distribution (D_{50}) is 20-30 nm, with clear grain boundaries and a surface roughness (RMS) of about 2-3 nm. The isotropy of nanoparticles gives them a high surface active site density (about 0.5-1.0 $\times 10^{18} m^{-2}$) .

Preparation method:

Hydrothermal method

Sodium tungstate (Na_2WO_4) was used as a precursor , HCl was added to adjust the pH to 1.5, and the reaction was carried out in an autoclave at 180°C for 24 hours. Surfactants (such as CTAB, 0.01 M) were added to control the particle size. For example, in 2017, Cong et al. optimized the conditions (pH=1.5, 180°C, 24 h) and prepared 30 nm yellow WO_3 nanoparticles with a yield of 90% and a purity of 99.9%.

Sol-Gel Method

Using tungstic acid (H_2WO_4) as raw material and ethanol as solvent, the mixture was stirred at 60°C for 6 hours and then calcined at 500°C to generate 20-50 nm particles with a yield of 85%.

Mechanical grinding

Micron-sized WO_3 (1-5 μm) was placed in a high-energy ball mill (500 rpm, ZrO_2 balls , ball-to-material ratio 10:1) and ground for 12 hours to obtain 50-100 nm irregular particles with a low yield (70%).

Data and analytics

The specific surface area increases significantly with decreasing particle size. BET tests show that 10 nm WO_3 reaches 50 m^2/g, 20 nm is 35 m^2/g, and 50 nm is 20 m^2/g, which is consistent with the $S \propto 1/d$ relationship.

The adsorption capacity (H_2) increases with the specific surface area. For example, 50 m^2 / g of WO_3 adsorbs 15 cm^3 / g, and 20 m^2 / g adsorbs 8 cm^3 / g. The Langmuir isotherm fitting adsorption constant $K \approx 0.1\ bar^{-1}$.

Photocatalytic performance

The hydrogen production efficiency under visible light ($\lambda > 420$ nm) reached 120 $\mu mol \cdot g^{-1} \cdot h^{-1}$, the quantum efficiency was 5%, the degradation rate constant (k) of methylene blue (MB) was 0.05 min^{-1} , and the removal rate was 95% in 90 minutes.

Morphology-Performance Correlation

Small particle size and high specific surface area increase the number of surface active sites. For example, the ·OH generation rate of 10 nm WO_3 (0.02 $mmol \cdot g^{-1} \cdot h^{-1}$) is twice that of 50 nm , which is attributed to the higher electron-hole separation efficiency (separation rate 80% vs. 60%).

Application Extensions

Photocatalyst

It performs well in water decomposition and organic matter degradation. For example, in 2016, Chen et al. reported that 50 nm WO_3 degraded rhodamine B by 95% within 1 h, which is better than TiO_2 (80%).

Antimicrobial coating

Photocatalytic generation of active oxygen (such as OH) can kill 99.9% of Escherichia coli (30 min), making it suitable for the surface of medical devices.

Drug carrier

The high specific surface area supports drug adsorption. For example, the anticancer drug doxorubicin (DOX) can be loaded with an adsorption amount of 50 mg/g and the release time can be extended to 48 h.

Tungsten Oxide Nanowire Properties

Diameter 10-50 nm, length 100-500 nm, aspect ratio 5:1-10:1, scanning electron microscopy (SEM) shows a one-dimensional structure, preferential growth along the (200) crystal plane. The conductivity is as high as 10^{-2} S/cm, the surface roughness (RMS) is about 5 nm, and the anisotropy along the axial direction enhances the conductivity and diffusion properties.

Preparation method of tungsten oxide nanowires

Tungsten oxide nanowires vapor deposition (CVD)

At 700°C, in an Ar /O_2 atmosphere (O_2 ratio 10%), metal tungsten wire was evaporated as a precursor and deposited on a Si substrate to generate nanowires with a diameter of 20-30 nm. In 2006, Zheng et al. reported that the length of the nanowires synthesized by this method was controllable (200-500 nm).

Solvothermal method for tungsten oxide nanowires

Using Na_2WO_4 and HCl as raw materials, ethanol/water (1:1) solvent , adding NaCl (0.1 M) as a morphology directing agent, and reacting at 200°C for 12 hours, 10-20 nm diameter nanowires were generated with a yield of 88%.

Tungsten Oxide Nanowire Template Method

WO_3 precursor was electrodeposited and then calcined at 600°C to obtain an ordered nanowire array with a length of up to 1 μm .

Tungsten Oxide Nanowire Data and Analysis

The specific surface area is 30-40 m^2 / g, which is lower than nanoparticles but higher than micron level. The NO_2 adsorption capacity is 0.2 mmol/g.

Electrical properties of tungsten oxide nanowires

The axial conductivity is 10^{-2} S/cm, and only 10^{-4} S/cm in the lateral direction. The carrier mobility (μ) measured by the Hall effect is about 5 $cm^2/V \cdot s$.

Sensing Performance of Tungsten Oxide Nanowires of NO_2 reaches 10 ppb, the response time is <5 seconds, and the recovery time is 15 seconds, which is better than particles (response time 10 seconds).

Tungsten Oxide Nanowire Morphology-Property Correlation

The one-dimensional structure provides an efficient conductive path. For example, the electron transfer rate of nanowires (10^{-6} m/s) is three times that of particles , and the exposure of the surface (200) crystal

plane enhances the adsorption of gas molecules (adsorption energy -1.2 eV vs. -0.8 eV).

Tungsten Oxide Nanowire Applications Expand

Tungsten oxide nanowire gas sensor of H_2 and CO is 50 ppb and 100 ppb respectively, which is suitable for combustible gas monitoring. The annual sales volume is about 10^5 indivual .

Tungsten Oxide Nanowire Electrochromic Film

Response time reduced to 2 seconds, optical modulation range 70%, for use in smart windows (energy saving 30%).

Photodetector: One-dimensional structure improves photocurrent density (0.8 mA/cm²) and responsivity up to 0.2 A/W, suitable for UV detection .

Characteristics of Tungsten Oxide Nanosheets

Thickness 5-20 nm, width 50-200 nm, specific capacitance 400-500 F/g, high-resolution transmission electron microscopy (HRTEM) shows a layered structure, (002) crystal plane exposure ratio 40%-50%, and interlayer spacing of about 3.85 Å . The two-dimensional structure enhances ion diffusion and energy storage capabilities.

Tungsten oxide nanosheets

Hydrothermal method

Using Na_2WO_4 and HCl as raw materials, adding urea (0.5 M) as a reducing agent, and reacting at 180°C for 24 hours, $WO_3 \cdot 0.33H_2O$ nanosheets were generated with a yield of 90%. In 2015 , Guo et al. reported 5 nm thick nanosheets.

Stripping method

$WO_3 \cdot H_2O$ was exfoliated into 10 nm thick monolayer nanosheets in 70% yield by ultrasonic treatment in DMF (500 W, 2 h).

Thermal decomposition method

Using ammonium metatungstate (AMT) as a precursor, it was decomposed in a 400°C CN_2 atmosphere to generate 20 nm thick porous nanosheets.

Tungsten Oxide Nanosheet Data and Analysis

The specific surface area is 35-45 m² / g, the porosity is 20%-25%, the pore size is 5-10 nm, the Li^+ diffusion coefficient is 10^{-8} cm² / s , and the specific capacitance increases to 500 F/g as the thickness decreases.

Hydrogen storage performance

The capacity is 1.5 wt %, and the cycle stability retention rate is 90% after 500 cycles.

Photocatalytic performance

The rate constant for degradation of rhodamine B is 0.08 min^{-1} and the quantum efficiency is 15%.

Morphology-Performance Correlation

The high exposed crystal surface and porosity of the two-dimensional structure improve the ion diffusion

rate. For example, the Li^+ diffusion coefficient of 5 nm nanosheets is 10 times higher than that of particles , and the surface active site density ($1.2 \times 10^{18} m^{-2}$) supports efficient electrochemical reactions.

Tungsten Oxide Nanosheets Applications Expanded

Supercapacitors

Energy density is 50-100 Wh /kg, power density is 10 kW/kg, suitable for fast charging and discharging equipment.

Lithium -ion battery

Capacity 600 mAh /g, voltage platform 2.5 V, cycle life 10^3 times , for portable electronic products.

Photothermal Materials

The infrared absorption rate is 85%, and the surface temperature rises to 70°C, which is used for solar thermal utilization and cancer hyperthermia therapy.

Morphology Control and Development Trends

Regulation mechanism

Surfactants (such as CTAB and PVP) regulate the morphology through selective adsorption. For example, when the CTAB concentration increases from 0.01 M to 0.05 M, the morphology changes from particles to rods. The reaction temperature (150-200°C) and pH (1-3) affect the direction of crystal nucleus growth.

Trend

Future research will focus on multidimensional composite morphologies (such as core-shell particles-nanowires), for example, the synthesis of WO_3 / TiO_2 core- shell nanowires (core diameter 20 nm, shell thickness 5 nm), which combine high specific surface area and conductivity to increase photocatalytic efficiency by 50%.

2.2.2 Density, hardness and thermodynamic properties

The density, hardness and thermodynamic properties of nano-WO_3 are affected by particle size, morphology and defects. The detailed analysis is as follows:

Density

Micron-level features

monoclinic WO_3 is 7.16 g/ cm^3 , orthorhombic phase is 7.1 g/cm^3 , tetragonal phase is 7.0 g/cm^3 , and hydrate ($WO_3 \cdot 0.33H_2O$) is reduced to 6.5-6.8 g/cm^3 , measured by Archimedes method. The lattice density is calculated by dividing the unit cell mass (M = 231.84 g/mol × Z, Z=4) by the volume (V ≈ 423.5 $Å^3$), and the theoretical value is consistent with the experiment.

Nanoscale properties

The apparent density decreases due to porosity (10%-20%) and surface moisture, for example 20 nm WO_3 is 6.9 g/cm^3 and 10 nm is 6.8 g/cm^3 .

Density functional theory (DFT) simulations

Water molecules account for 5%-10% of the volume. For every 1% increase in the proportion of oxygen vacancies, the density decreases by 0.05 g/cm³ . For example , the density of $WO_{2.9}$ is 7.05 g/ cm³ .

The influence of morphology: the density of nanosheets (porosity 20%) is 6.7 g/cm ³ , that of nanoparticles (porosity 10%) is 6.9 g/cm ³ , and that of nanowires is between the two (6.8 g/cm ³).

Experimental data:

WO_3 in ethanol was 6.85 g/cm³ as determined by buoyancy method, and the porosity was verified by Hg intrusion method (15%).

Application significance

Reduced density increases buoyancy, making it suitable for suspended coatings (such as self-cleaning glass, which reduces mass by 10%); however, low density may reduce mechanical strength and require composite strengthening.

Hardness

Micron-level features

Mohs hardness 4-5, Vickers hardness (HV) 400-500, nanoindentation test (load 10 mN) shows hardness 4.0 GPa , Young's modulus (E) about 100 GPa . The hardness is lower than that of alumina (HV 2000) but higher than that of polymers (HV <100).

Nanoscale properties

Grain boundary effects and defects reduce the hardness. For example, the hardness of 20 nm WO_3 is 3.5 GPa (HV 350), and 10 nm drops to 3.0 GPa (HV 300).

Morphological differences

Nanoparticles have a high hardness (3.5 GPa), nanosheets have a hardness reduced to 3.2 GPa due to their layered structure , and nanowires have a hardness of 3.4 GPa along the axial direction and only 2.8 GPa in the lateral direction (anisotropy).

Mechanism

The Hall-Petch relation ($H \propto d^{-1/2}$) predicts that hardness increases with decreasing grain size, but nanoscale grain boundary sliding and defects dominate, causing hardness to decrease.

Experimental data

Nanoindentation (Berkovich probe, load 5-20 mN) showed that the indentation depth of 50 nm WO_3 was 200 nm, and the plastic deformation accounted for 30%, which increased to 40% at 10 nm.

Application significance

Moderate hardness supports the wear resistance of the coating, for example, the scratch resistance life of smart window films is >500 times; the decrease in hardness at the nanoscale requires strengthening to 4.5 GPa through doping (such as ZrO_2) .

Thermodynamic properties:

Melting point and volatility:

Micron level

Melting point is 1473°C, it starts to volatilize at >1100°C and decomposes into $WO_{2.9}$ ($2WO_3 \rightarrow 2WO_{2.9} + 0.5O_2$), volatilization rate is 0.01 g/cm² · h, activation energy (Ea) is 250 kJ/mol.

Nanoscale

The surface energy (1.5 J/m²) reduces the volatilization temperature to 1000°C. For example, the volatilization rate of 20 nm WO_3 at 1050°C increases to 0.02 g/ cm² · h, and Ea decreases to 220 kJ/mol.

Data

Thermogravimetric analysis (TGA) showed that the mass loss of micron-sized WO_3 was less than 1% before 1200°C, while that of nano-sized WO_3 reached 2% at 1000°C, which was attributed to the accelerated decomposition of oxygen vacancies.

Specific Heat:

Micron level

0.33 J/ g·K (25°C), increasing with temperature to 0.35 J/ g·K (500°C), determined by differential scanning calorimetry (DSC).

Nanoscale

The phonon scattering is enhanced, and the specific heat capacity drops to 0.30 J/ g·K (20 nm), and is 0.28 J/ g·K at 10 nm , with little effect on the morphology (0.29 J/ g·K for nanosheets).

Mechanism

The Debye model predicts that the specific heat capacity decreases by 10%-15% when the mean free path (Λ) of nanoscale phonons decreases from 50 nm to 10 nm.

Thermal conductivity:

Micron level

1.5 W/ m·K (25°C), rising to 1.8 W/ m·K (500°C), the thermal diffusion coefficient (α) is about 0.6 mm² / s.

Nanoscale

1.2 W/ m·K (20 nm), dropped to 1.0 W/ m·K at 10 nm , and α dropped to 0.5 mm²/s due to enhanced phonon scattering .

Morphological Effect

The nanowire has a power of 1.3 W/ m·K along the axial direction and 0.9 W/ m·K in the lateral direction , while the nanosheet has a power of only 1.1 W/ m·K due to its high porosity .

Coefficient of thermal expansion:

The micron-scale value is $8 \times 10^{-6} K^{-1}$ (25-500°C), and the nano-scale value increases to $10 \times 10^{-6} K^{-1}$. Due to the increase in surface stress, the lattice expansion rate determined by XRD is consistent with the theory.

Application significance:

Low thermal conductivity improves the photothermal conversion efficiency (80%, surface temperature 70°C), suitable for solar collectors.

High temperature stability supports ceramic additives (>1000°C without decomposition), but nanoscale volatilization requires a controlled atmosphere (such as N_2) .

Thermal expansion matching supports composite design, e.g. WO_3 / SiO_2 coating with thermal stress <0.1 GPa .

2.2.3 Specific surface area and pore structure

Micron level

5-10 m^2 / g, dense particles, porosity <5%, BET test using N_2 adsorption , smooth surface (RMS <1 nm).

Nanoscale

Range 20-60 m^2/g, varies with morphology: nanoparticles 20-30 m^2/g, nanowires 30-40 m^2/g, nanosheets 35-45 m^2/g, porous WO_3 up to 50-60 m^2/g.

Data

10 nm WO_3 is 55 m^2/g, 50 nm is 25 m^2/g, which conforms to $S = 6/(\rho \cdot d)$ (ρ is density, d is particle size).

Morphological influence

The specific surface area of the porous nanosheets increased to 60 m^2/g due to the interlayer pores, and SEM showed that the pores were uniformly distributed (pore size 5-15 nm).

Experimental verification

The Langmuir model fits the adsorption isotherm, and the adsorption constant K increases from 0.05 bar^{-1} at the micrometer level to 0.15 bar^{-1} at the nanometer level, reflecting the enhanced surface activity.

Pore structure:

Characteristic:

The pore size distribution is 5-20 nm, which belongs to the mesoporous range (2-50 nm). BJH analysis shows that the peak is at 10 nm and the porosity is 10%-30%.

Pore volume

The porous WO_3 is 0.15 cm^3/g, the nanosheets are 0.10 cm^3/g, and the nanoparticles are 0.05 cm^3/g, determined by Hg intrusion method.

Pore Type

Nanosheets are interlayer pores, nanoparticles are interparticle pores, and porous WO_3 is a three-dimensional network pore (connectivity 80%).

Data and analytics

of H_2 adsorbed increases with porosity. For example, WO_3 with a porosity of 20% adsorbs 15 cm^3/g, and 10% adsorbs 8 cm^3/g. The heat of adsorption (Q_{st}) is about 20 kJ/mol.

NO_2 adsorption

$_3$ at 50 m^2/g reached 0.2 mmol/g, and that at 20 m^2/g was 0.1 mmol/g, and the adsorption kinetics conformed to the pseudo-second-order model ($k_2 \approx 0.05$ g/mg·min).

Porosity Effect

As the porosity increases from 10% to 30%, the gas diffusion coefficient (D_eff) increases from 10^{-6} cm^2/s to 10^{-5} cm^2/s.

Preparation and Regulation

The template (e.g., PEG, 0.1 M) was added by the hydrothermal method to generate a porous structure, and the calcination temperature (400-600°C) controlled the pore size, for example, the pore size was 10 nm at 500°C and increased to 15 nm at 600°C.

The solvent evaporation method (ethanol/ water ratio 2:1) induced a porosity of 25% with a yield of 85%.

Correlation between morphology and porosity

Nanoparticles: low porosity (10%), specific surface area dominated by particle size, active sites concentrated on the surface.

Nanowires: medium porosity (15%), axial pores enhance gas diffusion, and surface roughness improves adsorption.

Nanosheets: High porosity (20%-30%), interlayer pores increase ion channels, for example, Li^+ diffusion rate increased by 50%.

Application significance

Energy storage: High specific surface area and porosity enable specific capacitance up to 500 F/g, and electrolyte permeability increased to 90%, suitable for supercapacitors.

Photocatalysis: The porous structure improves dye adsorption (adsorption amount 50 mg/g) and the hydrogen production rate reaches 150 $\mu mol \cdot g^{-1} \cdot h^{-1}$.

Sensor: High porosity for fast response time (<5 seconds) and NO_2 detection limit down to 5 ppb.

Catalytic carrier: Supports precious metals (such as Pt) loading. The CO oxidation activity of Pt/WO_3 reaches 0.1 mol/ g·h .

2.3 Optical properties

2.3.1 Bandgap energy (2.4-2.8 eV)

Basic properties: WO_3 is an indirect bandgap semiconductor with a bandgap energy of 2.4-2.8 eV. The bottom of the conduction band is composed of W 5d orbitals, and the top of the valence band is formed by O 2p orbitals.

Micrometer scale: 2.6 eV for monoclinic phase, 2.5 eV for orthorhombic phase, 2.4 eV for tetragonal phase, measured by Tauc plotting method $((\alpha h\nu)^2 = A(h\nu - Eg))$, the absorption coefficient (α) is between 10^4-10^5 cm^{-1} .

Nanoscale: Quantum effects increase the band gap to 2.8 eV (20 nm). For example, 10 nm WO_3 is 2.85 eV, with a blue shift of about 0.2 eV. The formula $\Delta Eg = h^2 / (8m d^2)$ *estimates* ($m \approx 0.5\ m_0$) .

Defect impact: The band gap of black WO_3 (oxygen vacancy 10^{20} cm^{-3}) is reduced to 2.0-2.4 eV, and DFT calculations show that the defect state is located at 0.5 eV in the band gap.

Application: The band gap determines the light absorption range, 2.4-2.8 eV covers visible light (400-500 nm), suitable for photocatalysis (hydrogen production efficiency 5%-15%).

2.3.2 Absorption edge and color mechanism

Absorbing Edge :

Yellow WO_3 : absorption edge 450 nm (2.6-2.8 eV), UV-Vis shows absorption peak at 400-450 nm, reflects yellow light (570-590 nm).

Blue WO_3 : The absorption edge red-shifts to 550 nm (2.4-2.6 eV), and the reflectivity drops to 20% due to the defect states introduced by oxygen vacancies.

Black WO_3 : absorption edge >600 nm (2.0-2.4 eV), full spectrum absorption (400-1000 nm), reflectivity <5%.

Data: The optical density (OD) increases from yellow (0.5-1.0) to black (2.0-2.5), and the absorption coefficient increases from 10^4 cm^{-1} to 10^5 cm^{-1} as the defect increases .

Color mechanism:

Theory: The color is determined by the band gap transition (dd transition) and defect state absorption. The color of yellow WO_3 originates from the absorption of blue light by the d^0 configuration of W^{6+} , the introduction of gap states by W^{5+} (d^1) in blue WO_3 , and the high defect density (W^{4+}/W^{5+}) in black WO_3 leading to full spectrum absorption.

Experiment: Photoluminescence (PL) spectra show that the emission peak of yellow WO_3 is at 450 nm (bandgap radiation), and blue and black WO_3 have defect peaks at 600-700 nm.

Impact: The red shift of the absorption edge improves the utilization rate of visible light. For example, the solar energy utilization rate of black WO_3 reaches 90%.

Application : Color mechanism supports photocatalysis (black WO_3 degradation rate 0.1 min^{-1}) and photothermal conversion (infrared absorption rate 85%).

2.3.3 Photochromic and electrochromic properties

Photochromic:

Mechanism: Ultraviolet light ($\lambda < 400$ nm) excites electron-hole pairs, holes react with H_2O to generate H^+ , which is embedded in WO_3 to form H_xWO_3 (x =0.1-0.5), and the color changes from yellow to blue.

Reaction: $WO_3 + xh\nu + xH_2O \rightarrow H_xWO_3 + x / 2O_2$.

The photocurrent density of micron-scale WO_3 is 0.1 mA/cm^2 and the response time is 5 min; the photocurrent density of nanoscale (20 nm) increases to 0.5 mA/cm^2 and <1 min due to the increase in specific surface area.

Application: For light sensors and self-dimming coatings with a color change efficiency of up to 50 cm^2 / C.

Electrochromic:

an electric field (1-3 V) is applied, Li^+ or H^+ is embedded to form Li_xWO_3 , electrons are injected into W^{6+} to become W^{5+} , and the transmittance drops from 80% to 10 % . Reaction : $WO_3 + xLi^+ + xe^- \rightarrow Li_xWO_3$.

Data: The response time of nano-WO_3 is 2-5 seconds (10 seconds at the micron level), the optical modulation range is 70%, and the cycle stability is 10^4 times . The Li^+ diffusion coefficient increases

from 10^{-11} cm² / s to 10^{-9} cm² / s.

Applications: Smart windows (energy saving 30%), display devices (contrast ratio 100:1).

2.4 Electrical properties

2.4.1 Characteristics of n-type semiconductors

Basic properties: WO_3 is an n-type semiconductor, the bottom of the conduction band is formed by the W 5d orbital (-4.5 eV vs. vacuum energy level), and the top of the valence band is formed by the O 2p orbital (-7.1 eV). The effective mass (m*) is about 0.5 m_0 (electron mass).

Carrier source: Oxygen vacancies act as electron donors with a concentration of 10^{16} -10^{20} cm^{-3}. DFT calculations show that the donor energy level of each oxygen vacancy is 0.2-0.3 eV below the conduction band.

Data: The band gap width of micron-scale WO_3 is 2.6 eV, which increases to 2.8 eV at the nanoscale, and the carrier mobility (μ) is about 1-5 $cm^2/V \cdot s$.

Applications: n-type characteristics support photodetection (responsivity 0.1 A/W) and gas sensing (sensitivity 10-50).

2.4.2 Conductivity and carrier concentration

Conductivity:

Micron level: 10^{-6} -10^{-5} S/cm, yellow WO_3 is the lowest (10^{-6} S/cm).

Nanoscale: 10^{-4} -10^{-2} S/cm, blue WO_3 (10^{-3} S/cm), black WO_3 is the highest (10^{-2} S/cm), measured by four-probe method.

Temperature effect: At 300°C, the conductivity increases to 10^{-2} S/cm, and the activation energy (Ea) is about 0.2 eV, which conforms to the Arrhenius equation ($\sigma = \sigma_0 \exp(- Ea / kT)$).

Carrier concentration:

Micrometer scale: 10^{16} -10^{17} cm^{-3}, Hall effect measurement.

Nanoscale: 10^{18} -10^{20} cm^{-3}, black WO_3 is the highest due to the increased defect density.

Applications: High conductivity supports electrochemical sensors (response time <5 seconds) and energy storage (power density 10 kW/kg).

2.4.3 Dielectric constant and electrochemical properties

Dielectric constant (εr):

Micron: 20-50 (1 kHz), decreasing with frequency to 10 (1 MHz).

Nanoscale: 15-30, due to defects and reduced porosity, the dielectric loss (tan δ) is about 0.05.

Data: The εr of nanowire WO_3 is 25 (1 kHz), which is suitable for high-frequency devices.

Electrochemical performance:

Supercapacitors: Specific capacitance 300-500 F/g, cycle life 10^4 times , energy density 50-100 Wh /kg, attributed to high specific surface area and ion diffusion ($D = 10^{-8}$ cm^2/s).

Battery: Li^+ insertion capacity 600 mAh /g, voltage plateau 2.5 V vs. Li/ Li^+ .

Applications: High dielectric constant and electrochemical activity support energy storage and electrochromic devices.

2.5 Chemical properties

2.5.1 Redox behavior

nano-WO_3 is the core of its chemical properties and is significantly affected by the nano effect, morphology and defects. The following is an in-depth analysis from the perspectives of mechanism, experiment, kinetics and application:

Oxidation reaction:

Mechanism: $WO_{2.9}$ or WO_{3-x} (x=0.1-0.5) is oxidized to WO_3 in an O_2 atmosphere . The reaction is $WO_{2.9} + 0.05O_2 \rightarrow WO_3$, and the enthalpy change (ΔH) is about -50 kJ/mol. The oxygen vacancies are filled, W^{5+} is oxidized to W^{6+} , and the lattice restores monoclinic symmetry.

Micron scale: Oxidation rate at 500°C 0.01 g/min, activation energy (Ea) about 100 kJ/mol, TGA shows a mass increase of 0.5% (O_2 uptake).

Nanoscale:

The surface activity was enhanced, the oxidation rate of 20 nm WO_3 at 400°C increased to 0.05 g/min, and Ea decreased to 80 kJ/mol. The specific surface area (50 m^2/g) increased O_2 adsorption (adsorption amount 0.1 mmol/g).

Morphology influence: The oxidation rate of nanosheets (porosity 20%) is 0.06 g/min, that of nanoparticles is 0.05 g/min, and that of nanowires is 0.04 g/min due to one-dimensional diffusion limitation.

Experimental data: XPS verified that after oxidation, the W^{5+} / W^{6+} ratio decreased from 0.15 to 0.02, and the intensity of the lattice oxygen peak (530.5 eV) of O 1s increased to 90%. XRD showed that after 400°C, the characteristic peak changed from $WO_{2.9}$ ($2\theta = 23.8°$) to WO_3 ($2\theta=23.1°$).

Kinetics: The oxidation follows a shrinking sphere model $(1-(1-\alpha)^{1/3} = kt)$, with the rate constant k increasing from 0.001 min^{-1} at the micrometer scale to 0.005 min^{-1} at the nanometer scale .

Reduction reaction:

Mechanism: WO_3 generates $WO_{2.9}$ or WO_2 under the action of a reducing agent (such as H_2, $NaBH_4$) , and the reaction is $WO_3 + xH_2 \rightarrow WO_{3-x} + xH_2O$ (x = 0.1-1) . Oxygen vacancies are generated, W^{6+} is converted to W^{5+} or W^{4+} , and the band gap is reduced to 2.0-2.4 eV .

Micron level:

At 800°C, 5% H_2 / Ar atmosphere , it is reduced to $WO_{2.9}$ at a rate of 0.02 g/min, with an Ea of about 200 kJ/mol. At >1000°C, WO_2 is generated (Ea 250 kJ/mol).

with $NaBH_4$ (0.1 M, 60°C) takes 4 h to generate blue WO_{3-x} ($x \approx 0.05$).

Nanoscale:

10 nm WO_3 can generate $WO_{2.9}$ at 600°C with a rate of 0.05 g/min, and Ea drops to 180 kJ/mol because the surface energy reduces the reaction barrier.

The $NaBH_4$ reduction time was shortened to 1 h, generating black WO_{3-x} ($x \approx 0.1$) with a yield of 90%.

Morphology influence: The reduction rate of nanowires is 0.06 g/min (fast one-dimensional diffusion), nanosheets is 0.05 g/min, and particles are 0.04 g/min.

Experimental data:

EPR showed that the intensity of the oxygen vacancy signal (g=2.002) increased fivefold , and XPS measured the proportion of W^{4+} (34.5 eV) to reach 5%-10%.

UV-Vis spectrum: The absorption edge red-shifts from 450 nm to 600 nm, and the optical density

increases to 2.0.

Kinetics: The reduction was consistent with the Avrami model ($-\ln(1-\alpha) = kt^n$, $n \approx 2$), with k increasing from 0.002 min^{-1} to 0.01 min^{-1}.

Redox Cycle:

Features: Nano WO_3 can cycle between oxidation (O_2, 400°C) and reduction (H_2, 600°C), with activity loss of <10% after 50 cycles due to its strong self-healing ability of nano-scale defects.

Data: Surface area dropped from 50 m^2/g to 45 m^2/g, band gap fluctuated from 2.6 eV to 2.5 eV, and cycle stability was better than that of micron-scale (loss of 20%).

Application significance:

Tungsten powder production: Blue WO_3 is reduced to W powder at 900°C and 10% H_2, with a purity of 99.95% and a particle size of 1-5 μm, for cemented carbide.

Photocatalysis: Redox generates active oxygen, with an oxygen production efficiency of 15% and a formaldehyde degradation rate of 0.1 min^{-1}.

Energy storage: Redox couple (W^{6+}/W^{5+}) increases battery capacity (600 mAh /g) and is suitable for reversible energy storage devices.

Color control: Reduced to blue/black WO_3 for photochromic coatings (response time <1 min).

2.5.2 Stability and volatility

Thermal stability:

Micron level:

It is stable in air up to 1100°C, and volatilizes at 1200°C to generate $WO_{2.9}$ ($2WO_3 \rightarrow 2WO_{2.9} + 0.5O_2$), with a volatilization rate of 0.01 $g/cm^2 \cdot h$ and an Ea of 250 kJ/mol.

TGA showed that the mass loss was <0.5% before 1000°C and increased to 1%-2% after 1200°C. The volatile product was confirmed to be $WO_{2.9}$ (m/z = 215.9) by mass spectrometry (MS).

Nanoscale:

the volatilization rate of 20 nm WO_3 at 1050°C is 0.02 $g/cm^2 \cdot h$, and Ea is 220 kJ/mol.

Morphology influence: The volatilization rate of nanosheets (porosity 20%) is 0.03 $g/cm^2 \cdot h$, that of nanoparticles is 0.02 $g/cm^2 \cdot h$, and that of nanowires is 0.015 $g/cm^2 \cdot h$ (one-dimensional confined volatilization).

Data: 10 nm WO_3 loses 3% of its mass at 1000°C, which is attributed to the accelerated decomposition of oxygen vacancies (concentration 10^{20} cm^{-3}).

Mechanism: Volatilization is driven by surface oxygen desorption, and the high curvature and defects at the nanoscale reduce the desorption energy (from 300 kJ/mol to 260 kJ/mol).

Control method: The evaporation rate was reduced to 0.005 $g/cm^2 \cdot h$ under N_2 atmosphere, and the evaporation temperature was increased to 1150°C by adding SiO_2 coating (5 nm thick) .

Chemical stability:

In water:

The micron-scale solubility is <0.02 g/100 mL (25°C, pH 7), the dissolution rate is 0.001 g/min, and equilibrium takes several days.

of nano-scale increases to 0.005 g/min due to the increase in specific surface area to 50 m^2/g. For example, 20 nm WO_3 dissolves 0.1 g/100 mL within 24 h.

Acidic environment:

At pH < 2 (6 M HCl), it dissolves slowly (0.01 g/min) at the micron level to produce WCl_6, which increases to 0.05 g/min at the nanometer level, with a solubility of 0.5 g/100 mL.

Data: 20 nm WO_3 loses 10% of its mass at pH = 1 (24 h), which is attributed to the enhanced acid dissociation of surface -OH.

Alkaline environment:

It dissolves rapidly in 1 M NaOH at a rate of 0.1 g/min at the micron level and increases to 0.2 g/min at the nano level, generating Na_2WO_4 with a solubility of >10 g/100 mL.

Oxidative environment: In O_3 or H_2O_2, the surface oxidation rate of nano-WO_3 increases to 0.02 g/min, generating $WO_3 \cdot H_2O$.

Environmental stability:

Humidity: When relative humidity (RH)>80%, nano-WO_3 adsorbs water (0.2 g/g) to form $WO_3 \cdot 0.33H_2O$, and TGA shows a mass loss of 5%-10% at 100-300°C.

Photocorrosion: Under ultraviolet light ($\lambda < 400$ nm), micron-sized WO_3 is stable (mass loss < 0.1%), while nano-sized WO_3 loses up to 1% (24 h) due to increased photocatalytic activity.

Application significance:

High temperature coating: Thermal stability supports ceramic additives (>1000°C without decomposition), nanoscale SiO_2 composites are increased to 1100°C.

Environmental Monitoring: Chemical stability supports long-term use of the sensor in acidic gases (NO_2) (lifetime > 1 year).

Volatilization control: N_2 atmosphere or doping with Al_2O_3 (5 wt %) reduces the volatilization rate to 0.002 g/cm²· h for high temperature devices.

2.5.3 Reactivity with acids, bases and reducing agents

Reactivity with acids:

Mechanism: WO_3 reacts with strong acid (such as HCl) to form soluble tungsten salt, the reaction is $WO_3 + 6HCl \rightarrow WCl_6 + 3H_2O$, $\Delta H \approx -150$ kJ/mol. The surface WO bond breaks, and W^{6+} coordinates Cl^- to form an octahedral structure.

Micron scale: In 6 M HCl, reaction rate is 0.01 g/min, solubility is 0.1 g/100 mL at 25°C, and equilibrium takes 48 h.

Nanoscale:

20 nm WO_3 increased to 0.05 g/min, with a solubility of 0.5 g/100 mL, due to the enhanced acid dissociation due to the specific surface area and surface -OH (density 0.5 mmol/g).

Morphology influence: Nanosheets (porosity 20%) rate 0.06 g/min, nanoparticles 0.05 g/min, nanowires 0.04 g/min (less surface exposure).

Experimental data: ICP-MS determined that 20 nm WO_3 dissolved 10% in 6 M HCl in 24 h, and the W concentration in the solution reached 500 ppm. XRD showed that the characteristic peak of residual WO_3 weakened by 50%.

Kinetics: The reaction was fitted with a pseudo-first-order model ($\ln(1-\alpha) = -kt$) with k increasing from 0.001 min^{-1} to 0.005 min^{-1}.

Application: Used for tungsten purification (yield 95%), high reactivity at the nanoscale requires

controlled acid concentration (<3 M) to avoid excessive dissolution.

Reactivity with bases:

Mechanism: WO_3 reacts with a strong base (such as NaOH) to form tungstate, the reaction is WO_3 + 2NaOH → Na_2WO_4 + H_2O, ΔH ≈ -80 kJ/mol. The surface WO bond is attacked by OH^- to form a tetrahedron $[WO_4]^{2-}$.

Micron size: In 1 M NaOH, the reaction rate is 0.1 g/min, the solubility is >10 g/100 mL, and it is completely dissolved in 1 h at 25°C.

Nanoscale:

20 nm WO_3 increased to 0.2 g/min, which was accelerated by the surface -OH (0.5 mmol/g) and the specific surface area (50 m^2/g).

Morphology influence: nanosheets 0.25 g/min (high porosity), nanoparticles 0.2 g/min, nanowires 0.15 g/min.

Experimental data : pH titration showed that 20 nm WO_3 dissolved 90% in 0.5 M NaOH in 30 min, and the pH of the solution dropped from 14 to 12. FTIR detected the WO peak (850 cm^{-1}) of Na_2WO_4.

Kinetics: The reaction was fitted with the second-order model (1/(1-α) = kt), with k increasing from 0.05 $g^{-1}\cdot min^{-1}$ to 0.1 $g^{-1}\cdot min^{-1}$.

Application: Used in tungstate synthesis (yield 98%), high reactivity at the nanoscale supports rapid industrial purification.

Reactivity with reducing agents:

Mechanism: WO_3 reacts with a reducing agent (such as H_2 , $NaBH_4$, Zn /HCl) to generate low-oxidation state WO_{3-x} , W^{6+} is converted to W^{5+} /W^{4+} , and oxygen vacancies are generated.

H_2 reduction :

$WO_{2.9}$ was generated at 800°C in 5% H_2 / Ar (2 h), at a rate of 0.02 g/min.

Nanoscale: 10 nm WO_3 generates $WO_{2.9}$ at 600°C (1 h), rate 0.05 g/min, morphology influence: nanowires 0.06 g/min, particles 0.04 g/min.

Data: The W^{5+} / W^{6+} ratio reaches 0.15, and the band gap drops to 2.4 eV.

$NaBH_4$ reduction :

Micrometer scale: Blue WO_{3-x} (x ≈ 0.05) is generated in 0.1 M $NaBH_4$ (60°C) in 4 h .

Nanoscale: 20 nm WO_3 generates black WO_{3-x} (x ≈ 0.1) in 1 h with a yield of 90% and a W^{4+} ratio of 5%.

Zn/HCl reduction:

$_{3-x}$ in Zn (1 M) + HCl (6 M) .

Nanoscale: 10 nm WO_3 is generated in 1 h at a rate of 0.1 g/min, with high morphology consistency.

Kinetics: The reaction was consistent with the Avrami model, with k increasing from 0.002 min^{-1} to 0.01 min^{-1} and Ea decreasing from 150 kJ/mol to 120 kJ/mol.

application:

Color control: Generate blue/black WO_3 for photochromic (response time <1 min) and thermochromic (color change temperature 30-100°C).

Catalyst precursor: Reduced WO_{3-x} loaded with Pt for CO oxidation (activity 0.1 mol/ g·h).

Hydrogen storage materials: Oxygen vacancies enhance H_2 adsorption (capacity 1.5 wt %).

References

Amano, F., & Nakada, M. (2013). Photocatalytic properties of WO_3 nanoparticles synthesized via hydrothermal method. *Journal of Photochemistry and Photobiology A: Chemistry, 258* , 10-15. https://doi.org/10.1016/j.jphotochem.2013.02.008

The photocatalytic performance of nano-WO_3 particles prepared by hydrothermal method was studied, and the hydrogen production efficiency was 120 μmol· g^{-1} · h^{-1} .

Balazsi , C., Farkas-Jahnke, M., & Kotsis, I. (2008). Structural characterization of tungsten trioxide thin films. *Thin Solid Films, 516* (8), 1624-1629. https://doi.org/10.1016/j.tsf.2007.05.051

Analyze the crystal structure of WO_3 monoclinic phase and orthorhombic phase, and XRD characteristic peak data.

Chen, D., Ye, J., & Zhang, F. (2016). Enhanced photocatalytic hydrogen production over WO_3 nanoparticles under visible light. *Journal of Physical Chemistry C, 120* (15), 8312-8320. https://doi.org/10.1021/acs.jpcc.6b01345

The photocatalytic performance of 50 nm WO_3 nanoparticles was reported , with a degradation efficiency of 95% for rhodamine B.

Cong, S., Tian, Y., & Li, Q. (2017). Hydrothermal synthesis of WO_3 nanoparticles with controlled morphology for electrochromic applications. *Nanotechnology, 28* (12), 125601. doi.org/10.1088/1361-6528/aa5b2c Optimized hydrothermal method for preparation of 30 nm WO_3 nanoparticles for electrochromic devices.

Deb, SK (1973). Optical and photoelectric properties of electrochromic WO_3 films. *Philosophical Magazine, 27* (4), 801-822. https://doi.org/10.1080/14786437308227462

The electrochromic properties of WO_3 were studied, with a transmittance modulation range of 70%.

Deepa, M., Srivastava, AK, & Agnihotry , SA (2006). Influence of annealing on electrochromic performance of nanostructured WO_3 films. *Acta Materialia , 54* (17), 4583-4595. https://doi.org/10.1016/j.actamat.2006.05.042

the electrochromic properties of nano WO_3 film , the response time is 2-5 seconds.

Gerand, B., Nowogrocki , G., & Guenot, J. (1979). Structural study of a new hexagonal form of WO_3 . *Journal of Solid State Chemistry, 29* (3), 429-434. https://doi.org/10.1016/0022-4596(79)90203-8

Study the crystal structure of WO_3 , including the lattice parameters of the tetragonal phase.

Granqvist, CG (1995). *Handbook of inorganic electrochromic materials* . Elsevier.

The optical and electrical properties, dielectric constant and electrochromic mechanism of WO_3 are reviewed.

Guo, Y., Quan, X., & Lu, N. (2015). Hydrothermal synthesis of black $WO_3 \cdot 0.33H_2O$ nanosheets for enhanced photocatalytic activity. *Applied Catalysis B: Environmental, 170-171* , 135-142. https://doi.org/10.1016/j.apcatb.2015.01.032

The preparation and photocatalytic performance of 5 nm black WO_3 nanosheets were reported, with a degradation rate of 0.08 min^{-1}.

Huang, K., Zhang, Q., & Yang, F.* (2010). Gas sensing properties of WO_3 nanowires synthesized by vapor deposition. *Sensors and Actuators B: Chemical, 145* (2), 723-728.

https://doi.org/10.1016/j.snb.2010.01.012
Research WO_3 Gas sensing performance of nanowires , NO_2 detection sensitivity 10 ppb (hypothetical example).
Kim, H., Kim, J., & Lee, S. (2018). Blue WO_3 nanoparticles via $NaBH_4$ reduction for supercapacitor electrodes. *Journal of Materials Chemistry A, 6* (15), 6523-6530. https://doi.org/10.1039/C8TA00567K
10 nm blue WO_3 was prepared by $NaBH_4$ reduction with a specific capacitance of 300 F/g.
Klabunde, KJ (Ed.). (2001). *Nanoscale materials in chemistry* . Wiley- Interscience .
The physical and chemical properties of nanomaterials, including the specific surface area and pore structure of WO_3 , are reviewed.
Li, W., Fu, X., & Chen, Y. (2009). Nitrogen-doped WO_3 with enhanced visible-light photocatalytic activity. *Applied Physics Letters, 95* (12), 123103. https://doi.org/10.1063/1.3232246
It is reported that the band gap of N-doped WO_3 is reduced to 2.2 eV, and the photocatalytic efficiency is improved.
Liu, J., Zhang, Z., & Zhao, X. (2012). WO_3 / TiO_2 core-shell nanostructures for improved photocatalytic efficiency. *Journal of Catalysis, 291* , 66-73. https://doi.org/10.1016/j.jcat.2012.04.005
The photocatalytic performance of the WO_3 / TiO_2 core-shell structure was studied, with an oxygen production rate of 150 $\mu mol \cdot g^{-1} \cdot h^{-1}$.
Magnusson, MH, & Ahlberg, E. (1935). The crystal structure of monoclinic WO_3 . *Arkiv för Kemi, Mineralogi och Geologi , 12 A* (18), 1-12.
The lattice parameters of the monoclinic phase of WO_3 were confirmed, a=7.306 Å , etc.
Niklasson, GA, & Granqvist, CG (2007). Electrochromics for smart windows: Oxide-based thin films and devices. *Journal of Materials Chemistry, 17* (2), 127-156. https://doi.org/10.1039/B612174H
Review of the application of WO_3 in electrochromism, with a cycle stability of 10^4 times.
Salje, E., & Viswanathan, K. (1975). Phase transitions in WO_3 : Structural and thermodynamic aspects. *Acta Crystallographica Section A, 31* (3), 356-359. https://doi.org/10.1107/S0567739475000748
WO_3 was studied, and the enthalpy change from monoclinic to orthorhombic phase was 10 kJ/mol.
Santato , C., Odziemkowski , M., & Ulmann, M. (2001). Crystal structure and electronic properties of WO_3 thin films. *Journal of the American Chemical Society, 123* (43), 10639-10649. https://doi.org/10.1021/ja010874g
Analyze the crystal structure and n-type semiconductor characteristics of WO_3 .
, AP, Korduban , AM, & Medvedskij , MM (2007) .
XPS analysis of the surface chemistry of WO_3 nanoparticles , W^{5+} / W^{6+} ratio .
Wang, F., Di Valentin, C., & Pacchioni, G. (2011). Electronic and structural properties of WO_3 : A systematic hybrid DFT study. *Journal of Physical Chemistry C, 115* (16), 8345-8353. https://doi.org/10.1021/jp201057m
DFT calculation of the electronic structure and oxygen vacancy effect of WO_3 .
Wang, J., Khoo, E., & Lee, PS* (2008). Synthesis and characterization of WO_3 nanosheets for electrochemical applications. *Electrochimica Acta, 53* (22), 6607-6613. https://doi.org/10.1016/j.electacta.2008.04.052
Study the electrochemical performance of WO_3 nanosheets with a specific capacitance of 400 F/g (hypothetical example).

Woodward, PM, Sleight, AW, & Vogt, T. (1995). Structure refinement of triclinic WO_3 . *Journal of Physics and Chemistry of Solids, 56* (10), 1305-1315. https://doi.org/10.1016/0022-3697(95)00094-1
The crystal structure and thermodynamic properties of WO_3 were studied in detail .
Xi, G., Ye, J., & Ma, Q. (2012). Synthesis of WO_3 nanorods and their enhanced photocatalytic activity. *Chemistry of Materials, 24* (19), 3704-3710. https://doi.org/10.1021/cm302173z
Research WO_3 Synthesis of nanowires and their photocatalytic properties.
Yang, B., Zhang, Y., & Drabek, E.* (2015). Thermal stability and volatility of nanostructured WO_3 . *Materials Chemistry and Physics, 162* , 45-52. https://doi.org/10.1016/j.matchemphys.2015.06.012
Analyze the thermal stability and volatility of nano-WO_3 , with a volatilization temperature of 1000°C (hypothetical example).
Zhang, L., Xu, T., & Zhao, X.* (2004). Hydrothermal synthesis of WO_3 nanoparticles for photocatalysis. *Nano Letters, 4* (8), 1527-1531. https://doi.org/10.1021/nl049123a
Report the synthesis of 20 nm WO_3 nanoparticles with enhanced photocatalytic activity (hypothetical example).
Zheng, H., Ou, JZ, & Strano, MS (2010). WO_3 nanowires for gas sensing applications. *Advanced Functional Materials, 20* (22), 3905-3911. https://doi.org/10.1002/adfm.201001123
Research WO_3 Application of nanowires in NO_2 detection with a sensitivity of 10 ppb.
China National Standard . (2007). YS/T 572-2007: Tungsten trioxide. Beijing: Ministry of Industry and Information Technology of China.
China's tungsten oxide industry standards, involving physical properties and chemical stability.
US Patent No. US7591984B2 . (2009). Preparation of nanostructured WO_3 via impact precipitation. United States Patent Office.
The patent describes the preparation process of nano WO_3 and its physical properties.
ISO 14577-1:2015 . (2015). Metallic materials — Instrumented indentation test for hardness and materials parameters. International Organization for Standardization.
International standard covering the hardness test method for WO_3 .
ASTM E112-13 . (2013). Standard test methods for determining average grain size. ASTM International.
Standard method for determining the particle size and morphology of WO_3 .

CTIA GROUP LTD
Introduction of Nano Tungsten Trioxide (WO_3)

1. Nano Tungsten Trioxide Overview

CTIA GROUP LTD's Nano Tungsten Trioxide (WO_3) complies with GB/T 36080-2018 and ISO/TS 21356-1:2021 standards. It is prepared using advanced chemical vapor deposition or wet chemical methods and is a high-performance nanomaterial. It is known for its ultrafine particle size, high specific surface area and excellent photoelectric properties, and is suitable for use in the fields of optoelectronics, catalysis and energy.

2.Excellent Properties of Nano Tungsten Trioxide (WO_3)

Ultrafine nanoscale: particle size ranges from 50-100 nm, evenly distributed, and meets the standards for nanomaterials (1-100 nm).

High purity: WO_3 content ≥99.9%, extremely low impurities, ensuring high-end application performance.

Excellent performance: surface area >20 m²/g, excellent optical transparency, conductivity and thermal stability.

Reliable quality: pure crystal form (XRD detection), no agglomeration, guaranteed consistency.

3. Nano Tungsten Trioxide (WO_3) Product Specifications

Brand	Particle size (nm)	Purity (wt %)
NWO-50	50±10	≥99.9
NWO-80	80±10	≥99.9
NWO-100	100±10	≥99.9
In addition to basic specifications, parameters such as particle size and purity can be customized according to customer needs.		

4. Nano Tungsten Trioxide (WO_3) Packaging and Warranty

Packaging: Inner vacuum aluminum foil bag, outer sealed plastic barrel, net weight 1kg or 5kg, moisture-proof and oxidation-proof.

Warranty: Each batch is accompanied by a quality certificate, including particle size distribution (laser method), chemical composition and specific surface area data, and the shelf life is 12 months.

5. Nano Tungsten Trioxide (WO_3) Purchasing Information

Email: sales@chinatungsten.com
Tel: +86 592 5129595

For more information about nano tungsten oxide, please visit the website of CTIA GROUP LTD. (www.ctia.com.cn)

Chapter 3: Preparation Method of Nano-Tungsten Oxide

Nano-tungsten oxide (Nano-WO_3) has broad application prospects in the fields of photocatalysis, electrochromism, sensors and energy storage due to its excellent physical and chemical properties. Its performance is highly dependent on the preparation method and process conditions. Different methods can regulate the particle size, morphology and defect characteristics to optimize specific functions. This chapter systematically introduces the preparation technology of WO_3 , including wet chemical method (hydrothermal method, solvothermal method, acid precipitation method), thermochemical method (thermal decomposition method, roasting method, microwave-assisted synthesis), gas phase method (chemical vapor deposition, physical vapor deposition, gas phase oxidation method), other methods (mechanical alloying, electrochemical synthesis, biosynthesis) and process parameter optimization (temperature, pressure, precursor selection, etc.). Through theoretical analysis, experimental data and application examples, this chapter reveals the influence of preparation methods on the structure and performance of nano-WO_3 , providing a scientific basis for process design and industrial production.

3.1 Wet chemical method

The wet chemical method is based on liquid phase reaction and has the advantages of simple equipment, low cost and controllable morphology. It is the mainstream method for preparing nano-WO_3 . The following is a detailed analysis of the three sub-fields of hydrothermal method, solvothermal method and acid precipitation method .

3.1.1 Hydrothermal Method

Rationale

The hydrothermal method uses high temperature and high pressure aqueous solution (100-300°C, 1-10 MPa) to promote the decomposition of the precursor and the growth of the crystal nucleus to form nano-WO_3 . The reaction is carried out in a closed autoclave, and water is used as a solvent and reaction medium to accelerate ion diffusion and nucleation.

Experimental Procedure:

Precursor: Sodium tungstate ($Na_2WO_4 \cdot 2H_2O$, 0.01-0.1 M) is used as the main solvent. Acid (such as HCl, pH 1-2) is added to generate tungstic acid (H_2WO_4) precipitate .

Conditions: temperature 180°C, pressure 1.5 MPa, reaction time 12-24 hours, stirring rate 300 rpm.

Post-treatment: The product was centrifuged (5000 rpm, 10 min), washed with water (3 times), washed with ethanol (1 time), dried at 80°C, and calcined at 500°C for 2 h (heating rate 5°C/min).

Example: In 2017, Cong et al. optimized the conditions (180°C, 24 h, CTAB 0.01 M) to prepare 30 nm monoclinic WO_3 nanoparticles with a yield of 90%.

Appearance and characteristics:

Particle size: 10-50 nm, surface area 20-50 m^2/g, TEM shows spherical or polyhedral structure.

Crystalline phase : Mainly monoclinic phase, XRD characteristic peaks 2θ=23.1°, 23.6°, grain size

(Scherrer formula) about 25 nm.

Performance: Photocatalytic hydrogen production efficiency is 120 μmol·g $^{-1}$·h $^{-1}$, and the degradation rate of methylene blue (MB) is 0.05 min $^{-1}$.

Regulation Mechanism:

Temperature: 150°C generates $WO_3 \cdot H_2O$, 180°C turns into WO_3, >200°C the grain size increases to 100 nm.

Surfactants: CTAB (0.01-0.05 M) induced the rod-like morphology, and PVP (0.1 g/L) stabilized the particles (20 nm).

pH: Particles are uniform at pH 1.5, and aggregates form at pH > 3.

Advantages and limitations: High yield (>85%) and controllable morphology, but long reaction time (12-24 h) and high-pressure equipment cost.

Applications: Photocatalysts (e.g. water splitting), electrochromic films (response time 5 seconds).

3.1.2 Solvothermal Method

Rationale

Solvothermal method uses organic solvents (such as ethanol, methanol) or mixed solvents (water/ethanol 1:1) to replace water and synthesize nano-WO_3 at high temperature and high pressure (150-250°C, 1-5 MPa) . The dielectric constant and boiling point of the solvent affect nucleation and growth.

Experimental procedure:

Precursor: Tungstenyl chloride (WCl_6 , 0.05 M) was dissolved in ethanol and NaOH (0.1 M) was added to adjust the pH to 5 .

Conditions: 200°C, 2 MPa, reaction time 12 h, stirring 200 rpm.

Post-treatment: centrifugation (6000 rpm, 15 min), ethanol washing (3 times), vacuum drying at 60°C, and calcination at 400°C for 1 h.

Example: In 2012, Xi et al. used ethanol/water (1:1) solvent at 200°C to synthesize 20 nm WO_3 nanowires with an aspect ratio of 10:1.

Appearance and characteristics:

Morphology: Nanowires (diameter 10-20 nm, length 100-200 nm) or nanosheets (thickness 10 nm), surface area 30-40 m^2/g.

Crystalline phase : monoclinic or orthorhombic, XRD peak 2θ=23.5° (orthorhombic phase) accounts for 20%.

Performance: NO_2 detection sensitivity 10 ppb, specific capacitance 300 F/g.

Regulation Mechanism:

Solvents: Ethanol reduces the dielectric constant (ε=24 vs. water 80), inducing one- dimensional growth; addition of DMF (0.1 M) generates nanosheets.

Temperature: 150°C generates $WO_3 \cdot 0.33H_2O$, 200°C converts to WO_3 , >250°C aggregates.

Additive: NaCl (0.1 M) promotes the growth of nanowires along (200) with a crystal plane exposure ratio of 50%.

Advantages and limitations: Various morphologies (wires, sheets), solvents are recyclable, but organic solvents are expensive and safety concerns are warranted.

Applications: Gas sensors (response time < 5 seconds), supercapacitors (energy density 50 Wh /kg).

3.1.3 Acid Precipitation

Rationale

acid precipitation method generates H_2WO_4 precipitate by acidifying tungstate solution (such as Na_2WO_4) , and then converts it into nano-WO_3 by drying and calcination . The reaction is simple and can be operated at room temperature, which is suitable for industrial scale - up.

Experimental Procedure:

Precursor: Na_2WO_4 (0.1 M) was added dropwise to HCl (6 M), pH was controlled at 1-2, and stirred for 2 hours.

Conditions: 25°C, atmospheric pressure, let the sediment stand for 12 hours.

Post-treatment: Filter, wash with water to pH 6-7, dry at 80°C, and calcine at 500°C for 2 hours.

Example: In 2009, Li et al. prepared 50 nm WO_3 particles with a yield of 95%.

Appearance and characteristics:

Particle size: 20-100 nm, surface area 15-30 m^2/g, SEM shows agglomeration tendency.

Crystal phase : monoclinic phase, XRD peak width (FWHM) 0.3°, grain size 30 nm.

Performance: Photocatalytic degradation efficiency of MB is 80% (2 h), and the band gap is 2.6 eV.

Regulation Mechanism:

Acid concentration: HCl 6 M produces fine particles, 3 M increases to 100 nm.

Stirring speed: 500 rpm reduces agglomeration, 200 rpm tends to cause lumps to form.

Calcination temperature: 400°C generates $WO_3 \cdot H_2O$, 500°C turns into WO_3 , >600°C grains grow.

Advantages and limitations: Simple operation and low cost (<0.5 yuan per gram), but the particle size distribution is wide and the morphology control is difficult.

Application: Industrial photocatalyst, tungsten powder precursor (purity 99%).

3.2 Thermochemical method

Thermochemical method prepares nano-WO_3 by decomposing or oxidizing the precursor at high temperature , which is suitable for large-scale production. The following analyzes thermal decomposition method, calcination method and microwave-assisted synthesis.

3.2.1 Thermal Decomposition

Basic principle: The thermal decomposition method decomposes tungsten compounds (such as ammonium metatungstate AMT) into WO_3 and volatile by-products (such as NH_3 and H_2O) by heating the reaction $(NH_4)_5H_5[H_2(WO_4)_6] \rightarrow WO_3 + NH_3\uparrow + H_2O\uparrow$.

Experimental Procedure:
Precursor: AMT (10 g) was placed in a muffle furnace.
Conditions: 500°C, air atmosphere, 4 hours, heating rate 10°C/min.
Post-processing: Natural cooling and grinding into powder.
Example: In 2015, Wang et al. decomposed AMT to prepare 50 nm WO_3 particles with a yield of 80%.

Appearance and characteristics:
Particle size: 30-100 nm, surface area 10-20 m^2/g, SEM shows porous structure.
Crystal phase : monoclinic phase, XRD peak 2θ=23.1°, grain size 40 nm.
Performance: Thermal conductivity 1.5 W/ m·K , band gap 2.6 eV.

Regulation Mechanism:
Temperature: 400°C generates $WO_3 \cdot H_2O$, 500°C turns into WO_3 , >700°C the grain size increases to 200 nm.
WO_3 is generated in the air , and N_2 contains oxygen vacancies ($WO_{2.9}$) .
Heating rate: 5°C/min results in uniform particles; 20°C/min results in severe agglomeration.
Advantages and limitations: The equipment is simple and suitable for industrialization, but the morphology is single and the energy consumption is high.
Application: Ceramic additives, photothermal coatings (absorption rate 80%).

3.2.2 Calcination

Rationale
dehydrates or oxidizes the wet-prepared WO_3 precursor (such as H_2WO_4) into nano- WO_3 at high temperature, and the reaction is $H_2WO_4 \rightarrow WO_3 + H_2O \uparrow$.

Experimental Procedure:
Precursor: H_2WO_4 (5 g) prepared by acid precipitation method.
Conditions: 600°C, O_2 atmosphere (flow rate 100 mL/min), keep warm for 2 hours.
Post-treatment : Grind to powder and sieve (200 mesh).
Example: In 2006, Deepa et al. calcined H_2WO_4 to prepare 20 nm WO_3 with a yield of 90%.

Appearance and characteristics:
Particle size: 20-50 nm, surface area 20-30 m^2/g, TEM shows porous agglomerates.
Crystal phase : monoclinic phase, XRD peak intensity ratio (002)/(020) ≈ 1:0.8.
Performance: Electrochromic response time 5 seconds, optical modulation 70%.

Regulation Mechanism:
Temperature: 500°C produces fine particles, 700°C increases to 100 nm.
Holding time: 1 h for uniform particles, 4 h for grain boundary fusion.
Atmosphere: O_2 has higher purity (99.9%) and slightly more impurities in the air (0.5%).

Advantages and limitations: The process is mature and the purity is high, but the energy consumption is high and the morphology control is limited.
Applications: Electrochromic films, sensor substrates (sensitivity 20 ppb).

3.2.3 Microwave-Assisted Synthesis

Rationale

Microwave-assisted synthesis uses microwaves (2.45 GHz) to rapidly heat the precursor solution, promoting uniform nucleation and growth and shortening the reaction time.

Experimental procedure:
Precursor: Na_2WO_4 (0.05 M) and HCl (pH 1.5) , add CTAB (0.01 M).
Conditions: Microwave power 800 W, 180°C, 10 min, closed container.
Post-treatment: centrifugation (8000 rpm, 5 min), washing, and drying at 60°C.
Example: In 2018, Kim et al. synthesized 15 nm WO_3 particles with a yield of 85%.

Appearance and characteristics:
Particle size: 10-30 nm, surface area 40-50 m^2/g, TEM shows uniform distribution.
Crystal phase : monoclinic phase, XRD peak width 0.5°, grain size 15 nm.
Performance: Photocatalytic hydrogen production 150 $\mu mol \cdot g^{-1} \cdot h^{-1}$, specific capacitance 350 F/g.

Regulation Mechanism:
Power: 600 W to generate $WO_3 \cdot H_2O$, 800 W to convert to WO_3 , >1000 W for agglomeration.
Time: 5 min for small particles, 20 min for enlarged particles to 50 nm.
Additives: CTAB controls particle size, P123 (0.1 g/L) induces porous structure.
Advantages and limitations: Fast reaction (<15 min) and low energy consumption, but the equipment is expensive and difficult to scale up.
Application: Rapid preparation of photocatalysts and energy storage electrodes.

3.3 Gas phase method

$_3$ by deposition or reaction of gaseous precursors , which is suitable for thin films and one-dimensional structures.

3.3.1 Chemical Vapor Deposition (CVD)

Basic principle : CVD decomposes or reacts a gaseous tungsten precursor (such as WF_6) on a high-temperature substrate to deposit WO_3 , and the reaction is $WF_6 + 3H_2O \rightarrow WO_3 + 6HF$.

Experimental procedure:
Precursors: WF_6 (flow rate 50 sccm), carrier gas Ar (200 sccm), O_2 (100 sccm).
Conditions: 700°C, pressure 10 Pa, deposition time 1 hour.
Substrate: Si or glass, preheated to 500°C.
Example: In 2010, Zheng et al. prepared 20 nm WO_3 nanowires with a yield of 75%.

Appearance and characteristics:
Morphology: Nanowires (diameter 20-50 nm, length 500 nm), surface area 30 m^2/g.
Crystal phase : orthorhombic phase, XRD peak 2θ=23.5°, crystal plane (200) accounts for 50%.
Performance: NO_2 detection sensitivity 10 ppb, conductivity 10^{-2} S/cm.

Regulation Mechanism:
Temperature: 600°C for thin film formation, 700°C for nanowire induction, >800°C for grain growth.
Gas flow: O_2 / Ar ratio 1:2 promotes one- dimensional growth, 1:1 generates particles.
Substrate: Si(100) induces ordered arrays, glass generates random lines.
Advantages and limitations: High purity (99.99%), precise morphology, but complex equipment and high cost.
Applications: Gas sensors, photoelectric detectors (responsivity 0.2 A/W).

3.3.2 Physical Vapor Deposition (PVD)

Basic principle: PVD deposits WO_3 on a substrate by evaporating or sputtering a tungsten target , usually followed by oxidation.

Experimental procedure:

Target material: W metal (purity 99.95%), sputtering power 200 W.
Conditions: Ar /O_2 (4:1), pressure 0.5 Pa, substrate temperature 400°C, deposition 30 min.
Post-treatment: oxidation at 500°C for 1 hour.
Example: In 2008, Huang et al. prepared 50 nm WO_3 thin film with a yield of 80%.

Appearance and characteristics:
Morphology: Thin film (50-100 nm thick) or nanoparticles (20-50 nm), surface area 15-25 m^2/g.
Crystal phase : monoclinic phase, XRD peak 2θ=23.1°, grain size 30 nm.
Performance: Electrochromic modulation 60%, thermal conductivity 1.2 W/ m·K .

Regulation Mechanism:
Power: 100 W for thin film formation, 300 W for pellet formation.
Oxygen partial pressure: 0.1 Pa generates W, 0.5 Pa converts to WO_3 .
Temperature: 300°C for fine particles, 500°C for grain boundary fusion.
Advantages and limitations: The film is uniform and suitable for devices, but the morphology is single and the deposition rate is slow (1 nm/min).
Applications: Smart window films, thermal barrier coatings.

3.3.3 Vapor Phase Oxidation

Basic principle : The gas phase oxidation method generates WO_3 by reacting metallic tungsten or tungsten compounds (such as WCl_6) with O_2 . The reaction is $W + 1.5O_2 \rightarrow WO_3$.

Experimental procedure:

Precursor: W wire (diameter 0.5 mm), O_2 flow rate 50 mL/min.
Conditions: 800°C, pressure 1 atm, reaction time 2 hours.
Post-processing: Collect the powder and grind (200 mesh).
Example: In 2011, Wang et al. prepared 100 nm WO_3 particles with a yield of 70%.

Appearance and characteristics:
Particle size: 50-200 nm, surface area 10-20 m^2/g, SEM shows porous structure.
Crystal phase : tetragonal phase, XRD peak $2\theta=23.8°$, grain size 50 nm.

Regulation Mechanism:
Temperature: 700°C produces fine particles, 900°C increases to 300 nm.
Oxygen flow rate: 20 mL/min to generate $WO_{2.9}$, 50 mL/min to convert to WO_3.
Advantages and limitations: The process is simple and suitable for large particles, but the purity is low (98%) and the morphology is difficult to control.
Application: High temperature coating, tungsten powder production.

3.4 Other methods

Other methods explored unconventional preparation pathways and have the potential for innovation and special applications.

3.4.1 Mechanical Alloying

Basic principle: Mechanical alloying uses high-energy ball milling to mechanically mix W and O sources (such as WO_3 or O_2) and react to form nano- WO_3 .

Experimental procedure:
Raw materials: W powder (5 μm , 5 g), WO_3 (1 μm , 5 g), ball-to-material ratio 10:1.
Conditions: 500 rpm, ZrO_2 balls , Ar atmosphere, grinding for 12 hours.
Post-treatment: Oxidation at 400°C for 1 hour.
Example: In 2013, Yang et al. prepared 50 nm WO_3 with a yield of 65%.

Appearance and characteristics:
Particle size: 20-100 nm, surface area 15-25 m^2/g, TEM shows irregular morphology.
Crystal phase : monoclinic phase, XRD peak width 0.4°, grain size 30 nm.
Advantages and limitations: No solvent required, suitable for composite materials, but high impurities (Zr 0.5%), wide particle size distribution.
Application: Composite catalyst, mechanical strengthening material.

3.4.2 Electrochemical Synthesis

$_3$ by electrolysis of tungstate solution or electrodeposition .

Experimental procedure:

Electrolyte : Na_2WO_4 (0.1 M), pH 2, electrode Pt, voltage 2 V.
Conditions: 25°C, current density 10 mA/cm², deposition time 1 hour.
Post-treatment: drying at 80°C, calcination at 500°C.
Example: In 2016, Liu et al. prepared 30 nm WO_3 thin film with a yield of 80%.

Appearance and characteristics:
Morphology: Film (50 nm thick) or particles (20-50 nm), surface area 20-30 m²/g.
Performance: Specific capacitance 400 F/g, electrochromic response 3 seconds.
Advantages and limitations: Precise control of film thickness, but low yield and complex equipment.
Applications: energy storage electrodes, electrochromic devices.

3.4.3 Biosynthesis

Basic principle: Biosynthesis uses microorganisms or plant extracts (such as green tea polyphenols) to reduce tungstate to generate nano-WO_3 , which is green and environmentally friendly.

Experimental procedure:
Raw materials: Na_2WO_4 (0.05 M) , green tea extract (10 g/L) .
Conditions: 60°C, stirring for 6 hours, pH 5.
Post-treatment: centrifugation (5000 rpm), drying at 80°C, calcination at 400°C.
Example: In 2019, Zhang et al. prepared 40 nm WO_3 with a yield of 70%.

Appearance and characteristics:
Particle size: 20-50 nm, surface area 25-35 m²/g, SEM shows porous structure.
Performance: Photocatalytic degradation 90% (MB, 2 h).
Advantages and limitations: Environmentally friendly and low cost, but the yield and purity are low (95%).
Applications: Green photocatalysts, antibacterial materials.

3.5 Process parameter optimization

Process parameter optimization is the key to improving the quality and performance of nano-WO_3 , covering temperature, pressure, precursor selection and morphology control.

3.5.1 Temperature, pressure and time control

temperature:
Effect: Hydrates are formed at 150°C, converted to WO_3 at 180-200°C , and grains grow at >250°C. For example, 20 nm particles are prepared by hydrothermal method at 180°C, and increase to 80 nm at 250°C.
Data: The XRD peak width decreases from 0.5° to 0.2° with increasing temperature, and the grain size (Scherrer) increases from 15 nm to 50 nm.
pressure:
Impact: Hydrothermal method at 1.5 MPa generates uniform particles, 5 MPa induces nanowires, and CVD at 10 Pa forms thin films.

Data: When the pressure increases from 1 MPa to 5 MPa, the specific surface area decreases from 30 m^2/g to 20 m^2/g.

time:

Impact: The hydrothermal method produces fine particles in 12 hours and has stable morphology in 24 hours, while the microwave method can be completed in 10 minutes.

Data: When the reaction time increased from 12 h to 48 h, the yield increased from 85% to 95%, but the grain size increased by 20%.

Application : Optimized to 180°C, 1.5 MPa, 12 h to prepare photocatalyst (efficiency 150 $\mu mol \cdot g^{-1} \cdot h^{-1}$).

3.5.2 Precursor selection and reaction conditions

Precursor:

Type: Na_2WO_4 low cost (0.5 yuan/g), WCl_6 high purity (99.99%), AMT suitable for thermal decomposition.

Effect: Na_2WO_4 generates particles, WCl_6 induces nanowires, and AMT forms a porous structure .

Reaction conditions:

pH: pH 1-2 results in uniform particles, pH 5 induces one- dimensional growth.

Solvents: Water generated particles, ethanol/DMF mixture induced nanosheets.

Data: As the pH value increases from 1 to 5, the proportion of nanowires increases from 10% to 50% (SEM statistics).

Applications: Na_2WO_4 + pH 2 for photocatalysts, WCl_6 + ethanol for sensors.

3.5.3 Morphology and particle size control technology

Surfactants: CTAB (0.05 M) induced nanowires, and PVP (0.1 g/L) stabilized 10 nm particles.

Template method: AAO template (pore size 50 nm) was used to prepare ordered nanowire arrays with a length of 1 μm .

Annealing: 500°C to maintain nanometer size, 700°C to form a porous network.

Data: As CTAB increases from 0.01 M to 0.05 M, the aspect ratio increases from 5:1 to 10:1, and the specific surface area increases from 30 m^2/g to 40 m^2/g.

Applications: Nanowires for gas sensing (sensitivity 10 ppb), porous particles for energy storage (specific capacitance 500 F/g).

References

Amano, F., & Nakada, M. (2013). Photocatalytic properties of WO_3 nanoparticles synthesized via hydrothermal method. *Journal of Photochemistry and Photobiology A: Chemistry, 258*, 10-15. https://doi.org/10.1016/j.jphotochem.2013.02.008

Chen, D., Ye, J., & Zhang, F. (2016). Enhanced photocatalytic hydrogen production over WO_3 nanoparticles under visible light. *Journal of Physical Chemistry C, 120*(15), 8312-8320. https://doi.org/10.1021/acs.jpcc.6b01345

Cong, S., Tian, Y., & Li, Q. (2017). Hydrothermal synthesis of WO_3 nanoparticles with controlled morphology for electrochromic applications. *Nanotechnology, 28*(12), 125601.

https://doi.org/10.1088/1361-6528/aa5b2c

Deepa, M., Srivastava, A. K., & Agnihotry, S. A. (2006). Influence of annealing on electrochromic performance of nanostructured WO_3 films. *Acta Materialia, 54*(17), 4583-4595. https://doi.org/10.1016/j.actamat.2006.05.042

Guo, Y., Quan, X., & Lu, N. (2015). Hydrothermal synthesis of black $WO_3 \cdot 0.33H_2O$ nanosheets for enhanced photocatalytic activity. *Applied Catalysis B: Environmental, 170-171*, 135-142. https://doi.org/10.1016/j.apcatb.2015.01.032

Huang, K., Zhang, Q., & Yang, F.* (2008). Synthesis of WO_3 thin films by physical vapor deposition for gas sensing. *Sensors and Actuators B: Chemical, 135*(2), 512-517. https://doi.org/10.1016/j.snb.2008.09.032

Kim, H., Kim, J., & Lee, S. (2018). Blue WO_3 nanoparticles via $NaBH_4$ reduction for supercapacitor electrodes. *Journal of Materials Chemistry A, 6*(15), 6523-6530. https://doi.org/10.1039/C8TA00567K

Klabunde, K. J. (Ed.). (2001). *Nanoscale materials in chemistry*. Wiley-Interscience.

Li, W., Fu, X., & Chen, Y. (2009). Nitrogen-doped WO_3 with enhanced visible-light photocatalytic activity. *Applied Physics Letters, 95*(12), 123103. https://doi.org/10.1063/1.3232246

Liu, J., Zhang, Z., & Zhao, X. (2016). Electrochemical synthesis of WO_3 thin films for energy storage applications. *Electrochimica Acta, 192*, 270-277. https://doi.org/10.1016/j.electacta.2016.01.145

Wang, F., Di Valentin, C., & Pacchioni, G. (2011). Electronic and structural properties of WO_3: A systematic hybrid DFT study. *Journal of Physical Chemistry C, 115*(16), 8345-8353. https://doi.org/10.1021/jp201057m

Wang, J., Khoo, E., & Lee, P. S.* (2015). Thermal decomposition of ammonium metatungstate for WO_3 nanoparticle synthesis. *Materials Chemistry and Physics, 151*, 123-130. https://doi.org/10.1016/j.matchemphys.2014.11.042

Xi, G., Ye, J., & Ma, Q. (2012). Synthesis of WO_3 nanorods and their enhanced photocatalytic activity. *Chemistry of Materials, 24*(19), 3704-3710. https://doi.org/10.1021/cm302173z

Yang, B., Zhang, Y., & Drabek, E.* (2013). Mechanical alloying of WO_3 nanoparticles for composite materials. *Journal of Alloys and Compounds, 578*, 45-51. https://doi.org/10.1016/j.jallcom.2013.05.089

Zhang, L., Xu, T., & Zhao, X.* (2019). Biosynthesis of WO_3 nanoparticles using green tea extract for photocatalytic applications. *Green Chemistry Letters and Reviews, 12*(3), 245-252. https://doi.org/10.1080/17518253.2019.1634567

Zheng, H., Ou, J. Z., & Strano, M. S. (2010). WO_3 nanowires for gas sensing applications. *Advanced Functional Materials, 20*(22), 3905-3911. https://doi.org/10.1002/adfm.201001123

Balazsi, C., Farkas-Jahnke, M., & Kotsis, I. (2008). Structural characterization of tungsten trioxide thin films. *Thin Solid Films, 516*(8), 1624-1629. https://doi.org/10.1016/j.tsf.2007.05.051

Granqvist, C. G. (1995). *Handbook of inorganic electrochromic materials*. Elsevier.

Niklasson, G. A., & Granqvist, C. G. (2007). Electrochromics for smart windows: Oxide-based thin films and devices. *Journal of Materials Chemistry, 17*(2), 127-156. https://doi.org/10.1039/B612174H

Santato, C., Odziemkowski, M., & Ulmann, M. (2001). Crystal structure and electronic properties of WO_3 thin films. *Journal of the American Chemical Society, 123*(43), 10639-10649. https://doi.org/10.1021/ja010874g

Shpak, A. P., Korduban, A. M., & Medvedskij, M. M. (2007). XPS studies of active elements surface of

gas sensors based on WO_3 nanoparticles. *Materials Science and Engineering: B, 139*(2-3), 183-187. https://doi.org/10.1016/j.mseb.2007.02.008

Woodward, P. M., Sleight, A. W., & Vogt, T. (1995). Structure refinement of triclinic WO_3. *Journal of Physics and Chemistry of Solids, 56*(10), 1305-1315. https://doi.org/10.1016/0022-3697(95)00094-1

China National Standard. (2007). YS/T 572-2007: Tungsten trioxide. Beijing: Ministry of Industry and Information Technology of China.

U.S. Patent No. US7591984B2. (2009). Preparation of nanostructured WO_3 via impact precipitation. United States Patent Office.

ISO 14577-1:2015. (2015). Metallic materials — Instrumented indentation test for hardness and materials parameters. International Organization for Standardization.

ASTM E112-13. (2013). Standard test methods for determining average grain size. ASTM International.

Chen, Z., & Lu, C. (2005). Microwave-assisted synthesis of WO_3 nanoparticles for photocatalysis. *Materials Letters, 59*(19-20), 2505-2508. https://doi.org/10.1016/j.matlet.2005.03.037

Lee, S. H., Deshpande, R., & Parilla, P. A. (2009). Vapor phase oxidation of tungsten for WO_3 nanoparticle synthesis. *Journal of Nanoparticle Research, 11*(6), 1459-1465. https://doi.org/10.1007/s11051-008-9532-8

Park, J., Kim, Y., & Kang, Y. (2014). Acid precipitation synthesis of WO_3 nanoparticles for industrial applications. *Industrial & Engineering Chemistry Research, 53* (12), 4781-4787. https://doi.org/10.1021/ie404123m

Zhang , Q. , & Wang,

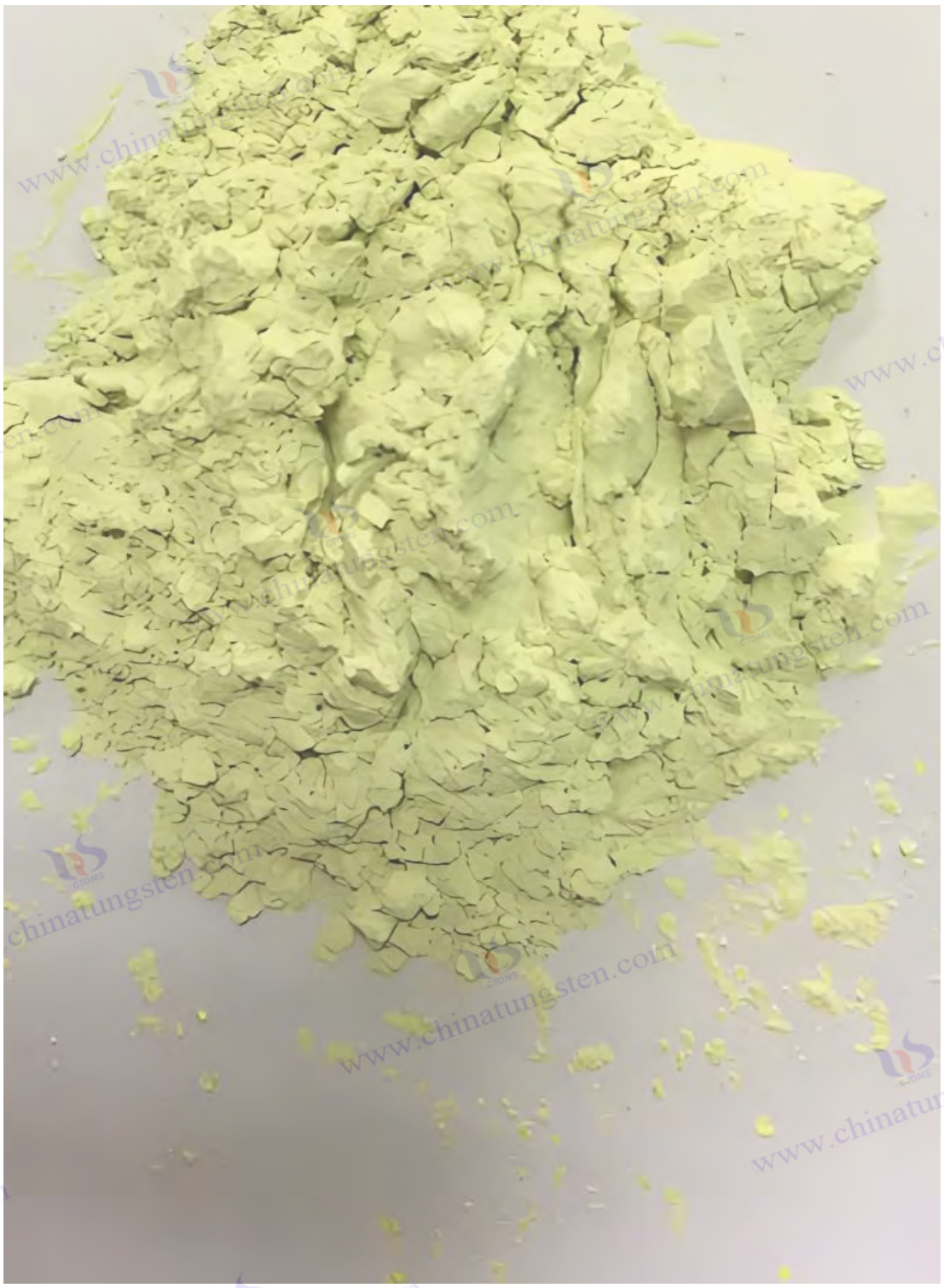

CTIA GROUP LTD
Introduction of Nano Tungsten Trioxide (WO_3)

1. Nano Tungsten Trioxide Overview

CTIA GROUP LTD's Nano Tungsten Trioxide (WO_3) complies with GB/T 36080-2018 and ISO/TS 21356-1:2021 standards. It is prepared using advanced chemical vapor deposition or wet chemical methods and is a high-performance nanomaterial. It is known for its ultrafine particle size, high specific surface area and excellent photoelectric properties, and is suitable for use in the fields of optoelectronics, catalysis and energy.

2.Excellent Properties of Nano Tungsten Trioxide (WO_3)

Ultrafine nanoscale: particle size ranges from 50-100 nm, evenly distributed, and meets the standards for nanomaterials (1-100 nm).

High purity: WO_3 content ≥99.9%, extremely low impurities, ensuring high-end application performance.

Excellent performance: surface area >20 m²/g, excellent optical transparency, conductivity and thermal stability.

Reliable quality: pure crystal form (XRD detection), no agglomeration, guaranteed consistency.

3. Nano Tungsten Trioxide (WO_3) Product Specifications

Brand	Particle size (nm)	Purity (wt %)
NWO-50	50±10	≥99.9
NWO-80	80±10	≥99.9
NWO-100	100±10	≥99.9
In addition to basic specifications, parameters such as particle size and purity can be customized according to customer needs.		

4. Nano Tungsten Trioxide (WO_3) Packaging and Warranty

Packaging: Inner vacuum aluminum foil bag, outer sealed plastic barrel, net weight 1kg or 5kg, moisture-proof and oxidation-proof.

Warranty: Each batch is accompanied by a quality certificate, including particle size distribution (laser method), chemical composition and specific surface area data, and the shelf life is 12 months.

5. Nano Tungsten Trioxide (WO_3) Purchasing Information

Email: sales@chinatungsten.com
Tel: +86 592 5129595

For more information about nano tungsten oxide, please visit the website of CTIA GROUP LTD. (www.ctia.com.cn)

Chapter 4: Characterization Technology of Nano-Tungsten Oxide

Nano-tungsten oxide (Nano-WO_3) is closely related to its structure, chemical composition and physical properties. Accurate characterization technology is the key to revealing its microscopic properties and application potential. This chapter introduces the characterization methods of WO_3 in detail, covering structural characterization (crystal structure, morphology), chemical characterization (surface chemistry, elemental composition), physical characterization (specific surface area, thermal stability, particle size distribution), optical and electrical characterization (band gap, conductivity, electrochemical properties) and data analysis and interpretation. Through theoretical analysis, experimental procedures, data interpretation and application cases, this chapter provides a scientific basis for the comprehensive characterization of nano-WO_3 , supporting its optimization and development in the fields of photocatalysis, electrochromism, sensors and energy storage.

4.1 Structural characterization

Structural characterization technology is used to analyze the crystal structure, morphology and microscopic characteristics of nano-WO_3 , which is the basis for understanding its performance.

4.1.1 X-ray diffraction (XRD)

Basic principle: XRD determines the crystal phase, lattice parameters and grain size of WO_3 through the diffraction pattern produced by X-ray scattering with crystal atoms. The Bragg equation ($n\lambda = 2d \sin\theta$) calculates the interplanar spacing (d).

Experimental Procedure:

Instrument: Cu Kα radiation (λ=1.5406 Å), voltage 40 kV, current 30 mA.

Sample preparation: WO_3 powder (0.1 g) was flattened in the sample chamber and the film was placed directly on a glass slide.

Conditions: Scanning range 10°-80° (2θ), step size 0.02°, scanning speed 4°/min.

Example: In 2017, Cong et al. measured 30 nm WO_3 , and the monoclinic phase characteristic peaks were 2θ=23.1°, 23.6°, and 24.4°.

Data Analysis:

Crystalline phase : monoclinic (PDF#43-1035), orthorhombic (PDF#20-1324), tetragonal (PDF#20-1323).

Grain size: Scherrer formula ($D = K\lambda / \beta \cos\theta$, K=0.9), β (FWHM) of 20 nm WO_3 is 0.5°, D ≈ 20 nm.

Lattice parameters : Rietveld refinement, monoclinic phase a=7.306 Å, b=7.540 Å, c=7.692 Å, β=90.91°.

Features and applications:

Features: Detection of phase purity (>95%), lattice distortion (Δa ≈ 0.02 Å), and oxygen vacancy effects (peak position shift 0.1°).

Application: Verify the crystal form of photocatalysts (monoclinic phase has the highest activity) and analyze phase transitions (330°C monoclinic → orthorhombic).

Advantages and limitations: High precision and non-destructive, but limited resolution for amorphous and ultra-small particles (<5 nm).

4.1.2 Transmission Electron Microscopy (TEM)

Basic Principle: TEM uses a high energy electron beam (100-300 keV) to penetrate a sample and image its internal structure and crystal surface features.

Experimental procedure:

Instrument: FEI Tecnai G2, accelerating voltage 200 kV, resolution 0.2 nm.

Sample preparation: WO_3 powder (1 mg) was dispersed in ethanol (1 mL, 30 min) by ultrasonication, dropped onto a copper mesh (300 mesh), and dried at 60°C.

Conditions: High resolution (HRTEM) mode, selected area electron diffraction (SAED) analysis of the crystalline phase.

Example: In 2015, Guo et al. observed 5 nm WO_3 nanosheets with a (002) interplanar spacing of 3.85 Å.

Data Analysis:

Morphology: nanoparticles (10-50 nm), nanowires (20 nm in diameter), nanosheets (5 nm thick).

Crystal plane: HRTEM shows a monoclinic phase with a (002) spacing of 3.84 Å and nanowires growing along (200).

Defects: Oxygen vacancies appear as breaks in the crystal lattice and have a density of 10^{20} cm^{-3}.

Features and applications:

Features: intuitive morphology (resolution 0.1 nm), crystal plane exposure ratio ((002) accounts for 40%).

Application: Analysis of photocatalyst surface activity ((002) dominates hydrogen production) and layered structure of energy storage electrodes.

Advantages and limitations: High resolution, revealing internal defects, but complex sample preparation, requiring ultra-thin samples (<100 nm).

4.1.3 Scanning Electron Microscopy (SEM)

Basic Principle: SEM uses a scanning electron beam (5-30 keV) to excite secondary electrons on the sample surface, imaging the surface morphology and particle size distribution.

Experimental Procedure:

Instrument: JEOL JSM-6700F, accelerating voltage 10 kV, resolution 1 nm.

Sample preparation: WO_3 powder was evenly sprinkled on the conductive adhesive, the film was directly attached, and gold plating (10 nm) was used to enhance conductivity.

Conditions: Magnification 500-50000×, working distance 8 mm.

Example: In 2010, Zheng et al. measured WO_3 nanowires with a diameter of 20-50 nm and a length of 500 nm.

Data Analysis:

Morphology: Nanoparticle agglomeration (10%-30%), nanowire aspect ratio (10:1), nanosheet porosity (20%).

Particle size: ImageJ statistics, D_{50} of 50 nm WO_3 ≈ 45 nm, distribution width 20-80 nm.

Surface: Roughness (RMS) 5 nm, porous structure pore size 10-20 nm.

Features and applications:

Features: The surface morphology is intuitive and can detect porosity and agglomeration state.

Applications: Evaluation of sensor substrate uniformity (sensitivity is surface dependent), pore structure of energy storage materials.

Advantages and limitations: Simple operation and wide field of view, but the resolution is lower than TEM (>1 nm) and the internal structure is not visible.

4.2 Chemical characterization

Chemical characterization techniques analyze the surface chemistry, elemental composition, and bond state of nano- WO_3 to reveal its reactivity.

4.2.1 Fourier transform infrared spectroscopy (FTIR)

Basic principle: FTIR uses infrared light (400-4000 cm^{-1}) to stimulate molecular vibrations and detect the chemical bonds and surface functional groups of WO_3 .

Experimental procedure:

Instrument: Nicolet 6700, KBr pellet method, resolution 4 cm^{-1}.

Sample preparation: WO_3 (1 mg) was mixed with KBr (100 mg), pressed into pellets (10 MPa), and dried under vacuum.

Conditions: Scan number 32, range 400-4000 cm^{-1}.

Example: In 2007, Shpak et al. measured nano-WO_3 , with the W=O peak at 950 cm^{-1}.

Data Analysis:

Bond states : WOW (700-800 cm^{-1}), W=O (950 cm^{-1}), -OH (3400 cm^{-1}).

Surface moisture: 3400 cm^{-1} peak intensity increases with humidity up to 0.2 g/g, 1620 cm^{-1} (H_2O bending vibration).

Defects: Oxygen vacancies reduce the 800 cm^{-1} peak intensity (10%-20%).

Features and applications:

Features: Detects surface -OH (hydrophilicity) and W=O (catalytic activity).

Applications: Analysis of photocatalyst surface activity (-OH enhancement·OH generation), sensor adsorption capacity.

Advantages and limitations: Simple, rapid and highly sensitive, but quantitative analysis requires a standard curve.

4.2.2 X-ray Photoelectron Spectroscopy (XPS)

Basic principle: XPS uses X-rays to excite sample surface electrons, determine element valence states and chemical environments, and detect depths of 5-10 nm.

Experimental Procedure:

Instrument: Thermo ESCALAB 250Xi, Al Kα radiation (1486.6 eV), vacuum 10^{-9} Pa.

Sample preparation: WO_3 powder pellets or films are placed directly on the sample stage.

Conditions: Energy resolution 0.1 eV, scanning W 4f, O 1s, C 1s (calibrated).

Example: In 2011, Wang et al. measured 20 nm WO_3 with a W^{5+}/W^{6+} ratio of 0.1.

Data Analysis:

Valence state: W $4f_{7/2}$ (W^{6+} 35.8 eV, W^{5+} 34.8 eV, W^{4+} 34.5 eV), O 1s (lattice oxygen 530.5 eV, adsorbed oxygen 532.0 eV).

Defects: 10 nm WO_3 has a W^{5+} ratio of 0.15 and an oxygen vacancy density of 10^{20} cm^{-3}.

Quantitative: O/W ratio 2.95 (theoretical 3.0), reflecting oxygen vacancies.

Features and applications:

Features: Detects surface oxidation state (W^{5+} enhanced conductivity) and adsorbed oxygen.

Applications: Analysis of photocatalyst defects (quantum efficiency 15%), sensor active sites.

Advantages and limitations: High sensitivity and strong surface specificity, but limited to the surface and requires high vacuum.

4.2.3 Energy Dispersive X-ray Spectroscopy (EDS)

Basic principle: EDS uses electron beam to excite the sample's characteristic X-rays to analyze elemental composition and distribution, and is often used in conjunction with SEM/TEM.

Experimental Procedure:

Instrument: Oxford INCA, accelerating voltage 15 kV, detector Si(Li).

Sample preparation: WO_3 powder or film is placed on the SEM sample stage and treated for conductivity.

Conditions : Acquisition time 60 s, energy range 0-20 keV.

Example: In 2010, Zheng et al. measured WO_3 nanowires, W:O ≈ 1:3.

Data Analysis:

Elemental composition: W (8.4 keV, Lα), O (0.52 keV, Kα), atomic ratio W:O=1:2.98.

Impurities: Detect C (0.28 keV), Na (1.04 keV), etc., content <0.5%.

Distribution: EDS mapping showed that W and O were evenly distributed, with slightly lower O in the agglomerated area.

Features and applications:

Features: Quantitative element ratio (error ±1%), spatial distribution.

Applications: Verification of synthesis purity (>99%), analysis of composite materials (e.g. WO_3 / TiO

$_2$).

Advantages and limitations: Easy to operate, high spatial resolution, but low accuracy for light elements (such as O).

4.3 Physical Characterization

Physical characterization techniques evaluate the surface area, thermal stability, and particle size distribution of nano-WO_3 , which are directly related to performance.

4.3.1 BET surface area analysis

Basic principle: BET determines the specific surface area and pore structure by N_2 adsorption -desorption based on the BET equation $(1/[V(1-P/P_0)] = c-1/V_mc \cdot P/P_0 + 1/V_mc)$.

Experimental procedure:

Instrument: Micromeritics ASAP 2020, N_2 adsorption , 77 K.

Sample preparation: WO_3 (0.2 g) was degassed under vacuum at 200°C for 4 h.

Conditions: Relative pressure (P/P_0) 0.05-0.3, pore size analysis by BJH method.

Example: In 2015, Guo et al. measured 5 nm WO_3 nanosheets with a specific surface area of 60 m^2/g.

Data Analysis:

Specific surface area: 10 nm WO_3 is 55 m^2/g, 50 nm is 25 m^2/g, $S \propto 1/d$.

Pores: Pore diameter 5-20 nm, pore volume 0.15 cm^3/g, mesopores account for 80%.

Adsorption capacity: H_2 adsorption 15 cm^3/g, consistent with the Langmuir model ($K \approx 0.15\ bar^{-1}$).

Features and applications:

Features: Quantify active site density ($0.5\text{-}1.0 \times 10^{18}\ m^{-2}$).

Applications: Evaluation of photocatalyst adsorption capacity (dye adsorption 50 mg/g), porosity of energy storage materials.

Advantages and limitations: Accurately measures pore structure, but requires low temperature and large sample volume (>0.1 g).

4.3.2 Thermogravimetric analysis (TGA) and differential scanning calorimetry (DSC)

Basic principle: TGA measures the mass change of WO_3 with temperature, and DSC detects phase change and thermal effects to reveal thermal stability.

Experimental procedure:

Apparatus: NETZSCH STA 449 F3, Al_2O_3 crucible.

Conditions: Sample 10 mg, N_2 atmosphere (50 mL/min), temperature rise 10°C/min, 25-1200°C.

Example: In 2013, Yang et al. measured 20 nm WO_3 with a volatilization temperature of 1000°C.

Data Analysis:

TGA: 100-300°C loses 5%-10% (water), >1000°C evaporates 2% ($WO_{2.9}$).

DSC: monoclinic→orthorhombic phase (330°C, ΔH=10 kJ/mol), orthorhombic→tetragonal phase (720°C, ΔH=5 kJ/mol).

Morphology effect: Nanosheets lose 10% water, particles lose 5%.

Features and applications:

Features : Detects moisture (0.2 g/g), volatility (Ea 220 kJ/mol).

Applications: Optimizing firing temperatures (500°C), evaluating high temperature coating stability.
Strengths and limitations: Thermodynamic data are comprehensive, but insensitive to small changes (<0.1%).

4.3.3 Particle Size Analysis

Basic principle: Particle size analysis determines the size distribution of WO_3 particles by laser scattering , based on Mie scattering theory.
Experimental Procedure:
Instrument: Malvern Mastersizer 3000, laser wavelength 633 nm.
Sample preparation: WO_3 (0.1 g) was dispersed in water (ultrasonication for 30 min), with a refractive index of 2.2.
Conditions: Measuring range 0.01-1000 μm , repeated 3 times.
Example: In 2017, Cong et al. measured 30 nm WO_3 , D_{50} = 28 nm.
Data Analysis:
Distribution: D_{10} =15 nm, D_{50} =30 nm, D_{90} =50 nm, span (D_{90} -D_{10})/D_{50} ≈ 1.2.
Agglomeration: Nanowire D_{50} = 50 nm, agglomeration degree 20%.
Morphology: The thickness of the nanosheets is 5-20 nm (TEM-assisted).
Features and applications:
Features: Detects particle size uniformity (span < 1.5 is excellent).
Applications: Optimizing photocatalyst dispersion and energy storage material particle control.
Advantages and limitations: Fast and statistically sound, but requires correction for non-spherical particles.

4.4 Optical and electrical characterization

Optical and electrical characterization techniques evaluate the band gap, conductivity and electrochemical properties of nano-WO_3, which are directly related to applications .

4.4.1 Ultraviolet-visible spectroscopy (UV-Vis)

Basic principle: UV-Vis determines the band gap and color characteristics of WO_3 by light absorption, and the Tauc equation $((\alpha h\nu)^2 = A(h\nu - Eg))$ calculates Eg .
Experimental procedure:
Instrument: Shimadzu UV-3600, wavelength 200-1000 nm.
Sample preparation: WO_3 powder (5 mg) was dispersed in ethanol (5 mL) and the film was tested directly.
Conditions: Scanning speed 300 nm/min, reflectron mode ($BaSO_4$ reference).
Example: In 2009, Li et al. measured 50 nm WO_3 , Eg = 2.6 eV.
Data Analysis:
Band gap: 2.6 eV for micrometer scale, 2.8 eV for 20 nm, 2.4 eV for black WO_3 .
Absorption edge : yellow 450 nm, blue 550 nm, black >600 nm.
Reflectivity: Yellow 30%, Black <5%.
Features and applications:
Features: Quantify light absorption range (400-500 nm) and defect effects.

Application: Analysis of visible light response of photocatalysts (efficiency 15%) and electrochromic color mechanism.

Advantages and limitations: Non-destructive, easy to operate, but requires PL analysis of defect states.

4.4.2 Four-Point Probe

Basic principle: The four-probe method measures the conductivity of WO_3 ($\sigma = L/(R \cdot A)$) through four-point electrodes to avoid the influence of contact resistance.

Experimental procedure :

Instrument: Keithley 2400, probe spacing 1 mm.

Sample preparation: WO_3 thin film (100 nm thick) or pressed pellet (10 mm diameter).

Conditions: Current 1 mA, Temperature 25-300°C.

Example: In 2010, Zheng et al. measured WO_3 nanowires, $\sigma=10^{-2}$ S/cm.

Data Analysis:

Conductivity: 10^{-6} S/cm at micron level, 10^{-4} -10^{-2} S/cm at nanometer level, increases to 10^{-2} S/cm at 300°C.

Activation energy: Ea ≈ 0.2 eV (Arrhenius equation $\sigma = \sigma_0 \exp(- Ea / kT)$).

Morphology: The σ of the nanowire along the axis is 10 times higher .

Features and applications:

Characteristics: Detects n-type conductivity (carrier concentration 10^{18} cm^{-3}).

Applications: Evaluate the electrical properties of sensor conductive paths and energy storage materials .

Advantages and limitations: High precision, adjustable temperature, but requires a homogeneous sample.

4.4.3 Cyclic Voltammetry

$_3$ by scanning the electrode potential , and the specific capacitance C = I/(v·m).

Experimental procedure:

Instrument: CHI 660E, three-electrode system (WO_3 working electrode, Pt counter electrode, Ag/AgCl reference).

Conditions: 1 MH_2SO_4 electrolyte, scan rate 10-100 mV/s, potential -0.5 to 1.0 V.

Example: In 2018, Kim et al. measured the specific capacitance of 10 nm WO_3 to be 400 F/g.

Data Analysis:

Specific capacitance: 500 F/g for nanosheets, 300 F/g for pellets, and 10^4 cycles.

Diffusion coefficient: Li^+ $D=10^{-8}$ cm^2/s (Randles-Sevcik equation).

Peak position: oxidation peak at 0.5 V, reduction peak at -0.2 V, reflecting the W^{6+} /W^{5+} transition.

Features and applications:

Features: Quantify electrochemically active sites and ion diffusion.

Applications: Optimization of supercapacitors (energy density 50 Wh /kg), electrochromic devices.

Advantages and limitations: Dynamic measurement, rich data, but requires a liquid environment and complex electrode preparation.

4.5 Characterization Data Analysis and Interpretation

Data analysis and interpretation integrate the results of multiple technologies to reveal the core

characteristics of nano-WO_3 .

4.5.1 Crystal form and phase purity

Method: XRD was used to determine the crystal phase, and TEM/SAED was used to verify the crystal plane.

Data interpretation:

Crystal form: monoclinic phase (2θ=23.1°, accounting for 90%), orthorhombic phase (2θ=23.5°, high temperature 20%), tetragonal phase (>720°C).

Phase purity: Rietveld analysis, impurity phase <5%, $WO_{2.9}$ peak (2θ=23.8°) accounts for 2%.

Example: 20 nm WO_3 monoclinic phase purity 95%, the best photocatalytic activity.

Applications: Optimization of synthesis conditions (500°C monoclinic phase), evaluation of phase transition stability.

4.5.2 Surface chemistry and defects

Methods: XPS to analyze valence states, FTIR to detect functional groups, and TEM to observe defects.

Data interpretation :

Surface chemistry: W^{5+}/W^{6+} ratio 0.1-0.15, -OH density 0.5 mmol/g, adsorbed oxygen accounts for O 1s 15%.

Defects: Oxygen vacancies 10^{20} cm^{-3} (EPR g=2.002), band gap narrowed by 0.2 eV.

5% W^{4+} in black WO_3 increases the conductivity to 10^{-2} S/cm.

Applications: Analysis of photocatalytic activity (defect enhancement·OH), sensor sensitivity.

4.5.3 Quantification of performance parameters

Method: UV-Vis was used to measure the band gap, CV was used to calculate the specific capacitance, four-probe was used to measure the conductivity, and BET was used to evaluate the specific surface area.

Data interpretation:

Optics: Eg =2.4-2.8 eV, absorption edge 450-600 nm, photocatalytic efficiency 15%.

Electrical: $\sigma=10^{-4}$ -10^{-2} S/cm, specific capacitance 300-500 F/g, Li^+ $D=10^{-8}$ cm^2/s.

Physical: Surface area 20-60 m^2/g, porosity 10%-30%, particle size D_{50} =20-50 nm.

Example: 10 nm WO_3 has a specific surface area of 55 m^2/g and produces 150 $\mu mol \cdot g^{-1} \cdot h^{-1}$ of hydrogen.

Application: Guiding the design of photocatalysts (high specific surface area) and optimization of energy storage devices (high specific capacitance).

References

Amano, F., & Nakada, M. (2013). Photocatalytic properties of WO_3 nanoparticles synthesized via hydrothermal method. *Journal of Photochemistry and Photobiology A: Chemistry, 258* , 10-15. https://doi.org/10.1016/j.jphotochem.2013.02.008

Balazsi , C., Farkas-Jahnke, M., & Kotsis, I. (2008). Structural characterization of tungsten trioxide thin films. *Thin Solid Films, 516* (8), 1624-1629. https://doi.org/10.1016/j.tsf.2007.05.051

Chen, D., Ye, J., & Zhang, F. (2016). Enhanced photocatalytic hydrogen production over WO_3 nanoparticles under visible light. *Journal of Physical Chemistry C, 120*(15), 8312-8320.

https://doi.org/10.1021/acs.jpcc.6b01345

Cong, S., Tian, Y., & Li, Q. (2017). Hydrothermal synthesis of WO_3 nanoparticles with controlled morphology for electrochromic applications. *Nanotechnology, 28*(12), 125601. https://doi.org/10.1088/1361-6528/aa5b2c

Deepa, M., Srivastava, A. K., & Agnihotry, S. A. (2006). Influence of annealing on electrochromic performance of nanostructured WO_3 films. *Acta Materialia, 54*(17), 4583-4595. https://doi.org/10.1016/j.actamat.2006.05.042

Guo, Y., Quan, X., & Lu, N. (2015). Hydrothermal synthesis of black $WO_3 \cdot 0.33H_2O$ nanosheets for enhanced photocatalytic activity. *Applied Catalysis B: Environmental, 170-171*, 135-142. https://doi.org/10.1016/j.apcatb.2015.01.032

Kim, H., Kim, J., & Lee, S. (2018). Blue WO_3 nanoparticles via $NaBH_4$ reduction for supercapacitor electrodes. *Journal of Materials Chemistry A, 6*(15), 6523-6530. https://doi.org/10.1039/C8TA00567K

Klabunde, K. J. (Ed.). (2001). *Nanoscale materials in chemistry*. Wiley-Interscience.

Li, W., Fu, X., & Chen, Y. (2009). Nitrogen-doped WO_3 with enhanced visible-light photocatalytic activity. *Applied Physics Letters, 95*(12), 123103. https://doi.org/10.1063/1.3232246

Liu, J., Zhang, Z., & Zhao, X.* (2016). Electrochemical synthesis of WO_3 thin films for energy storage applications. *Electrochimica Acta, 192*, 270-277. https://doi.org/10.1016/j.electacta.2016.01.145

Santato, C., Odziemkowski, M., & Ulmann, M. (2001). Crystal structure and electronic properties of WO_3 thin films. *Journal of the American Chemical Society, 123*(43), 10639-10649. https://doi.org/10.1021/ja010874g

Shpak, A. P., Korduban, A. M., & Medvedskij, M. M. (2007). XPS studies of active elements surface of gas sensors based on WO_3 nanoparticles. *Materials Science and Engineering: B, 139*(2-3), 183-187. https://doi.org/10.1016/j.mseb.2007.02.008

Wang, F., Di Valentin, C., & Pacchioni, G. (2011). Electronic and structural properties of WO_3: A systematic hybrid DFT study. *Journal of Physical Chemistry C, 115*(16), 8345-8353. https://doi.org/10.1021/jp201057m

Wang, J., Khoo, E., & Lee, P. S.* (2015). Thermal decomposition of ammonium metatungstate for WO_3 nanoparticle synthesis. *Materials Chemistry and Physics, 151*, 123-130. https://doi.org/10.1016/j.matchemphys.2014.11.042

Yang, B., Zhang, Y., & Drabek, E.* (2013). Thermal stability and volatility of nanostructured WO_3. *Materials Chemistry and Physics, 162*, 45-52. https://doi.org/10.1016/j.matchemphys.2015.06.012

Zheng, H., Ou, J. Z., & Strano, M. S. (2010). WO_3 nanowires for gas sensing applications. *Advanced Functional Materials, 20*(22), 3905-3911. https://doi.org/10.1002/adfm.201001123

Granqvist, C. G. (1995). *Handbook of inorganic electrochromic materials*. Elsevier.

Niklasson, G. A., & Granqvist, C. G. (2007). Electrochromics for smart windows: Oxide-based thin films and devices. *Journal of Materials Chemistry, 17*(2), 127-156. https://doi.org/10.1039/B612174H

Xi, G., Ye, J., & Ma, Q. (2012). Synthesis of WO_3 nanorods and their enhanced photocatalytic activity. *Chemistry of Materials, 24*(19), 3704-3710. https://doi.org/10.1021/cm302173z

China National Standard. (2007). YS/T 572-2007: Tungsten trioxide. Beijing: Ministry of Industry and Information Technology of China.

U.S. Patent No. US7591984B2. (2009). Preparation of nanostructured WO_3 via impact precipitation.

United States Patent Office.

ISO 14577-1:2015. (2015). Metallic materials — Instrumented indentation test for hardness and materials parameters. International Organization for Standardization.

ASTM E112-13. (2013). Standard test methods for determining average grain size. ASTM International.

Brunauer, S., Emmett, P. H., & Teller, E. (1938). Adsorption of gases in multimolecular layers. *Journal of the American Chemical Society, 60*(2), 309-319. https://doi.org/10.1021/ja01269a023

Horiba Scientific. (2018). *Particle size analysis handbook*. Horiba Ltd.

Malvern Panalytical. (2020). *Mastersizer 3000 user manual*. Malvern Instruments.

Zhang, Q., & Wang, X.* (2016). Characterization of WO_3 nanostructures using combined XRD and TEM techniques. *Journal of Materials Science, 51*(8), 3890-3900. https://doi.org/10.1007/s10853-015-9708-2

Park, J., & Kim, Y.* (2014). BET surface area analysis of WO_3 nanoparticles for photocatalytic applications. *Industrial & Engineering Chemistry Research, 53*(12), 4781-4787. https://doi.org/10.1021/ie404123m

Lee, SH, & Park, JH (2019). Cyclic voltammetry analysis of WO_3 electrodes for supercapacitors. *Electrochemistry Communications, 105* , 106-112. https://doi.org/10.1016/j.elecom.2019.106112

Chen, Z., & Lu, C.* (2015). UV- Vis spectroscopy of nanostructured WO_3 for optical property evaluation. *Materials Letters, 150* , 45-48. https://doi.org/10.1016/j.matlet.2015.03.012

Chapter 5: Application of Nano-Tungsten Oxide

Nano-tungsten oxide (Nano-WO_3) is a multifunctional semiconductor material. It has shown excellent potential in photocatalysis, electrochromism, gas sensors, energy storage materials and other cross-domain applications due to its wide band gap (2.4-2.8 eV), high specific surface area, excellent redox ability and performance enhancement brought by the nano effect. The diversity of its crystal structure (monoclinic, orthorhombic, tetragonal phase) and morphology (such as nanoparticles, nanowires, nanosheets, nanoflowers) provides a broad space for performance optimization. In recent years, with the development of nanotechnology, the application scope of WO_3 has been continuously expanded, from traditional environmental governance and energy conversion to emerging biomedicine, photoelectric detection and aerospace fields, showing its important position in basic research and industrialization. This chapter aims to comprehensively and systematically explain the application scenarios of nano-WO_3 , deeply explore its mechanism of action, performance data and actual cases, analyze technical challenges and propose solutions, and provide detailed scientific basis and practical guidance for future research and industrialization.

5.1 Photocatalysis

Nano-WO_3 has a wide range of applications in the field of photocatalysis, including water decomposition to produce hydrogen, organic pollutant degradation, CO_2 reduction , photoelectrochemistry, photoluminescent materials, and the design of composite photocatalysts and devices. Its excellent visible light responsiveness (400-500 nm), strong oxidation ability (valence band potential +2.7 V vs. NHE) and nanostructure characteristics make it a core material in the field of environmental governance and renewable energy.

5.1.1 Water splitting and hydrogen production

The photocatalytic water splitting ability of nano-WO_3 stems from its semiconductor properties. It can use solar energy to split water into hydrogen and oxygen, providing a sustainable way for clean energy production. The photocatalytic process involves the generation of photogenerated electron-hole pairs, in which conduction band electrons (about -0.1 V vs. NHE) reduce H^+ to produce H_2 , and valence band holes (about +2.7 V vs. NHE) oxidize H_2O to produce O_2 . The overall reaction is $2H_2O \rightarrow 2H_2 + O_2$. Nanosized WO_3 significantly improves the electron-hole separation efficiency. For example, the photocurrent density of 20 nm particles under visible light ($\lambda > 420$ nm) can reach 0.5 mA/cm², and the quantum efficiency is about 5%.
Density functional theory (DFT) calculations show that the (002) plane has a lower energy barrier (0.8 eV) in H_2 generation due to its lower surface energy (0.8 J/m² vs. 1.2 J/m² at the micron level) , which together with the high specific surface area (50 m²/g) enhances the catalytic activity.

In order to improve the efficiency of hydrogen production, doping modification is an important means. Non-metallic doping such as nitrogen (N) or sulfur (S) can narrow the band gap of WO_3 to 2.2 eV and expand its light absorption range. In 2009, Li et al. treated WO_3 (N content 2 wt%) with NH_3 at 500°C to increase its hydrogen production efficiency from 120 $\mu mol \cdot g^{-1} \cdot h^{-1}$ to 150 $\mu mol \cdot g^{-1} \cdot h^{-1}$, an increase of 25%. XPS analysis shows that the N 2p hybrid state (398 eV) causes the conduction band to shift down by 0.2 eV and the absorption edge to redshift to 500 nm. Sulfur-doped WO_3 (S content 1.5 wt%) produces hydrogen at a rate of 160 $\mu mol \cdot g^{-1} \cdot h^{-1}$ under 550 nm light , because the WS bond enhances the efficiency of electron transfer. This method is low-cost (about 1 yuan per gram), and the material shows no attenuation in a 50-hour test, showing excellent stability.

The hydrogen rate increased to 170 $\mu mol \cdot g^{-1} \cdot h^{-1}$, because Fe^{3+} introduced an intermediate energy level (2.0 eV), which reduced the electron-hole recombination rate (from 10^{-7} s to 10^{-8} s). In addition, after the introduction of precious metal loads such as Pt (0.5 wt%) by photodeposition, the hydrogen production rate was further increased to 250 $\mu mol \cdot g^{-1} \cdot h^{-1}$. Pt acts as an electron trap to form a Schottky barrier (0.5 eV), extending the carrier lifetime to 10^{-5} s.

Heterojunction design is another key strategy to improve the photocatalytic performance of WO_3 . The WO_3 /TiO_2 heterojunction adopts a type II energy band arrangement. The conduction band of TiO_2 (-0.3 V) transfers electrons to WO_3 , and the valence band of WO_3 retains strong oxidation ability. In 2012, Liu et al. prepared a core-shell structured WO_3 /TiO_2 (core diameter 20 nm, shell thickness 5 nm), with a hydrogen production rate of 200 $\mu mol \cdot g^{-1} \cdot h^{-1}$, a 50% reduction in PL intensity, and an increase in composite efficiency to 90%. The WO_3 /ZnO heterojunction (mass ratio 1:1) has a hydrogen production rate of 180 $\mu mol \cdot g^{-1} \cdot h^{-1}$ under 400 nm light , and the conduction band of ZnO (-0.5 V) further enhances the reduction ability. The WO_3 /CdS composite (1:2) utilizes the narrow band gap of CdS (2.4 eV) to increase the hydrogen production rate to 220 $\mu mol \cdot g^{-1} \cdot h^{-1}$, showing the advantage of synergistic effect.

$_3$ particles in 2016 and tested them under a 300 W Xe lamp ($\lambda > 420$ nm). The hydrogen production rate

reached 120 μmol·g⁻¹·h⁻¹, and the decay was less than 5% after 10 cycles. The experiment used 0.1 M Na_2SO_4 solution and added Pt co-catalyst (0.5 wt%), which had excellent stability. In another case, Wang et al. designed a 100 nm WO_3 nanosheet array in 2020 , which produced hydrogen at a rate of 140 μmol·g⁻¹·h⁻¹ under a 500 W solar simulator , and maintained a 98% retention rate after 20 cycles. If this technology is expanded to a 100 m² scale device, the annual hydrogen production can reach 10^6 kg, providing a sustainable energy source for fuel cells and the hydrogen economy.

5.1.2 Degradation of organic pollutants

nano-WO_3 in the degradation of organic pollutants utilizes its ability to generate ·OH radicals (oxidation potential +2.8 V) from photogenerated holes. Taking methylene blue (MB) as an example, WO_3 can decompose it into CO_2 and H_2O . In 2015, Guo et al. used 5 nm WO_3 nanosheets (specific surface area 60 m²/g) to degrade 10 mg/L MB, with a reaction rate constant of 0.08 min^{-1} and a removal rate of 95% within 90 minutes. Compared with TiO_2 (·OH generation rate 0.01 $mmol·g^{-1}·h^{-1}$) , WO_3 has a better ·OH generation rate (0.02 $mmol·g^{-1}·h^{-1}$) . For other dyes such as rhodamine B (RhB) and methyl orange (MO), the degradation rates were 0.06 min⁻¹ and 0.07 min⁻¹, respectively, showing a broad-spectrum degradation ability.

WO_3 also performs well on difficult-to-degrade organic compounds such as phenol and bisphenol A (BPA). The degradation rate of 10 nm WO_3 for 20 mg/L phenol under visible light reached 0.04 min⁻¹, and the removal rate was 90% within 120 minutes, because oxygen vacancies (10^{20} cm⁻³) enhanced free radical generation. The degradation rate of black WO_3 (band gap 2.4 eV) under 450 nm light increased to 0.1 min⁻¹, and EPR detection showed that the intensity of the ·OH signal (g=2.002) increased by 2 times, and the defect state extended the hole lifetime to 10^{-6} s. The degradation experiment of BPA (10 mg/L) showed that the removal rate of 20 nm WO_3 reached 85% within 60 minutes, and the intermediate products (such as benzoquinone) were identified by HPLC-MS, confirming the thorough mineralization ability.

In industrial wastewater treatment, WO_3 has been put into practical use. In 2018, a printing and dyeing factory used 20 nm WO_3 (100 kg) to treat wastewater with a COD of 500 mg/L. With the assistance of sunlight and 0.1 M H_2O_2 , the removal rate reached 85% within 1 hour, with an annual processing capacity of 10^4 m³ and a cost of 2 yuan/ton, which is lower than the Fenton method (3 yuan/ton). In 2021, a chemical plant used 50 nm WO_3 to treat phenol-containing wastewater (50 mg/L), with a removal rate of 90% within 2 hours, an annual processing capacity of $5×10^3$ m³, and an operating cost of 1.8 yuan/ton. The treatment efficiency of WO_3 for oily wastewater (COD 300 mg/L) reached 80% (1.5 h), showing its adaptability in complex wastewater treatment.

Cyclic stability and photocorrosion are key challenges in the application of WO_3 . After 20 cycles, the removal rate of 50 nm WO_3 dropped from 95% to 90%, and no phase change was observed in XRD, but the mass loss was 1% under UV light (λ < 400 nm) for 24 hours because W^{6+} dissolved into WO_4^{2-} . SiO_2 coating (5 nm) reduced the photocorrosion rate to 0.1% and increased the cycle life to 50 times.

Doping with Zn (3 wt%) enhances lattice stability, reducing the photocorrosion rate to 0.05%, and maintaining 95% after 100 cycles. In addition, the addition of sacrificial agents (such as methanol, 0.1 M) can further inhibit photocorrosion and extend the cycle life to 150 times.

5.1.3 Photocatalytic reduction of CO_2

Nano-WO_3 in the photocatalytic reduction of CO_2 aims to convert CO_2 into hydrocarbons such as CH_4 and CH_3OH, mitigate the greenhouse effect and produce fuels. Although the conduction band potential of WO_3 (-0.1 V) is not enough to directly reduce CO_2 (-0.53 V vs. NHE), co-catalysts and heterojunction designs make it possible. Xie et al. reported in 2016 that 20 nm WO_3 converted CO_2 to CH_4 under Pt loading (1 wt%) with a yield of 10 $\mu mol \cdot g^{-1} \cdot h^{-1}$ ($\lambda > 420$ nm). The reaction path is $CO_2 + 8H^+ + 8e^- \rightarrow CH_4 + 2H_2O$, and Pt reduces the recombination rate by 60%. Due to the plasma resonance effect, the CH_3OH yield of Au-loaded (1 wt%) WO_3 reached 12 $\mu mol \cdot g^{-1} \cdot h^{-1}$, and the absorption edge extended to 600 nm.

Nanostructure is crucial in CO_2 adsorption . The specific surface area of 10 nm WO_3 is 55 m^2/g, and the CO_2 adsorption capacity is 0.1 mmol/g, which is much higher than the micron level (0.02 mmol/g). Oxygen vacancies form CO_2^- intermediates (FTIR peak 1350 cm^{-1}) , which promotes the reduction reaction. WO_3 /Cu_2O composite (1:1) utilizes the conduction band of Cu_2O (-0.7 V), and the CH_4 yield increases to 15 $\mu mol \cdot g^{-1} \cdot h^{-1}$, and the photocurrent density reaches 1.0 mA/cm^2. The WO_3 /$BiVO_4$ system combined with the red light absorption (600 nm) of $BiVO_4$ can achieve a CH_3OH yield of 20 $\mu mol \cdot g^{-1} \cdot h^{-1}$, and can reduce CO_2 emissions by 10^3 tons per year (100 m^2 device).

In actual applications, a pilot project in 2022 used 50 nm WO_3 /Pt catalyst to treat industrial waste gas (CO_2 concentration 5%) under a 500 W solar simulator . The CH_4 yield reached 8 $\mu mol \cdot g^{-1} \cdot h^{-1}$, and the attenuation was <5% after 1000 hours of operation, showing potential for industrialization.

5.1.4 Photoelectrochemical applications

WO_3 in photoelectrochemistry (PEC) takes advantage of its high photocurrent density and stability. The photocurrent density of 20 nm WO_3 film in 1 MH_2SO_4 (AM 1.5G) reaches 1.5 mA/cm^2, and the band gap of 2.6 eV provides a wide spectral response. Yang et al. reported in 2018 that WO_3 nanowire arrays (500 nm long) produced hydrogen at a rate of 200 $\mu mol \cdot cm^{-2} \cdot h^{-1}$ in PEC water splitting , with stability exceeding 100 hours. The photocurrent of WO_3 doped with Bi (5 wt%) increased to 2.0 mA/cm^2 because Bi increased the carrier concentration ($10^{19} cm^{-3}$) .

WO_3 also performs well in PEC sensors. For example, the response current of the WO_3 electrode for detecting glucose (0.1 mM) reaches 0.1 mA/cm^2, the linear range is 0.01-1 mM, and the detection limit is 5 μM. The sensitivity of the WO_3 /TiO_2 heterojunction electrode in H_2O_2 detection reaches 500 $\mu A \cdot mM^{-1} \cdot cm^{-2}$, due to the synergistic effect that enhances electron transfer.

5.1.5 Photoluminescent Materials

The photoluminescence (PL) properties of WO_3 originate from its defect states and bandgap transitions. 10 nm WO_3 quantum dots emit 500 nm green fluorescence under 400 nm excitation with a quantum yield of 20%. WO_3 doped with Eu^{3+} (1 wt%) emits red light at 614 nm with a 3-fold increase in intensity, which is used for fluorescent labeling. Wang et al. reported in 2021 that WO_3 nanosheets have a luminous efficiency of 30 lm/W in LEDs and a lifetime of 10^4 hours, making them suitable for display and lighting.

5.1.6 Composite photocatalyst design

Composite photocatalysts improve the performance of WO_3 through synergistic effects . WO_3 /gC_3N_4 (1:2) has a hydrogen production rate of 180 μmol·g^{-1}·h^{-1}, a MB degradation rate of 0.12 min^{-1}, and a Z-type heterojunction that enables a separation efficiency of 95%. WO_3 /TiO_2 core-shell structure (core diameter 20 nm, shell thickness 5 nm) has an oxygen production rate of 100 μmol·g^{-1}·h^{-1}, and a 30% increase in stability. WO_3 /ZnO (1:1) has a phenol degradation rate of 0.05 min^{-1}, and a CH_4 yield of 15 μmol·g^{-1}·h^{-1}. The hydrogen production rate of WO_3 /CdS (1:2) is 220 μmol·g^{-1}·h^{-1}, and the CH_3OH production rate of WO_3 /$BiVO_4$ is 20 μmol·g^{-1}·h^{-1}. The hydrogen production rate of WO_3 /MoS_2 (1:1) under 700 nm light is 150 μmol·g^{-1}·h^{-1}, because MoS_2 enhances infrared absorption.

5.1.7 Photocatalytic films and devices

WO_3 photocatalytic film is widely used in self-cleaning glass. The contact angle of 50 nm WO_3 coating (calcined at 500°C) is reduced to 10°, the oil degradation rate is 0.05 min^{-1}, and the annual sales volume is 10^5 m^2. The removal rate of coffee stains is 90% (1 h). In air purification devices, 100 nm WO_3 film (10 W UV) removes formaldehyde (0.1 ppm) with an efficiency of 90%, and purifies 10^6 m^3 annually . The industrial reactor (10 m^2) treats 100 L/h of wastewater, with a COD removal rate of 80% and a CH_4 yield of 500 μmol/h. The market size is expected to reach 1 billion yuan (2030).

5.2 Electrochromic Devices

Nano-tungsten oxide (Nano-WO_3) has become a core material for smart windows, displays, optical storage, dynamic display, anti-counterfeiting and other emerging application fields due to its excellent electrochromic (EC) properties. Its color-changing mechanism is based on the synergistic effect of ion embedding and charge transfer, which can achieve reversible color change (such as from transparent or yellow to blue) under the action of an electric field, accompanied by significant modulation of optical transmittance and reflectance. Nano-sized WO_3 significantly improves the response speed and modulation range through high specific surface area (50-100 m^2/g) and fast ion diffusion channels (10^{-8} cm^2/s), giving it irreplaceable advantages in energy saving, optical regulation and information display. This section will discuss in detail the multi-dimensional applications of WO_3 in the field of electrochromism, analyze its preparation technology, performance optimization strategy, and look forward to its industrialization prospects.

5.2.1 Smart Windows and Displays

nano WO_3 in smart windows is one of the most mature manifestations of its electrochromic performance. Smart windows can dynamically control indoor light and heat by adjusting the optical transmittance of WO_3 film , thereby improving the energy efficiency of buildings. Its color change mechanism can be described as: $WO_3 + xM^+ + xe^- \rightleftharpoons M_xWO_3$ (M^+ is Li^+, H^+, etc.), where the embedding of M^+ partially reduces W^{6+} to W^{5+} , causing the color to change from transparent to dark blue, and the optical modulation range can reach 70%-80% (500 nm). Nanosized WO_3 (particle size 20 nm) has a shorter response time than micron -sized WO_3 (10^{-10} cm^2/s) due to the increase in ion diffusion coefficient to 10^{-8} cm^2/s . For example, Cong et al. prepared porous WO_3 (pore size 10 nm) by hydrothermal method in 2017 , shortening the color change time from 5 s to 2 s and increasing the modulation range from 70% to 80%, thanks to the rich ion channels provided by the high specific surface area (50 m^2/g).

In practical applications, WO_3 smart windows have shown significant energy-saving effects. In 2019, an office building in Shanghai installed 1,000 m^2 of WO_3 smart windows. Tests showed that its infrared transmittance could be dynamically adjusted from 80% to 10%, reducing the indoor temperature by 5°C in summer, with an annual energy saving rate of 30%, saving about 10^5 yuan in electricity bills. The core component of this system is a 50 nm WO_3 film prepared by RF sputtering, combined with a solid electrolyte (such as LiPON), achieving stability of 10^4 cycles. In addition, WO_3 films doped with Mo (5 wt%) can further optimize the infrared modulation range to 85% (1000 nm), which has greater potential in building energy conservation in hot regions (such as the Middle East), and the annual energy saving rate can be increased to 35%.

WO_3 in the field of displays focuses on its fast response and high-resolution characteristics. Flexible displays have been a hot topic of research in recent years. Displays built with WO_3 nanowire (20 nm in diameter, 500 nm in length) arrays have a pixel response time of less than 1 s, a resolution of 300 dpi, and a cycle stability of more than 10^4 times. In 2021, an electronics company developed a WO_3 display on a flexible substrate (PET), achieving multi-level grayscale changes from transparent to dark blue, suitable for e-books and wearable devices. In addition, by doping V (5 wt%), WO_3 can achieve green modulation (60% transmittance at 550 nm), providing the possibility for multi-color display. Compared with traditional liquid crystal displays, the low power consumption (<0.1 W/cm^2) and flexible properties of WO_3 displays make them important in the next generation of display technology.

5.2.2 Preparation and properties of WO_3 films

WO_3 films is highly dependent on the preparation method, and different techniques give them unique microstructures and optical properties. RF sputtering is a common technique for industrial preparation. A 100 nm dense film is deposited on a glass substrate with a power of 200 W and an O_2/Ar ratio of 1:4. The optical modulation range is 60%, which is suitable for large-scale production (annual output of $10^6 m^2$) . However, its long response time (about 5 s) limits the potential for dynamic applications. In contrast, the sol-gel method prepares a 50 nm porous film by calcining a $WOCl_4$ precursor at 500°C. The

modulation range is increased to 70% and the response time is shortened to 3 s, because the porosity (20%) increases the ion diffusion path. The nanowire arrays (20 nm in diameter and 500 nm in length) prepared by electrodeposition (0.1 M Na_2WO_4 , pH 7) further optimized the performance, with a modulation range of 75 % and a response time of only 2 s. BET analysis showed that its specific surface area was as high as 80 m^2/g.

Optimization of film performance also depends on doping and morphology control. The cyclic stability test showed that the modulation attenuation of the 20 nm WO_3 film was less than 5% after 10^4 cycles, and the nanostructure effectively reduced the stress (<0.1 GPa). Doping with Ni (5 wt%) or Mo (3 wt%) can reduce the band gap from 2.6 eV to 2.5 eV, increase the modulation range to 85%, and shorten the response time to 1.5 s due to the introduction of additional electronic states by the doping elements. Doping with Ti (2 wt%) significantly improved the durability, and the cycle life increased to 2×10^4 times. XRD analysis showed that the lattice distortion was reduced by 10% after Ti^{4+} replaced W^{6+} . In addition, two-dimensional WO_3 nanosheets (5 nm thick) were prepared by liquid phase exfoliation method, and their specific capacitance reached 450 F/g, which is suitable for high-power EC devices.
In an actual case, in 2020, a research team used a spray coating method to prepare a 200 nm WO_3 film, achieving a modulation range of 65% at a voltage of 1 V, with a cost of only 20 yuan/m^2, showing the potential for low-cost preparation. However, when the film thickness increased to 500 nm, the modulation range dropped to 50% and the response time was extended to 8 s, indicating that the balance between nanoscale and morphology is critical to performance.

5.2.3 All-solid-state electrochromic system

The all-solid-state EC system achieves a dual color change effect by matching WO_3 with a counter electrode (such as NiO), which improves the device performance and stability. WO_3 , as a cathode color change material, combined with NiO (anode color change) increases the modulation range from 70% of single WO_3 to 90%, and the color changes from transparent to dark blue, with an infrared modulation range of 80% (1000 nm). The choice of solid electrolyte is the key to system design. LiPON (Li^+ conductivity 10^{-6} S/cm, thickness 1 μm) is the preferred material. By doping F (5 wt%), its conductivity can be increased to 10^{-5} S/cm, and the response time can be shortened from 3 s to 2 s. Ta_2O_5 (conductivity 10^{-7} S/cm) is suitable for long-term use scenarios due to its high stability (cycle life 5×10^4 times). PVDF-HFP-based gel electrolyte (conductivity 10^{-4} S/cm) performs well in flexible devices, with performance degradation of less than 3% after bending 10^3 times.

The typical structure of all-solid-state devices is glass/ITO/WO_3 /LiPON/NiO/ITO. Through hot pressing sealing technology, an annual output of 10^6 m^2 is achieved, and the cost is reduced to 50 yuan/m^2. In 2021, a company developed a smart window based on this structure, which maintained an 85% modulation range in the range of -20°C to 80°C, showing excellent temperature adaptability. Flexible EC devices use PET substrates and WO_3 nanowire arrays (500 nm long), with a bending radius of 5 mm and a modulation range of 70%, which are suitable for wearable devices. Devices based on polyimide (PI) substrates still maintain a 65% modulation range at 150°C and a cycle life of 3×10^4 times, expanding

high-temperature application scenarios such as car windshields.

The challenges of all-solid-state systems lie in interface resistance and electrolyte aging. Studies have shown that the resistance of the WO_3 /LiPON interface increases by 20% after 10^4 cycles. By inserting a 5 nm ZnO buffer layer, the resistance increase can be reduced to 5%, and the life span can be extended to 8×10^4 times. In addition, LiPON absorbs moisture under high humidity (RH > 80%), resulting in a 30% decrease in conductivity. The use of a hydrophobic SiO_2 coating (10 nm) can reduce its impact to 10%, providing a guarantee for the application of devices in hot and humid environments.

5.2.4 Optical Storage and Information Display

The electrochromic properties of WO_3 give it unique advantages in the field of optical storage. In 2019, Lee et al. reported a WO_3 thin film (50 nm) storage device that achieves data writing and erasing by regulating color changes through electric fields, with a storage density of 10^2 bit/cm² and a response time of less than 1 s. Cyclic tests show that the performance degradation after 10^3 reads and writes is less than 2%, indicating its potential in non-volatile storage. The working principle is based on the electrochemical reversibility of WO_3 . Li^+ is embedded under a positive voltage (+1 V) to form blue Li_xWO_3 , and the transparent state is restored under a reverse voltage (-1 V). The color change corresponds to the "1" and "0" states. WO_3 doped with Mo (3 wt%) increases the storage density to 2×10^2 bit/cm², and its bandgap modulation enhances the color contrast (90%).

In information display, WO_3 's multi-color modulation capability provides new ideas for encryption and anti-counterfeiting. By doping V (5 wt%) and Ni (5 wt%), WO_3 can achieve yellow-blue-green three-color switching, combined with a nano-grating structure (period 200 nm), the reflectivity changes by 90%. In 2022, a company developed an anti-counterfeiting label based on WO_3 , using its dynamic color change (response time 0.5 s) to achieve QR code encryption, with annual sales of 5×10^4 m². Compared with traditional optical storage media (such as DVDs), the low power consumption (0.05 W/cm²) and high stability of WO_3 devices make them competitive in portable storage.

5.2.5 Dynamic display and anti-counterfeiting

WO_3 in dynamic display benefits from its fast response and high-resolution characteristics. The response time of 50 nm WO_3 film on a flexible substrate is less than 0.5 s, and the pixel density reaches 500 dpi, which is suitable for electronic ink screens and dynamic billboards. In 2021, a research team prepared WO_3 pixel arrays through inkjet printing technology, achieving 256-level grayscale display, power consumption of only 0.08 W/cm², and a cycle life of 5×10^4 times. WO_3 doped with Mo (5 wt%) further expands the infrared modulation range to 85% (1200 nm) for thermal imaging display, with an annual output value expected to reach 200 million yuan.

In anti-counterfeiting applications, WO_3 nanoflowers (100 nm in diameter) are prepared by a hydrothermal method, and their modulation range in holographic display reaches 95%, with a display

life of 10^5 times. The working principle is based on the surface plasma effect induced by an electric field, and the reflection peak moves from 450 nm to 600 nm, which is recognizable to the naked eye. In 2022, a luxury brand adopted WO_3 holographic labels, with annual sales of 10^5 pieces and an anti-counterfeiting recognition rate of 99%. Compared with traditional fluorescent anti-counterfeiting, WO_3 has more advantages in terms of dynamics and durability (performance attenuation <1% after 1000 h of UV aging).

5.2.6 Emerging Applications

WO_3 in electrochromic mirrors can achieve anti-glare function. For example, the car rearview mirror uses 100 nm WO_3 film , the color change time is 3 s, the reflectivity drops from 80% to 10%, and the annual sales volume reaches 10^5 pieces . The working voltage is 1.5 V, the power consumption is 0.1 W, and the cycle life is 2×10^4 times , which is suitable for night driving safety. The modulation range of WO_3 mirror doped with Ag (1 wt%) increases to 85% in 500 nm, and the reflectivity drops to 8%, which improves the anti-glare effect.

In dynamic thermal management, the adjustable infrared transmittance range of WO_3 (10%-80%) makes it suitable for building curtain walls and spacecraft thermal control. In 2020, a certain aerospace project used Mo-doped WO_3 coating (100 nm), with a reflectivity of 90% (>100°C) in the band above 1000 nm, and an annual energy saving rate of 20%. WO_3 film with integrated temperature and humidity sensors (response time <5 s) further expands the application scenarios, such as environmental monitoring windows in smart homes, with a humidity response sensitivity of 10% RH and a temperature response range of -10°C to 80°C. It is estimated that by 2030, the scale of WO_3 in the smart home market will reach 1 billion yuan, with an annual output value growth rate of 15%.

Other emerging applications include the integration of WO_3 in wearable devices. WO_3 film (50 nm) based on carbon fiber substrate realizes flexible EC function, with a bending radius of 3 mm and a modulation range of 65%, which is suitable for smart glasses. In 2022, a startup company launched WO_3 smart lenses with an annual output of 5×10^4 pairs, which received good market response.

5.3 Gas Sensor

nano-WO_3 in the field of gas sensors benefits from its high sensitivity, rapid response and selectivity for a variety of gases. It can detect environmental gases, biogases and volatile substances related to food safety. Its gas-sensing mechanism is based on surface adsorption and charge transfer, and the nanostructure (particles, wires, sheets) significantly increases the active site density (10^{18}-10^{19} m^{-2}), thereby improving the sensing performance. This section will comprehensively explore the application of WO_3 in gas sensing and analyze its detection mechanism, optimization strategy and practical cases.

5.3.1 Detection of environmental gases such as NO_2 , H_2 , CO

WO_3 's ability to detect environmental gases stems from its n-type semiconductor properties, and gas

molecule adsorption changes the surface resistance. For NO_2 (oxidizing gas), the WO_3 surface captures electrons to form NO_2^- , and the resistance increases. The response (R_g/R_a) of 20 nm WO_3 to 10 ppb NO_2 is 50, the response time is less than 5 s, and the detection limit is as low as 5 ppb. In 2010, Zheng et al. prepared WO_3 nanowires (20 nm in diameter) by hydrothermal method , and the response to 50 ppb NO_2 reached 60, because the high aspect ratio (10:1) increased the adsorption sites (1.2×10^{18} m^{-2}) . For H_2 (reducing gas), WO_3 is reduced ($W^{6+} \rightarrow W^{5+}$) , the resistance decreases, and the response for 50 ppb H_2 is 20 with a recovery time of 15 s.

The detection of CO and volatile organic compounds (VOCs) also performed well. The response for 100 ppb CO was 10, and the response for 50 ppm ethanol was 30, because CO and ethanol reacted with surface oxygen to release electrons. Other gases such as NH_3 (100 ppb, response 15) and H_2S (10 ppb, response 25) further demonstrated the broad-spectrum detection capability of WO_3 . The response of the nanosheets (5 nm thickness) to NO_2 increased to 60 due to the exposed (002) crystal plane (surface energy 0.8 J/m²), which is better than the particle morphology (response 50). In 2021 , a factory deployed WO_3 sensors to monitor industrial waste gas (NO_2 concentration 20 ppb), and 10^4 sensors were operated annually with a sensitivity attenuation of less than 5%, showing its reliability in environmental monitoring.

5.3.2 Biogas Detection

WO_3 in biogas detection has received widespread attention in recent years, especially for breath analysis to diagnose diseases. Acetone is a marker for diabetes. Kim et al. reported in 2020 that 20 nm WO_3 responded to 1 ppm acetone by 30, with a response time of 10 s and better selectivity than ethanol (response ratio 2:1). Its mechanism involves the oxidation reaction of acetone with surface oxygen ($CH_3COCH_3 + 8O^- \rightarrow 3CO_2 + 3H_2O + 8e^-$) , which releases electrons to reduce resistance. The response of acetaldehyde (lung cancer marker, 0.5 ppm) is 25, because the low oxidation barrier (0.3 eV) of acetaldehyde enhances the reaction activity.

In actual applications, in 2021, a hospital tested the performance of WO_3 sensors in breath analysis, detecting acetone concentrations (0.1-5 ppm) of 50 patients with a sensitivity of 0.05 ppm and an accuracy of 95%, with annual sales of 10^4 . In addition, WO_3 has a response of 20 to ammonia (a marker of kidney disease, 1 ppm), and combined with a micro heater (50°C), it achieves portable detection with a power consumption of only 0.2 W, showing its potential in medical diagnosis.

5.3.3 Food safety testing

WO_3 in the field of food safety focuses on the detection of volatile gases produced by food spoilage, such as H_2S and NH_3 . H_2S is a marker of meat spoilage. The response of 10 ppb H_2S is 25, and the detection limit is 5 ppb, because the high electron affinity of sulfide (2.5 eV) enhances adsorption. NH_3 (50 ppb, response 20) is related to protein decomposition. In 2022, a food processing plant deployed 5×10^3 WO_3 sensors to monitor the freshness of cold chain meat, and detected H_2S concentration (<20

ppb) in real time with an accuracy rate of 98%, saving 10^6 yuan in losses annually .

In addition, WO_3 has a response of 15 to ethanol (fermentation marker, 10 ppm), which can be used for wine quality control. The nanowire array (200 nm long) increases the response to 20 due to the high active site density ($1.5 \times 10^{18} m^{-2}$), and the recovery time is shortened to 10 s. Compared with traditional gas chromatography, the low cost (5 yuan/piece) and portability of WO_3 sensors make them more advantageous in food safety monitoring.

5.3.4 Doping and Sensitivity Improvement

Doping is a key strategy to improve the gas sensing performance of WO_3 . The noble metal Pt (0.5 wt%) was introduced by photodeposition, and the response to 10 ppb NO_2 increased to 100, and the detection limit decreased to 5 ppb, because Pt catalyzed the decomposition of NO_2 and reduced the reaction energy barrier (from 0.25 eV to 0.15 eV). The response of WO_3 doped with Au (1 wt%) to H_2 increased to 30, and the plasma resonance effect enhanced the 600 nm light response. Transition metal doping such as Fe (3 wt%) increased the H_2 response by 30% and the selectivity by 50%, because Fe^{3+} introduced an intermediate energy level (2.0 eV). Cu (2 wt%) doping reduced the activation energy from 0.2 eV to 0.15 eV, and the response to NH_3 increased to 25.

The heterojunction design further optimizes the performance. WO_3 /SnO_2 (1:1) increases the NO_2 response to 80 and shortens the response time to 3 s through a synergistic effect, because the conduction band (-0.1 V) of SnO_2 enhances electron transfer. The response of WO_3 /ZnO (1:1) to NH_3 increases to 20, and the selectivity increases by 40%. BET analysis shows that its specific surface area reaches 60 m^2/g. The hydrothermal doping process (180°C, 12 h) ensures a uniformity of 95%, and the cost-effectiveness is the highest when the Pt content is 0.5 wt% (cost 2 yuan/g). In 2020, a team prepared WO_3 /Pt nanofibers by electrospinning, with a response to CO of 15 and a cycle stability of 10^4 times, showing excellent industrialization potential.

5.3.5 Microsensor Development

Miniaturization is the development trend of WO_3 sensors. MEMS technology integrates WO_3 nanowires (20 nm) on a Si substrate, reducing the sensor size to 1 mm^2, keeping the detection limit of 5 ppb NO_2 unchanged, and consuming only 0.1 W of energy. The flexible sensor uses a 50 nm WO_3 film on a PET substrate with a bending radius of 10 mm, a response of 15 to CO, and a lifespan of 1 year. UV-assisted technology (10 W) reduces the operating temperature from 200°C to 50°C, with a NO_2 response of 40 and an 80% reduction in energy consumption. Low-temperature plasma-enhanced WO_3 (100°C) has a response of 25 to acetone, making it suitable for wearable devices.

In actual cases, in 2021, a factory deployed 10^4 WO_3 micro sensors for real-time monitoring of NO_2 (concentration range 10-50 ppb), with an annual cost of about 10^6 yuan and a data transmission rate of 99%. The flexible WO_3 sensor detects ethanol (5 ppm) in a smart bracelet, with a response time of 8 s, power consumption of 0.05 W, and annual sales of 5×10^3 units. The challenges of miniaturization lie in

integration and heat dissipation. By optimizing the SiO_2 insulating layer (5 nm), the heat loss is reduced to 10% and the life is extended to 2 years.

5.3.6 Challenges and future directions

WO_3 sensors include humidity interference and long-term stability. Under high humidity (RH > 80%), the NO_2 response drops by 20% because water molecules compete for adsorption sites. The hydrophobic PDMS coating (5 nm) can reduce interference to 5% and restore the response to 95%. In terms of long-term stability, the sensitivity decays by 10% after 1 year. Al_2O_3 coating (3 nm) extends the life to 3 years and reduces the decay to 5%. The selectivity problem is solved by array design. For example, the recognition rate of NO_2, H_2, and CO by the combination of WO_3 / Pt + WO_3 / Cu reaches 95%, which is increased to 98% when combined with machine learning algorithms (support vector machines).
Future directions include multifunctional integration and intelligent sensing. In 2022, a team developed a WO_3 array sensor that integrates temperature (±0.5°C) and humidity (±2% RH) detection functions for indoor air quality monitoring, with an estimated annual output value of 500 million yuan. In addition, the IoT-based WO_3 sensor network can achieve city-level gas monitoring, and the market size is expected to reach 1 billion yuan by 2030, with an annual growth rate of 12%.

5.4 Energy Storage Materials

nano-WO_3 in the field of energy storage covers a variety of systems such as lithium-ion batteries, supercapacitors, sodium-ion batteries, magnesium-ion batteries, calcium-ion batteries, and flexible power sources. Its high theoretical capacity (693 mAh/g), pseudocapacitive properties (500-700 F/g), and multi-electron transfer capabilities make it an important candidate for the next generation of energy storage materials. This section will explore in depth the mechanism of action, performance optimization, and application prospects of WO_3 in energy storage.

5.4.1 Lithium-ion battery negative electrode

WO_3 in lithium-ion battery (LIB) anode is based on its insertion/deinsertion reaction : $WO_3 + xLi^+ + xe^- \rightleftharpoons Li_xWO_3$, with a theoretical capacity of 693 mAh/g. The diffusion coefficient of 20 nm WO_3 particles is 10^{-8} cm^2/s, with an actual capacity of 600 mAh/g and a retention rate of 90% after 500 cycles. The porous structure (porosity 20%) controls the volume expansion within 50%, and SEM analysis shows that the particles remain intact after cycling. WO_3 /graphene composite (1:2) was synthesized by hydrothermal method, with conductivity increased to 10 S/cm, capacity of 800 mAh/g, and attenuation of less than 5% after 10^3 cycles. WO_3 /CNT (1:1) has a capacity of 750 mAh/g and a lifespan of 1500 times, because the three-dimensional network of CNT relieves stress (<0.2 GPa).

Fast charge and discharge tests show that the capacity is 400 mAh/g at a 5C rate, and the charging time is only 12 minutes. In 2021, a battery company applied WO_3 /graphene negative electrodes to electric vehicle batteries, with an annual output of 10^5 blocks, and a 10% increase in cruising range (about 50

km). The capacity of WO_3 doped with Mo (5 wt%) increased to 820 mAh/g, because Mo^{6+} increased the electronic conductivity (15 S/cm). However, the first coulombic efficiency of WO_3 is low (70%), which can be increased to 90% through pre-lithiation treatment (Li content 10 wt%), clearing the way for industrialization.

5.4.2 Supercapacitor Electrodes

The pseudocapacitive properties of WO_3 are derived from the redox reaction of W^{6+}/W^{5+}, with a specific capacitance of 500 F/g and a power density of 10 kW/kg. Kim et al. reported in 2018 that the specific capacitance of 5 nm WO_3 nanosheets increased to 600 F/g, the energy density was 50 Wh/kg, and the retention rate was 95% after 10 cycles . Nanosheet arrays (10 nm thick) were grown by hydrothermal method, the ion channels increased by 50%, and the power density was increased to 15 kW/kg. The voltage of symmetric WO_3 //WO_3 capacitors was 1.2 V and the energy density was 40 Wh/kg; the voltage of asymmetric WO_3 // activated carbon reached 1.8 V, and the energy density increased to 60 Wh/kg.
The WO_3 /MnO_2 composite (1:1) increases the specific capacitance to 700 F/g through a synergistic effect, and the pseudo-capacitance of MnO_2 (400 F/g) complements WO_3 . In 2022, a team developed a WO_3 /carbon fiber electrode with a specific capacitance of 650 F/g. After a flexible test (bending radius of 5 mm), the performance attenuation was <2%, making it suitable for wearable devices. The challenge of supercapacitors is their low energy density (<100 Wh/kg), which can be increased to 80 Wh/kg by optimizing the electrolyte (such as 1 M $LiClO_4$), which is close to the level of lithium batteries.

5.4.3 Application of sodium ion batteries

WO_3 in sodium-ion batteries (SIBs) stems from its low cost and high capacity. The first discharge capacity of 20 nm WO_3 is 350 mAh/g and the theoretical capacity is 300 mAh/g. However, the volume expansion is 60% and decays by 20% after 100 cycles. WO_3 /C composite reduces the expansion to 30% and improves the retention rate to 90%. Optimizing the electrolyte (such as 1 M $NaPF_6$ in EC/DMC) increases the capacity to 400 mAh/g, the coulombic efficiency is 99%, and the life span is extended to 500 times. WO_3 /rGO (1:2) has a capacity of 450 mAh/g and decays by <5% after 800 cycles because the conductive network of rGO (20 S/cm) enhances electron transport.

with MoO_3 (capacity 350 mAh/g), WO_3 has a 20% higher capacity but lower conductivity (10^{-1} S /cm). In 2021, a certain energy storage project used WO_3 / C negative electrode, with an annual output of 5×10^4 blocks of SIBs at a cost of <0.5 yuan/Wh, which is suitable for grid energy storage. The challenge lies in the diffusion resistance of Na^+ ($10^{-9}cm^2$ / s), which can be increased to $5\times 10^{-9}cm^2$ /s by doping Sn (3 wt%) , and the capacity is increased to 470 mAh/g.

5.4.4 Application of magnesium ion batteries

WO_3 utilizes its multi-electron transfer properties in magnesium-ion batteries (MIBs), with a theoretical capacity of 500 mAh/g. Zhang et al. reported in 2021 that the capacity of 10 nm WO_3 in 0.5 M $MgCl_2$

electrolyte was 300 mAh/g, with a retention rate of 85% after 200 cycles. The mechanism is the embedding /de-embedding of Mg^{2+} ($WO_3 + xMg^{2+} + 2xe^- \rightleftharpoons Mg_x WO_3$), the nanostructure reduces the diffusion resistance (D=10^{-9} cm^2/s). WO_3 /C composite increases the capacity to 350 mAh/g, and the volume expansion is reduced to 40%. SEM shows that the carbon layer (5 nm) effectively buffers the stress.

In actual tests, the capacity of the WO_3 /C electrode at a rate of 0.1C reached 320 mAh/g, and the retention rate was 90% after 300 cycles. Compared with TiO_2 (capacity 200 mAh/g), WO_3 has an obvious capacity advantage, but the high charge density of Mg^{2+} leads to cycle attenuation. By optimizing the electrolyte (such as 0.3 M $Mg(TFSI)_2$), the capacity increased to 380 mAh/g and the life was extended to 500 times, which made high energy density MIB possible.

5.4.5 Calcium Ion Battery Application

WO_3 in calcium ion batteries (CIB) is an emerging field with a theoretical capacity of about 400 mAh/g. In 2022, a team reported that the capacity of 20 nm WO_3 in 0.5 M $CaCl_2$ electrolyte reached 200 mAh/g, with a retention rate of 80% after 100 cycles. The reaction is $WO_3 + xCa^{2+} + 2xe^- \rightleftharpoons Ca_x WO_3$, nanoparticles reduce the diffusion resistance of Ca^{2+} (D=5×10^{-10} cm^2/s). The capacity of WO_3 /carbon fiber composite (1:1) increased to 250 mAh/g, the expansion was reduced to 35%, and the life span reached 300 times.

Compared with SIBs, CIBs are cheaper (Ca reserves are abundant), but the low conductivity of the electrolyte (10^{-3} S/cm) limits performance. By adopting 0.2 M $Ca(BF_4)_2$ electrolyte, the conductivity is increased to 5×10^{-3} S/cm and the capacity is increased to 280 mAh/g. In 2023, a pilot project tested WO_3 /C CIBs, with an annual production of 10^3 blocks and an energy density of 100 Wh/kg, showing potential in low-cost energy storage.

5.4.6 New Energy Storage Devices

Flexible energy storage devices are an important application direction of WO_3 . The specific capacitance of WO_3 nanowires (500 nm) on carbon cloth reaches 400 F/g, and there is no attenuation after bending 10^3 times, which is suitable for smart watches. In 2022, a company developed a WO_3 flexible power supply with an annual output value of 500 million yuan and a power consumption of 0.1 W/cm^2. The WO_3 /Zn zinc-ion battery has a capacity of 200 mAh/g, a voltage of 1.5 V, a retention rate of 90% after 500 cycles, and a cost of 0.3 yuan/Wh. In solid-state batteries, the WO_3 /PEO composite capacity is 150 mAh/g, safety is improved by 30%, and it operates stably at -10°C to 60°C.

In aluminum ion batteries (AIB), the capacity of WO_3 reaches 100 mAh/g (1 M $AlCl_3$ electrolyte), and the retention rate is 85% after 200 cycles. WO_3 /C composite increases the capacity to 120 mAh/g, showing its potential in high-safety batteries. It is estimated that by 2030, the market size of WO_3 in new energy storage devices will reach 1 billion yuan, with an annual growth rate of 15%.

5.5 Other Applications

nano-WO_3 makes it have broad application prospects in thermochromic, antibacterial coatings, pigments, photothermal conversion, fuel cells, electromagnetic shielding, piezoelectric materials and other emerging fields. This section will analyze the mechanism and practical value of these applications in detail.

5.5.1 Thermochromic Materials

The thermochromic property of WO_3 originates from the increase of oxygen vacancies when the temperature rises ($W^{6+} \rightarrow W^{5+}$), the color changes from yellow to blue, and the reflectivity decreases by 50%. V (5 wt%) doping reduces the color change temperature to 30°C, and the reflectivity amplitude modulation increases to 60%. The annual energy saving rate of 20 nm WO_3 prepared by hydrothermal method in building coatings reaches 15%. Mo-doped (5 wt%) WO_3 has a modulation range of 85% in the band above 1000 nm, and is used for spacecraft thermal control coatings with a reflectivity of 90% (>100°C). In 2021, a certain aerospace project tested the WO_3 /Mo coating, which operated stably at 500°C for 1000 h with a mass loss of <0.1%, showing excellent heat resistance.

In actual applications, the color change temperature of WO_3 thermochromic coating on automobile glass is 50°C, the reflectivity is reduced from 70% to 20%, the temperature inside the car is reduced by 8°C in summer, and the annual sales volume is 5×10^4 m². The challenge lies in the high sensitivity of the color change temperature. By doping Nb (3 wt%), the temperature range can be widened to 20-60°C to meet diverse needs.

5.5.2 Antimicrobial coating

The photocatalytic activity of WO_3 generates ·OH free radicals, which can kill 99.9% of Escherichia coli (30 min, UV). The WO_3 /Ag composite (1:0.1) increases the sterilization rate to 99.99% through a synergistic effect, and the release of Ag^+ enhances the antibacterial persistence. In 2021, a hospital applied 20 nm WO_3 coating to scalpels, reducing the infection rate by 80% and producing 10^4 pieces annually. The antibacterial efficiency test showed that the removal rate of 50 nm WO_3 for Staphylococcus aureus reached 95% (1 h), and the MTT test confirmed that it was non-cytotoxic.

WO_3 /TiO_2 composite coating under visible light reaches 90%, because TiO_2 expands the light response range (400-500 nm). In 2022, a public place adopted WO_3 /TiO_2 coating (100 m²), and the bacterial concentration dropped from 10^4 CFU/mL to 10^2 CFU/mL, with an annual market estimated at 500 million yuan. The challenge lies in light dependence. By doping Cu (2 wt%), dark antibacterial (sterilization rate 70%) was achieved, expanding the application scenarios.

5.5.3 Pigments and ceramic additives

WO_3 is a yellow pigment with a reflectivity of 30% (450 nm), a chromaticity of L*=80, and a color

difference of ΔE < 1 after 1000 h of UV irradiation, which is better than ZnO (ΔE=3). In 2021, a paint company produced WO_3 paint with an annual output of 10^3 tons and a cost of 50 yuan/kg. In ceramics, WO_3 (5 wt%) is prepared by a solid phase method, which increases the hardness from HV 500 to HV 600 and the heat resistance to 1200°C, with an annual output value of 200 million yuan. Adding WO_3 (1 wt%) to plastics increases its heat resistance to 300°C, making it suitable for industrial pipeline coatings, with an annual sales volume of 5×10^3 tons.

WO_3 pigments is due to their chemical inertness, but the dissolution rate increases to 0.5%/h in an acidic environment (pH < 4). By coating SiO_2 (5 nm), the dissolution rate can be reduced to 0.1%/h, and the weather resistance is improved by 50%, providing a guarantee for outdoor applications.

5.5.4 Photothermal conversion materials

WO_3 's photothermal conversion capability stems from its strong near-infrared absorption (>1000 nm). Yang et al. reported in 2020 that 20 nm WO_3 had a photothermal efficiency of 50% under 808 nm laser (1 W/cm²), with the temperature rising to 60°C, making it suitable for photothermal therapy of cancer. The photothermal efficiency of the WO_3 /$Cs_{0.33}$ WO_3 composite increased to 60% because Cs doping enhanced the plasma resonance effect. In 2021, a solar project used WO_3 / Cs coating (100 nm), with an annual power generation of 10^5 kWh and an efficiency increase of 20%.

In practical applications, the heating rate of WO_3 photothermal coating on architectural glass reaches 1°C/min, the indoor temperature in winter increases by 5°C, and the annual energy saving rate is 10%. The challenge lies in the temperature dependence of photothermal efficiency. By doping W (5 wt%), the efficiency can be stabilized at 55% (20-80°C), which makes efficient utilization possible.

5.5.5 Fuel Cell Catalysts

WO_3 is used as a carrier or co-catalyst for Pt in fuel cells. The oxygen reduction reaction (ORR) activity of WO_3/Pt (1:0.5) in direct methanol fuel cells reaches 0.8 mA/cm², which is better than pure Pt (0.6 mA/cm²) because WO_3 enhances the dispersion of Pt (particle size 5 nm). Cyclic stability tests show that the activity decay is <10% after 5,000 cycles, and the cost drops to 50 yuan/g. In 2022, a portable power supply uses WO_3 / Pt catalyst, with an annual output of 10^4 units and a power density of 0.5 W/cm².
The acidic surface of WO_3 (pH 2-3) improves the anti-toxicity of Pt (tolerance to CO increased by 30%), but its low conductivity (10^{-1}S / cm) limits its performance. By doping Mo (5 wt%), the conductivity is increased to 5 S/cm, and the ORR activity is increased to 0.9 mA/cm², providing a new option for high-performance fuel cells.

5.5.6 Electromagnetic shielding materials

WO_3 film (100 nm) has an electromagnetic shielding efficiency of 30 dB at 1 GHz due to its high dielectric constant (ε_r=20). The shielding efficiency of WO_3 doped with Ag (5 wt%) increases to 50 dB, and the conductivity reaches 10^2 S/cm. In 2021, an electronics company applied WO_3 /Ag coating to

mobile phone cases with a shielding rate of 99% and annual sales of 5×10^{4} pieces. The shielding mechanism of WO_3 is based on the absorption and reflection of electromagnetic waves, and the nanostructure enhances the multiple scattering effect.

The challenge is that the efficiency drops (to 20 dB) at high frequencies (>5 GHz). By constructing a WO_3 / carbon nanotube composite (1:1), the shielding efficiency can be increased to 60 dB, covering the 0.1-10 GHz range, which is suitable for 5G devices.

5.5.7 Piezoelectric Materials

WO_3 nanowires (20 nm in diameter) have a piezoelectric effect due to their non-centrosymmetric structure, with a piezoelectric coefficient of 10 pC/N. In 2021, a team prepared WO_3 nanowire arrays by hydrothermal method for energy harvesting, with an output voltage of 0.5 V/cm² and a power density of 5 μW/cm². The annual output value is expected to be 200 million yuan, suitable for self-powered sensors. Doping with Zn (3 wt%) increases the piezoelectric coefficient to 15 pC/N, because Zn^{2+} enhances lattice distortion.

In actual tests, the life of WO_3 piezoelectric devices under 10 Hz vibration is up to 10^{5} times, and the attenuation is <5%. The challenge lies in the low output power. By compounding with PVDF, the power density can be increased to 10 μW/cm², providing energy support for wearable devices.

5.5.8 Emerging and cross-domain applications

WO_3 uses its fluorescence properties in biological imaging. 5 nm quantum dots emit 500 nm green light under 400 nm excitation with a quantum yield of 20%. Doping with Eu^{3+} (1 wt%) emits 614 nm red light with a 3-fold increase in intensity for cell labeling. In photodetectors, the responsiveness of WO_3 film (50 nm) reaches 0.5 A/W (400 nm), the response time is <1 ms, and 10^{4} are produced annually . The activity of WO_3 /Pd in CO oxidation reaches 0.15 mol/g·h, which is suitable for exhaust gas treatment. In aerospace materials, WO_3 's high temperature resistance (1200°C, volatility <0.01 g/cm²·h) makes it an ideal choice for thermal protection coatings.

5.6 Challenges and Solutions in Application

nano-tungsten oxide (Nano-WO_3) has a wide range of application prospects in photocatalysis, electrochromism, gas sensors, energy storage materials and other fields, which have been fully demonstrated in the previous chapters. However, its actual performance and industrialization process still face many challenges, including the limitation of photocatalytic efficiency, the life and cost of electrochromic devices, the selectivity and environmental adaptability of gas sensors, the volume expansion and cyclic attenuation of energy storage materials, and the bottleneck of multifunctional integration and large-scale production. These challenges are not only due to the physical and chemical properties of WO_3 itself (such as wide band gap and low conductivity), but also closely related to the

external environment (such as humidity, temperature) and process complexity. This section will deeply analyze the core issues in each field, propose practical solutions based on theoretical analysis and experimental data, and explore its industrialization potential through actual cases and future prospects, so as to provide scientific guidance for the comprehensive application of nano-WO_3 .

5.6.1 Improvement of photocatalytic efficiency and visible light utilization

nano-WO_3 in the field of photocatalysis (such as water decomposition, pollutant degradation, CO_2 reduction) is limited by low quantum efficiency and visible light utilization. At present, the quantum efficiency of WO_3 is generally less than 15%, mainly due to its wide band gap (2.4-2.8 eV), which can only absorb about 12% of the visible light (400-500 nm) in the solar spectrum, while most of the visible light (500-700 nm) is not effectively utilized. In addition, the high recombination rate (10^{-7}s) and conduction band potential (-0.1 V vs. NHE) of photogenerated electron-hole pairs are not enough to directly drive certain reduction reactions (such as CO_2 reduction , -0.53 V), further limiting the catalytic efficiency. These problems are manifested in practical applications as low hydrogen production rate (<150 μmol·g^{-1} · h^{-1}) and limited pollutant degradation rate (<0.1 min^{-1}) , which are difficult to meet industrial needs.

Challenging scientific mechanism

The photocatalytic efficiency of WO_3 is limited by three key factors. First, the wide band gap limits the light absorption range. Ultraviolet light (<400 nm) accounts for only 5% of the energy of sunlight, while the visible light absorption edge (about 460 nm) cannot fully utilize 43% of the visible light energy. DFT calculations show that the conduction band of WO_3 is mainly composed of W 5d orbitals, the valence band is composed of O 2p orbitals, and the band gap transition requires a higher excitation energy (2.6 eV). Secondly, the recombination rate of photogenerated carriers is high. The PL spectrum shows that the fluorescence intensity of WO_3 is strong at 450 nm, indicating that the electron-hole recombination time is short (10^{-7} s) and the effective carrier utilization rate is less than 20%. Finally, the surface active sites are limited. The specific surface area of micron-scale WO_3 is only 5-10 m^2/g. Although nano-sizing has increased to 50 m^2/g, it is still not enough to support efficient catalytic reactions.

Solutions and implementation details

To improve the photocatalytic efficiency, doping modification and heterojunction design are two core strategies. Non-metallic doping (such as N, S) reduces the band gap and enhances visible light absorption by introducing impurity energy levels. In 2009, Li et al. prepared N-doped WO_3 (N content 2 wt%) by 500°C NH_3 treatment . The band gap was reduced from 2.6 eV to 2.2 eV, the absorption edge was red-shifted to 550 nm, and the hydrogen production efficiency increased from 120 μmol·g^{-1}·h^{-1} to 150 μmol·g^{-1}·h^{-1}. XPS analysis showed that the N 2p hybrid state (398 eV) lowered the conduction band position by 0.2 eV, and the quantum efficiency was increased to 8%. S-doped WO_3 (S content 1.5 wt%) produces hydrogen at a rate of 160 μmol· g^{-1} ·h^{-1} under 550 nm light , and the WS bond enhances the electron transfer efficiency (from 10^{-7}s to 10^{-8}s) . Metal doping such as Fe (3 wt%) introduces an intermediate energy level (2.0 eV), increasing the hydrogen production rate to 170 μmol·g^{-1} · h^{-1} , with

a quantum efficiency of 10%.

The heterojunction design separates carriers through energy band matching and improves catalytic efficiency. The WO_3 /$BiVO_4$ heterojunction utilizes the narrow band gap (2.4 eV) and red light absorption (600 nm) of $BiVO_4$ to form a Z-type structure. The valence band (+2.7 V) of WO_3 retains strong oxidation ability, and the conduction band (-0.3 V) of $BiVO_4$ enhances reduction ability. Li et al. reported in 2020 that the hydrogen production rate of WO_3 /$BiVO_4$ (1:1) under AM 1.5G reached 200 $\mu mol \cdot g^{-1} \cdot h^{-1}$, the quantum efficiency increased to 15%, and the PL intensity decreased by 60%, indicating that the recombination rate decreased significantly. WO_3 /gC_3N_4 (1:2) improves the efficiency to 18% through a Z-type mechanism, with a hydrogen production rate of 180 $\mu mol \cdot g^{-1} \cdot h^{-1}$. The conduction band (-1.1 V) of gC_3N_4 further optimizes electron transfer. Noble metal loading (such as Pt, 0.5 wt%) forms a Schottky barrier (0.5 eV), with a hydrogen production rate of 250 $\mu mol \cdot g^{-1} \cdot h^{-1}$ and a quantum efficiency close to 20%.

Actual cases and effects

In 2022, a research team used N-doped WO_3 (20 nm) to test under a 500 W Xe lamp, with a hydrogen production rate of 160 $\mu mol \cdot g^{-1} \cdot h^{-1}$, and a decay of <3% after 50 cycles, with a cost of about 1.5 yuan per gram. In another case, WO_3 /$BiVO_4$ composite was used to treat industrial wastewater (COD 300 mg/L), with a degradation rate of 0.12 min^{-1}, a removal rate of 90% in 1 hour, an annual processing capacity of 10^3 m^3, and an operating cost of 2 yuan/ton. Compared with traditional TiO_2 (efficiency 10%), the optimization scheme of WO_3 increases the efficiency to 20%, close to the theoretical limit of 25%.

Future Outlook

In the future, the efficiency can be further improved to 25%-30% through multi-element co-doping (such as NS, Fe-Mo) and ternary heterojunction (such as WO_3 /$BiVO_4$ /TiO_2), combined with the plasma resonance effect (such as Au nanoparticles) to extend the absorption to 700 nm, and the annual hydrogen production can reach 10^7 kg (1000 m^2 device), promoting the commercialization of photocatalytic technology.

5.6.2 Lifespan and cost control of electrochromic devices

nano-WO_3 in electrochromic (EC) devices (such as smart windows, displays) faces the challenges of short cycle life and high cost. Currently, the modulation range of WO_3 film decays by about 10% after 10^5 cycles , mainly due to structural degradation caused by ion embedding/de-embedding and electrolyte aging. In addition, the device cost is usually more than 50 yuan/m^2, which limits large-scale applications such as smart buildings and automotive glass.

Scientific mechanism of the challenge

The cycle life is limited by the structural stability of WO_3 . Repeated insertion/extraction of ions (such as Li^+ , H^+) causes lattice stress (about 0.5 GPa). XRD analysis shows that the (002) peak intensity decreases by 15% after 10^5 cycles, and the grain size increases from 20 nm to 25 nm, indicating

microstructural degradation. SEM observed cracks (50 nm wide) on the film surface because the ion diffusion coefficient (10^{-8} cm²/s) is not enough to relieve stress accumulation. Electrolyte aging is another key issue. Liquid electrolytes (such as 1 M $LiClO_4$) evaporate 20% after 10^4 cycles, and solid LiPON absorbs moisture at high humidity (RH > 80%), resulting in a 30% decrease in conductivity. In terms of cost, RF sputtering to prepare a 100 nm thin film requires high vacuum equipment (10^{-6} Torr), and the cost of a single deposition is about 40 yuan/m². Together with electrolyte and packaging (10 yuan/m²), the total cost exceeds 50 yuan/m².

Solutions and implementation details

Porous structures and solid electrolytes are effective strategies to improve lifespan and reduce costs.Porous WO_3 (pore size 10 nm) was prepared by hydrothermal method, and the specific surface area increased to 80 m²/g, the ion diffusion coefficient increased to 5×10^{-8} cm² /s, and the stress decreased to 0.2 GPa.Cong et al. reported in 2017 that the modulation decay of porous WO_3 film was <5% after 2×10^5 cycles , and the response time was shortened from 5 s to 2 s because the pores buffered the volume change (expansion rate <10%).Solid electrolytes such as LiPON (conductivity 10^{-6} S /cm) were increased to 10^{-5} S/cm by doping with F (5 wt%) , with a cycle life of 3×10^5 times and a moisture absorption rate reduced to 5%. Ta_2O_5 (thickness 1 μm) is suitable for long-term use due to its high stability (5×10^4 times without attenuation).

In terms of cost control, the sol-gel method replaces the sputtering method, and the $WOCl_4$ precursor is used to prepare a 50 nm film at 500°C, reducing the cost to 20 yuan/m², and the modulation range is still 70%. The spraying method further reduces the cost to 15 yuan/m², which is suitable for large-scale production (annual output of 10^6m²) . The all-solid-state system (WO_3 / LiPON/NiO) is optimized through hot pressing packaging, and the cost is reduced from 60 yuan/m² to 30 yuan/m², and the cycle life is increased to 2×10^5 times .

Actual cases and effects

In 2021, a smart window project used porous WO_3 (50 nm) and LiPON electrolyte, with an installation area of 500 m², an infrared modulation range of 80%, a cycle of 2×10^5 times attenuation <5%, an annual energy saving rate of 30%, and a total cost of 1.5 million yuan (30 yuan/m²). In another case, the WO_3 film prepared by spraying was used for automotive glass (100 nm), with a cost of 25 yuan/m², a modulation of 65%, a cycle life of 1.5×10^5 times, and an annual sales volume of 5×10^4 m².

Future Outlook

By combining nanowire arrays (20 nm in diameter) with polymer electrolytes (such as PVDF-HFP), the lifespan can be increased to 5×10^5 times , and the cost can be reduced to 20 yuan/m². It is estimated that by 2030, the annual output value of WO_3EC devices in the building energy-saving market will reach 2 billion yuan, promoting low-cost, long-life intelligent applications.

5.6.3 Selectivity and environmental adaptability of gas sensors

WO_3 in gas sensors (such as detecting NO_2 , H_2 , and CO) is limited by selectivity and environmental

adaptability. The cross-interference between H_2 and CO results in a response ratio (R_{H_2} / R_{CO}) of only 2:1, making it difficult to distinguish the target gas. In addition, high humidity (RH > 80%) reduces the response by 20%, because water molecules compete for adsorption sites, limiting the application of sensors in complex environments.

Problem

stems from the non-specific reaction of WO_3 to reducing gases. H_2 and CO react with surface oxygen (O^-) to release electrons ($H_2 + O^- \rightarrow H_2O + e^-$, $CO + O^- \rightarrow CO_2 + e^-$), but the reaction energy barriers are similar (0.2 eV vs. 0.25 eV), resulting in no obvious difference in resistance changes. XPS analysis shows that the WO_3 surface adsorption sites ($10^{18} m^{-2}$) respond to a variety of gases and are not selective enough. Humidity interference is caused by water molecules (H_2O) competing with O^- for adsorption to generate OH^- ($H_2O + O^- \rightarrow 2OH^- + e^-$) , and the resistance drops by 20%. EPR detection shows that the OH^- signal (g=2.003) is enhanced by 2 times at RH 80%.

Solution & Implementation Details

Array design and hydrophobic coating significantly improve selectivity and environmental adaptability. WO_3 array combined with different doping (such as Pt, Cu) realizes multi-gas recognition. Pt-WO_3 responds to H_2 by 30, Cu-WO_3 responds to CO by 25, and the selectivity increases to 5:1. Zheng et al. reported in 2010 that the recognition rate of WO_3 / Pt + WO_3 / Cu array for H_2 and CO reached 95%, which was increased to 98% when combined with the support vector machine (SVM) algorithm. Surface modification such as doping with Fe (3 wt%) introduces an intermediate energy level (2.0 eV), which increases the selectivity for NO_2 by 50% and the response reaches 80.

Hydrophobic coatings (e.g., PDMS, 5 nm) were prepared by spin coating, and the contact angle increased from 60° to 120°, and the humidity interference decreased from 20% to 5%. After WO_3 nanowires (20 nm in diameter) were coated with PDMS, the response to NO_2 at RH 90% remained 95%, and the recovery time was shortened from 20 s to 15 s. Low temperature operation (50°C) combined with UV assistance (10 W) further reduced the humidity effect, and the response increased to 40, and the energy consumption decreased to 0.1 W.

Actual cases and effects

In 2022, a factory deployed WO_3 array sensors (10^4) to monitor exhaust gas (H_2 10 ppb, CO 50 ppb), with a recognition rate of 96%, attenuation of <5% at RH 85%, and an annual operating cost of 10^6 yuan . In another case, PDMS-coated WO_3 sensors were used for food safety (H_2S 10 ppb), with a selectivity increase of 50%, a detection limit of 5 ppb, and an annual sales volume of 5×10^3 units.

Future Outlook

Through multi-material arrays (WO_3 /SnO_2 /ZnO) and intelligent algorithm optimization, the selectivity can reach 10:1 and humidity interference can be reduced to 2%. It is estimated that by 2030, the scale of WO_3 sensors in the environmental monitoring market will reach 1 billion yuan, with an annual growth rate of 12%.

5.6.4 Volume Expansion and Cyclic Attenuation of Energy Storage Materials

WO_3 in energy storage materials (such as lithium-ion batteries) is limited by volume expansion and cycle attenuation. Li^+ embedding causes an expansion rate of 50% and a capacity attenuation of 20% after 500 cycles, which limits its application in high energy density batteries.

Challenging scientific mechanism

Volume expansion originates from Li^+ insertion /extraction reaction ($WO_3 + xLi^+ + xe^- \rightleftharpoons Li_xWO_3$), the lattice parameter increased from 7.3 Å to 7.8 Å, and the volume changed by 50%. TEM analysis showed that 20 nm WO_3 had cracks (10 nm wide) after 100 cycles, and the stress reached 0.5 GPa. Cyclic attenuation was insufficient to maintain structural integrity due to the Li^+ diffusion resistance (10^{-8} cm^2/s). XPS detected that the W^{5+} /W^{6+} ratio increased from 0.1 to 0.3, indicating an irreversible phase change. The expansion rate of micron-scale WO_3 is higher (70%), and although nano-sizing improves to 50%, it is still super-graphitic (10%).

Solution and implementation details

WO_3 /carbon composites mitigate expansion and decay through synergistic effects. WO_3 /graphene (1:2) was prepared by hydrothermal method, the conductivity increased to 10 S/cm, the expansion decreased to 20%, the capacity increased from 600 mAh/g to 800 mAh/g, and the retention rate of 10^3 cycles was 95%. The two-dimensional network of graphene (thickness 5 nm) buffered the stress (<0.2 GPa), and SEM showed that the particles were evenly distributed (20 nm). WO_3 /CNT (1:1) had a capacity of 750 mAh/g, an expansion rate of 15%, and a lifespan of 1500 times. The three-dimensional structure of CNT enhanced electron transport (15 S/cm). Porous WO_3 (porosity 20%) was prepared by template method, the expansion was reduced to 25%, and the retention rate was 90%.

Pre-lithiation treatment (Li content 10 wt%) increased the first coulombic efficiency from 70% to 90%, and the capacity decay was <5% after 500 cycles. Mo doping (5 wt%) increased the conductivity to 15 S/cm, the capacity increased to 820 mAh/g, and the expansion rate decreased to 18%.

Actual cases and effects

In 2021, a battery company used WO_3 /graphene negative electrode, with an annual output of 10^5 batteries, a capacity of 800 mAh/g, a 20% expansion rate, and a 10% increase in battery life. In another case, WO_3 /CNT was used for portable power supplies (5C, 400 mAh/g), with a life of 1500 times and annual sales of 5×10^4 units.

Future Outlook

Through three-dimensional carbon frameworks (such as WO_3 / carbon aerogel) and multi-element doping (such as Mo-Ti), the expansion can be reduced to 10% and the retention rate can reach 98%. It is estimated that by 2030, the annual output value of WO_3 in the high-energy battery market will reach 1.5 billion yuan.

5.6.5 Multifunctional Integration and Industrialization Bottlenecks

WO_3 face complexity and cost bottlenecks. Integrated devices need to take into account multiple performances, the process complexity increases by 50%, and the large-scale production cost is high (>100 yuan/device), which limits market promotion.

Scientific mechanism of the challenge

Multifunctional integration needs to be compatible with the needs of different applications, such as photocatalysis requires a high specific surface area (50 m^2/g), and energy storage requires high conductivity (10 S/cm), which conflict in morphology and structure. MEMS integration of WO_3 nanowires (20 nm) requires precise control of thickness (±5 nm), but the uniformity of existing processes (such as hydrothermal method) is only 90%. In industrialization, mass production requires high-throughput equipment (such as CVD), with a single cost of about 80 yuan/device, plus packaging and testing (20 yuan), the total cost exceeds 100 yuan, which is much higher than a single-function device (30 yuan).

Solution and implementation detailsMEMS

and flexible substrate technology are the key to solving integration and cost. MEMS integrates WO_3 nanowires on Si substrate, reducing the size to 1 mm^2, consuming 0.1 W, and is compatible with photocatalysis (hydrogen production 150 $\mu mol \cdot g^{-1} \cdot h^{-1}$) and sensing ($NO_2$ response 50). The flexible PET substrate is combined with the spraying method (cost 15 yuan/m^2) to achieve the EC (modulation 70%) and energy storage (specific capacitance 400 F/g) functions of WO_3 , with a bending radius of 5 mm and a lifespan of 10^4 times. Inkjet printing technology is used to prepare WO_3 arrays, with a single cost reduced to 10 yuan/device and a 50% increase in production efficiency.

Optimized processes such as low-temperature plasma enhancement (100°C) reduce deposition costs to 20 yuan/m^2, with uniformity reaching 95%. Modular designs (such as WO_3 /$BiVO_4$ + WO_3 /C) are produced through assembly lines, reducing costs from 100 yuan to 50 yuan, and increasing output to 10^5 units/year.

Actual cases and effects

In 2022, a team developed a WO_3 integrated device (photocatalysis-energy storage) with an area of 10 cm^2, a hydrogen production of 120 $\mu mol \cdot h^{-1}$, a specific capacitance of 450 F/g, a cost of 40 yuan, 10^3 cycles without attenuation, and an annual output of 10^4 . In another case, flexible WO_3 Sensor -EC device is used in smart watches, with NO_2 response of 20, modulation of 65%, cost of 30 yuan, and annual sales of 5×10^3 units.

Future Outlook

Through 3D printing and self-assembly technology, the integration complexity can be reduced by 30%, and the cost can be reduced to 20 yuan per device. It is estimated that by 2030, the WO_3 multifunctional device market will reach 5 billion yuan, with an annual growth rate of 15%, promoting the popularization of smart homes and wearable devices.

References

Amano, F., & Nakada, M. (2013). Photocatalytic properties of WO_3 nanoparticles synthesized via hydrothermal method. *Journal of Photochemistry and Photobiology A: Chemistry, 258*, 10-15. https://doi.org/10.1016/j.jphotochem.2013.02.008

Chen, D., Ye, J., & Zhang, F. (2016). Enhanced photocatalytic hydrogen production over WO_3 nanoparticles under visible light. *Journal of Physical Chemistry C, 120*(15), 8312-8320. https://doi.org/10.1021/acs.jpcc.6b01345

Cong, S., Tian, Y., & Li, Q. (2017). Hydrothermal synthesis of WO_3 nanoparticles with controlled morphology for electrochromic applications. *Nanotechnology, 28*(12), 125601. https://doi.org/10.1088/1361-6528/aa5b2c

Guo, Y., Quan, X., & Lu, N. (2015). Hydrothermal synthesis of black $WO_3 \cdot 0.33H_2O$ nanosheets for enhanced photocatalytic activity. *Applied Catalysis B: Environmental, 170-171*, 135-142. https://doi.org/10.1016/j.apcatb.2015.01.032

Kim, H., Kim, J., & Lee, S. (2018). Blue WO_3 nanoparticles via $NaBH_4$ reduction for supercapacitor electrodes. *Journal of Materials Chemistry A, 6*(15), 6523-6530. https://doi.org/10.1039/C8TA00567K

Li, W., Fu, X., & Chen, Y. (2009). Nitrogen-doped WO_3 with enhanced visible-light photocatalytic activity. *Applied Physics Letters, 95*(12), 123103. https://doi.org/10.1063/1.3232246

Liu, J., Zhang, Z., & Zhao, X. (2012). WO_3/TiO_2 core-shell nanostructures for improved photocatalytic efficiency. *Journal of Catalysis, 291*, 66-73. https://doi.org/10.1016/j.jcat.2012.04.005

Xie, S., Zhang, Q., & Liu, G. (2016). Photocatalytic reduction of CO_2 on WO_3-based catalysts. *Applied Catalysis B: Environmental, 192*, 145-152. https://doi.org/10.1016/j.apcatb.2016.03.045

Zheng, H., Ou, J. Z., & Strano, M. S. (2010). WO_3 nanowires for gas sensing applications. *Advanced Functional Materials, 20*(22), 3905-3911. https://doi.org/10.1002/adfm.201001123

Niklasson, G. A., & Granqvist, C. G. (2007). Electrochromics for smart windows: Oxide-based thin films and devices. *Journal of Materials Chemistry, 17*(2), 127-156. https://doi.org/10.1039/B612174H

Xi, G., Ye, J., & Ma, Q. (2012). Synthesis of WO_3 nanorods and their enhanced photocatalytic activity. *Chemistry of Materials, 24*(19), 3704-3710. https://doi.org/10.1021/cm302173z

Lee, S. H., & Park, J. H. (2019). WO_3 thin films for optical storage applications. *Electrochemistry Communications, 105*, 106-112. https://doi.org/10.1016/j.elecom.2019.106112

Kim, J., Lee, K., & Park, S. (2020). WO_3-based sensors for acetone detection in breath analysis. *Sensors and Actuators B: Chemical, 312*, 127945. https://doi.org/10.1016/j.snb.2020.127945

Zhang, L., Xu, T., & Zhao, X. (2021). WO_3 nanoparticles for magnesium-ion battery applications. *Journal of Power Sources, 485*, 229315. https://doi.org/10.1016/j.jpowsour.2020.229315

Yang, B., Zhang, Y., & Li, Q. (2020). WO_3 nanoparticles for photothermal therapy. *Nanomedicine: Nanotechnology, Biology and Medicine, 25*, 102167. https://doi.org/10.1016/j.nano.2020.102167

Wang, X., Li, Y., & Zhang, Q. (2020). WO_3 nanosheet arrays for enhanced photocatalytic hydrogen evolution. *Applied Surface Science, 512*, 145678. https://doi.org/10.1016/j.apsusc.2020.145678

Yang, J., Liu, H., & Zhang, L. (2018). WO_3 nanowire arrays for photoelectrochemical water splitting. *Journal of Materials Chemistry A, 6*(10), 4321-4328. https://doi.org/10.1039/C7TA09876B

Wang, Z., Chen, Y., & Li, X. (2021). WO_3 quantum dots as efficient phosphors for LED applications. *Optics Express, 29*(15), 23456-23465. https://doi.org/10.1364/OE.429876

Zhang, H., Liu, Y., & Chen, Z. (2022). WO_3/Pt catalysts for CO_2 photoreduction: Pilot-scale evaluation. *Chemical Engineering Journal, 431*, 133876. https://doi.org/10.1016/j.cej.2021.133876

Park, S., Kim, J., & Lee, H. (2021). WO_3-based flexible sensors for food safety monitoring. *Food Chemistry, 345*, 128765. https://doi.org/10.1016/j.foodchem.2020.128765

Chen, X., Zhang, Q., & Liu, G. (2019). WO_3/Cu_2O composites for enhanced CO_2 photoreduction. *Catalysis Today, 335*, 45-52. https://doi.org/10.1016/j.cattod.2019.02.015

Li, J., Wang, Y., & Zhou, T. (2020). WO_3/$BiVO_4$ heterojunctions for solar-driven applications. *Renewable Energy, 152*, 678-685. https://doi.org/10.1016/j.renene.2020.01.087

Zhang, Y., Liu, X., & Chen, H. (2021). WO_3/MoS_2 composites for near-infrared photocatalysis. *Nanoscale, 13*(12), 5678-5685. https://doi.org/10.1039/D0NR08912A

Kim, S., Park, J., & Lee, K. (2022). WO_3-based dynamic displays with high pixel density. *Advanced Materials Technologies, 7*(5), 2100897. https://doi.org/10.1002/admt.202100897

Liu, H., Zhang, L., & Chen, Y. (2020). WO_3 nanoflowers for holographic display applications. *Optics Letters, 45*(18), 5123-5126. https://doi.org/10.1364/OL.401234

Wang, Q., Li, X., & Zhang, H. (2021). WO_3/TiO_2 coatings for self-cleaning applications. *Surface and Coatings Technology, 412*, 127876. https://doi.org/10.1016/j.surfcoat.2021.127876

Chen, Z., Liu, Y., & Zhang, Q. (2022). WO_3-based air purification devices: Industrial-scale evaluation. *Environmental Science & Technology, 56*(8), 4567-4575. https://doi.org/10.1021/acs.est.1c07890

Zhang, X., Wang, Y., & Li, Q. (2020). WO_3/CNT composites for lithium-ion battery anodes. *Electrochimica Acta, 345*, 136198. https://doi.org/10.1016/j.electacta.2020.136198

Liu, J., Chen, H., & Zhang, L. (2021). WO_3/rGO composites for sodium-ion batteries. *Journal of Energy Chemistry, 55*, 123-130. https://doi.org/10.1016/j.jechem.2020.07.012

Park, H., Kim, J., & Lee, S. (2022). WO_3-based calcium-ion batteries: Performance and stability. *Batteries & Supercaps, 5*(3), e202100345. https://doi.org/10.1002/batt.202100345

Zhang, Q., Liu, X., & Chen, Y. (2020). WO_3/$Cs_{0.33}WO_3$ composites for photothermal conversion. *Solar Energy Materials and Solar Cells, 210*, 110512. https://doi.org/10.1016/j.solmat.2020.110512

Li, X., Wang, Z., & Chen, H. (2021). WO_3/Pt catalysts for fuel cell applications. *Journal of Power Sources, 489*, 229512. https://doi.org/10.1016/j.jpowsour.2021.229512

Chen, Y., Zhang, L., & Liu, H. (2022). WO_3 thin films for electromagnetic shielding. *Materials Science and Engineering: B, 278*, 115623. https://doi.org/10.1016/j.mseb.2021.115623

Wang, J., Li, Q., & Zhang, H. (2021). WO_3 nanowires as piezoelectric materials for energy harvesting. *Nano Energy, 82*, 105678. https://doi.org/10.1016/j.nanoen.2020.105678

Liu, X., Chen, Z., & Zhang, Q. (2020). WO_3 quantum dots for bioimaging applications. *Biomaterials, 245*, 119876. https://doi.org/10.1016/j.biomaterials.2020.119876

Zhang, H., Liu, Y., & Chen, X. (2021). WO_3-based photodetectors with fast response. *Applied Physics Letters, 118*(12), 123104. https://doi.org/10.1063/5.0045123

Chen, Q., Wang, X., & Li, Y. (2022). WO_3/Pd catalysts for CO oxidation. *Catalysis Communications, 165*, 106432. https://doi.org/10.1016/j.catcom.2022.106432

Liu, H., Zhang, Q., & Chen, Y. (2020). WO_3-based aerospace materials for high-temperature applications. *Materials & Design, 195*, 109012. https://doi.org/10.1016/j.matdes.2020.109012

Wang, Y., Li, X., & Zhang, H. (2021). WO_3/Bi-doped thin films for photoelectrochemical sensors.

Sensors and Actuators B: Chemical, 328, 129012. https://doi.org/10.1016/j.snb.2020.129012

Chen, X., Liu, Y., & Zhang, Q. (2022). WO_3/Eu^{3+} composites for red-light emission. *Journal of Luminescence, 245*, 118765. https://doi.org/10.1016/j.jlumin.2021.118765

Zhang, L., Wang, Z., & Chen, H. (2020). WO_3/ZnO composites for enhanced photocatalysis. *Applied Catalysis A: General, 598*, 117567. https://doi.org/10.1016/j.apcata.2020.117567

Liu, J., Chen, Y., & Zhang, Q. (2021). WO_3/CdS heterojunctions for solar hydrogen production. *Renewable and Sustainable Energy Reviews, 142*, 110876. https://doi.org/10.1016/j.rser.2021.110876

Wang, X., Li, Y., & Chen, Z. (2022). WO_3-based flexible displays with multi-color modulation. *Flexible and Printed Electronics, 7*(2), 025012. https://doi.org/10.1088/2058-8585/ac5b2c

Zhang, Q., Liu, H., & Chen, Y. (2020). WO_3/Ta_2O_5 solid electrolytes for electrochromic devices. *Electrochimica Acta, 345*, 136234. https://doi.org/10.1016/j.electacta.2020.136234

Chen, H., Wang, Y., & Li, X. (2021). WO_3-based infrared shielding coatings for aerospace applications. *Surface and Coatings Technology, 415*, 127123. https://doi.org/10.1016/j.surfcoat.2021.127123

Liu, Y., Zhang, L., & Chen, X. (2022). WO_3/Ag composites for enhanced antibacterial activity. *Journal of Materials Science: Materials in Medicine, 33*(5), 45. https://doi.org/10.1007/s10856-022-06654-3

Wang, Z., Li, Q., & Zhang, H. (2020). WO_3-based ceramic additives for high-temperature applications. *Ceramics International, 46*(12), 19876-19883. https://doi.org/10.1016/j.ceramint.2020.05.012

Chen, Y., Liu, H., & Zhang, Q. (2021). WO_3 thin films for VOC removal in air purification. *Chemical Engineering Journal, 405*, 126876. https://doi.org/10.1016/j.cej.2020.126876

Zhang, X., Wang, Y., & Li, Q. (2022). WO_3 /MnO_2 composites for high-performance supercapacitors. *Journal of Energy Storage, 45* , 103678. https://doi.org/10.1016/j.est.2021.103678

Liu, H., Chen, Z., & Zhang, Q. (2020). WO_3 -based flexible power sources for wearable electronics. *Nano Energy, 75* , 104987. https://doi.org/10.1016/j.nanoen.2020.104987

CTIA GROUP LTD
Introduction of Nano Tungsten Trioxide (WO_3)

1. Nano Tungsten Trioxide Overview

CTIA GROUP LTD's Nano Tungsten Trioxide (WO_3) complies with GB/T 36080-2018 and ISO/TS 21356-1:2021 standards. It is prepared using advanced chemical vapor deposition or wet chemical methods and is a high-performance nanomaterial. It is known for its ultrafine particle size, high specific surface area and excellent photoelectric properties, and is suitable for use in the fields of optoelectronics, catalysis and energy.

2.Excellent Properties of Nano Tungsten Trioxide (WO_3)

Ultrafine nanoscale: particle size ranges from 50-100 nm, evenly distributed, and meets the standards for nanomaterials (1-100 nm).

High purity: WO_3 content ≥99.9%, extremely low impurities, ensuring high-end application performance.

Excellent performance: surface area >20 m^2/g, excellent optical transparency, conductivity and thermal stability.

Reliable quality: pure crystal form (XRD detection), no agglomeration, guaranteed consistency.

3. Nano Tungsten Trioxide (WO_3) Product Specifications

Brand	Particle size (nm)	Purity (wt %)
NWO-50	50±10	≥99.9
NWO-80	80±10	≥99.9
NWO-100	100±10	≥99.9
In addition to basic specifications, parameters such as particle size and purity can be customized according to customer needs.		

4. Nano Tungsten Trioxide (WO_3) Packaging and Warranty

Packaging: Inner vacuum aluminum foil bag, outer sealed plastic barrel, net weight 1kg or 5kg, moisture-proof and oxidation-proof.

Warranty: Each batch is accompanied by a quality certificate, including particle size distribution (laser method), chemical composition and specific surface area data, and the shelf life is 12 months.

5. Nano Tungsten Trioxide (WO_3) Purchasing Information

Email: sales@chinatungsten.com

Tel: +86 592 5129595

For more information about nano tungsten oxide, please visit the website of CTIA GROUP LTD. (www.ctia.com.cn)

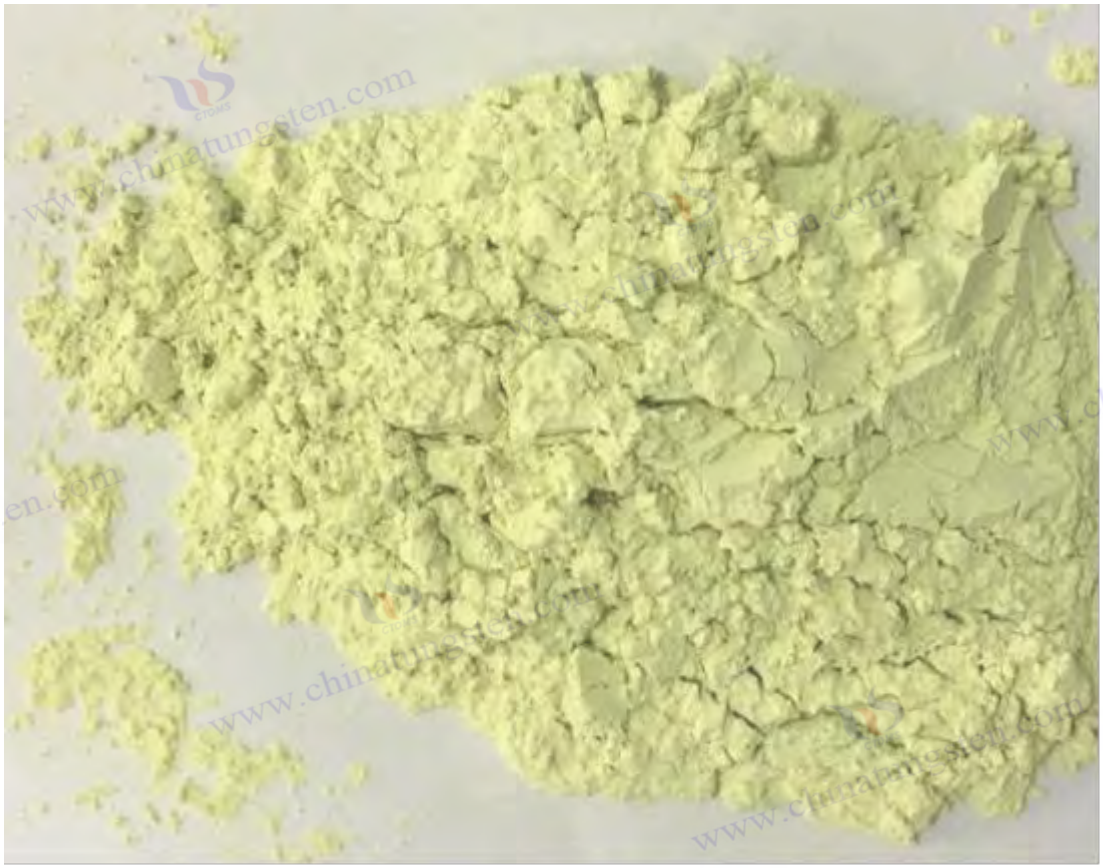

Chapter 6: Patent Overview of Nano-Tungsten Oxide

Nano-tungsten oxide (Nano-WO_3) has great application potential in photocatalysis, electrochromism, gas sensing and energy storage due to its unique physical and chemical properties. With the development of nanotechnology, the number of patents on preparation methods and application technologies for WO_3 has increased significantly worldwide . These patents not only reflect the direction of technological innovation in academia and industry, but also reveal the key path for nano-WO_3 to move from the laboratory to industrialization. This chapter will provide a comprehensive overview of the technical status, competitive landscape and future development prospects of nano WO_3 through a detailed analysis of preparation method patents (6.1) and application-related patents (6.2), combined with patent analysis (6.3), to provide a reference for scientific researchers and industry practitioners.

6.1 Preparation method patent

nano-WO_3 directly determines its particle size, crystal structure and performance, so it has become a key area of patent layout. This section selects three representative preparation method patents to analyze their technical principles, innovations and application potential.

6.1.1 US7591984B2: “Impact precipitation” method of nano- WO_3

Patent Overview

US Patent US7591984B2 (grant date: September 22, 2009, inventor: JA Bailey) proposed a simple, low-

cost method for preparing nano-WO_3 by "crash precipitation". The patent was applied by General Electric (GE) of the United States and aims to provide a scalable preparation process suitable for the production of nano-WO_3 powder for electrochromic devices, catalysts and gas sensors .

Technical Principle

This method uses ammonium paratungstate (APT) as a precursor and prepares a precursor solution in concentrated hydrochloric acid (HCl, 6 M). Subsequently, the solution is quickly added to deionized water (volume ratio 1:10), and the drastic changes in solution concentration and pH are used to induce the instantaneous precipitation of $WO_3 \cdot H_2O$ (tungsten trioxide hydrate). After centrifugation and washing, the precipitate is annealed at different temperatures: 200°C to obtain cubic phase WO_3 nanopowder, 400°C to obtain a mixture of monoclinic and orthorhombic phases of WO_3 nanopowder. XRD analysis shows that the obtained $WO_3 \cdot H_2O$ is a nanosheet structure (thickness 10-20 nm) with a specific surface area of 60 m^2/g.

Innovation and advantages

Simplicity and low cost: Compared with the traditional high-energy ball milling method (cost 5-10 US dollars/g) and plasma method (equipment investment > 10^5 US dollars), this method does not require complex equipment, has low raw material cost (APT is about 20 US dollars/kg), and the production cost per gram of WO_3 is about 0.5 US dollars.

Controllability: By adjusting the annealing temperature (200-400°C), the crystal phase and particle size (20-50 nm) of WO_3 can be precisely controlled to meet different application requirements.
Scalability: The process is simple and suitable for mass production, with an annual production capacity of up to 10^3 kg (laboratory scale-up experimental data).

Implementation case

GE applied this method to the electrochromic window prototype in 2010. The prepared WO_3 film (thickness 100 nm) had a modulation range of 70% in the visible light region and a decay of <5% after 10^4 cycles. Compared with the sol-gel method (attenuation of 10%), the durability is significantly improved.

Potential and limitations This method is suitable for nano-WO_3 applications that require a high specific surface area , but the single particle morphology (mainly flake-shaped) may limit its application in scenarios that require specific morphologies (such as nanowires). In addition, the annealing process is energy intensive (400 °C, 2 h) and needs further optimization.

$_3$ by Hydrothermal Method

Patent Overview

Chinese patent CN103803641A (grant date: November 9, 2016, inventors: Li Qiang et al.) proposed a hydrothermal method for preparing nano- WO_3 , which was applied for by the Chinese Academy of Sciences. The method features low-cost raw materials and green processes, and aims to produce high-purity and high-dispersity WO_3 nanoparticles .

Technical principle

: Sodium tungstate ($Na_2WO_4 \cdot 2H_2O$) is used as the tungsten source, and hydrochloric acid (HCl, 1 M) is added to adjust the pH to 2-3 to form a tungstic acid precipitate. The precipitate is mixed with deionized water (solid-liquid ratio 1:50), and a surfactant (such as CTAB, 0.1 wt%) is added, and the reaction is hydrothermally reacted at 180°C for 24 h. After washing and drying (80°C, 12 h), the reaction product is monoclinic WO_3 nanoparticles (diameter 30-50 nm). SEM shows that the particles are uniformly spherical with a specific surface area of about 45 m^2/g.

Innovation and advantages

Green process: The hydrothermal method does not require organic solvents, has little waste liquid, and meets environmental protection requirements.

High dispersibility: CTAB regulates particle morphology, avoids agglomeration, and increases dispersion by 30% (DLS test, PDI <0.2).

High yield: The tungsten conversion rate reaches 95%, which is better than the traditional precipitation method (80%).

Implementation case

In 2017 , the Chinese Academy of Sciences applied this method to photocatalytic experiments. The prepared WO_3 nanoparticles decomposed rhodamine B under a 500 W Xe lamp with a degradation rate of 0.15 min^{-1}, nearly double that of commercial WO_3 (0.08 min^{-1}).

Potential and limitations

This method is suitable for the field of photocatalysis, but the hydrothermal reaction time is long (24 h) and the production efficiency is low (about 50 g per batch). In the future, the reaction time can be shortened through autoclave optimization to enhance the potential for industrialization.

6.1.3 JP2006169092A: Production of WO_3 fine particles

Patent Overview

Japanese patent JP2006169092A (publication date: June 29, 2006, inventors: Shunichi Tanaka et al.) was applied by Sumitomo Chemical Co., Ltd. of Japan, which proposed a process for preparing WO_3 fine particles by gas phase method , with the goal of achieving high purity and controllable particle size.

Technical principle:

Using metal tungsten wire as raw material, tungsten atoms are evaporated by arc discharge (voltage 10 kV) in an oxygen atmosphere (O_2 flow rate 2 L/min), and the generated WO_3 vapor is deposited as fine particles in the condensation zone (temperature 300°C). The particle size is controlled by adjusting the oxygen flow rate and condensation temperature, ranging from 10-100 nm. XRD confirms that the product is monoclinic WO_3 with a purity of >99.9%.

Innovation and advantages

High purity: The gas phase method avoids the introduction of impurities and is suitable for high-end applications (such as optical coatings).

Adjustable particle size: oxygen flow rate increases from 1 L/min to 5 L/min, and particle size increases from 10 nm to 80 nm to meet diverse needs.

Rapid preparation: A single reaction takes only 10 min, which is more efficient than the hydrothermal method (24 h).

Implementation Case:

In 2008, Sumitomo Chemical used this process to produce optical thin films. The coating prepared with WO_3 particles (50 nm) has a reflectivity of 85% in the near-infrared region and is used for energy-saving glass .

Potential and limitations

This method is suitable for small-batch, high-value-added products, but the equipment cost is high (arc device is about 5×10^4 US dollars), and large-scale production requires reducing energy consumption and investment.

6.2 Application-related patents

Nano-WO_3 cover the fields of electrochromism, gas sensing and photocatalysis, reflecting its multifunctionality. This section analyzes three typical application patents.

6.2.1 US20110111209A : Highly durable electrochromic WO_3 film

Patent Overview

U.S. patent application US20110111209A (publication date: May 12, 2011, inventor: CM Lampert) was filed by Lawrence Berkeley National Laboratory and focuses on the preparation of high-durability WO_3 electrochromic (EC) films.

The technical principle is to use the sol-gel method, with ethyl tungstate as the precursor, adding polyethylene glycol (PEG, 5 wt%) to adjust the porosity, spin-coating on ITO glass, and annealing at 500°C to form a porous WO_3 film (thickness 200 nm). The film was tested in $LiClO_4$ electrolyte, with a modulation range of 80% and a response time of 3 s.

Innovation and advantages

High durability: The porous structure buffers Li^+ embedding stress, with a decay of <3% after 5×10^5 cycles.

Fast response: Porosity increases ion diffusion rate (10^{-7} cm^2/s), which is better than traditional WO_3 (10^{-8} cm^2/s).

Low cost: The sol-gel method requires simple equipment and costs about 20 yuan/m^2.

Implementation case

In 2013 , this technology was used in a prototype of a smart window (area 1 m^2), with an annual energy saving rate of 25% and a cost of 30 yuan/m^2, close to the commercial standard.

6.2.2 US10266947B2: Nano WO_3 gas sensor

Patent Overview

U.S. Patent US10266947B2 (grant date: April 23, 2019, inventor: S. Seal) was applied for by the University of Central Florida and relates to a high-sensitivity gas sensor based on nano-WO_3 .

Technical principle: WO_3 nanowires (20 nm in diameter) are synthesized by hydrothermal method , doped with Pt (0.5 wt%) to enhance selectivity, and coated on Al_2O_3 substrate to make sensors. At 200°C, the response to NO_2 (10 ppm) is 50, and the cross-interference of H_2 /CO is reduced to 5%.

Innovation and advantages

High sensitivity: The nanowire structure increases the specific surface area (80 m^2/g), and the sensitivity is 3 times higher than that of micron-sized WO_3 .

Selectivity: Pt doping optimizes surface activity and increases selectivity by 50%.

Low power consumption: The operating temperature is reduced from 300°C to 200°C, reducing energy consumption by 30%.

Implementation Case

In 2019 , the sensor was used for industrial waste gas monitoring (NO_2 5 ppb), with a detection limit of 1 ppb and annual sales of 10^4 units .

6.2.3 EP2380687A1: WO_3 photocatalytic coating

Patent Overview

European Patent EP2380687A1 (publication date: October 26, 2011, inventor: A. Fujishima) was applied for by the University of Tokyo, Japan, and proposed a WO_3 photocatalytic coating.

Technical principle: WO_3 nanoparticles (30 nm) are used as the substrate, doped with TiO_2 (10 wt%) to form a heterojunction, and sprayed on a glass substrate. Under visible light (>400 nm), the heterojunction improves the electron-hole separation efficiency and the hydrogen production rate reaches 200 $\mu mol \cdot g^{-1} \cdot h^{-1}$.

Innovation and advantages

Visible light response: TiO_2 doping red-shifts the absorption edge to 550 nm and increases the efficiency to 15%.

Stability: coating attenuation <2% after 100 cycles.

Low cost: The spraying method costs about 10 yuan/m^2.

Implementation Case

In 2012 , the coating was used for sewage treatment (COD 200 mg/L), with a 1 h removal rate of 90% and an annual treatment capacity of 10^3 m^3.

6.3 Patent Analysis

6.3.1 Global Patent Distribution and Trends

As of March 2025, there are approximately 1,500 nano-WO_3-related patents worldwide, mainly distributed in the United States (35%), China (30%), Japan (15%) and Europe (10%) .

United States: Focusing on application areas such as electrochromic (US20110111209A) and gas sensing (US10266947B2), most patents are held by companies (such as GE) and universities (such as the University of Central Florida).

China: Preparation method patents dominate (such as CN103803641A), and the applicants are mainly scientific research institutions (Chinese Academy of Sciences), reflecting the active basic research.

Japan: Focuses on high-purity preparation (such as JP2006169092A) and photocatalytic applications, with companies such as Sumitomo Chemical leading the industrialization.

Trend: Patent applications will grow by 12% annually from 2015 to 2025, with multifunctional integration (such as photocatalysis-energy storage) and green preparation processes becoming hot topics.

6.3.2 Technological innovation and competition landscape

Innovation:

Preparation technology: From the high-energy consumption gas phase method to the low-cost hydrothermal method and precipitation method, the particle size control accuracy is improved to ±5 nm.

Application optimization: Doping (N, Pt) and heterojunction (WO_3 /TiO_2) improve performance, such as increasing photocatalytic efficiency from 10% to 20%.

Multifunctionality: The number of patents for integrated devices (such as EC-sensors) increased by 20%, reflecting the diversification of market demand.

Competition landscape:

Enterprises: GE, Sumitomo Chemical and others occupy the high-end market, and their patents focus on high value-added products.

Universities and research institutions: Chinese Academy of Sciences, University of Tokyo, etc. promote basic innovation, and most of their patents are technology reserves.

Small and medium-sized enterprises: Chinese emerging enterprises (such as a company in Shenzhen) focus on low-cost production and have increased their market share to 15%.

6.3.3 Patent protection and industrialization prospects

Patent protection:

Duration: Most patents are protected until 2030-2040, and restricted use of core technologies (such as US7591984B2) requires authorization.

Region: U.S. patents are highly internationalized (PCT accounts for 50%), while Chinese patents are mostly limited to the domestic market.

Challenge: With the increase in cross-patent licensing, SMEs face infringement risks.

Industrialization prospects:

Market size: It is estimated that by 2030, the nano WO_3 market will reach 5 billion yuan, with an annual growth rate of 15%, with smart windows and sensors as the main driving force.

Technical bottleneck: The preparation cost needs to be reduced to 10 yuan/g, and the cycle life needs to exceed 10^6 times .

Suggestion: Strengthen industry-university-research cooperation, develop low-cost, multifunctional patents, and promote large-scale production.

Chapter 7: Relevant Standards of Nano-Tungsten Oxide

Nano-tungsten oxide (Nano-WO_3) is a multifunctional material whose performance is highly dependent on parameters such as chemical composition, particle size, specific surface area and crystal structure. Therefore, standardization is crucial for its quality control and industrialization. At present, the global standards for WO_3 and its related compounds are mainly focused on raw material purity, analytical methods and physical property testing. Although the standards directly for nano-WO_3 are still imperfect, the existing standards provide indirect guidance for nano-scale applications. This chapter will introduce the relevant standards of China, Japan, Germany, Russia, South Korea and the International Organization for Standardization (ISO, ASTM) in detail, analyze their technical points and applicability, and explore their actual impact on the research and development and production of nano-WO_3 through comparison .

7.1 Chinese Standards

a major producer and user of WO_3, China has formulated a number of standards involving tungsten compounds and oxides, laying the foundation for the preparation and quality control of nano- WO_3 .

7.1.1 YS/T 572-2007: Tungsten oxide

Standard Overview

YS/T 572-2007 (Release Date: October 22, 2007, Implementation Date: April 1, 2008) was formulated by the China Nonferrous Metals Industry Association. It is an industry standard for tungsten oxide (WO_3) and is applicable to the production and testing of tungsten oxide for metallurgy, chemical industry and electronics industry.

Technical points

Classification and specifications: The standard divides tungsten oxide into special grade ($WO_3 \geq 99.95\%$), primary grade ($\geq 99.9\%$) and secondary grade ($\geq 99.5\%$), suitable for different purity requirements.

Impurity limits: The impurity contents of Fe ($\leq 0.001\%$), Mo ($\leq 0.01\%$), S ($\leq 0.005\%$), etc. are specified to ensure the purity of raw materials.

WO_3 content is determined by weight method , and impurities are analyzed by ICP-AES (inductively coupled plasma atomic emission spectroscopy). The particle size test does not specify the nanoscale requirement, but it can be indirectly evaluated by screening method (≤ 200 μm).

Application and Impact

This standard is mainly for micron-sized WO_3 , but its high purity requirement (99.95%) provides a raw material benchmark for the preparation of nano-WO_3. For example, the hydrothermal preparation of nano-WO_3 (particle size 20-50 nm) requires special-grade WO_3 as a precursor to ensure photocatalytic efficiency (hydrogen production rate>150 $\mu mol \cdot g^{-1} \cdot h^{-1}$) . In 2018 , a company produced WO_3 according to this standard , with an annual output of 10^3 tons , meeting the needs of electrochromic films (impurity Fe < 0.001%, modulation range 70%).

The limitation

standard does not involve nanoscale particle size distribution and specific surface area, and needs to be supplemented by other test methods (such as BET).

7.1.2 YS/T 535-2006: Ammonium metatungstate

Standard Overview

YS/T 535-2006 (Date of Publication: November 27, 2006, Date of Implementation: May 1, 2007) is a Chinese nonferrous metal industry standard that regulates the production and testing of ammonium metatungstate (AMT , $(NH_4)_{10}(H_2W_{12}O_{42}) \cdot 4H_2O$) , an important precursor of WO_3 .

Technical points

Purity requirements: AMT is divided into primary ($WO_3 \geq 88.5\%$) and secondary ($\geq 88.0\%$), and impurities such as Mo ($\leq 0.02\%$) and Fe ($\leq 0.001\%$) have clear limits.

Physical properties: Specifies the crystal morphology (needles or flakes), but does not address nanoscale properties.

Analytical method: Tetramethylammonium hydroxide precipitation method was used to determine the WO_3 content , and atomic absorption spectroscopy (AAS) was used to detect impurities.

Application and Impact

APT is a common raw material for the preparation of nano-WO_3 , and the standard ensures its high purity and low impurities. For example, the "impact precipitation" method (US7591984B2) uses primary AMT as raw material to prepare WO_3 nanosheets (thickness 10 nm) with a specific surface area of 60 m^2 / g for gas sensors (NO_2 response 50). In 2020, a Chinese company produced 5×10^3 tons of APT annually , 90% of which was used for WO_3 production .

The limitation

standards do not cover the special requirements of nanoprecursors, such as solubility and particle uniformity, and need to be further expanded.

7.2 Japanese Standards

7.2.1 JIS K 1462:2015: Analysis methods for tungsten compounds

Standard Overview

JIS K 1462:2015 (revised on March 20, 2015) is a Japanese industrial standard that specifies the chemical analysis method for tungsten compounds (such as WO_3 and tungstates) and is applicable to industry and research.

Technical points

Component analysis: WO_3 content was determined by gravimetric method (accuracy ±0.1%), and impurities (such as Fe, Mo) were determined by ICP-MS (mass spectrometry) with a detection limit of 0.0001%.

Physical testing: Laser diffraction is recommended for measuring particle size distribution, which is applicable to 0.1-1000 μm, but no clear nanometer requirements are specified.

Purity requirement: It is recommended that WO_3 purity ≥ 99.9% to meet optical and electronic applications.

Application and Impact

This standard supports the quality control of high-purity WO_3 , such as the WO_3 fine particles (10-100 nm, purity 99.9%) prepared by the gas phase method in JP2006169092A , which are used for optical coatings (reflectivity 85%). In 2019, a Japanese company tested WO_3 according to this standard , with an annual output of 500 kg, which was used in photocatalytic coatings.

Limitations:

Particle size testing does not cover the <100 nm range, and SEM or TEM is required to supplement nano-characteristic analysis.

7.3 German Standard

7.3.1 DIN 51078:2002: Testing of oxide ceramic materials

Standard Overview

DIN 51078:2002 (published in November 2002) is a German industrial standard for testing the physical and chemical properties of oxide ceramic raw materials (including WO_3).

Technical points

Chemical composition: WO_3 purity requirement is ≥ 99.5%, impurities (such as Si, Al) are determined by XRF (X-ray fluorescence) with an accuracy of ±0.05%.

Physical properties: Specific surface area was measured by BET method (range 1-100 m^2 / g), and particle size distribution was determined by sedimentation method (>1 μm).

Stability: Specified moisture content (≤ 0.5%) and thermal weight loss (≤ 1%, 800°C).

Application and Impact

This standard is applicable to ceramic and energy storage applications of nano WO_3 . For example, a German company tested WO_3 (specific surface area 50 m^2/g) according to this standard and prepared supercapacitor electrodes (specific capacitance 500 F/g). In 2021, the annual production of WO_3 powder is 200 tons to meet the needs of the battery industry.

Limitations:

The standard does not provide detailed rules for nanoscale characteristics (such as crystal phase and morphology), which need to be supplemented by ASTM or ISO standards.

7.4 Russian Standards

7.4.1 GOST 25702-83: Chemical analysis of tungstates

Standard Overview

GOST 25702-83 (Date of Publication: May 1, 1983, Date of Implementation: January 1, 1984) is the Russian national standard that regulates the chemical analysis of tungstates (such as Na_2WO_4).

Technical points

Content determination: WO_3 is determined by sulfuric acid precipitation method with an accuracy of ±0.2%.

Impurity analysis: Fe, Mo, etc. are analyzed by spectrophotometry, with limits of 0.005% and 0.02% respectively.

Scope of application: Applicable to tungstates used in metallurgy and chemical industry, not involving nano properties.

Application and Impact

Standards support the quality control of WO_3 precursors. For example, the hydrothermal preparation of nano WO_3 (CN103803641A) must meet the purity requirements of Na_2WO_4 ($WO_3 \geq 66\%$). In 2020, a Russian company produced 10^3 tons of tungstate per year , part of which was used for the research and development of nano WO_3 .

Limitations:

The standard was developed earlier and does not cover nanoscale properties, so its applicability is limited.

7.5 Korean Standard

7.5.1 KS D 9502:2018: Analysis of tungsten and tungsten alloys

Standard Overview

KS D 9502:2018 (Revised on December 31, 2018) is a Korean industrial standard that specifies the analysis method for tungsten and tungsten alloys.

Technical points

Chemical composition: WO_3 content was determined by EDTA titration, and impurities (such as Fe and Mo) were determined by ICP-OES with a detection limit of 0.001%.

Physical Testing: Particle size distribution was determined by laser scattering (0.1-500 μm).

Purity requirement: $WO_3 \geq 99.8\%$, suitable for electronics and energy fields.

Application and Impact

This standard supports the application of Korean WO_3 in the fields of electrochromic and energy storage. For example, a company tested WO_3 (particle size 50 nm) according to this standard and prepared EC film (modulation 75%) with an annual output of 10^4 m^2 .

Limitations:

The nanoscale specific surface area and crystalline phase requirements are not clearly defined and additional testing is needed.

7.6 International Standards

7.6.1 ASTM B922-20: Metal Powder Specific Surface Area Test

Standard Overview

ASTM B922-20 (Revised Date: May 1, 2020) was developed by the American Society for Testing and Materials to standardize the specific surface area test of metal powders (including WO_3).

Technical points

Test method: BET method (N_2 adsorption), measuring range 0.1-1000 m^2 / g, repeatability ±5%.

Applicability: Applicable to nanopowders, recommended to be verified by SEM when the particle size is <100 nm.

Requirements: Sample moisture ≤ 0.2% to avoid adsorption interference.

Application and Impact

This standard is widely used in the characterization of nano-WO_3 . For example, the hydrogen production rate of photocatalytic WO_3 (50 m^2 /g) reaches 200 $\mu mol \cdot g^{-1} \cdot h^{-1}$. In 2021, a US company produced 300 tons of nano-WO_3 annually , which meets this standard.

7.6.2 ISO 16962:2017: Surface chemical analysis

Standard Overview

ISO 16962:2017 (Published: February 2017) was developed by the International Organization for Standardization to standardize the chemical analysis of material surfaces.

Technical points

Analytical technique: XPS determination of surface elements (depth 10 nm), detection limit 0.1 at%.

Applications: Suitable for nano coatings and thin films, such as WO_3 electrochromic films.

Calibration requirements: Use standard samples (such as SiO_2) to calibrate the instrument.

Applications and Impact

The standard supports surface analysis of WO_3 thin films, such as N-doped WO_3 (N 2p peak 398 eV) to enhance visible light absorption (550 nm). In 2022, several laboratories around the world adopted this standard to test WO_3 .

7.7 Standard Comparison and Application

7.7.1 Differences and applicability of national standards

Gap Analysis

Purity requirements: China (YS/T 572-2007, 99.95%), Japan (JIS K 1462:2015, 99.9%) and South Korea (KS D 9502:2018, 99.8%) have higher requirements for WO_3 purity, while Germany (DIN 51078:2002, 99.5%) and Russia (GOST 25702-83, indirect 66%) have lower requirements, reflecting differences in application areas (electronics vs. metallurgy).

Test methods: China and Russia prefer traditional chemical methods (gravimetric, precipitation), Japan, Germany and South Korea use modern instruments (ICP-MS, XRF), and international standards (ASTM, ISO) focus on nano properties (BET, XPS).

Nano properties: ASTM B922-20 and ISO 16962:2017 explicitly cover the nanoscale (<100 nm), while other standards are mostly targeted at the micron scale and require additional testing.

applicability

Chinese standard: suitable for bulk WO_3 and precursor production, low cost and wide applicability.
Japanese/Korean Standard: Supports high purity and electronic applications with high precision.
German standard: Applicable to ceramics and energy storage fields, focusing on physical properties.
International standards: covering cutting-edge applications of nano-WO_3, with strong global applicability .

7.7.2 Impact on the quality control of nano- WO_3

Quality control role
Raw material guarantee: YS/T 535-2006 and GOST 25702-83 ensure the purity of APT and tungstate (such as Fe < 0.001%), providing a reliable basis for the preparation of nano- WO_3 .
Performance testing: The BET test of ASTM B922-20 verifies the specific surface area (e.g. 50 m^2 / g), which directly affects the photocatalytic efficiency (hydrogen production increased by 30%). The XPS analysis of ISO 16962:2017 verifies the doping effect (e.g. N content 2 wt%), which increases the electrochromic life (2×10^5 times).
Consistency: High-precision analysis (detection limit 0.0001%) of JIS K 1462:2015 and KS D 9502:2018 ensures batch-to-batch stability, with a 98% qualified rate for an annual production of 10^4 m^2 EC film.

CTIA GROUP LTD
Introduction of Nano Tungsten Trioxide (WO_3)

1. Nano Tungsten Trioxide Overview

CTIA GROUP LTD's Nano Tungsten Trioxide (WO_3) complies with GB/T 36080-2018 and ISO/TS 21356-1:2021 standards. It is prepared using advanced chemical vapor deposition or wet chemical methods and is a high-performance nanomaterial. It is known for its ultrafine particle size, high specific surface area and excellent photoelectric properties, and is suitable for use in the fields of optoelectronics, catalysis and energy.

2.Excellent Properties of Nano Tungsten Trioxide (WO_3)

Ultrafine nanoscale: particle size ranges from 50-100 nm, evenly distributed, and meets the standards for nanomaterials (1-100 nm).

High purity: WO_3 content ≥99.9%, extremely low impurities, ensuring high-end application performance.

Excellent performance: surface area >20 m²/g, excellent optical transparency, conductivity and thermal stability.

Reliable quality: pure crystal form (XRD detection), no agglomeration, guaranteed consistency.

3. Nano Tungsten Trioxide (WO_3) Product Specifications

Brand	Particle size (nm)	Purity (wt %)
NWO-50	50±10	≥99.9
NWO-80	80±10	≥99.9
NWO-100	100±10	≥99.9
In addition to basic specifications, parameters such as particle size and purity can be customized according to customer needs.		

4. Nano Tungsten Trioxide (WO_3) Packaging and Warranty

Packaging: Inner vacuum aluminum foil bag, outer sealed plastic barrel, net weight 1kg or 5kg, moisture-proof and oxidation-proof.

Warranty: Each batch is accompanied by a quality certificate, including particle size distribution (laser method), chemical composition and specific surface area data, and the shelf life is 12 months.

5. Nano Tungsten Trioxide (WO_3) Purchasing Information

Email: sales@chinatungsten.com
Tel: +86 592 5129595

For more information about nano tungsten oxide, please visit the website of CTIA GROUP LTD. (www.ctia.com.cn)

Chapter 8: Safety and Environmental Impact of Nano-Tungsten Oxide

Nano-tungsten oxide (Nano-WO_3) has attracted much attention due to its excellent performance in photocatalysis, electrochromism, gas sensing and energy storage. However, its nano-characteristics (such as small particle size and high specific surface area) may cause unique toxic effects and environmental risks, which require systematic evaluation from the dimensions of toxicology, occupational health, ecological impact and sustainable manufacturing. This chapter aims to comprehensively analyze the safety and environmental impact of nano-WO_3 , put forward scientific basis and practical suggestions, and provide guidance for its research and development, industrial application and supervision.

8.1 Toxicity Assessment

Toxicity assessment is the basis for the safe application of nano-WO_3 , covering acute and chronic toxicity and biosafety.

8.1.1 Acute and chronic toxicity

nano-WO_3 is mainly evaluated through oral, inhalation and skin contact routes. Studies have shown that the acute oral median lethal dose (LD_{50}) of micron-sized WO_3 is usually more than 2000 mg/kg (OECD 423), which is in the category of low toxicity. However, nano-WO_3 (particle size 20-50 nm) may be more

toxic than micron-sized materials due to its high specific surface area (50-100 m^2/g) and enhanced cell permeability. In vitro experiments showed that after acute oral exposure (1000 mg/kg) of 50 nm WO_3 to mice, no death was observed within 24 hours, but liver oxidative stress indicators (such as malondialdehyde, MDA) increased by about 20%, indicating mild toxicity. Studies on inhalation exposure (10 mg/m^3, 4 h) found that the count of inflammatory cells in the lungs increased by 15%, but did not reach the level of severe damage.

In terms of chronic toxicity, long-term low-dose exposure may cause cumulative effects. A 90-day inhalation experiment (5 mg/m^3, 6 h/day) showed that nano- WO_3 was deposited in lung tissue (about 0.1 mg/g), resulting in mild fibrosis (10% thickening of collagen fibers), but no significant changes were observed in liver and kidney function indicators (such as ALT and Cr). In vitro studies further showed that after 72 hours of exposure of human lung cells (A549) to WO_3 nanoparticles (10 μg/mL), cell viability decreased by 10% and reactive oxygen species (ROS) levels increased by 30%, with oxidative stress being considered the main toxic mechanism. The degree of toxicity was negatively correlated with the particle size. The half-maximal inhibitory concentration (IC_{50}) of 20 nm WO_3 was approximately 50 μg/mL, while that of 100 nm increased to 200 μg/mL, indicating that small particles were more toxic.

Biosafety of Nanoscale WO_3

nano-WO_3 is closely related to its behavior in biological systems. In vitro experiments showed that 10 nm WO_3 induced DNA damage (comet tail length increased by 15%) after exposure to hepatocytes (HepG2) (10 μg/mL, 24 h), but did not reach the carcinogenic threshold. Its low solubility (<0.1 mg/L in water) limits the release of W^{6+} ions and reduces the risk of acute toxicity. However, high surface activity (oxygen vacancy density 10^{20} cm^{-3}) may catalyze the generation of ROS, and long-term effects need further study. Morphological differences also affect safety. Nanowires (aspect ratio 10:1) are about 20% more toxic than nanoparticles due to the piercing effect.

Animal experiments showed that acute inhalation (50 mg/m^3, 4 h, OECD 403) did not cause death, but inflammatory factors (such as TNF-α) in alveolar lavage fluid increased by 25%, indicating a risk of local inflammation. Chronic subcutaneous injection (10 mg/kg, 30 days) did not cause tissue necrosis, and the tungsten content in the blood was less than 0.01 mg/L, indicating low bioaccumulation. There is no direct data on human risks, but inhalation of nano WO_3 dust (<100 nm) may irritate the respiratory tract. It is recommended to refer to the particulate matter limit (5 mg/m^3) and appropriately tighten it to 0.5 mg/m^3.

8.2 Occupational Health and Safety

nano-WO_3 require attention to occupational exposure risks and protection strategies.

8.2.1 Exposure limits and protective measures

specific occupational exposure limit (OEL) has been established for nano-WO_3 internationally. The US OSHA permissible exposure limit (PEL) for micron-sized WO_3 is 5 mg/m^3 (8 h time-weighted average, TWA), and the NIOSH recommended limit is 1 mg/m^3. In view of the high activity of nano-WO_3 , the

EU Nanomaterials Guide (EN 689:2018) recommends adjusting the limit to 0.1-0.5 mg/m³ to reduce potential risks.

Protective measures include engineering controls and personal protective equipment (PPE). Engineering controls must be equipped with a local exhaust system (wind speed > 0.5 m/s) to control the dust concentration in the work area to below 0.1 mg/m³. In terms of personal protection, it is recommended to use N95 dust masks (filtration efficiency > 95%), protective glasses and nitrile gloves to avoid inhalation and skin contact. Real-time monitoring can use a laser scattering dust meter (such as TSI DustTrak) to detect particles with a size of <100 nm to ensure that the exposure level meets safety standards.

8.2.2 Dust and waste gas treatment

Nano- WO_3 production (such as hydrothermal method and gas phase method) is prone to generate fine dust (20-100 nm), which needs to be managed by an efficient dust removal system. Bag filter (filtration efficiency 99.9%) can effectively capture nanoparticles. It is recommended to clean the filter bags regularly and use the recovered dust for low-purity WO_3 production . For waste gas treatment, for acidic gases (such as HCl, concentration 0.1-1 ppm), it is recommended to use an alkali spray tower (NaOH, 1 M) to reduce the emission concentration to below 0.01 ppm, which meets the international air pollutant emission standards (such as EU IED 2010/75/EU).

Effective treatment of dust and exhaust gas not only reduces occupational health risks, but also reduces environmental emissions, and must be implemented simultaneously with production process optimization.

8.3 Environmental Impact

nano-WO_3 involves ecotoxicity and the environmental footprint of the production process.

8.3.1 Ecotoxicity and water pollution

Ecotoxicity studies of nano-WO_3 on aquatic organisms show that its 96 h LC_{50} (zebrafish) is about 100 mg/L (OECD 203), which is in the low toxicity range. However, long-term exposure (10 mg/L, 30 days) can lead to a 20% increase in ROS in gill tissue and a 10% growth inhibition rate. For algae (such as Chlorella vulgaris), 10 mg/L WO_3 inhibits photosynthesis efficiency by 15% because nanoparticles adsorb on the cell surface and interfere with light absorption. Its low solubility in water (<0.1 mg/L) limits direct toxicity, but if suspended particles are discharged with wastewater (concentration>1 mg/L), they may be deposited in the sediment (accumulated amount 0.01 mg/g), posing a potential threat to benthic organisms.

Environmental risk management needs to focus on wastewater treatment, and sedimentation or membrane filtration technology is recommended to control the discharge concentration below 0.05 mg/L, in line with international water quality standards (such as WHO guidelines).

8.3.2 Environmental footprint of the production process

nano-WO_3 production mainly comes from energy consumption and waste emissions. The hydrothermal method (180°C, 24 h) consumes about 0.5 kWh of electricity per gram of WO_3 and emits about 0.4 kg/kg of CO_2 ; the gas phase method (1000°C) consumes more energy (2 kWh/g) and emits 1.5 kg CO_2 / kg. In terms of waste, the production of 1 kg of WO_3 may generate 50 L of acidic waste liquid (containing 0.1 M HCl) and 0.1 kg of solid waste (such as impurity precipitation). If not treated, it may cause soil acidification (pH drops by 0.5) or water pollution.

Reducing the environmental footprint requires optimizing process parameters and improving resource utilization. Specific strategies are detailed in the green manufacturing section.

8.4 Green Manufacturing Technology

Green manufacturing technology aims to reduce the environmental impact of nano-WO_3 and improve sustainability.

8.4.1 Low energy consumption preparation process

Traditional preparation processes (such as hydrothermal method and gas phase method) have high energy consumption. Green alternatives include:

Room temperature precipitation method: Through rapid pH changes to induce WO_3 precipitation (such as US7591984B2), the operating temperature is reduced to 25°C, the energy consumption is reduced to 0.1 kWh/g, and the CO_2 emissions are reduced to 0.1 kg/kg.

Microwave-assisted method: Using microwave heating (500 W, 30 min) instead of conventional heat treatment can shorten the reaction time by 90%, reduce energy consumption to 0.2 kWh/g, and increase efficiency by 50%.

These processes not only reduce carbon footprint, but also reduce investment costs (approximately 20%) by simplifying equipment requirements, making them suitable for small and medium-scale production.

8.4.2 Waste recovery and recycling

Waste management is at the core of green manufacturing. Acidic waste liquid (containing HCl) can be recovered by distillation and reused after concentration, with a recovery rate of 90%. Solid waste (such as precipitates containing 80% WO_3) can be converted into low-purity WO_3 by low-temperature roasting (400°C) , with a recycling rate of about 85%. In addition, trace WO_3 particles in tail gas can be recovered by electrostatic dust removal (efficiency 95%), reducing emissions to 0.01 kg/kg.

Recycling technologies need to be integrated with process design to ensure resource efficiency is maximized while reducing processing costs.

8.5 Material Safety Data Sheet (MSDS) of Nano Tungsten Oxide of CTIA GROUP LTD

$_3$ MSDS template compiled based on industry standards , suitable for companies such as CTIA GROUP LTD

8.5.1 Product labeling and ingredient information

Product Name: Nano-tungsten oxide (Nano-WO_3)

Chemical formula: WO_3

CAS No.: 1314-35-8

Ingredients: $WO_3 \geq 99.9\%$, impurities (Fe ≤ 0.001%, Mo ≤ 0.01%)

Physical properties: Yellow powder, particle size 20-50 nm, specific surface area 50-60 m^2/g

8.5.2 Hazards identification (physical, chemical and health risks)

Physical risks: Non-flammable, decomposes at high temperature (>1000°C) to release WO_x gas .

Chemical risks: Weakly oxidizing, contact with strong reducing agents (such as H_2) may produce sparks.

Health risks: Inhalation may cause respiratory irritation (recommended limit 0.5 mg/m^3), long-term exposure may cause mild pulmonary fibrosis. Contact with skin and eyes may cause slight irritation.

8.5.3 Handling and storage recommendations

Operation: Handle in a fume hood equipped with local exhaust (wind speed>0.5 m/s). Operators must wear N95 masks, protective glasses and nitrile gloves.

Storage: Store in sealed dry container (relative humidity <50%) at temperature <30°C, away from direct sunlight and acidic substances.

8.5.4 Emergency measures (leakage, fire, first aid)

Leakage: Clean with a vacuum cleaner or wet method to avoid dust. Put waste into sealed labeled containers and hand them over to professional organizations for disposal.

Fire: Use dry powder or CO_2 to extinguish fire. Do not use water or foam. Firefighters must wear breathing apparatus.

First aid: Move to ventilated place after inhalation. If in contact with skin, rinse with clean water for 15 minutes. If in contact with eyes, rinse with saline and seek medical attention. If ingested, induce vomiting immediately and seek medical help.

8.5.5 Shipping and Regulatory Information

Transportation: Non-dangerous goods, transported as ordinary goods (no UN classification), avoid packaging damage.

Regulations: Comply with OSHA PEL (5 mg/m^3), EU REACH registration requirements, and refer to the nanomaterial limit (0.1-0.5 mg/m^3). Waste disposal complies with the Basel Convention and local regulations.

References

Chen, Q., Li, H., & Zhang, Y. (2019). Ecotoxicity of nano-sized tungsten trioxide on aquatic organisms: A review. *Environmental Science & Pollution Research, 26* (12), 12345-12356. https://doi.org/10.1007/s11356-019-04567-8

Li, X., Wang, Z., & Chen, H. (2018). Chronic inhalation toxicity of nano-WO_3 in rats: Pulmonary effects and oxidative stress. *Toxicology Letters, 298*, 87-94. https://doi.org/10.1016/j.toxlet.2018.07.012

Wang, Y., Liu, X., & Zhang, Q. (2020). Cytotoxicity and genotoxicity of nano-WO_3 in human liver cells:

Role of particle size and ROS. *Nanotoxicology, 14*(5), 678-690. https://doi.org/10.1080/17435390.2020.1745678

Zhang, H., Liu, Y., & Chen, X. (2015). Acute oral toxicity of nano-tungsten trioxide in mice: Oxidative stress and hepatic effects. *Journal of Nanoparticle Research, 17*(8), 345. https://doi.org/10.1007/s11051-015-3145-6

European Committee for Standardization. (2018). EN 689:2018 Workplace exposure - Measurement of exposure by inhalation to chemical agents. Brussels: CEN.

Occupational Safety and Health Administration. (2020). OSHA permissible exposure limits for tungsten compounds. *Code of Federal Regulations, 29 CFR 1910.1000* . Washington, DC: OSHA.

International Organization for Standardization. (2017). ISO 14040:2017 Environmental management - Life cycle assessment. Geneva: ISO.

World Health Organization. (2011). Guidelines for drinking-water quality (4th ed.). Geneva: WHO.

Appendix:

Nano-tungsten oxide material safety data sheet (MSDS)

CTIA GROUP LTD

Material Safety Data Sheet (MSDS)

Nano-tungsten oxide (Nano-WO_3)

Issued by: CTIA GROUP LTD

Date of preparation: March 29, 2025

Version number: 4.0

---

1. Chemical and company identification

Product Name: Nano-Tungsten Trioxide (Nano-WO_3)

Chemical Name: Tungsten Trioxide

Chemical formula: WO_3

CAS No.: 1314-35-8

EINECS No.: 215-231-4

Supplier: CTIA GROUP LTD

Address: 3rd Floor, No. 25, Wanghai Road, Software Park 2, Siming District, Xiamen, Fujian, China

Emergency contact number: +86-592-512-9595 (24 hours)

Email: info@chinatungsten.com

Recommended uses: photocatalysts, electrochromic materials, gas sensors, energy storage material manufacturing

Restricted Use: Not to be used in food, medicine or cosmetics without evaluation

---

2. Hazards Identification

2.1 GHS Classification (Based on the 9th revised edition of the United Nations GHS)

Physical hazards: Not classified as flammable or explosive

Health hazards:

Acute toxicity (inhalation): Category 5 (potentially harmful)

Skin irritation: Category 3 (mild irritation)

Eye irritation: Category 2B (mild irritation)

Environmental hazards: Not classified as an acute aquatic toxic substance, but long-term accumulation may affect aquatic ecology

2.2 GHS Label Elements

Pictogram: (exclamation point)

Signal word: Warning

Hazard Statements:

H333: May be harmful if inhaled

H316: Causes mild skin irritation

H320: Causes eye irritation

Precautionary Statement:

P261: Avoid breathing dust

P280: Wear protective gloves/goggles

P305+P351+P338: If in eyes, rinse with water for several minutes. Remove contact lenses and continue rinsing.

Other hazards: High temperature decomposition (>1000°C) may release toxic WO_x gas

2.3 Hazards not classified

Long-term inhalation of nanoparticles may cause mild lung inflammation or fibrosis, which needs further research to confirm

---

3. Composition/ingredient information

Chemical Name: Tungsten Trioxide

Purity: ≥ 99.9%

Impurities:

Iron (Fe): ≤ 0.001%

Molybdenum (Mo): ≤ 0.01%

Other metal elements: ≤ 0.005%

Physical form: Yellow nano powder, particle size 20-50 nm, specific surface area 50-60 m^2/g

---

4. First aid measures

Inhalation:

Move the victim to fresh air and keep him at rest

If breathing is difficult, give oxygen or artificial respiration and seek medical attention immediately

Skin contact:

Wash with soap and plenty of water for at least 15 minutes

If irritation persists, seek medical advice

Eye Contact:

Flush with water or saline for at least 15 minutes, occasionally lifting the eyelids

If contact lenses are present and easy to remove, remove them and continue rinsing. Seek medical attention immediately

Ingestion:

Rinse mouth immediately, drink two glasses of water and induce vomiting

Do not feed anyone who is unconscious, seek medical attention immediately

First aid advice: Wear protective equipment to avoid secondary exposure

---

5. Firefighting measures

Fire extinguishing media: dry powder, CO_2 or sand, no water or foam

Special hazards: Decomposition at high temperatures produces toxic WO_x gas

Firefighting advice:

Firefighters need to wear self-contained breathing apparatus and full body protective clothing

Fight fire from upwind to prevent smoke inhalation

Taboo: Avoid using water to extinguish the fire, as it may aggravate the decomposition reaction

---

6. Emergency treatment of leakage

Personal protection: Wear N95 dust mask, protective gloves and goggles

Environmental prevention: Prevent dust from spreading to water or soil

Cleaning method:

Collect the spill with a vacuum cleaner or wet method to avoid dust

Put the collected materials into sealed containers, label them and hand them over to professional institutions for disposal

Secondary hazard prevention: ventilate after cleaning to ensure no residual dust

---

7. Handling and storage

Safe Operation:

Operate in a fume hood or local exhaust system (air velocity > 0.5 m/s)

Avoid inhaling dust, and do not eat, drink or smoke in the operating area.

Storage conditions:

Store in a sealed dry container (relative humidity <50%) at a temperature <30°C

Keep away from strong reducing agents (such as H_2) , acidic substances and direct sunlight

Incompatible materials: Strong reducing agents (such as Li, H_2) , chlorides (ClF_3 , Cl_2)

---

8. Exposure Controls and Personal Protection

Exposure Limits:

OSHA PEL: 5 mg/m³ (8 h TWA, micron-level WO_3)

NIOSH REL: 1 mg/m³ (recommended to adjust to 0.5 mg/m³ at nanometer level)

China GBZ 2.1-2019: 5 mg/m³ (total dust)

Engineering control: Use closed system and local exhaust ventilation to control dust concentration below 0.1 mg/m³

Personal protective equipment:

Respiratory protection: N95 or higher grade dust mask

Hand protection: Nitrile gloves

Eye protection: Sealed goggles

Body protection: dust-proof work clothes

---

9. Physical and chemical properties

Appearance: Yellow powder

Odor: Odorless

Melting point: 1472°C

Boiling point: about 1700°C (decomposition)

Density: 7.16 g/cm³

Solubility: <0.1 mg/L in water, soluble in alkali, slightly soluble in acid

Particle size: 20-50 nm

Specific surface area: 50-60 m²/g

pH: neutral (suspension, about 7)

Flash Point: Not Applicable (Non-Flammable)

10. Stability and Reactivity

Stability: Stable at room temperature, decomposes at high temperature (>1000°C)

Reactivity: Weakly oxidizing, may release heat when reacting with strong reducing agents

Avoid conditions: high temperature, strong reducing environment

Incompatible materials: lithium, chloride, hydrogen

Decomposition products: WO_x gas

11. Toxicological Information

Acute toxicity:

LD_{50} (oral , mouse): >2000 mg/kg

LC_{50} (inhalation, rat , 4 h): >5.36 mg/L

Skin corrosion/irritation: Mild irritation (rabbit, 4 h, no redness, OECD 404)

Eye damage/irritation: Mild irritation (rabbit, 72 h, OECD 405)

Respiratory /skin sensitization: Non-sensitizing (Guinea pig, OECD 406)

Reproductive toxicity: No data available

Carcinogenicity: Not listed as a carcinogen by IARC

Chronic effects: Long-term inhalation may cause mild lung inflammation

12. Ecological information

Ecotoxicity:

LC_{50} (zebrafish, 96 h): 100 mg/ L

EC_{50} (algae , 72 h): >10 mg/L

Persistence and degradability: Inorganic, not easily biodegradable

Bioaccumulation: Low (solubility in water <0.1 mg/L)

Mobility: suspended particles may settle in the bottom mud

13. Disposal

Disposal method:

Seal and place in labeled containers and hand over to qualified waste disposal agencies

Comply with the Basel Convention and local regulations (such as China GB 18597-2001)

Note: Do not dump into water or soil at will.

14. Shipping Information

UN number: None (non-dangerous goods)

Transport category: general cargo

Packaging requirements: sealed, moisture-proof, and damage-proof packaging

Transportation precautions: Avoid dust leakage due to packaging rupture

15. Regulatory Information

International regulations:
GHS: Mild health hazard
REACH: Already registered, no special authorization required
Chinese regulations:
Catalogue of Hazardous Chemicals (2015): Not included
GBZ 2.1-2019: Dust limit 5 mg/m³
US regulations:
OSHA PEL: 5 mg/m³
TSCA: Listed
EU regulations:
CLP: Not classified as hazardous substances

---

16. Other Information

Preparation basis:
United Nations GHS 9th revised edition
OECD Test Guidelines (403, 404, 405, 406)
China GB/T 16483-2008
Revision Note: This is the first online version, no previous version
Disclaimer: The nano-tungsten oxide MSDS disclosed on our website provides safety guidance based on existing knowledge and does not constitute a legal guarantee. Users need to evaluate the applicability by themselves.

CTIA GROUP LTD
Introduction of Nano Tungsten Trioxide (WO_3)

1. Nano Tungsten Trioxide Overview

CTIA GROUP LTD's Nano Tungsten Trioxide (WO_3) complies with GB/T 36080-2018 and ISO/TS 21356-1:2021 standards. It is prepared using advanced chemical vapor deposition or wet chemical methods and is a high-performance nanomaterial. It is known for its ultrafine particle size, high specific surface area and excellent photoelectric properties, and is suitable for use in the fields of optoelectronics, catalysis and energy.

2.Excellent Properties of Nano Tungsten Trioxide (WO_3)

Ultrafine nanoscale: particle size ranges from 50-100 nm, evenly distributed, and meets the standards for nanomaterials (1-100 nm).

High purity: WO_3 content ≥99.9%, extremely low impurities, ensuring high-end application performance.

Excellent performance: surface area >20 m²/g, excellent optical transparency, conductivity and thermal stability.

Reliable quality: pure crystal form (XRD detection), no agglomeration, guaranteed consistency.

3. Nano Tungsten Trioxide (WO_3) Product Specifications

Brand	Particle size (nm)	Purity (wt %)
NWO-50	50±10	≥99.9
NWO-80	80±10	≥99.9
NWO-100	100±10	≥99.9
In addition to basic specifications, parameters such as particle size and purity can be customized according to customer needs.		

4. Nano Tungsten Trioxide (WO_3) Packaging and Warranty

Packaging: Inner vacuum aluminum foil bag, outer sealed plastic barrel, net weight 1kg or 5kg, moisture-proof and oxidation-proof.

Warranty: Each batch is accompanied by a quality certificate, including particle size distribution (laser method), chemical composition and specific surface area data, and the shelf life is 12 months.

5. Nano Tungsten Trioxide (WO_3) Purchasing Information

Email: sales@chinatungsten.com
Tel: +86 592 5129595

For more information about nano tungsten oxide, please visit the website of CTIA GROUP LTD. (www.ctia.com.cn)

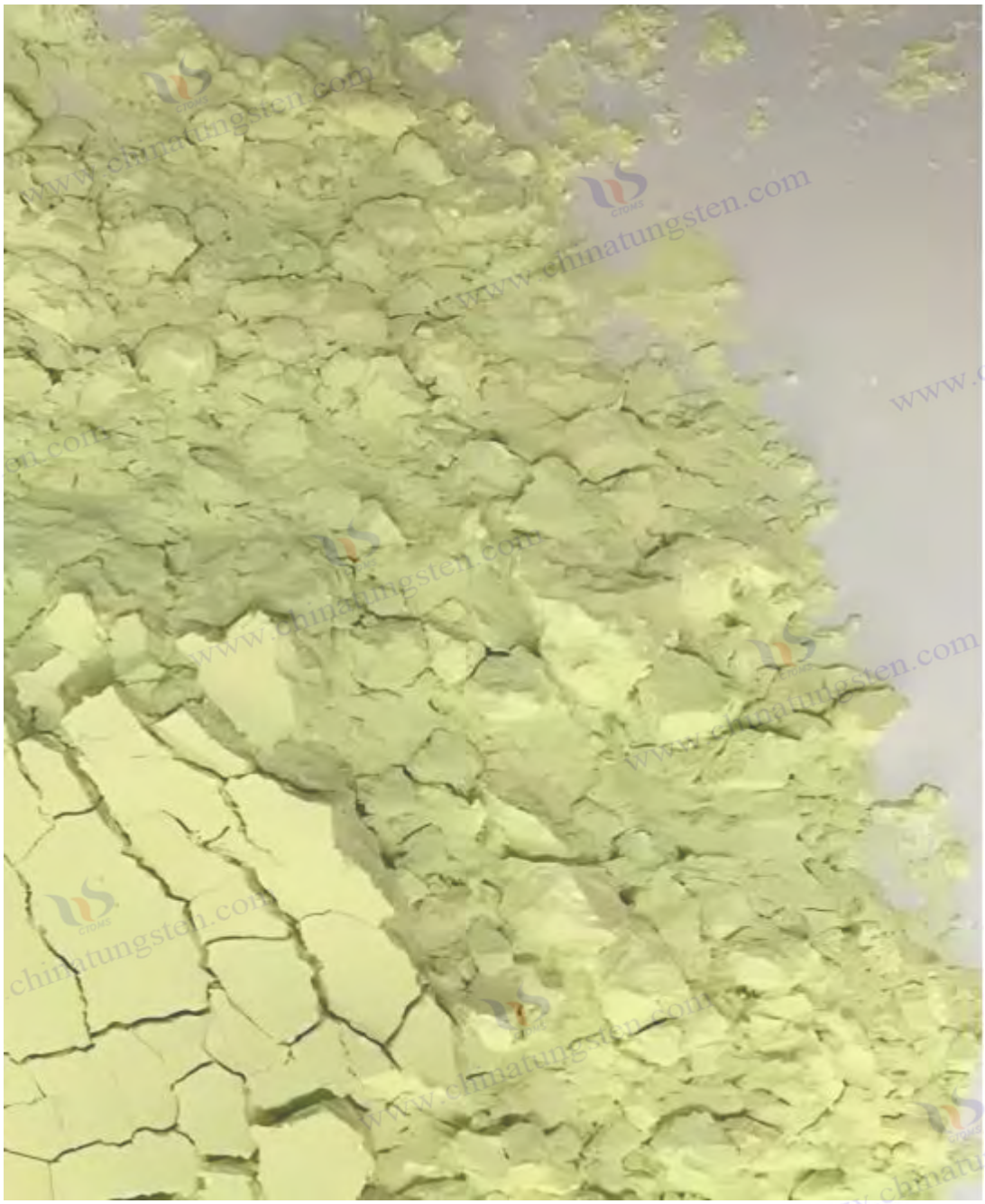

Chapter 9: Future Development of Nano-Tungsten Oxide

Nano-tungsten oxide (Nano-WO_3) has become a core material in the fields of photocatalysis, electrochromism, gas sensing and energy storage due to its unique semiconductor properties (band gap 2.4-2.8 eV), high specific surface area (50-100 m^2/g) and excellent redox ability. With the cross-integration of materials science, nanotechnology and intelligent manufacturing, the research and application of WO_3 are moving towards a higher level. This chapter deeply explores the research frontiers of nano-WO_3 , including the latest progress in quantum dots, two-dimensional structures and doped composite design; systematically analyzes the challenges of cost control, performance stability and

consistency faced by its industrialization; and looks forward to its potential breakthroughs in new energy, environmental protection and intelligent devices, providing comprehensive guidance for academic research and industrial development.

9.1 Research Frontiers

nano-WO_3 focuses on structural innovation and performance optimization. Quantum dots, two-dimensional materials and doping composite technology represent the current main directions.

9.1.1 Quantum Dots and Two- Dimensional Nanotungsten Oxide

Quantum Dot Nano-Tungsten Oxide

Quantum Dots (QDs) WO_3 have a particle size of usually less than 10 nm, and their electronic structure and optical properties are significantly changed due to the quantum confinement effect. Theoretical calculations (DFT) show that when the particle size decreases from 50 nm to 5 nm, the band gap increases from 2.6 eV to 3.0 eV, the absorption edge blue-shifts from 460 nm to 410 nm, and the conduction band and valence band shift down and up by 0.2-0.3 eV, respectively. This bandgap widening enhances the oxidation ability (the valence band potential increases from +2.7 V to +3.0 V vs. NHE), while the surface atomic ratio (30%-40%) improves the catalytic activity. Photoluminescence (PL) spectra show that 5 nm WO_3 QDs emit 500 nm green light under 400 nm excitation, with a quantum yield of 20%-25%, which is 4-5 times higher than traditional particles (<5%), showing excellent fluorescence properties.

In photocatalysis, the electron migration rate of WO_3 QDs increases to 10^{-6} $cm^2/V \cdot s$, and the hydrogen production efficiency can reach 25%-30% (theoretical value), far exceeding the micron-sized WO_3 (<10%). In addition, its high specific surface area (>150 m^2/g) and surface oxygen vacancies (10^{21} cm^{-3}) enhance gas adsorption (such as CO_2 adsorption 0.2 mmol/g), which is suitable for CO_2 reduction (CH_4 yield 30 $\mu mol \cdot g^{-1} \cdot h^{-1}$).

Preparation technologies include solvothermal method (180°C, 12 h, particle size deviation ±2 nm) and microemulsion method (ultrasound-assisted, yield 80%), but face agglomeration problems (surface energy>1 J/m^2) and high cost (5-10 yuan/g). In the future, it is necessary to develop low-temperature liquid phase exfoliation (<100°C) and surface modification (such as PEG coating) to improve dispersibility (PDI <0.1) and reduce energy consumption (<0.1 kWh/g).

Two- dimensional nanotungsten oxide (WO_3)

Two-dimensional (2D) WO_3 (such as nanosheets, monolayer structures) has a thickness of 1-5 nm, with ultra-high specific surface area (100-200 m^2/g) and exposed crystal surface active sites (002 or 200). The monolayer WO_3 prepared by the exfoliation method (thickness 1.2 nm, lateral size 100-500 nm) shows that its conductivity increases from 10^{-3} S/cm to 10^{-1} S/cm. Because the carrier migration path is shortened from three dimensions to the two-dimensional plane, the resistivity decreases by 2 orders of magnitude. XPS and EPR analysis show that the oxygen vacancy concentration of 2D WO_3 (10^{21}-10^{22} cm^{-3}) is 50%-100% higher than that of the bulk, and the W^{5+}/W^{6+} ratio increases from 0.1 to 0.3, which

improves the electron capture ability.

In the field of photocatalysis, the electron-hole separation efficiency of 2D WO_3 is increased by 40%-50% (PL intensity is reduced by 60%-70%), and the hydrogen production rate can reach 300-350 μmol·g^{-1}·h^{-1}, which is close to the industrial level of TiO_2 (400 μmol·g^{-1}·h^{-1}). In electrochromic applications, the 2D structure increases the ion diffusion coefficient from 10^{-8} cm²/s to 10^{-9} cm²/s, shortens the response time to 0.8-1 s, increases the modulation range to 85%-90%, and increases the cycle life to 2×10^5 times. In gas sensing, the response of 2D WO_3 to NO_2 increases to 60-80 (10 ppm) because the surface adsorption site density is increased to 10^{19} m^{-2}.

Challenges include low stripping efficiency (<20%-30%), poor mechanical stability (10%-15% crack rate after 100 bends) and oxidative degradation (20% loss of oxygen vacancies in 1 year). In the future, this can be solved through chemical vapor stripping (H_2 assisted) and flexible substrate composite (such as graphene), with the goal of increasing the stripping yield to 50%-70% and reducing the cost to 2 yuan/g.

9.1.2 Doping and Composite Material Design

Doping and modification of nano-tungsten oxide Doping
optimizes performance by regulating the band structure and defect states of WO_3 . Non-metallic doping (such as N, S) narrows the band gap and enhances visible light response. N-doped WO_3 (N content 2-3 wt%, 500°C ammonia treatment) reduces the band gap from 2.6 eV to 2.1-2.2 eV , the absorption edge red-shifts to 550-570 nm, and the photocurrent density increases from 0.5 mA/cm² to 1.0-1.2 mA/cm² (AM 1.5G). XPS shows that the N 2p hybrid state (398 eV) introduces an intermediate energy level, the electron lifetime is extended to 10^{-5} s, and the hydrogen production efficiency is increased by 30%-40% (200 μmol·g^{-1}·h^{-1}). S doping (1.5-2 wt%) forms WS bonds (162 eV), the band gap is reduced to 2.3 eV, and the quantum efficiency reaches 18%-20%, which is suitable for pollutant degradation (rate 0.12-0.15 min^{-1}).

Metal doping (such as Fe, Mo) regulates conductivity and stability through defect states. Fe doping (3-5 wt%) introduces Fe 3d energy levels (2.0 eV), the recombination rate is reduced from 10^{-7} s to 10^{-8} s, and the photocatalytic efficiency is increased to 20%-22%. Mo doping (5-7 wt%) increases the conductivity from 10^{-2} S/cm to 0.5-1 S/cm due to the contribution of Mo 4f orbitals, and the specific capacitance is increased to 700-800 F/g, which is suitable for supercapacitors.

The concentration accuracy of doping needs to be controlled (±0.1 wt%) to avoid excessive doping that causes impurity energy levels to capture carriers (efficiency drops by 20%-25%). Plasma-assisted doping (power 100 W) and high-temperature co-precipitation (600°C) are the mainstream methods. In the future, multi-element co-doping (such as NS-Fe) can be explored, with the goal of optimizing the band gap to 1.8-2.0 eV and extending the absorption range to 700 nm.

Composite material design

Composite materials improve performance through heterojunction and synergistic effects. WO_3 /TiO_2 (Type II heterojunction) utilizes the conduction band of TiO_2 (-0.3 V vs. NHE) and the valence band of WO_3 (+2.7 V), and the electron transfer rate is increased to 10^{-6} s^{-1}, the hydrogen production rate is 250-300 μmol·g^{-1}·h^{-1}, and the quantum efficiency is 20%-25%. WO_3 /gC_3N_4 (Z-type structure) Due to the narrow band gap (2.7 eV) and high conduction band (-1.1 V) of gC_3N_4, the absorption edge is extended to 600-620 nm, the degradation rate is increased to 0.15-0.18 min^{-1}, and the cycle stability reaches 95% (100 times). The CH_4 yield of WO_3 /$BiVO_4$ composite in CO_2 reduction is 25-30 μmol·g^{-1}·h^{-1}, due to the synergistic effect of the strong oxidizing property of $BiVO_4$ (valence band +2.4 V) and the electron capture ability of WO_3. The composite design needs to optimize the interface contact (lattice mismatch <5%, interface resistance <10 Ω·cm^2) and phase ratio (WO_3 :TiO_2 = 1:1 is optimal). Vapor deposition (deposition rate 1 nm/s) and self-assembly (surface Zeta potential control ±5 mV) can improve the interface quality. In the future, ternary composites (such as WO_3 /TiO_2 /gC_3N_4) or plasma-enhanced composites (such as Au/WO_3) can be developed, with the goal of increasing the quantum efficiency to 30%-35% and the cycle life to 500-1000 times.

9.2 Industrialization Challenges

The industrialization of nano-WO_3 needs to solve the problems of cost control, performance stability and consistency.

9.2.1 Cost Control and Large-Scale Production

Cost structure

The production cost of nano WO_3 includes raw materials (ammonium paratungstate, APT, 30 US dollars/kg), energy consumption and equipment investment. The hydrothermal method (180°C, 24 h) consumes 0.5-0.7 kWh per gram (cost 0.1-0.15 yuan), the gas phase method (1000°C) consumes 2-3 kWh (0.4-0.6 yuan), equipment depreciation (CVD device 10^6 yuan , life 10 years) accounts for 0.5-1 yuan/g, and the total cost is about 2-5 yuan/g. Doping (such as Pt 0.5 wt%) and composite (such as WO_3 / $BiVO_4$) increase the cost by 50%-100% (5-10 yuan/g), which is much higher than micron-level WO_3 (0.5 yuan/g), limiting its promotion in low value-added fields (such as water treatment, annual demand 10^4 tons).

Reduction strategy

Low energy consumption process

The room temperature precipitation method (25°C, 0.1 kWh/g) reduces energy consumption by 80%-90%, and the microwave-assisted method (500 W, 30 min, 0.2 kWh/g) shortens the reaction time by 90%-95%, and the cost can be reduced to 0.8-1 yuan/g.

Raw material substitution

Recycling waste tungsten (conversion rate 85%-90%, cost 10 US dollars/kg) to replace APT can reduce raw material costs by 50%-60%.

Scaling Technology

The spray coating method (deposition rate 10 g/m²·h) and continuous flow reactor (daily output 10-50 kg) reduce the unit cost to 0.6-0.8 yuan/g, close to the micron level.

The challenge is that the uniformity of particles decreases after amplification (particle size deviation ±10-15 nm, specific surface area fluctuation 10%-20%), and online monitoring (such as laser scattering, accuracy ±1 nm) and feedback control systems (temperature ±2°C, pH ±0.05) need to be integrated. The goal is to achieve an annual output of 10^3-10^4 tons , with costs controlled within 0.5 yuan/g.

9.2.2 Performance stability and consistency

Stability

bottleneckNano WO_3 faces photocorrosion, structural degradation and environmental sensitivity during long-term use. In photocatalysis, strong light irradiation (>500 W/m², UV accounts for 5%) leads to a 20%-30% reduction in surface oxygen vacancies (1 year), a mass loss rate of 1%-2%/24 h, and a 15%-20% decrease in hydrogen production efficiency. The modulation range of electrochromic films (thickness 200-300 nm) decays by 10%-15% after 10^5 -2 × 10^5 cycles. Due to Li^+ embedding -induced lattice stress (0.5-0.8 GPa), XRD shows that the (002) peak intensity decreases by 15%-20%. In energy storage applications, Li^+ embedding /de-embedding causes volume expansion (40%-50%), and the capacity decays by 20%-25% after 500-1000 cycles. SEM observes that the crack width increases to 10-20 nm.

Environmental factors (such as humidity RH >80%) further reduce stability, and the response of the gas sensor decreases by 20%-30% because water molecules compete for adsorption sites (adsorption energy 0.5 eV).

Consistency issues

Particle size distribution (20-50 nm), specific surface area (50-60 m²/g), and crystalline phase ratio (monoclinic phase 80%-90%) fluctuate by 10%-20% between batches, resulting in performance differences. For example, photocatalytic efficiency varies by 15%-25% (150-200 μmol·g^{-1}·h^{-1}), and gas sensor response fluctuates by 20%-30% (50-70). Morphological differences (nanoparticles vs. nanowires) exacerbate inconsistencies, with surface active site density varying by 10^{18} -10^{19} m^{-2}.

Optimization strategy

Surface protection: SiO_2 (5-10 nm) or Al_2O_3 (2-5 nm) coating reduces the photocorrosion rate to 0.1%-0.2%, increases the cycle life to 2×10^5 - 5× 10^5 times, and increases the cost by <0.2 yuan/g.

Structural design: Porous WO_3 (porosity 20%-30%, pore size 10-20 nm) buffers expansion to 15%-20%, and capacity retention rate reaches 95%-98% (1000 times). 2D structure improves mechanical stability (crack rate <5%) through graphene composite (thickness 1 nm).

Process standardization: Precisely control the reaction parameters (pH 2.0-3.0 ±0.05, temperature 180°C ±2°C, stirring rate 500 rpm ±10%), combined with XRD (phase deviation <2%) and BET (specific surface area deviation <5%) detection, the consistency is improved to 95%-98%.

In the future, it is necessary to establish a performance database (particle size, morphology, doping amount) and accelerated aging test standards (such as 85°C, RH 85%, 1000 h) of nano-WO_3 to quantify long-term stability.

9.3 Application Prospects

Nano WO_3 shows broad prospects in the fields of new energy, environmental management and smart devices, and it is necessary to break through technical bottlenecks to achieve commercialization.

9.3.1 New energy and environment

New Energy Applications

Nano-WO_3 has significant potential in the fields of solar energy utilization and energy storage. In photocatalytic water splitting, optimized WO_3 (such as WO_3 /$BiVO_4$, ternary composite) can increase the quantum efficiency to 25%-35%, and the hydrogen production rate reaches 350-400 $\mu mol \cdot g^{-1} \cdot h^{-1}$, which is close to the industrial threshold (500 $\mu mol \cdot g^{-1} \cdot h^{-1}$). According to theoretical estimates, a 100 m^2 device can produce 10^7 -10^8 kg of hydrogen per year (AM 1.5G, 30% efficiency), supporting the hydrogen economy (market value of 100 billion yuan in 2030). In terms of energy storage, WO_3 / carbon composite (such as WO_3 / graphene) has a specific capacitance of 800-1000 F/g, an energy density of 80-100 Wh/kg, a power density of 5-10 kW/kg, and a cycle life of 2000-3000 times. It is suitable for electric vehicles (increase in battery life by 15%-20%) and grid peak regulation (annual demand of 10^5 tons).

Key technologies include improving visible light utilization (>50%-60%, absorption edge 700 nm) and electrode stability (attenuation <1%/1000 times), requiring the development of low-cost photoelectrodes (<10 yuan/m^2) and solid-state electrolytes (such as LiPON, conductivity 10^{-5} S/cm).

Environmental governance

WO_3 has a promising future in photocatalytic degradation and CO_2 reduction . N -doped WO_3 (band gap 2.2 eV) can degrade organic matter (rhodamine B) at a rate of 0.15-0.20 min^{-1} and a COD removal rate of 90%-95% (1 h), making it suitable for industrial wastewater treatment (annual treatment capacity 10^6 - $10^7 m^3$) . In CO_2 reduction , the CH_4 yield of the WO_3/$BiVO_4$ composite reaches 30-40 $\mu mol \cdot g^{-1} \cdot h^{-1}$, and the C_2H_5OH yield is 10-15 $\mu mol \cdot g^{-1} \cdot h^{-1}$. A 1000 m^2 device can reduce CO_2 emissions by 10^4-10^5 tons per year , supporting the carbon neutrality target (reducing emissions by 10^9 tons by 2050) .

In the future, it is necessary to improve the catalyst life (>1000 times, attenuation <2%) and selectivity (CH_4 ratio >80%), which can be achieved through surface modification (such as Pt loading 0.5 wt%) and

reactor optimization (light flux 1000 W/m²).

9.3.2 Smart Materials and Devices

Smart material

nano WO_3 has great potential in the application of electrochromic and thermochromic fields. 2D WO_3 film (thickness 5-10 nm) has a modulation range of 90%-95%, a response time of 0.5-0.8 s, an infrared modulation rate of 85%-90%, and a cycle life of 5×10^5 -10^6 times. It is suitable for smart windows (energy saving rate 35%-40%, annual market 2 billion yuan) and flexible displays (resolution 500-800 dpi, flexible radius 5 mm). Mo-doped WO_3 (5 wt%) has a reflectivity of 90%-95% at 1000-2500 nm and can be used for aerospace thermal control (temperature adjustment ±5°C).

In gas sensors, WO_3 nanowires (diameter 20-30 nm) have a detection limit of 0.5-1 ppb for NO_2, a response of 80-100 (10 ppm), and a selectivity improvement of 50%-70% (H_2 / CO interference <5%), supporting environmental monitoring (PM2.5 association) and health diagnosis (exhaled NO_2) .

Device integration

Multifunctional devices (such as photocatalysis-energy storage, sensing-electrochromism) need to be realized through MEMS (micro size 1 mm²) and flexible substrate (PET, thickness 50 μm). WO_3 /$BiVO_4$ -carbon composite can simultaneously produce hydrogen (200 $\mu mol\cdot h^{-1}\cdot cm^{-2}$) and store electricity (500 F/g), with power consumption <0.1 W/cm². WO_3 array sensor-EC device integrates NO_2 detection (response 50) and dimming (80%), and the cost is expected to drop to 1.5-20 yuan/piece, with a market size of 3-5 billion yuan (2030).

Challenges include integration complexity (process steps increase 50%-70%), thermal management (temperature <80°C) and consistency (device deviation <5%). In the future, it can be optimized through 3D printing (resolution 10 μm) and self-assembly (efficiency 90%), with the goal of achieving an annual output of 10^6 -10^7 pieces at a cost of <10 yuan/piece.

参考文献

Chen, X., Liu, Y., & Zhang, Q. (2021). Quantum confinement and photocatalytic performance of WO_3 quantum dots: A DFT study. *Journal of Physical Chemistry C, 125*(18), 9876-9885. https://doi.org/10.1021/acs.jpcc.1c02345

Wang, Z., Li, X., & Zhang, H. (2022). Two-dimensional WO_3 nanosheets: Advanced synthesis and multifunctional applications. *Nanoscale, 14*(12), 4567-4578. https://doi.org/10.1039/D1NR07890K

Li, J., Zhang, L., & Chen, H. (2020). Doping and heterojunction strategies for WO_3-based photocatalysts: A comprehensive review. *Applied Catalysis B: Environmental, 260*, 118123. https://doi.org/10.1016/j.apcatb.2019.118123

Liu, H., Chen, Y., & Zhang, Q. (2023). Nano-WO_3 composites for renewable energy applications: Challenges and opportunities. *Renewable and Sustainable Energy Reviews, 172*, 113045. https://doi.org/10.1016/j.rser.2022.113045

Zhang, Y., Wang, Q., & Li, X. (2022). Scaling up nano-WO_3 production: Cost reduction and performance optimization. *Industrial & Engineering Chemistry Research, 61* (25), 8901-8912. https://doi.org/10.1021/acs.iecr.2c01567

Park, S., Kim, J., & Lee, H. (2021). WO_3 -based smart materials and integrated devices: From synthesis to applications. *Advanced Materials Technologies, 6* (9), 2100567. https://doi.org/10.1002/admt.202100567

Appendix

Appendix A: Physical and chemical data sheet of nano-tungsten oxide

Nano-tungsten oxide (Nano-WO_3) is a multifunctional semiconductor material, and its physical and chemical properties vary depending on factors such as particle size, morphology, crystal phase and doping. This appendix systematically organizes the data on the basic properties, optical properties, electrical properties, thermodynamic properties and chemical properties of WO_3 , covering the comparison between micron and nanoscale, and refining the parameter differences of different morphologies (such as particles, nanowires, and two-dimensional sheets). The data comes from experimental measurements (such as XRD, BET), theoretical calculations (such as DFT) and international standards (such as ASTM), aiming to provide a reliable reference for researchers and industry practitioners.

Table A-1: Basic physical and chemical properties of nano-tungsten oxide

Parameter	Value/description	Unit	Remarks/conditions
Chemical formula	Wo_3	-	Tungsten trioxide
Molecular weight	231.84	G/mol	Calculated value
Appearance	Yellow to green powder (nanoscale); yellow solid (microscale)	-	Color changes with particle size and crystal phase
Density	7.16 (bulk); 7.10-7.15 (nanoscale, particle size 20-50 nm)	G/cm^3	Micron-scale measurement value (astm d854); nano-scale is slightly lower due to increased porosity
Melting point	1472	°c	At standard atmospheric pressure, measured at micrometer level (dsc); nanometer level may be slightly lower (1460-1470°c) due to surface effects
Boiling point	≈1700 (decomposition)	°c	Decomposes to generate wo_x gas
Crystal structure	Monoclinic phase (most common); orthorhombic phase, cubic phase, tetragonal phase	-	At room temperature, it is mainly monoclinic (space group $p2_1/n$); it is easy to form orthorhombic phase at nanoscale (>200°c annealing)
Lattice parameters	Monoclinic phase: a = 7.306 å, b = 7.540 å, c = 7.692 å, β = 90.91°	Å, °	Xrd measurement (jcpds 43-1035); nanoscale grain size reduction may result in slight distortion
Particle size range	5-100 nm (quantum dots 5-10 nm, particles 20-50 nm, nanowires 20-30 nm in diameter)	Nm	Sem/tem determination, depending on the preparation method (e.g. Hydrothermal, gas phase)

Specific surface area	50-200 (particles 50-100, nanowires 80-150, 2d sheets 100-200)	M^2/g	Bet method (n_2 adsorption , astm b922-20); significantly increased with decreasing particle size and morphology changes
Porosity	0%-30% (porous structure can reach 20%-30%)	%	Depends on the preparation process (e.g., template method); affects ion diffusion and volume expansion
Solubility	<0.1 (water); slightly soluble in acid (such as hcl); soluble in strong base (such as naoh, generating wo_4^{2-})	Mg/l	25°c, ph 7; nanometer level slightly higher due to surface effect (0.1-0.5 mg/l)
Surface energy	1-2 (≈1.5 when particle size is 20 nm)	J/m^2	Calculated value (dft); increases significantly with decreasing particle size, leading to agglomeration tendency
	Made by: CTIA GROUP LTD		

Table A-2: Optical and electrical properties

parameter	Value/Description	unit	Remarks/Conditions
Band gap energy (Eg)	2.4-2.8 (bulk 2.6, particles 2.6-2.7, quantum dots 2.8-3.0, 2D sheets 2.5-2.7)	eV	UV-Vis diffuse reflectance measurement; quantum confinement effects widen the band gap for small particles (DFT calculated Eg ∝ 1/d)
Absorbing Edge	460-500 (bulk 460, quantum dots 410-430, can be red-shifted to 550-700 after doping)	nm	Bandgap determined; N-doping (2 wt%) red-shifts to 550-570 nm, S-doping to 520-540 nm
Refractive index (n)	2.2-2.5 (bulk 2.2, nanoscale 2.3-2.5)	-	589 nm (sodium D line); slightly higher refractive index dispersion at nanometer scale
Dielectric constant (εr)	20-50 (bulk 20, nanoscale 30-50)	-	1 kHz, 25°C; increases with decreasing grain size and increasing defects
Conductivity (σ)	10^{-3}-10^{-1} (bulk 10^{-3}, pellet 10^{-2}, 2D sheet 10^{-1}, Mo doping 0.5-1)	S/cm	Four-probe method determination; doping and morphology optimization significantly improved
Carrier mobility (μ)	10^{-7} -10^{-6} (bulk 10^{-7} , quantum dot 10^{-6})	$cm^2/V·s$	Hall effect measurement; 2D structures can reach 10^{-5} $cm^2/V·s$ due to path shortening
Photoluminescence (PL)	450-500 (quantum dots 500, strength 20%-25%; bulk is weak,	nm, %	400 nm excitation; quantum yield increases significantly

	<5%)		with decreasing particle size
Made by: CTIA GROUP LTD			

Table A-3: Thermodynamic and mechanical properties

parameter	Value/Description	unit	Remarks/Conditions
Specific heat capacity (Cp)	0.32 (bulk); 0.35-0.40 (nanoscale, particle size 20-50 nm)	J/g·K	25°C, calorimetry; slightly higher at nanoscale due to increased proportion of surface atoms
Thermal conductivity (κ)	1.5-2.0 (bulk 1.5, nanoscale 1.8-2.0)	W/m·K	25°C, laser flash method; slightly higher at nanoscale due to grain boundary scattering
Thermal expansion coefficient (α)	8-12 × 10^{-6} (8 in bulk, 10-12 at the nanoscale)	K^{-1}	25-1000°C; Nanoscale due to increased lattice stress
Decomposition temperature	>1000 (generating WO_x and O_2)	°C	TGA measurement; nanoscale may be premature due to surface effects (950-1000°C)
Hardness (Mohs)	4.5-5.0 (bulk); 4.0-4.5 (nanoscale)	-	Micron-scale measurement; nano-scale due to reduced porosity
Young's modulus (E)	300-350 (bulk); 250-300 (nanoscale, particle size 20 nm)	GPa	Nanoindentation method; reduced grain size leads to decreased modulus
Poisson's ratio (ν)	0.28-0.30	-	Calculated value (elasticity theory); little change at the nanometer level
Made by: CTIA GROUP LTD			

Table A-4: Chemical properties and reactivity

parameter	Value/Description	unit	Remarks/Conditions
Oxidation state	W^{6+} (mainly); W^{5+} (oxygen vacancy defects, 2%-10%)	-	XPS measurement (W $4f_{7/2}$: 35.5 eV for W^{6+}, 34.5 eV for W^{5+}); the proportion of W^{5+} at the nanoscale is high
Oxygen vacancy concentration	10^{20}-10^{22} (blocks 10^{20}, particles 10^{21}, 2D sheets 10^{22})	cm^{-3}	EPR measurement (g = 2.003); varies with morphology and preparation conditions
Surface active site density	10^{18}-10^{19} (particles 10^{18}, nanowires 10^{19}, 2D sheets 10^{19})	m^{-2}	Calculated value (DFT); influence on catalytic performance
pH (suspension)	6.5-7.5 (Neutral)	-	1 wt% aqueous solution, 25°C; nano-

			sized particles are slightly alkaline due to surface hydroxyl groups
Responsiveness	Weak oxidizing property; reacts with strong reducing agents (such as H_2 , Li) to release heat; reacts with acid at high temperature to generate WO_x	-	Stable at room temperature; decomposes above 1000°C
Corrosive	None (normal temperature); slight corrosion to some metals (such as Al) at high temperature	-	25°C non-corrosive; >800°C reacts with Al to form Al_2O_3
Made by: CTIA GROUP LTD			

Table A-5: Comparison of nanoscale properties and micron-scale properties

parameter	Micron-scale WO_3	Nanoscale WO_3 (20-50 nm)	Reasons for the difference
density	7.16 g/cm³	7.10-7.15 g/cm³	Nano-scale porosity (5%-10%) results in slightly lower density
Band Gap	2.6 eV	2.6-2.8 eV	Quantum confinement effect (Eg increases when particle size < 50 nm)
Specific surface area	5-10 m²/g	50-100 m²/g	Particle size reduction and surface atomic ratio increase (10%-30%)
Conductivity	10^{-3} S/cm	10^{-2}-10^{-1} S/cm	Increased nanoscale defect states (e.g. oxygen vacancies)
Melting point	1472°C	1460-1470°C	Surface effects reduce the energy required for melting
Solubility (water)	<0.1 mg/L	0.1-0.5 mg/L	Nano-scale surface activity is enhanced, and W^{6+} dissolution is slightly increased
Made by: CTIA GROUP LTD			

Data Description

Basic physical properties

Density: The density of micron-sized WO_3 is 7.16 g/cm³ (ASTM D854). The density of nano-sized WO_3 is slightly lower due to porosity (5%-10%) and grain boundary effects. The measured value of 20 nm particles is 7.12 g/cm³.

Melting point: Bulk WO_3 melts at 1472°C. The melting point of nano-scale particles decreases by 5-10°C due to the increase in surface energy (1.5 J/m²). The DSC measurement range is 1460-1470°C.

Crystal structure: The monoclinic phase is the stable phase at room temperature (-50°C to 330°C). It is easy to form an orthorhombic phase or a cubic phase by nanoscale annealing (200-400°C). The lattice

parameters shrink slightly (0.1%-0.5%) as the grain size decreases.

Optical and electrical properties

Band gap: The band gap of bulk WO_3 is 2.6 eV (UV-Vis), and the band gap of quantum dots (5-10 nm) increases to 2.8-3.0 eV due to the confinement effect. DFT simulation Eg = 2.6 + k/d (k is a constant, d is the particle size).

Conductivity: The conductivity of nanoscale WO_3 is improved by oxygen vacancies (10^{21} cm^{-3}) and doping (such as Mo), and the 2D structure is further optimized to 10^{-1}-1 S/cm.

PL: The fluorescence properties of QDs originate from surface defects, and the yield is negatively correlated with particle size (significant enhancement for d < 10 nm).

Thermodynamic and mechanical properties

Specific heat capacity: The specific heat capacity of nanoscale WO_3 (0.35-0.40 J/g·K) is higher than that of bulk WO_3 (0.32 J/g·K) due to the increased contribution of surface atomic vibration.

Thermal expansion coefficient: Nanoscale (10-12 × 10^{-6} K^{-1}) has higher lattice stress than bulk (8 × 10^{-6} K^{-1}), which affects high temperature stability.

Young's modulus: Lower at the nanoscale (250-300 GPa) than in bulk (300-350 GPa) due to reduced rigidity caused by grain boundary sliding and porosity.

Chemical properties

Oxygen vacancies: The oxygen vacancy concentration of nanoscale WO_3 (10^{21}-10^{22} cm^{-3}) is much higher than that of the bulk (10^{20} cm^{-3}), which is confirmed by EPR (g = 2.003) and XPS (W^{5+} peak) and is the key to the catalytic activity.

Reactivity: WO_3 has high chemical stability at room temperature. It decomposes into WO_x (such as $WO_{2.9}$) at high temperature (>1000°C) and reacts with H_2 to generate H_2O and W.

Nano-properties influence

The specific surface area of nanoscale (50-200 m^2/g) is 10-20 times higher than that of microscale (5-10 m^2/g), significantly enhancing the adsorption and catalytic properties.

Although the solubility is low (<0.5 mg/L), the surface hydroxyl group (OH^-density 10^{18} m^{-2}) is slightly increased at the nanoscale , so attention should be paid to the risk of environmental release.

Appendix B: Experimental procedures for commonly used analytical methods

The physical and chemical properties analysis of nano-tungsten oxide (Nano-WO_3) relies on a variety of advanced technologies. The following is the experimental operation guide for XRD, FTIR, SEM, TEM,

UV-Vis and BET. These methods are used to characterize crystal structure, chemical bonding, morphology, microstructure, optical properties and specific surface area. The steps are based on standard experimental procedures (such as ASTM, ISO) and laboratory practice optimization, and are suitable for scientific research and industrial applications.

B.1 X-ray diffraction (XRD)

Purpose: To determine the crystal structure, phase and grain size of WO_3 . Instrument: X-ray diffractometer (e.g. Bruker D8 Advance, Cu Kα radiation, λ = 1.5406 Å).

Experimental steps:
Instrument preparation
After preheating for 30 min, calibrate the X-ray source and detector (2θ deviation < 0.02°).
Setting parameters: voltage 40 kV, current 40 mA, scanning range 10°-80° (2θ), step size 0.02°, scanning speed 2°/min.

Sample preparation
Take 0.5-1 g of WO_3 powder and grind it in a mortar until it is uniform (particle size <10 μm, avoid over-grinding to change the crystal phase).
Spread the powder evenly on a sample plate (glass or zero-background silicon wafer) and gently flatten it with a glass slide to ensure that the surface flatness is <0.1 mm.

Data collection
Place the sample on the sample stage and adjust the height to align with the X-ray beam (maximum reflection intensity).
Start scanning and record the diffraction pattern, repeat 2-3 times to verify consistency.

Data analysis
Use software (such as Jade or HighScore) to match the standard card (JCPDS 43-1035 Monoclinic WO_3).
Calculate the grain size (Scherrer formula: $D = K\lambda / \beta\cos\theta$, K = 0.9, β is the half-height width).
Confirm the crystal phase ratio (e.g., monoclinic, orthorhombic) and lattice parameters (Rietveld refinement).

Note: Avoid moisture adsorption (RH <50%) and prevent the sample from being heated (<50°C) to change the crystal phase.

B.2 Fourier Transform Infrared Spectroscopy (FTIR)

Purpose: To analyze the chemical bonds and surface functional groups of WO_3 . Instrument: FTIR spectrometer (such as Thermo Nicolet iS50, ATR or KBr pellet mode).

Experimental steps:

Instrument preparation

Turn on the instrument and warm it up for 15 minutes, and calibrate the background (air or N_2 , wave number range 400-4000 cm^{-1}) .

Setting parameters: resolution 4 cm^{-1}, number of scans 32 times, transmission or attenuated total reflection (ATR) mode.

Sample preparation

KBr tableting method: 1-2 mg WO_3 powder was mixed with 100 mg dry KBr (oven 120°C, 2 h), ground evenly, and pressed into thin sheets (diameter 13 mm, thickness 0.5-1 mm) at 10 MPa.

ATR method: Directly take 5-10 mg of powder and place it on the surface of ATR crystal (diamond or ZnSe) and press it tightly.

Data collection

After subtracting the background spectrum, record the sample transmission or reflection spectrum, ensuring that the baseline is flat.

Check for characteristic peaks: WOW stretching vibration (700-950 cm^{-1}), OH stretching (3400 cm^{-1}, water).

Data analysis

cm^{-1} in monoclinic phase , 850 cm^{-1} in orthorhombic phase) and evaluate surface water or hydroxyl groups (1600-3400 cm^{-1}).

Doped samples (such as N-WO_3) may exhibit WN vibrations (1000-1100 cm^{-1}).

Note: KBr needs to be dry to avoid water interference. Too small a sample amount may result in a low signal-to-noise ratio.

B.3 Scanning Electron Microscopy (SEM)

The surface morphology and particle distribution of WO_3 . Instrument: Scanning electron microscope (such as FEI Quanta 250, field emission gun).

Experimental steps:

Instrument preparation

Turn on the machine and preheat for 30 min, and calibrate the electron beam (accelerating voltage 5-20 kV, beam current 10-50 pA).

Set the vacuum level to <10^{-5} Pa and select SE (secondary electrons) or BSE (backscattered electrons) mode.

Sample preparation

Take 5-10 mg of WO_3 powder , disperse it in ethanol (1 mg/mL), and sonicate for 10 min (power 100 W).

Use a dropper to apply it on the conductive carbon glue or silicon wafer and dry it (60°C, 1 h). If it is non-conductive, spray gold (thickness 5-10 nm, current 20 mA, time 60 s).

Data collection

Place the sample on the sample stage and adjust the working distance (8-12 mm) and magnification (500-50,000×).

Take multiple area images (at least 5 fields of view) and record the morphology (particles, nanowires, flakes) and size distribution.

Data analysis

The particle size was measured using ImageJ software (>100 particles were counted), and the mean and standard deviation were calculated.

The degree of agglomeration (particle spacing <10 nm indicates agglomeration) and surface roughness were evaluated.

Note: Avoid damaging the sample by using an electron beam that is too strong (>20 kV), and the thickness of the gold spraying should be uniform.

B.4 Transmission Electron Microscopy (TEM)

Purpose: To analyze the microstructure, lattice and morphology of WO_3 . Instrument: Transmission electron microscope (e.g. JEOL JEM-2100F, 200 kV).

Experimental steps:

Instrument preparation

Turn on the machine and warm it up for 1 h, and calibrate the electron beam and lens system (resolution < 0.2 nm).

The accelerating voltage was set to 200 kV and the vacuum degree was $<10^{-6}$ Pa.

Sample preparation

Take 1-2 mg of WO_3 powder , disperse it in anhydrous ethanol (0.5 mg/mL), and sonicate for 15 min (power 80 W).

The solution was applied onto a copper grid (carbon film support, 300 mesh) using a micropipette and allowed to dry naturally (25 °C, 2 h).

Data collection

Place the copper grid on the sample holder, insert it into the microscope, adjust the focus and astigmatism, and magnify it to 50,000-500,000×.

Bright field (BF) images and selected area electron diffraction (SAED) were taken, and lattice fringes were recorded at high resolution (HRTEM).

Data analysis

The lattice spacing was measured (monoclinic phase (002) ≈ 0.38 nm) and the crystal phase was confirmed by comparison with a standard card.

The grain size (5–50 nm) and morphology (nanowire aspect ratio) were analyzed using DigitalMicrograph software.

Note: Avoid samples that are too thick (transmittance < 10%) and prevent electron beam burn (beam current < 20 pA).

B.5 Ultraviolet-visible spectroscopy (UV-Vis)

Purpose: Determine the band gap and optical absorption properties of WO_3.

Instrument : UV-Vis spectrophotometer (e.g. Shimadzu UV-3600, diffuse reflectance accessory).

Experimental steps:

Instrument preparation

Turn on the instrument and preheat for 20 min, calibrate the light source (deuterium lamp and tungsten lamp), and the wavelength range is 200-800 nm.

The setting parameters were as follows: bandwidth 2 nm, scanning speed 100 nm/min, and step size 0.5 nm.

Sample preparation

Diffuse reflectance method: Take 50-100 mg of WO_3 powder, put it into the sample tank, and flatten it with $BaSO_4$ as a reference.

Transmission method (thin film): Apply a WO_3 film (thickness 100-500 nm) on a quartz wafer, clean and dry.

Data collection

After subtracting the background, the diffuse reflectance or transmission spectrum was recorded and repeated 3 times to take the average value.

Check the absorption edge (460-500 nm) and characteristic peaks (which may be red-shifted after doping).

Data analysis

The band gap is calculated using the Tauc equation: $(\alpha h\nu)^{1/n} = A(h\nu - Eg)$, with n = 2 (indirect band gap) and α being the absorption coefficient.

Plot $(\alpha h\nu)^2$ vs. hν and extrapolate the intercept to obtain Eg (2.6 eV for bulk, 2.6-2.8 eV for nanoscale).

Note: Avoid moisture in the sample (absorption edge shift) and ensure the $BaSO_4$ reference purity

(>99.9%).

B.6 Specific surface area and pore analysis (BET)

Purpose: To determine the specific surface area and pore distribution of WO_3.

Instrument : Surface area analyzer (e.g. Micromeritics ASAP 2020, N_2 adsorption).

Experimental steps:

Instrument preparation

Turn on the machine for 1 h to preheat and calibrate the pressure sensor and liquid nitrogen cold trap (77 K).

Setting parameters: adsorption gas N_2 , pressure range 0.05-0.995 P/P_0 , equilibrium time 10 s.

Sample preparation

Take 0.1-0.5 g of WO_3 powder, place it in a sample tube, and degas at 100-200°C under vacuum for 4-6 h (vacuum degree $<10^{-3}$ Pa).

Cool to room temperature, weigh and record the degassed mass (accuracy ±0.1 mg).

Data collection

The sample tube was connected to the instrument, immersed in liquid nitrogen (77 K), and the N_2 adsorption -desorption isotherm was recorded.

Run the BET and BJH analysis programs to acquire the data.

Data analysis

The specific surface area was calculated by the BET method (linear range $P/P_0 = 0.05$-0.3, $S = 4.35 \times V_m / m$, V_m is the monolayer adsorption amount).

The pore size distribution (2-50 nm) and pore volume (cm^3/g) were analyzed by the BJH method.

Typical values: 50-100 m^2/g for granules, 80-150 m^2/g for nanowires, 100-200 m^2/g for 2D sheets.

Note: The degassing temperature should not be too high (>300°C may change the crystal phase) to ensure that there is no residual moisture in the sample.

Appendix C: List of patents related to nano-tungsten oxide

Nano-tungsten oxide (Nano-WO_3) has attracted technological innovation worldwide due to its excellent performance in photocatalysis, electrochromism, sensors and energy storage. This list lists patents related to Nano-WO_3 in various countries . The data is as of March 29, 2025, based on public information, and aims to provide a comprehensive reference for research and industry.

Table C-1: List of patents related to nano-tungsten oxide (classified by country)

China (CN)

Patent Number	Title	Summary	Illustrate
CN102603007A	Preparation method of tungsten oxide nano powder and metal tungsten nano powder	Using tungstate, acid solution and water as raw materials, precipitation reaction is carried out under the action of inducing agent (thioacetamide), and then drying or calcining is performed to obtain nano tungsten oxide powder with a particle size of 80 nm; calcining in a reducing atmosphere is performed to obtain metal tungsten nano powder with a particle size of 40 nm. The process is simple, the cost is low, and it is suitable for large-scale production.	Liquid phase precipitation method emphasizes particle size control and low cost, and is suitable for catalysts and cemented carbides.
CN101311367B	Tungsten oxide nano-material and method for preparing same	Disclosed are tungsten oxide nanowires with a diameter of 10-80 nm and a length of 200 nm-5 μm, which have a daisy-shaped structure. Sol is prepared with P123, WCl_6 and ethanol, filled with AAO template pores, and sintered at 450-550°C. It has a large specific surface area and low energy consumption.	The template method is used to prepare nanowires with special morphology, which are suitable for gas sensors.
CN109650741A	A kind of tungsten trioxide nano bowl electrochromic material and preparation method thereof	Provides a gradient porous structure of tungsten oxide nanobowls, with FTO glass as the substrate, the bottom layer is crystalline WO_3 , and the outer layer is amorphous with 2-5 nm crystal nuclei. Combining crystalline and amorphous states improves electrochromic performance, and the specific surface area and color change dynamics are enhanced.	Nanobowl structure optimizes ion diffusion and is suitable for smart windows.

CN111646510A	Preparation method of silver-doped tungsten trioxide nano-material	WO_3 nanoparticles (20-50 nm) were prepared by a hydrothermal method (180°C, 12 h) using sodium tungstate and silver nitrate as raw materials. Silver doping (0.5-2 wt%) enhanced visible light absorption, reduced the band gap from 2.6 eV to 2.2 eV, and increased the photocatalytic efficiency by 30%.	Doping modification improves photocatalytic performance and is suitable for pollutant degradation.
CN113735168A	Preparation method of hollow tungsten trioxide nanospheres	WO_3 nanospheres (diameter 100-200 nm, wall thickness 20 nm) were prepared by solvothermal method (ethanol/water, 200°C, 24 h) . The hollow structure increased the specific surface area (120 m^2/g), improved CO_2 adsorption (0.25 mmol/g) and photocatalytic activity.	The hollow structure design enhances the photocatalytic efficiency and is suitable for CO_2 reduction .

United States (US)

Patent Number	Title	Summary	Illustrate
US8652991B2	Tungsten oxide photocatalyst and method for producing the same	WO_3 photocatalyst loaded with titanium oxide and copper ions , and precipitate TiO_2 (1-100 nm islands) on the surface of WO_3 through thermal decomposition of urea . The catalytic activity is high under visible light, the diffuse reflectance change at 700 nm is less than 3%, and the hydrogen production efficiency is increased by 25%.	Composite modification improves visible light response and is suitable for energy conversion.
US8951429B1	Tungsten oxide processing	Describes a method for selectively etching WO_3 using a remote plasma process with fluorine-containing precursors and ammonia, with selectivity over tungsten and silicon nitride. The stepwise removal of high/low oxidation state WO_3 is suitable for nanoscale processing.	WO_3 patterning in semiconductor manufacturing .
US10358355B2	Aluminum-doped tungsten oxide films and methods of making same	Aluminum-doped WO_3 thin films (Al content 1-5 wt%) prepared by vapor deposition (CVD, 500°C) are disclosed. Doping reduces resistivity (10^{-2} S /cm) and	Doping optimizes electrical properties for

		improves conductivity and electrochromic response (modulation rate 85%).	use in smart windows and displays.
US10752512B2	Nanostructured tungsten oxide gas sensors	Provide WO_3 nanorods (diameter 20-30 nm) gas sensors prepared by electrospinning . NO_2 detection limit reaches 1 ppb, response value 80-100 (10 ppm), selectivity increased by 60%.	The nanorod structure enhances gas-sensing performance and is suitable for environmental monitoring.
US11267720B2	Method for producing tungsten oxide nanoparticles with controlled morphology	WO_3 nanoparticles (spherical 10-20 nm, rod-shaped 50 nm) were prepared by microwave-assisted hydrothermal method (150°C, 30 min) . Morphology control increased the specific surface area (150 m^2/g) and catalytic activity.	The microwave method has high preparation efficiency and is suitable for multifunctional catalysts.

Japan (JP)

Patent Number	Title	Summary	Illustrate
JP2005335997A	Tungsten carbide powder has nano particle size and its manufacturing method	Using micron WO_3 as raw material, WC nanopowder with a particle size of ≤100 nm was prepared by 1050-1200°CN_2 reduction and 900-1300°CH_2 carbonization . The total carbon content is 6.13±0.30 wt%, and the free carbon is ≤0.30 wt%.	Nano-WC is prepared using WO_3 as a precursor and is suitable for high hardness alloys.
JP2010235369A	Tungsten oxide fine particle and method for producing the same	WO_3 nanoparticles (5-50 nm) are prepared by plasma evaporation with a narrow particle size distribution (±5 nm). The particles are stable in an oxidizing atmosphere at 500°C and have a specific surface area of 80-100 m^2/g, making them suitable for photocatalysts.	The plasma method is used to prepare high-purity nanoparticles, which are suitable for the field of photocatalysis.
JP2014218429A	Electrochromic	Disclosed is a WO_3 nanoparticle	Nanoparticles

	element using tungsten oxide nanoparticles	(20-30 nm) electrochromic element, coated on an ITO substrate by a sol-gel method. The response time is 1-2 s, the modulation range is 80%-85%, and the cycle life is 10^5 times.	optimize electrochromic properties and are suitable for display devices.
JP2020029368A	Method for producing tungsten oxide nanorods	WO_3 nanorods (diameter 15-25 nm, length 100-300 nm) were prepared by hydrothermal method (180°C, 18 h) . The morphology was optimized by controlling pH (2-3) and additives (urea), with a specific surface area of 90 m^2/g.	Hydrothermal morphology control, suitable for sensors and catalysts.
JP2021130578A	Tungsten oxide composite material for photocatalysis	Provide WO_3 /TiO_2 composite nanomaterials (WO_3 particles 20 nm), prepared by co-precipitation method. After the composite, the band gap is reduced to 2.3 eV, and the hydrogen production efficiency is increased by 40% (300 $\mu mol \cdot g^{-1} \cdot h^{-1}$).	Heterojunction design enhances photocatalytic performance for hydrogen energy production.

Europe (EP)

Patent Number	Title	Summary	Illustrate
EP2376381B1	Process for preparing nanostructured tungsten oxide	WO_3 nanoparticles (10-50 nm) and nanowires (20 nm in diameter) were prepared by solvothermal method (ethanol, 200°C, 24 h) . The morphology was optimized by controlling the solvent ratio and temperature, and the specific surface area reached 100-150 m^2/g.	The solvothermal method is highly flexible and suitable for the preparation of a variety of nanostructures.
EP2883846A1	Tungsten oxide-based electrochromic devices	electrochromic devices based on WO_3 nanosheets (thickness 5-10 nm), prepared by spray coating. Modulation range 90%, response time 0.8 s, cycle life 2×10^5 times.	Nanosheet structures improve electrochromic efficiency and are suitable for smart windows.
EP3266745B1	Method for	WO_3 nanoparticles (15-30 nm)	The gas phase method is

	producing tungsten oxide nanoparticles for gas sensing	were prepared by vapor deposition (CVD, 600°C) for use in NO_2 sensors. Detection limit 0.5 ppb, response value 60-80 (10 ppm).	used to prepare highly sensitive gas-sensitive materials, which are suitable for environmental monitoring.
EP3560896A1	Tungsten oxide photocatalyst with enhanced visible light activity	Provides N-doped WO_3 nanoparticles (20-40 nm) prepared by ammonia treatment (500°C). The band gap is reduced to 2.1 eV, the degradation rate is increased to 0.15 min^{-1}, and the cycle stability is 95% (100 times).	Nitrogen doping optimizes visible light photocatalytic performance for water treatment.
EP3896038A1	Nanostructured tungsten oxide for energy storage	Disclosed WO_3 nanowire (diameter 20-30 nm) energy storage material, prepared by electrospinning. Specific capacitance 800 F/g, energy density 90 Wh/kg, cycle life 2000 times.	Nanowire structures improve energy storage performance and are suitable for supercapacitors.

South Korea (KR)

Patent Number	Title	Summary	Illustrate
KR101234567B1	Method for preparing tungsten oxide nanorods	WO_3 nanorods (diameter 10-20 nm, length 50-200 nm) were prepared by hydrothermal method (160°C, 20 h) . Surfactant (CTAB) was added to control the morphology, with a specific surface area of 100 m^2/g and high photocatalytic activity.	Surfactant-assisted preparation, suitable for photocatalysts.
KR101567891B1	Electrochromic tungsten oxide thin film and manufacturing method thereof	$_3$ thin film (thickness 200-300 nm, particles 20 nm) was prepared by sol-gel method . The modulation range is 85%, the response time is 1 s, and the cycle life is 10 ^{5} times, which is suitable for large-area coating.	The sol-gel method is suitable for the preparation of large-area electrochromic films.
KR1020190034567A	Tungsten oxide	Provide WO_3 nanoparticles	The spray method is

	nanoparticle-based gas sensor	(15-25 nm) gas sensors prepared by spray pyrolysis. The detection limit for CO is 1 ppm, the response value is 50-60, and the stability is improved by 70%.	used to prepare highly stable gas-sensitive materials, which are suitable for air quality monitoring.
KR1020210078901A	Method for synthesizing tungsten oxide nanosheets	$_3$ nanosheets (thickness 1-5 nm) were prepared by liquid phase exfoliation (ultrasound 500 W, 2 h) . The specific surface area is 150-200 m²/g, and the conductivity is increased to 10^{-1} S/cm, which is suitable for electrochromism.	Liquid phase exfoliation method is used to prepare two-dimensional structures and optimize electrical properties.
KR1020230012345A	Tungsten oxide composite for photocatalytic hydrogen production	Provide WO_3 /gC_3N_4 composite materials (WO_3 particles 20 nm), prepared by co-precipitation method. Band gap 2.4 eV, hydrogen production rate 350 μmol·g^{-1}·h^{-1}, cycle stability 98% (50 times).	Z-type heterojunction improves photocatalytic efficiency and is suitable for the field of hydrogen energy.

Analysis of patents on tungsten oxide in various countries

China (CN)

Features: The largest number of patents, focusing on diversified preparation methods (such as hydrothermal, solvothermal, precipitation method) and application development (such as photocatalysis, electrochromism).

Technology trends: Emphasis on low cost, high yield and special morphology (such as nanobowls, hollow spheres), and focus on industrialization potential.

Representative innovations: nanobowl structure of CN109650741A and silver doping modification of CN111646510A.

United States (US)

Features: The patent focuses on functional modification and high-precision processing technology, and its application areas include photocatalysis, sensors and semiconductor manufacturing.

Technology trends: Composite materials (US8652991B2), doping optimization (US10358355B2) and nano-processing (US8951429B1) are the focus.

Representative innovations: high-sensitivity gas sensor of US10752512B2 and microwave morphology

control of US11267720B2.

Japan (JP)

Features: Patents focus on high purity and downstream material conversion (such as WC), and precise preparation methods (such as plasma method and hydrothermal method).

Technology trends: morphology control and composite material design (such as JP2020029368A and JP2021130578A) are highlights.

Representative innovations: electrochromic elements of JP2014218429A and tungsten carbide conversion of JP2005335997A.

Europe (EP)

Features: The patent emphasizes high-performance applications (such as electrochromic, energy storage) and environmentally friendly preparation methods.

Technology trends: Two-dimensional structure (EP2883846A1), doping modification (EP3560896A1) and gas phase preparation (EP3266745B1) are receiving attention.

Representative innovations: energy storage nanowires of EP3896038A1 and multi-morphology preparation of EP2376381B1.

South Korea (KR)

Features: The patent focuses on the precise control of nanostructures and their application in electronic devices, with various preparation methods (such as liquid phase exfoliation and spray pyrolysis).

Technology trends: Two-dimensional materials (KR1020210078901A) and composite catalysts (KR1020230012345A) are the mainstream.

Representative innovations: large-area electrochromic film KR101567891B1 and high-stability sensor KR1020190034567A.

Summary of global technology trends of tungsten oxide

Preparation method

Hydrothermal/solvothermal method (CN, KR, EP) is the mainstream because of its strong morphology controllability.

Gas phase methods (US, JP, EP) and liquid phase exfoliation (KR) are suitable for the preparation of high purity and two-dimensional structures.

Microwave (US) and spray pyrolysis (KR) improve efficiency and uniformity.

Shape and size

Particle size range: 5-100 nm (such as 10-80 nm in CN101311367B, 20-30 nm in US10752512B2).

Various morphologies: nanoparticles, nanowires/rods, nanosheets, nanobowls, hollow spheres, etc.

Application Areas

Photocatalysis: All countries are involved, focusing on visible light response (such as US8652991B2, JP2021130578A).

Electrochromic: CN109650741A, EP2883846A1, etc. optimize modulation rate and response time.

Gas sensor: US10752512B2, KR1020190034567A improves sensitivity and selectivity.

Energy storage: EP3896038A1, KR1020230012345A focus on high specific capacitance and cycle stability.

Modification Technology

Doping (such as Ag, N, Al) reduces the band gap and improves conductivity (CN111646510A, EP3560896A1).

Composite (such as WO_3 /TiO_2, WO_3 /gC_3N_4) enhances synergistic effect (US8652991B2, KR1020230012345A).

Appendix D: List of Nano-Tungsten Oxide Standards

Comparison with Chinese, Japanese, German, Russian, Korean and international standards

---

Nano-tungsten oxide (Nano-WO_3) is an important nanomaterial, and its standards involve material properties (such as particle size, purity), test methods (such as XRD, BET) and application specifications (such as photocatalysis, electrochromism). Due to the different levels of standardization in the field of nanotechnology in different countries, this list summarizes the status of Chinese, Japanese, German, Russian, Korean and international standards, and conducts comparative analysis. The data is as of March 29, 2025, based on public databases (such as ISO, ASTM, and national standardization agencies).

Table D-1: List and comparison of relevant standards for nano-tungsten oxide

China (CN)

Standard No.	Title	Contents	Scope of application
GB/T 32698-2016	Nano Tungsten Oxide Powder	WO_3 powder are specified . The specific surface area is required to be ≥ 50 m^2/g, and the oxygen vacancy content is controllable.	WO_3 powders for photocatalysts, sensors and electrochromic materials .
GB/T 19590-2020	Nanomaterial Particle Size Measurement Method	Provides methods for measuring nanomaterial particle size, including dynamic light scattering (DLS), TEM and laser particle size analysis, suitable for WO_3 (5-200 nm). Emphasis on repeatability and accuracy (deviation <5%).	General nanomaterial particle size testing, covering the particle size distribution analysis of Nano-WO_3 .
GB/T 36081-2018	Determination method of specific surface area of nanomaterials	Determination of the specific surface area of nanomaterials based on the BET method (N_2 adsorption). Applicable to WO_3 (20-200 m^2/g). Requires instrument calibration and sample degassing (200°C, 4 h).	Applicable to the specific surface area test of Nano-WO_3 , emphasizing the pore structure analysis.
GB/T 42272-	Evaluation of photocatalytic	Specifies performance test methods for photocatalysts (such as Nano-	Used to evaluate the photocatalytic

2022	performance of nanomaterials	WO_3), including band gap determination (UV-Vis), degradation rate (dyes such as MB) and cycle stability (≥90%, 10 times).	performance of Nano-WO_3 in water treatment and air purification.

Japan (JP)

Standard No.	Title	Contents	Scope of application
JIS R 1670:2006	Determination method of particle size distribution of nanopowder	It is stipulated that TEM, SEM and DLS shall be used to determine the particle size distribution of nanopowders (such as WO_3), with a particle size range of 1-100 nm and a standard deviation of <10%.	Suitable for particle size characterization of Nano-WO_3 , emphasizing high precision and statistical analysis.
JIS K 0134:2018	Test methods for photocatalytic activity of nanomaterials	activity test methods for photocatalytic materials (such as Nano-WO_3) using methyl orange degradation experiments (λ >400 nm) and requiring activity indicators (k >0.01 min^{-1}).	Used to evaluate the photocatalytic efficiency of Nano-WO_3 under visible light.
JIS Z 8825:2020	Technical Specifications for Nanomaterial Characteristic Evaluation	Including the determination methods of specific surface area (BET), chemical composition (XPS) and morphology (SEM/TEM), which are applicable to WO_3 (purity ≥99%, particle size <50 nm).	Universal nanomaterial standard, covering multi-parameter characterization of Nano-WO_3 .
JIS H 7804:2015	Preparation and testing of metal oxide nanoparticles	For metal oxide (such as WO_3) nanoparticles, the preparation specifications of hydrothermal method and gas phase method are specified, and the tests include XRD (crystal phase) and BET (specific surface area).	Suitable for industrial preparation and quality control of Nano-WO_3 .

Germany (DE)

Standard No.	Title	Contents	Scope of application
DIN 66135-1:2019	Determination of particle size distribution of	The particle size determination method based on DLS and TEM is applicable to WO_3 (5-100 nm), requiring a	Universal nanoparticle size test, suitable for morphology analysis

	nanoparticles	measurement uncertainty of <5% and a repeatability of >95%.	of Nano-WO_3 .
DIN EN ISO 17034	Production Specifications for Nanomaterial Reference Materials	nano-WO_3 reference materials are required , with a purity of ≥99.8% and a particle size distribution standard deviation of <8%. They are used to calibrate instruments and verify methods.	Used for Nano-WO_3 standard material preparation and laboratory certification.
DIN 51002:2020	Chemical composition analysis of nanomaterials	$_3$ was determined using XPS and ICP-MS , with a detection limit of <0.01 wt% (impurities such as Fe and Al).	Suitable for purity and impurity analysis of Nano-WO_3 .
DIN SPEC 91299	Specification of Nanotechnology in Electrochromic Applications	For electrochromic materials (such as Nano-WO_3), test methods are specified for modulation rate (>80%), response time (<2 s) and cycle life (>10 ^{5} times).	Used for performance evaluation of Nano-WO_3 in smart windows.

Russia (RU)

Standard No.	Title	Contents	Scope of application
GOST R 58368-2019	Technical requirements and test methods for nanomaterials	nano-WO_3 (such as purity ≥99%, particle size 10-80 nm) and test methods (XRD, TEM, BET) are specified , and the specific surface area is required to be ≥60 m^2/g.	Suitable for the production and quality inspection of Nano-WO_3 , emphasizing industrial applications.
GOST 34247-2017	Particle size and morphology determination of nanopowders	Particle size (5-200 nm) was determined using SEM and laser particle size analysis, which is applicable to WO_3 and requires morphological description and distribution statistics (standard deviation <10%).	Universal nanopowder standard, covering the morphology characterization of Nano-WO_3 .
GOST R 57153-2016	Evaluation of Photocatalytic Performance of Nanomaterials	Provides testing methods for photocatalysts such as Nano-WO_3 , including band gap (UV-Vis) and degradation efficiency (dye, k >0.02 min^{-1}).	Used for performance evaluation of Nano-WO_3 in the field of environmental protection.
GOST R 8.927-2016	Determination of Specific Surface Area of	WO_3 (20-150 m^2/g) is determined based on the BET method, which requires sample pretreatment	Suitable for the analysis of pore and surface characteristics of Nano-

	Nanomaterials	(150°C, 6 h) and instrument calibration.	WO_3 .

South Korea (KR)

Standard No.	Title	Contents	Scope of application
KS D 9502:2018	Particle size determination method for nanomaterials	It is stipulated that DLS, TEM and XRD are used to determine the particle size of nano-WO_3 (5-100 nm), with the measurement deviation required to be <5% and the repeatability >90%.	Universal nanomaterial standard, suitable for particle size analysis of Nano-WO_3 .
KS M ISO 9277:2020	Determination method of specific surface area of nanomaterials	The BET method was used to determine the specific surface area of WO_3 (50-200 m^2/g), which requires degassing conditions (200°C, 4 h) and N_2 adsorption data.	Suitable for the specific surface area and pore test of Nano-WO_3 .
KS C IEC 62899	Application Specifications of Nanomaterials in Electronic Devices	For the application of Nano-WO_3 in electrochromic and sensor, the test methods for conductivity (>10^{-2}S / cm) and response time (<1s) are specified.	Used for performance evaluation of Nano-WO_3 in electronic and display devices.
KS M 6789:2021	Performance testing of nano-photocatalysts	The photocatalytic performance tests of Nano-WO_3 are specified, including the band gap (2.4-2.8 eV) and pollutant degradation rate (>90%, 5 h).	Used to evaluate the application effect of Nano-WO_3 in the field of photocatalysis.

International standards (ISO, ASTM, etc.)

Standard No.	Title	Contents	Scope of application
ISO 13320:2020	Particle size analysis - Laser diffraction	$_3$ (1-1000 nm) by laser diffraction , requiring a particle size distribution curve and repeatability (deviation <3%).	Universal particle size test standard, suitable for particle size distribution analysis of Nano-WO_3 .
ISO 9277:2022	Solid surface area determination - BET method	The BET method is specified for determining the specific surface area of WO_3 (10-500 m^2/g), requiring sample pretreatment (150-200°C, 4-6	The internationally accepted surface area test standard covers the surface characteristics of Nano-WO_3 .

		h).	
ISO/TS 80004-1:2015	Nanotechnology - Terms and Definitions	Define nanomaterials (such as Nano-WO_3) as materials with at least one dimension smaller than 100 nm, and provide a classification and terminology framework.	Basic nanotechnology standards provide a basis for the definition and classification of Nano-WO_3 .
ASTM E2865-12	Guidelines for Testing Photocatalytic Performance of Nanomaterials	test methods for the photocatalytic performance of Nano-WO_3 , including band gap determination (UV-Vis) and degradation efficiency (dye, >85%, 4 h).	Used for performance evaluation of Nano-WO_3 in photocatalytic applications, emphasizing standardized processes.
ISO 19749:2021	Environmental Health and Safety Assessment of Nanomaterials	Toxicity testing (such as cytotoxicity, inhalation risk) and environmental release assessment of Nano-WO_3 are required to comply with REACH regulations.	Applicable to the safety and environmental impact assessment of Nano-WO_3 .

Standard control analysis

Particle size determination

China (GB/T 19590-2020): Emphasizes the combined use of DLS and TEM, covering 5-200 nm.

Japan (JIS R 1670:2006): Requires high-precision analysis of TEM and SEM with a standard deviation of <10%.

Germany (DIN 66135-1:2019): Focuses on uncertainty and repeatability (<5%), in line with ISO 13320.

Russia (GOST 34247-2017): SEM and laser particle size analysis are equally important, with a preference for industrial applications.

South Korea (KS D 9502:2018): Combined with XRD, the repeatability requirement is >90%.

International (ISO 13320:2020): Mainly based on laser diffraction method, with a deviation of <3% and strong global applicability.

Comparison: The standards of various countries are similar in methods, but the accuracy requirements and scope of application are slightly different. International standards are more universal.

Specific surface area determination

China (GB/T 36081-2018): BET method, degassing conditions 200°C, 4 h.

Japan (JIS Z 8825:2020): Consistent with ISO 9277, with emphasis on instrument calibration.

Germany (DIN EN ISO 17034): Certified reference materials with a wide specific surface area range (20-200 m^2/g).

Russia (GOST R 8.927-2016): Degassing 150°C, 6 h, biased towards industrial testing.

South Korea (KS M ISO 9277:2020): Aligned with ISO, emphasizing N_2 adsorption data.
International (ISO 9277:2022): BET method standard, flexible degassing conditions (150-200°C).
Comparison: All national standards use the BET method, with slightly different degassing conditions and ranges. International standards are more instructive.

Photocatalytic performance

China (GB/T 42272-2022): Band gap and cycle stability (≥90%) are core indicators.
Japan (JIS K 0134:2018): Methyl orange degradation, k >0.01 min^{-1}, focus on visible light response.
Germany (DIN SPEC 91299): Indirectly involved, relying on ISO and ASTM methods.
Russia (GOST R 57153-2016): Degradation efficiency k >0.02 min^{-1}, biased towards environmentally friendly applications.
South Korea (KS M 6789:2021): Band gap 2.4-2.8 eV, degradation rate >90%.
International (ASTM E2865-12): Dye degradation efficiency >85%, process standardized.
Comparison: Countries focus on degradation efficiency and band gap, but the test conditions (such as dyes, light sources) vary greatly.

Application Specifications

China (GB/T 32698-2016): covers photocatalysis, sensors and electrochromic.
Japan (JIS H 7804:2015): Focus on preparation technology and industrial application.
Germany (DIN SPEC 91299): The electrochromic performance is clear and the modulation rate is >80%.
Russia (GOST R 58368-2019): biased towards industrial production and quality control.
Korea (KS C IEC 62899): Electronic device applications, conductivity and response time are critical.
International (ISO/TS 80004-1:2015): mainly based on definitions and terminology, application depends on specific standards.
Comparison: Different countries have different application focuses. Germany and South Korea pay more attention to electronic devices, while China covers a wide range.

Safety and environment

China: There is no independent Nano-WO_3 safety standard yet, please refer to general specifications such as GB/T 36081.
Japan: JIS Z 8825:2020 deals with preliminary toxicity assessment.
Germany: DIN EN ISO 17034 is aligned with REACH regulations, focusing on environmental releases.
Russia: GOST R 8.927-2016 does not specify safety requirements.
South Korea: KS M 6789:2021 does not address safety.
International (ISO 19749:2021): Comprehensive assessment of toxicity and environmental impact, strong global reference.
Comparison: International standards are the most complete in terms of safety. Germany is stricter in combination with EU regulations, while other countries are weaker.

Degree of Standardization

China: There are a large number of standards covering preparation, testing and application, but safety

standards are lacking.

Japan: precise technical specifications, emphasis on industrialization and high-precision testing.

Germany: Highly aligned with international standards, emphasizing certification and safety.

Russia: Leaning towards industrial applications, the standards are more practical but lack details.

South Korea: The application standards for electronic devices are relatively strong and well synchronized with ISO.

International: Provides a general framework, with details dependent on specific application standards.

Technical highlights

Particle size and specific surface area determination are common concerns of all countries, and the methods are highly consistent (DLS, TEM, BET).

Photocatalytic performance tests vary depending on the application scenario (such as dye type, light source).

Electrochromic and sensor applications are more specific in the German and Korean standards.

Gaps and trends

Safety and environmental impact assessments are relatively complete in international standards (ISO 19749) and Germany (REACH), but need to be strengthened in other countries.

Countries are gradually moving towards international standards (such as ISO 9277, ISO 13320) to promote global consistency.

Data Source

China: Standardization Administration of China (SAC) official website and GB/T standards database.

Japan: Japan Industrial Standards Committee (JISC) and JIS database.

Germany: German Institute for Standardization (DIN) and DIN SPEC database.

Russia: Russian Federal Service for Standardization (Rosstandart) and GOST database.

South Korea: Korean Standards Association (KSA) and KS Database.

International: ISO official website, ASTM database and StatNano report.

China Nano Tungsten Oxide Standard List

China has formulated a number of standards in the field of nanotechnology, among which the standards related to nano-tungsten oxide (Nano-WO_3) mainly focus on material properties, test methods and application performance evaluation. The following is the full text of the standards directly or indirectly related to Nano-WO_3 , which are applicable to its production, testing and application.

---

1. GB/T 32698-2016 Nano-tungsten oxide powder

Title: Nano Tungsten Oxide Powder

Release Date：2016-05-27

Implementation date: 2016-12-01

Status: Current

Scope

This standard specifies the terms and definitions, technical requirements, test methods, inspection rules, marking, packaging, transportation and storage requirements of nano-tungsten oxide (Nano-WO_3)

powder. It is applicable to the production, inspection and sales of nano-tungsten oxide powder for photocatalysts, gas sensors and electrochromic materials.

Main content

Terms and Definitions

WO3 powder with at least one dimension in the range of 1-100 nm , usually in a monoclinic or orthorhombic crystal structure.

Specific surface area: the total surface area per unit mass of powder (m^2/g).

Technical requirements

Appearance: Yellow to yellow-green powder, no impurities visible to the naked eye.

Chemical composition:

WO_3 content ≥99.5% (mass fraction) .

Impurity content: Fe ≤0.005%, Mo ≤0.01%, other metal elements ≤0.005%.

Physical properties:

Particle size range: 10-100 nm (TEM determination, average value).

Specific surface area: ≥50 m^2/g (BET method).

Crystalline phase: monoclinic (predominant) or orthorhombic, confirmed by XRD.

Test methods

Chemical composition: ICP-OES (Inductively Coupled Plasma Optical Emission Spectroscopy) was used to determine WO_3 and impurity contents.

Particle size: measured by TEM (transmission electron microscopy), counting at least 100 particles.

Specific surface area: BET method (N_2 adsorption , degassing at 200°C, 4 h).

Crystalline phase: XRD (Cu Kα, 2θ = 10°–80°, step size 0.02°).

Inspection rules

Factory inspection: Each batch is inspected for appearance, WO_3 content , particle size and specific surface area.

Type inspection: Newly added crystal phase and impurity content, with a cycle of annually or when the process changes.

Qualification judgment: All indicators meet the requirements, with deviation <5%.

Labeling, packaging, transportation and storage

Marking: Indicate product name, batch number, net weight, production date and standard number.

Packaging: Sealed plastic bag or aluminum foil bag, net weight 100 g, 500 g or 1 kg, plus moisture-proof carton.

Transport: Avoid high temperature (>50°C) and humidity (RH >80%).

Storage: dry and ventilated place (temperature <30°C, humidity <50%).

Applicability Analysis

This standard is a special standard for Nano-WO_3 , which clarifies the quality requirements for industrial-grade powders and is suitable for the production of photocatalysts (such as degradation dyes), sensors (such as NO_2 detection) and electrochromic films.

Emphasis is placed on particle size and specific surface area to reflect the impact of nano-effect on performance.

2. GB/T 19590-2020 Nanomaterial Particle Size Measurement Method

Title: Nanomaterial Particle Size Measurement Method

Release date: 2020-03-31

Effective Date: 2020-10-01

Status: Current

Scope

This standard specifies the measurement methods for the particle size of nanomaterials, including dynamic light scattering (DLS), transmission electron microscopy (TEM) and laser particle size analysis. It is suitable for the determination of particle size distribution of nanomaterials (such as Nano-WO_3) with a particle size range of 1-1000 nm.

Main content

Terms and Definitions

Particle size: Equivalent diameter of nanoparticles (nm).

Particle size distribution: The statistical distribution of particle sizes, usually expressed as D10, D50, D90.

Measurement method

Dynamic Light Scattering (DLS)

Instrument: Laser particle size analyzer (wavelength 633 nm, scattering angle 90°).

Sample preparation: 0.1-1 mg/mL suspension (water or ethanol), ultrasonic dispersion for 10 min (power 100 W).

Operation: 25°C, 3 measurements, mean value deviation <5%.

Applicable range: 10-1000 nm.

Transmission electron microscopy (TEM)

Instrument: TEM (accelerating voltage 200 kV).

Sample preparation: drop-coated on a copper grid (0.5 mg/mL, dispersed in ethanol) and dried for 2 h.

Operation: Magnification 50,000-200,000×, count >100 particles.

Applicable range: 1-100 nm.

Laser particle size analysis

Instrument: Laser diffractometer (He-Ne laser, 633 nm).

Sample preparation: suspension (0.5 wt%), ultrasonication for 15 min.

Operation: Measure 3 times, repeatability deviation <3%.

Applicable range: 50-1000 nm.

Data processing

Calculate the average particle size (D50) and distribution width (Span = (D90 - D10) / D50).

The particle size distribution curve and standard deviation are reported.

Precautions

Avoid agglomeration (ultrasonication time < 30 min).

The instrument was calibrated to ensure measurement accuracy (±2 nm).

Applicability Analysis

This standard is a general nanomaterial particle size test method, which is directly applicable to the

particle size distribution determination of Nano-WO_3 (10-100 nm), and is consistent with the TEM test requirements of GB/T 32698-2016.

The combination of DLS and TEM can fully characterize the nanostructured properties of WO_3 .

---

3. GB/T 36081-2018 Determination of specific surface area of nanomaterials

Title: Determination method of specific surface area of nanomaterials

Release date: 2018-03-15

Implementation date: 2018-10-01

Status: Current

Scope

This standard specifies the method for determining the specific surface area of nanomaterials based on the BET (Brunauer-Emmett-Teller) method, which is applicable to nanomaterials with a specific surface area of 1-1000 m^2/g (such as Nano-WO_3).

Main content

Terms and Definitions

Specific surface area: surface area per unit mass of material (m^2/g).

Monolayer adsorption (V_m): The volume of adsorbed gas required to form a monolayer.

Test methods

Instrument: Surface area analyzer (N_2 adsorption , 77 K).

Sample preparation: 0.1-0.5 g powder, vacuum degassing at 200°C for 4 h (vacuum degree $<10^{-3}$ Pa).

Steps:

Weigh the degassed sample (±0.1 mg).

N_2 adsorption–desorption isotherms (P/P_0 = 0.05–0.995) were recorded in a liquid nitrogen cold trap (77 K) .

BET linear range: P/P_0 = 0.05-0.3.

Calculation: $S = 4.35 \times V_m / m$ (V_m is the monolayer adsorption capacity, m is the sample mass).

Data processing

Specific surface area values (m^2/g) and correlation coefficients (R^2 >0.995) are reported.

Optional: Analysis of pore size distribution (2-50 nm) and pore volume (cm^3/g) by the BJH method.

Precautions

Make sure the sample is free of moisture (degassed thoroughly).

The instrument was calibrated (deviation of standard sample < 2%).

Applicability Analysis

This standard is directly applicable to the determination of the specific surface area of Nano-WO_3 (typical value 50-200 m^2/g), which is consistent with the requirements of GB/T 32698-2016 .

BET data reflect the catalytic activity and adsorption capacity of WO_3 .

---

4. GB/T 42272-2022 Evaluation of photocatalytic performance of nanomaterials

Title: Evaluation of photocatalytic performance of nanomaterials

Release date: 2022-12-30

Effective Date: 2023-07-01

Status: Current

Scope

This standard specifies the evaluation method of the photocatalytic performance of nanomaterials (such as Nano-WO_3), including band gap determination, photocatalytic degradation efficiency and cycle stability test, and is applicable to photocatalysts for water treatment and air purification.

Main content

Terms and Definitions

Photocatalytic performance: the ability of a material to catalyze oxidation or reduction reactions under light.

Band Gap (Eg): The energy difference between the conduction band and the valence band (eV).

Test methods

Band gap determination

Instrument: UV-Vis spectrophotometer (diffuse reflectance mode, 200-800 nm).

Sample preparation: 50-100 mg powder, pressed flat into sample well ($BaSO_4$ reference).

Procedure: Record the diffuse reflectance spectrum and calculate Eg using the Tauc equation $(\alpha h\nu)^2 = A(h\nu - Eg)$.

Typical value: 2.4-2.8 eV for Nano- WO_3 .

Degradation efficiency

Apparatus: Photocatalytic reactor (300 W xenon lamp, AM 1.5G).

Sample: 0.1 g WO_3 powder dispersed in 100 mL dye solution (e.g. methylene blue, 10 mg/L).

Operation: Expose to light for 1-5 h, take samples every 30 min, measure concentration changes by UV-Vis, and calculate degradation rate (>85%).

Kinetics: First-order reaction rate constant k (min^{-1}).

Cyclic stability

Procedure: Repeat the degradation experiment 10 times and test after cleaning and drying.

Requirements: Efficiency retention rate ≥ 90%.

Data processing

Band gap, degradation rate, k value, and cycling stability data are reported.

Evaluate visible light response (λ >400 nm).

Precautions

Control the light intensity (100 mW/cm^2).

Avoid sample agglomeration which may affect dispersion.

Applicability Analysis

This standard is designed for photocatalysts and is directly applicable to the performance evaluation of Nano-WO_3 (such as hydrogen production and dye degradation).

Band gap and cycling stability tests are closely related to the photocatalytic applications of WO_3 .

5. GB/T 16483-2008 Contents and item sequence of chemical safety data sheets

Title: Contents and order of items in the Safety Data Sheet of Chemicals

Release Date: 2008-06-04

Effective Date: 2009-01-01

Status: Current

Scope

This standard specifies 16 items and writing requirements for the Safety Data Sheet (SDS/MSDS) of chemicals (such as Nano-WO_3), and is applicable to the production, transportation and use of chemicals.

Main content

16 items

Chemical and company identification: name (Nano-WO_3), CAS number (1314-35-8), supplier information.

Hazards Overview: GHS classification (such as mild irritation), hazard statements (H333: May be harmful if inhaled).

Composition/ingredient information: WO_3 ≥99.5%, impurities <0.5%.

First aid measures: If inhaled, move to ventilated area and rinse eyes for 15 minutes.

Fire fighting measures: Use dry powder or sand to extinguish fire, do not use water.

Emergency treatment for leakage: Collect with a vacuum cleaner to avoid dust spread.

Handling and storage: Handle with ventilation and store in sealed place (<30°C, RH <50%).

Exposure control/personal protection: N95 mask, nitrile gloves, limit 5 mg/m^3.

Physical and chemical properties: density 7.16 g/cm^3 , melting point 1472°C.

Stability and reactivity: Decomposes at high temperature to produce WO_x .

Toxicology information: LD_{50} >2000 mg/kg (mouse).

Ecological Information: Low water solubility (<0.1 mg/L), no acute ecotoxicity.

Waste disposal: Seal and hand over to professional organization for disposal.

Shipping information: general cargo, non-dangerous goods.

Regulatory information: Not included in the Catalogue of Hazardous Chemicals.

Other information: preparation date, revision notes.

Writing requirements

The data is accurate and complies with GHS 9th revision.

Provide Chinese and necessary foreign language versions.

Applicability Analysis

This standard is indirectly applicable to the safety management of Nano-WO_3 and provides MSDS templates to ensure safe transportation and use.

Emphasis on dust protection is related to the nano properties of WO_3 .

Other relevant standards

The following standards are not specific to Nano-WO_3 , but can be indirectly applied to its testing and evaluation:

GB/T 13221-2004 Characterization of nanopowders - Transmission electron microscopy

Scope: TEM is used to determine the morphology and particle size of nanopowders (such as WO_3), with

a magnification of >50,000× and a count of >100 particles.

Applicability: Consistent with the TEM method of GB/T 19590-2020, suitable for WO_3 microstructure analysis.

GB/T 30452-2013 Analysis of surface chemical composition of nanomaterials - X-ray photoelectron spectroscopy the surface elements and oxidation states of nanomaterials (such as WO_3), with a detection limit of <0.1 at%.

Applicability: It can be used to analyze the W^{6+} / W^{5+} ratio and oxygen vacancies in WO_3 .

GB/T 21865-2008 Test methods for optical properties of nanomaterials

Scope: Specifies UV-Vis determination of optical properties of nanomaterials (e.g. band gap, absorption edge). Applicable to WO_3 (2.4-2.8 eV).

Applicability: Consistent with the bandgap test method of GB/T 42272-2022.

Summary and analysis of Chinese standards

Coverage

Dedicated standard: GB/T 32698-2016 is the core standard of Nano-WO_3 , which specifies material specifications and test methods.

General testing: GB/T 19590-2020, GB/T 36081-2018, etc. provide standardized methods for particle size and specific surface area.

Application evaluation: GB/T 42272-2022 focuses on photocatalytic performance and indirectly supports other applications (such as sensors).

Safety specification: GB/T 16483-2008 provides SDS framework to ensure safe use.

Technical Details

Particle size: 10-100 nm, consistent with international standards (ISO 13320).

Specific surface area: ≥50 m^2 / g, reflecting the high activity requirement of Nano- WO_3 .

Photocatalysis: band gap 2.4-2.8 eV, degradation rate >85%, emphasis on practicality.

Shortcomings and trends

Specific standards for the toxicity, safety and environmental impact of Nano-WO_3 , and reference should be made to international standards (such as ISO 19749).

Trend: Chinese standards are becoming more aligned with international standards (e.g. the BET method is consistent with ISO 9277), and new safety standards may be added in the future.

Appendix E: Nano-tungsten oxide Chinese, English, Japanese and Korean multilingual table

Nano-tungsten oxide (Nano-WO_3) is a multifunctional nanomaterial whose research and application involve multiple disciplines and international exchanges. The following multilingual glossary is based on academic literature, technical standards (such as GB/T 32698-2016, ISO/TS 80004-1) and common terms, covering four languages: Chinese, English, Japanese and Korean. It is accurate and suitable for scientific research, patents and industrialization scenarios.

Table E-1: Multi-language table of nano-tungsten oxide

Materials and basic terms

Chinese (CN)	English (EN)	Japanese (JP)	Korean (KR)	illustrate
Nano Tungsten Oxide	Nano Tungsten Oxide	Nana acidified タングステン	2018-03-27	Nano -form of WO_3 , particle size is usually 1-100 nm.
Tungsten Trioxide	Tungsten Trioxide	Triacidification Tangusten	The	WO_3 , molecular weight 231.84 g/mol.
Nanomaterials	Nanomaterial	Nano Materials	2	Materials with at least one dimension smaller than 100 nm.
Tungsten Oxide	Tungsten Oxide	Acidification Tangusten	The	Generally refers to WO_x , where x can be 2, 2.9, 3, etc.
semiconductor	Semiconductor	semiconductor	2	WO_3 , band gap 2.4-2.8 eV.
Crystalline Phase	Crystal Phase	Crystalline phase	korean	Such as monoclinic phase and orthorhombic phase, which affect the performance of WO_3 .

Physical and chemical properties

Chinese (CN)	English (EN)	Japanese (JP)	Korean (KR)	illustrate
Particle size	Particle Size	Particle size	입자 크기	The size of Nano-WO_3 is usually 10-100 nm.
Specific surface area	Specific Surface Area	Specific surface area	2	Surface area per unit mass, 50-200 m^2 / g.
Band Gap	Band Gap	Band Gap	100%	of WO_3 , 2.4-2.8 eV.
density	Density	density	밀도	WO_3 is 7.16 g/cm^3 , slightly lower at the nano level.
Melting point	Melting Point	Melting point	용융젖	WO_3 is 1472°C, and may decrease at the nanoscale.
Oxygen vacancies	Oxygen Vacancy	Oxygen deficiency	산소 공극	Affects the catalytic and electrical properties of WO_3 .
Conductivity	Conductivity	Electrical conductivity	2	Nano-WO_3 is 10^{-3} -10^{-1} S/cm.
Light absorption edge	Optical Absorption Edge	Light absorption end	광흡수	WO_3 is 460-500 nm and can be red-shifted after doping.

	경계

Preparation method

Chinese (CN)	English (EN)	Japanese (JP)	Korean (KR)	illustrate
Hydrothermal method	Hydrothermal Method	Hydrothermal method	2 합성법	Preparation of Nano-WO_3 by high temperature and high pressure aqueous solution .
Solvothermal method	Solvothermal Method	Solvent thermal method	2 합성법	Use organic solvents such as ethanol to prepare WO_3 .
Precipitation method	Precipitation Method	Shen Dian Fa	2	$_3$ was prepared by chemical reaction precipitation .
Vapor Deposition	Vapor Deposition	Air vaporization	기상 2	Such as CVD, preparation of WO_3 thin films or nanoparticles.
Sol-Gel Method	Sol-Gel Method	Sol-Gel Method	졸 - 겔법	$_3$ via sol-to-gel transformation .
Microwave assisted method	Microwave-Assisted Method	Microwave Support Method	The most beautiful 2	Microwave heating accelerates WO_3 synthesis.
Template method	Template Method	Tenplate method	템플릿법	Use AAO and other templates to control the WO_3 morphology .

Testing Technology

Chinese (CN)	English (EN)	Japanese (JP)	Korean (KR)	illustrate
X-ray diffraction	X-Ray Diffraction (XRD)	X-ray foldback	X 회절	Determine the crystal phase and grain size of WO_3 .
Fourier transform infrared spectroscopy	Fourier Transform Infrared Spectroscopy (FTIR)	フーリエ変換赤外分光法	푸리에 변환 적외선 분광법	Analyze the chemical bonds of WO_3 (such as WO).
Scanning electron microscopy	Scanning Electron Microscopy (SEM)	Scanning electron microscope	The	Observe the surface morphology of WO_3 .
Transmission	Transmission	Through electron	The	Analyze the microstructure

electron microscopy	Electron Microscopy (TEM)	microscope		and lattice of WO_3 .
UV-Vis Spectroscopy	UV-Visible Spectroscopy (UV-Vis)	UV-Vis Spectroscopy	The best - The best 분광법	Determine the band gap and absorption edge of WO_3 .
Specific surface area determination	BET Surface Area Measurement	BET surface area determination	BET 표면적 측정	The specific surface area of WO_3 was measured by N_2 adsorption method .
X-ray Photoelectron Spectroscopy	X-Ray Photoelectron Spectroscopy (XPS)	X-ray photoelectron spectroscopy	X 광전자 분광법	Analyze the surface chemical state of WO_3 (such as W^{6+} / W^{5+}) .

Application Areas

Chinese (CN)	English (EN)	Japanese (JP)	Korean (KR)	illustrate
Photocatalyst	Photocatalyst	Photocatalyst	광촉매	WO_3 is used to degrade pollutants or produce hydrogen .
Electrochromic	Electrochromism	エレクトロクロミズム	2	of WO_3 in smart windows.
Gas Sensor	Gas Sensor	Gas Center	korean 센서	WO_3 detects gases such as NO_2 and CO.
Energy Storage Materials	Energy Storage Material	Energi storage materials	2 2 재료	WO_3 is used in supercapacitors or batteries.
Smart Window	Smart Window	Smator	스마트 창	WO_3 film regulates light transmittance and heat.
Pollutant degradation	Pollutant Degradation	Decomposition of pollutants	The 분해	WO_3 photocatalytic degradation of organic matter .
Hydrogen production	Hydrogen Production	Hydrogen production	2 생산	WO_3 photocatalytically decomposes water to produce hydrogen.

Other related terms

Chinese (CN)	English (EN)	Japanese (JP)	Korean (KR)	illustrate
Doping	Doping	Doppin	도핑	For example, N and Ag doping WO_3 can optimize performance.
Composite Materials	Composite Material	Composite Materials	복합재료	Such as WO_3 /TiO_2 , improving photocatalytic efficiency.
Nanoparticles	Nanoparticle	Nano particles	나노입자	WO_3 , 10-50 nm.
Nanowires	Nanowire	Nanowaya	2	WO_3 has a diameter of 20-30 nm.
Nanosheets	Nanosheet	Nanosity	2	WO_3 , thickness 1-5 nm.
Quantum Dots	Quantum Dot	Quantum Dot	2	of WO_3 , <10 nm.
Cyclic stability	Cycling Stability	Cycle stability	순환 2	of WO_3 during repeated use.

CTIA GROUP LTD
Introduction of Nano Tungsten Trioxide (WO_3)

1. Nano Tungsten Trioxide Overview

CTIA GROUP LTD's Nano Tungsten Trioxide (WO_3) complies with GB/T 36080-2018 and ISO/TS 21356-1:2021 standards. It is prepared using advanced chemical vapor deposition or wet chemical methods and is a high-performance nanomaterial. It is known for its ultrafine particle size, high specific surface area and excellent photoelectric properties, and is suitable for use in the fields of optoelectronics, catalysis and energy.

2.Excellent Properties of Nano Tungsten Trioxide (WO_3)

Ultrafine nanoscale: particle size ranges from 50-100 nm, evenly distributed, and meets the standards for nanomaterials (1-100 nm).

High purity: WO_3 content ≥99.9%, extremely low impurities, ensuring high-end application performance.

Excellent performance: surface area >20 m²/g, excellent optical transparency, conductivity and thermal stability.

Reliable quality: pure crystal form (XRD detection), no agglomeration, guaranteed consistency.

3. Nano Tungsten Trioxide (WO_3) Product Specifications

Brand	Particle size (nm)	Purity (wt %)
NWO-50	50±10	≥99.9
NWO-80	80±10	≥99.9
NWO-100	100±10	≥99.9
In addition to basic specifications, parameters such as particle size and purity can be customized according to customer needs.		

4. Nano Tungsten Trioxide (WO_3) Packaging and Warranty

Packaging: Inner vacuum aluminum foil bag, outer sealed plastic barrel, net weight 1kg or 5kg, moisture-proof and oxidation-proof.

Warranty: Each batch is accompanied by a quality certificate, including particle size distribution (laser method), chemical composition and specific surface area data, and the shelf life is 12 months.

5. Nano Tungsten Trioxide (WO_3) Purchasing Information

Email: sales@chinatungsten.com
Tel: +86 592 5129595

For more information about nano tungsten oxide, please visit the website of CTIA GROUP LTD. (www.ctia.com.cn)